ASPECTS OF ELECTRONIC DEVICE PACKAGING

by

D.R. BRIDGE B.Sc.

For submission to the

degree of Doctor of Philosophy

University of Warwick

Department of Physics

December 1986

LIST OF CONTENTS

LIST OF FIGURES

LIST OF TABLES

Acknowledgements

DECLARATION

This dissertation is submitted to the University of Warwick in support of my application for admission to the degree of Doctor of Philosophy. It is an account of my work carried out in the Department of Physics, University of Warwick during the period October 1983 to August 1986 and, except where specifically acknowledged in the text, is a result of my own independent research. No part of this thesis has been submitted in respect of a degree to this or any other university.

DECEMBER 1986   D.R. BRIDGE

ABSTRACT

For this work cordierite has been investigated as a possible substitute substrate material for alumina, with particular emphasis on its role in multilayer device packaging. By limiting the processing temperatures to below 1000°C, copper could be used as the conductor material. Milled glass powder was made into thin sheet form by a doctor blading technique and, once dried, the copper screen printed on top. After lamination and firing, the conductor was completely encapsulated by the cordierite matrix. Copper diffusion occurred with metallic copper precipitating out although a small denuded zone was evident around the periphery of the conductor. This was due to compositional changes occurring there.

Experiment showed that the effects of glass particle shape, average size and size distribution lead to deviation in the shrinking of compacts from the theoretical sintering curves. An unstable μ phase was the first to appear on the glass particle surfaces although another, unidentifiable phase, was also found to exist during the very early stages of crystallization. This was followed shortly after by bulk crystallization of μ cordierite in the remaining glass, possibly being aided by a prior phase separation. Further heat treatment lead to the transformation to α cordierite and the formation of enstatite, the exact transformation temperature depending upon the minor oxide additives in the glass. At temperatures above ~1050°C protoenstatite formed and lead to a general degradation in material properties.

The benefit from having α cordierite as the principal phase is a low dielectric constant (5.35) and loss angle (5×10^{-4}), reasonable strength (130 MPa) and high resistivity (~10^{15} Ωcm). This makes it a suitable replacement for alumina although its low thermal conductivity (~2 $Wm^{-1}K^{-1}$) is a drawback. By adjusting the MgO/Al_2O_3 ratio, the material could be expansion matched to that of silicon.

LIST OF ABBREVIATIONS

CRN   –   Continuous Random Network

DTA   –   Differential Thermal Analysis

DTG   –   Differential Thermogravimetry

DSC   –   Differential Scanning Calorimetry

EDAX   –   Energy Dispersive Analysis of X-rays

IC   –   Integrated Circuit

IR   –   Infrared

JCPDS   –   Joint Committee for Powder Diffraction Standards

MAS   –   Magnesium Alumino Silicate

MAS NMR   –   Magic Angle Spinning Nuclear Magnetic Resonance

MCM   –   Multichip Module

MLC   –   Multilayer Ceramic

MOS   –   Metal Oxide Semiconductor

NBO   –   Non Bridging Oxygen

NMR   –   Nuclear Magnetic Resonance

ppm   –   Parts per Million

RD   –   Spin Lattice Relaxation Time

RF   –   Radio Frequency

SEM   –   Scanning Electron Microscope/Microscopy

TEM   –   Transmission Electron Microscope/Microscopy

TGA   –   Thermogravimetric Analysis

VLSI   –   Very Large Scale Integration

XRD   –   X-ray Diffraction

In memory of Professor P.W. McMillan

CHAPTER ONE - INTRODUCTION

In many high speed data processing units it is packaging technology
which determines or limits performance, cost and reliability (1) and may
be one of the limiting factors in further circuit integration and
increased device operating frequency (2). For the manufacturer there
are many requirements to be taken into account when designing a suitable
system:-

i)   Electrical signals must be able to pass between various components
whilst remaining electrically isolated from other current carrying
members. Ideally these signal paths must be short.

ii) Due consideration must be paid to power dissipation since excessive
thermal build up will lead to component failure.

iii) The integrated circuits (IC'S) themselves must remain hermetically
sealed since they are sensitive to atmospheric variations (humidity etc)
whilst the packaging as a whole must withstand the external environment
which may include large magnetic fields, radiation, hostile chemical
conditions etc.

iv) The package must be sufficiently robust to withstand the rigours of
assembly, transportation and use.

v)   Potential users will be looking for package reliability, space
efficiency and design flexibility.

The more general aspects of device packaging are dealt with more fully
in the book by Fogiel (3) and more recently by Ho (4) and Giess et al
(5).

Organic polymer material has been used to a great extent in device

encapsulation where the operating environment is fairly inert and device performance is not critical. The choice of substrate material can be crucial however in advanced applications since the material will effect the response, performance and possible uses of the system.

1.1 AIM OF THE THESIS

1.1.1 The Problems with Alumina

Beryllia (BeO) would be a good material, particularly as it has a high thermal conductivity, but because of its toxicity alumina has proved to be by far the most popular choice of substrate material due to its good sintering properties, high strength and reasonable thermal conductivity, see Flock (6). Many alumina substrates are commercially available with differing degrees of purity and surface finish. There are some disadvantages in its use however:-

i) Its high sintering temperature (1500-1600°C) limits the choice of conductor metal to the more refractory materials such as Mo, W, Pd or Pt. Molybdenum, or some alloy with it, appears to be the favoured metal since it is cheaper than the others, has a good shrinkage match to alumina and adheres well (7). All these metals however are generally expensive, Mo requires plating before soldering and they have high resistivities. The latter is an important consideration since the size of a substrate is influenced by the size of conductors on it.

Decreasing the width and/or thickness increases resistance R since

$$R = \rho l/A \qquad (1.1)$$

where ρ is the resistivity, l the length and A the cross sectional area.

High resistances also lead to larger voltage drops and localized heating.

ii) The thermal expansion of alumina is high $(65-70 \times 10^{-7} {}^{\circ}C^{-1})$ compared to that of silicon chips $(\sim 30 \times 10^{-7} {}^{\circ}C^{-1})$. This leads to possible failure due to stress at the solder pad connection, a problem which is likely to get worse if IC's increase in size (see Carlson et al (8)).

iii) The time delay, Td, of a signal propagating a length l down a conductor is given as

$$Td = \sqrt{K} l/c \qquad (1.2)$$

where c is the speed of light and K the dielectric constant of the surrounding medium. Alumina has a dielectric constant of about 10 which leads to small but noticeable delays ($\sim 10ns/m$).

Consequently there is a need for a low firing, sinterable material to replace alumina (9). Thus the aim of this work is to develop, and investigate the properties of, a glass ceramic that can be used in this process. It should have a maximum processing temperature of $\sim 1000^{\circ}C$ enabling cheaper and lower resistivity metals such as Au, Cu and Ag to be used. The general requirements of a ceramic packaging material have been discussed by Wilcox (10).

1.1.2 Alternative Materials to Date

Both SiC and Si_3N_4 have improved conductivities and SiO_2 has a low dielectric constant but all these ceramics have an excessive processing temperature. Thus much work has focused on glasses and glass ceramics. McMillan et al (11) devised a multilayer structure, which incorporated

copper conductors, in 1968. A lithium zinc silicate glass ceramic was used since it was required to match the thermal expansion of a copper heat sink ($\alpha \sim 170 \times 10^{-7} {}^{\circ}C^{-1}$). A lower expansion glass ceramic was investigated by Cornings and their boro-silicate glass is now commercially available (e.g. Corning 7052).

The possibility of using glass was first suggested by Byer (12) who looked at the encapsulation of conductors using photosensitive glasses. Both Greenstein et al (13) and Longston et al (14) suggested using thin films of bubble free glass onto which a suitable metal could be deposited. Again the required expansion was high since the glasses were bonded to a lower alumina substrate and glasses suffer generally from a poor thermal conductivity compared to glass ceramics. More recently alternative materials have been proposed. Shimada et al (15) have developed an alumina/lead boro-silicate glass mix that can be sintered at 900°C and has improved properties over pure alumina. An expansion coefficient of $42 \times 10^{-7} {}^{\circ}C^{-1}$ and dielectric constant of 7.5 was quoted. A material which sinters at 750°C and has a dielectric constant of 6 was put forward by Lau et al (16) although no composition was given and an expansion coefficient of $57 \times 10^{-7} {}^{\circ}C^{-1}$ is a little on the high side.

Finally a low firing temperature ceramic in the system $BaO-ZrO_2-SiO_2$ has been developed by Wakino et al (17) which can be cofired with copper.

From a knowledge of crystal phases, however, it would appear that two of the most likely contenders are either β spodumene ($Li_2O.Al_2O_3.4SiO_2$) or cordierite ($2MgO.2Al_2O_3.5SiO_2$). Glass ceramics where these are the principal crystalline phases have been investigated by Narken and Tummala (18) and Kumar et al (19). Both phases were found to be

suitable for substrate applications, particularly multilayer ceramic (MLC) substrates, with cordierite having a slightly better potential. Thus it was decided to investigate the use of glass ceramics in MLC fabrication by concentrating on cordierite based materials, specifically the phase development, the properties and the interaction between the various processing steps and properties.

1.2 PACKAGING EVOLUTION

The prime driving force behind device packaging is that of higher densities, i.e. the need to package more capability into a smaller space. Obviously as the number of circuit functions per chip (Nc) increases the number of required leads (Nt) increases also and this can become a limiting factor in package density. It has been shown empirically by Rent (20,21) that Nt is related to Nc by the following expression,

$$Nt = A(Nc)^B \qquad (1.2)$$

where A varies between about 4 and 2.5 whilst B is about $\frac{2}{3}$. Thus it is possible to break down a complicated system into clusters of circuits and sets of connected interfaces.

Initailly IC's were fairly simple and this was reflected in their packaging such as the TO series cans which were hermetically sealed metal cans with chips wire bonded to a ceramic base. One of the next most successful developments was that of the dual in-line package (DIP), favoured because of its ease of handling and mounting. Despite being one of the least space efficient IC packages in wide use it has become a standard through the actions taken by the Joint Election Device

Engineering Council (J.E.D.E.C.). More recently the demand for more terminals has lead to an alternative J.E.D.E.C. package where all four sides of the chip carrier are used instead of just the two with the DIP (22,23).

The circuit density per chip has continued to increase with no sign of abating, a typical VLSI chip today having 10^5-10^6 MOS circuits each (24) although this has not been matched by an increase in device dimensions. From equation 1.2 this implies that the interconnecting circuitry must become even more complex in what is essentially a non changing area. Furthermore, development of GaAs and high speed Si circuits has led to operating frequencies in the GHz region. Hence signal wavelengths have become comparable with package dimensions with resulting degradation due to reflections.

This had led to a fundamental change in packaging technology, away from the isolated 'flat packs', with their associated three level hierarchy of packaging, to multichip modules (MCM's) using MLC substrates.

Much of the innovative work has been done by the IBM corporation in America with MLC's being used in the IBM 4300 series (25-27) and the more recent 3081 series computer (1,7,28-30). They are also incorporated into the NEC SX supercomputer (31). For a review of packing within IBM see Seraphim and Feinberg (32) and for MLC evolution, Schwartz (33). MLC's are becoming increasingly common for microwave applications (34-35).

1.2.1 Advantages of MLC's

Part of a typical MCM is shown in Fig.1.1. The main advantage of this type of packaging is that the high density of IC's and wiring (see Ferry
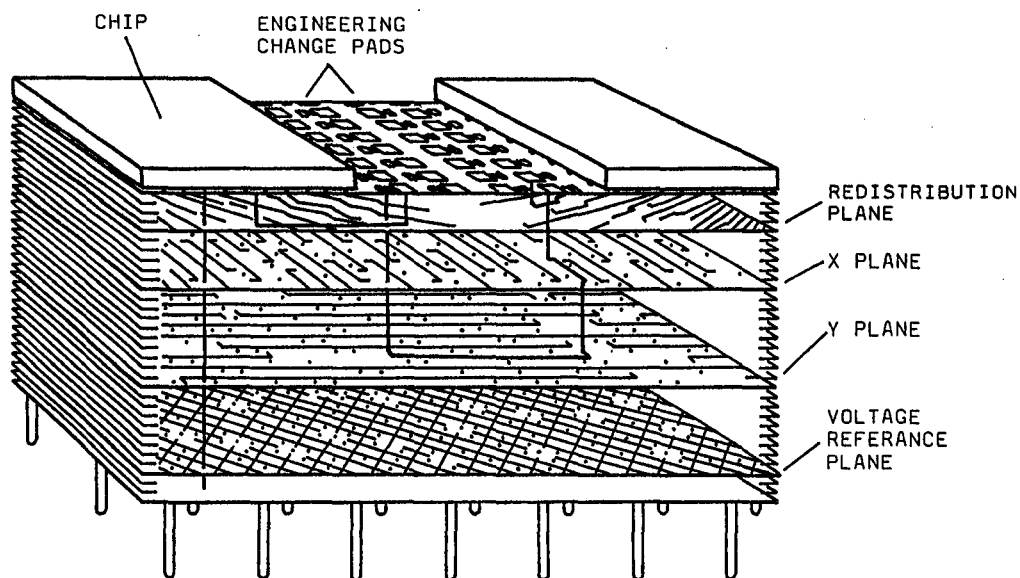
FIG.1.1   Section of part of a typical MLC substrate
          (after (1))
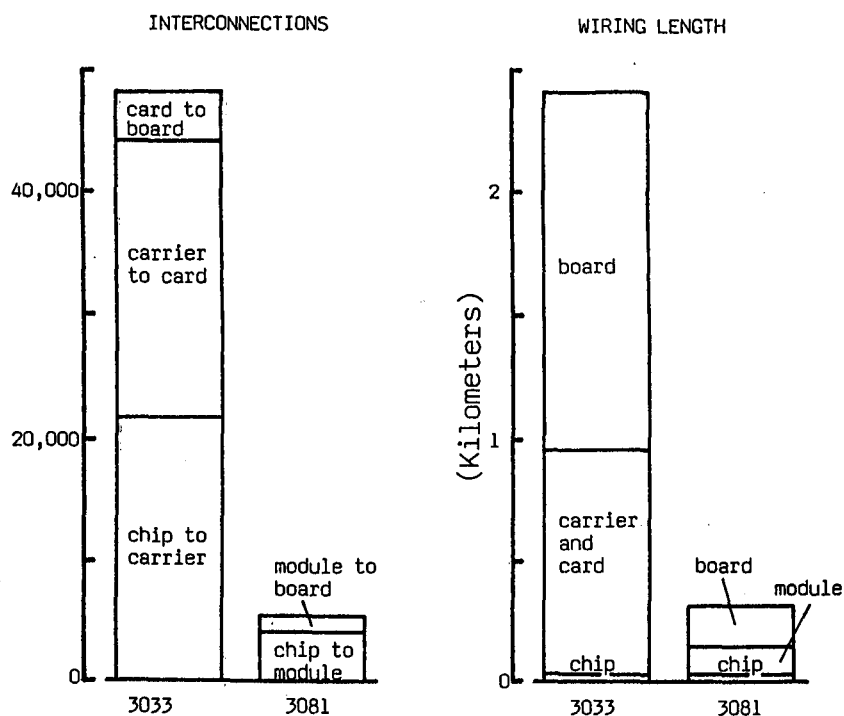
FIG1.2   Comparison of the number of interconnections
         and total wiring. length of the IBM 3033
computer (plug in card type) and the IBM 3081 computer
(MCM type). (After (1))

(36)) lead to greatly increased switching times, typically a nanosecond, and hence improved computer performance (37). The total number of interconnections is dramatically reduced and reduced connection lengths lead to a lower power consumption (Fig.1.2). Reduction in wasted space leads to more compact systems although this places increased demand upon heat dissipation especially in the central processor unit. The total cost is reduced and the system more reliable, an important factor when one considers that a field replacement unit is considerably more expensive.

The MCM of the 3081 measures ~80mm square and 5mm thick and within its 33 layers contains some 200m of wiring and more than 350,000 vertical linking vias. 133 IC's requiring 12,000 contact pads sit on the top surface fed by signals, power etc from 1800 pins in the bottom surface. Nine of these modules locate into a larger multilayer substrate which can supply up to 600 Amps (38). Generally these high technology substrates have been limited to the larger mainframe computers but there is considerable scope for a scaled down inclusion within smaller PC's (39).

1.2.2. Manufacture of MLC's

The method of construction for MLC's was originally suggested by Schwartz and Wilcox (40) based on ideas by Stetson and Schwartz (41). Since the work by Kaiser et al (42) the approach to manufacture has become fairly routine and many patents have been taken out based around the process (43-50).

Central to the production of MLC's is the manufacture of large, thin sheets of unfired ceramic called 'green sheets'. Alumina is ball milled

with a suitable solvent added to which is a binder, plasticizer, wetting agent and deflocculent (see park (51)). When the particle size is sufficiently small and the slip of the right consistancy (typically 1-1.5 poise) it is filtered and then doctor bladed out onto a continuous moving belt. The thickness of the sheet is carefully controlled. After passing through a drying oven the volatile components have evaporated leaving the alumina embedded in an organic binder mix. A fine particle size is required to give a smooth surface but this obviously necessitates a larger quantity of binder. Doctor blading is a critical operation since the sheets must be of uniform thickness (typically 0.1-0.8mm) and free from defects such as pinholes and cracks.

After blanking to the right size and punching registration holes the vias are punched. These provide for the vertical linking between layers and take the form of ~150μm diameter holes positioned on a 0.3-0.5mm grid. Up to 40,000 vias are required per sheet and these can be punched (52, 53), drilled (54) or cut by laser (38). An alternative method of via fabrication is discussed by Dougherty and Greer (55). Sheets are then cleaned to remove residual debris and then subjected to an optical verification, i.e. presence or absence of a via and its location.

The vias are filled by standard screen printing techniques since all holes are filled in one operation. By choosing an appropriately formulated conductive paste the shape of the vias can be altered so as to reduce stress concentrations (56). The next stage is metallization of the signal conduction lines which can be done using thin film techniques (57, 58) but is more usually done again by thick film screen printing. The metal used in the conductive paste depends upon the choice of ceramic and the maximum firing temperature, see Chance and

Wilcox (59). Lines are typically 100μm wide, 50μm thick and 100μm apart although these dimensions can be reduced using thin film depositions.

An alternative method of metallization exists whereby improvements on the resistivity of the conductor is achieved (40, 60, 61). Paste is deposited in the normal manner but its metal content is considerably reduced. After firing, lightly metallized hollow channels within the ceramic result which can then be capillary filled or infiltrated under pressure.

Following stacking of the sheets in the required order the next stage is lamination. In this process the individual layers fuse together and the ceramic/binder mix flows around the conductors. Gardener and Nufer (62) have shown that the bond strength, B, between layers is related to the lamination pressure, P, lamination temperture, T, and time, t, by the relation.

$$B = K_1 + K_2 \ln(PTt) \qquad (1.2)$$

where K_1 and K_2 are empirical constants that are determined for each ceramic/binder system. For good bonding a pressure of ~4.5-70 MPa at 60-135°C is required for a period of 5-15 minutes. However, an appropriate choice of binder enables pressure alone to be used (43, 63).

The laminate is then fired, as a single structure, to complete densification. During firing all binders must be completely evolved whilst for base or refractory metallurgies the furnace atmosphere must be suitably controlled. Considerable shrinkage occurs during sintering and since close tolerances are involved it is usually necessary to specify the shrinkage to ~0.15%. If so desired, by screening

appropriate metals to form a thermocouple, the internal temperature
gradient within the substrate can be monitored directly (64). Once
fired, the MLC is now a dense ceramic body with a 3D internal network of
conductors. These conductors are then subjected to an extensive
electrical test.

The final processes involve brazing in the lower contact pins (see
Babuka et al (65)) and usually Ni and Au plating prior to surface
mounting the chips. These are in what is known as a 'flip chip'
configuration in that the operational surface of the IC points towards
the top of the MLC. A tin-lead solder pad is placed between the chip
and the contact pad. On passing the MCM through a low temperature
bonding furnace the contacts melt, aligning the chip through surface
tension, the so called 'controlled collapse contact' (66-68). Final
electrical testing can now be performed. The manufacturing processes
are summarized in Fig.1.3. They are discussed further by Burger and
Wiegel (69) and reviewed by Schwartz (70). It should be pointed out
that MLC's can be made entirely by the thick film process which greatly
widens the choice of metallic conductor (71). However, it suffers from
the disadvantage that each layer must be fired before the next can be
deposited.

The high density of chips on the MCM generates too much heat to be
dissipated by air cooling, where the maximum heat flux is about $2W/cm^2$.
For the IBM 3081 processor this has led to the developemnt of the
Thermal Conduction Module (72), part of which is shown in Fig.1.4. The
chip is surrounded by helium since it has a higher thermal conductivity
than air. A metal cylinder conducts heat away from the back of the chip
to a chilled water channel. A chip dissipating 4W will operate at about

```
                    CERAMIC BALL MILLING ──────────────── BINDER
                            ↓ ◄────────────────────────── PREPARATION
                        BINDER ADDITIONS
                            ↓
                   CASTING SLIP PREPARATION
                            ↓
                        TAPE CASTING
                            ↓
                    DRYING AND STRIPPING
                            ↓
                     VISUAL INSPECTION
                            ↓
                         BLANKING
                            ↓
                       VIA PUNCHING
                            ↓
                         CLEANING
                            ↓
                     OPTICAL TESTING
                            ↓
                        SCREENING
                            ↓
                   STACKING/LAMINATION
                            ↓
PLATING SOLUTION             FIRING
PREPARATION ──────────────► ↓
                         PLATING
                            ↓
                         BRAZING
                            ↓
                   ELECTRICAL TESTING
                            ↓
                       CHIP JOINING
                            ↓
                         REFLOW
ENGINEERING ──────────────► ↓
CHANGES             VISUAL AND ELECTRICAL TESTS
      ▲─────────────────────────────── ↓
                         CAPPING
```

FIG.1.3 Flow diagram of MLC manufacture

WATER →

SPRING

PISTON

Ar GAS

SEAL

CHIP

MCM
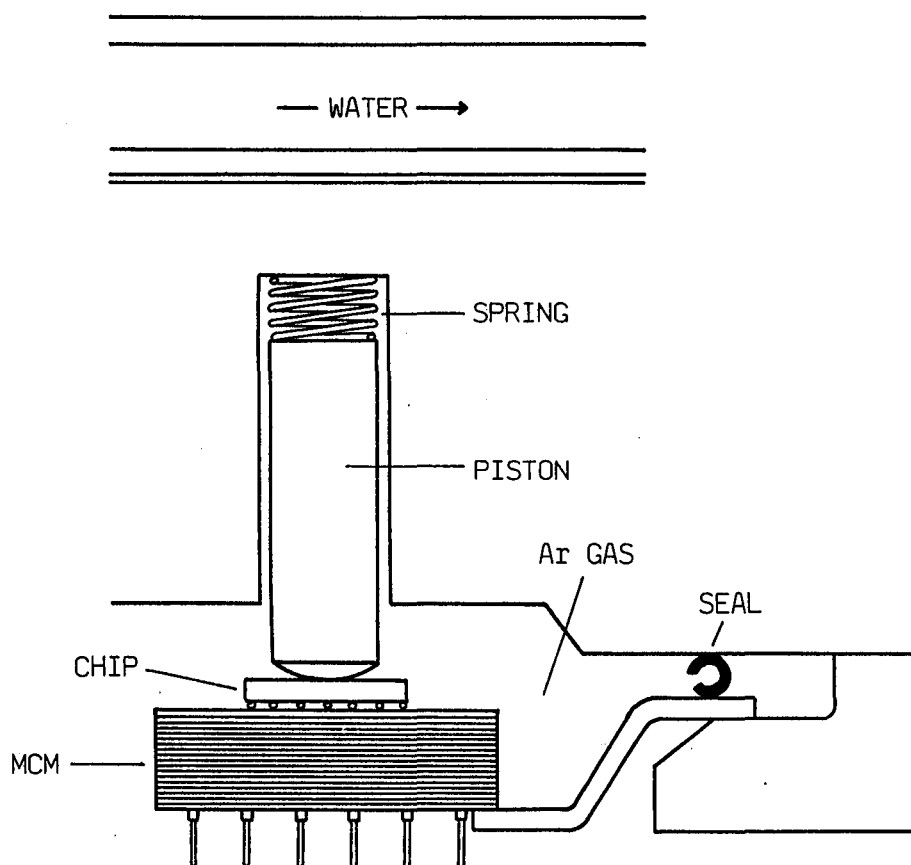
FIG.1.4 Section of the IBM Thermal Conduction
        Module

68°C which is well below its safe operating limit.

Consideration of fig. 1.1 shows the nature of the various components within a MCM. The top surface of the module contains the IC's plus engineering change pads which allow for external testing and a certain degree of rewiring. The next lowest levels are concerned with signal redistribution, essentially between the IC's and change pads. The layers below these provide for interchip communication, each alternating layer having conductors running parallel either to the x or y direction. The lowest layers are concerned with the distribution of both power and input/output signals. Between each layer is a voltage reference plane which is maintained either at ground or a fixed voltage. These cut down noise through inter-layer crosstalk and help define the impedance of the conductors. Absence of reference planes can lead up to 40% variation in connection capacitances (12).

1.3   GLASSES AND GLASS CERAMICS

1.3.1 Glasses

The term glass refers to a material which has many of the physical properties of a solid but has an atomic arrangement which lacks the long range periodicity of crystalline materials and instead has a liquid like short range order extended usually over only a few atomic spacings. The glasses of greatest technological interest are formed by melting together certain metal oxides and has led to a definition of a glass by the American Society for Materials Testing - 'a glass is an inorganic product of fusion which has cooled to a rigid condition without crystallizing.' It should be pointed out that organic materials can

also form glasses and methods other than melt cooling are also important.

The constituents of a glass can be divided into three categories, network formers, intermediates and modifers. Network formers (SiO_2, P_2O_5, B_2O_3 etc) are oxides which can form glasses directly on cooling to form a continuous, rigid 3D structure whilst intermediates (Al_2O_3, TiO_2 etc) do not themselves form glasses but are capable of entering into the network of glass formers. The effect of modifying oxides (MgO, Na_2O etc) is to change the properties of a glass by altering the network in some way. For instance, MgO added to silica reduces the viscosity by breaking Si-O-Si bonds to form non bridging oxygens (NBO.'s) i.e. $Si-O^{--}O-Si$ bonds with charge compensation by the Mg^{2+} ion.

One way of distinguishing between the various oxide forms is to measure the ability of the cation to form a covalent bond with oxygen. This is represented by the ionic field strength, F, given as (73,74)

$$F = Z/r^2 \qquad (1.5)$$

where Z is the valency and r the ionic radius. It is found that network formers have high field strengths (Si^{4+} = 23.8) and, due to their cation/anion radius ratio, readily form a tetrahedral unit of oxygen, with the cation at the centre. Modifers have low F values (Mg^{2+} = 4.7) whilst intermediates have values in between (Al^{3+} = 12.0).

One of the problems concerning glass, and which still remains largely unanswered, is its structure. Evidence for some degree of structure comes from diffraction data and a comparison of the pair distribution functions for a glass and ordinary liquid. Principally two schools of

thought exist.

The continuous random network mmodel (CRN) was first proposed by Zacharisen (75), based on the earlier work of Goldschmidt (76) and supported by the X-ray diffraction work of Warren (77). For example, in silica it assumes that the structure is built up of tetrahedral units with each oxygen being shared between two silicon atoms. Although the distance between any two neighbouring tetrahedra is deemed to be fairly constant in the extreme their relative orientations are completely random.

In fact, if this were so, then there would be a flat distribution of dihedral angles. In practice it is found that some angles are more probable than others (78) (although all angles are present) as is to be expected from orbital hybridisation and overlap requirements. The CRN model does not fully encompass glass properties, however, e.g. it fails to take into account thermal history and phase separation (79).

Although the diffraction patterns of amorphous materials show diffuse rings, some are more intense than others and these sometimes correspond to the intense peaks of the corresponding crystal phase, e.g. the (111) reflection of cristobalite. This has led to the proposal of the crystallite theory by Lebedev (80, see also 81) and is supported by the X-ray work of Randall et al (82) and Valenkov and Porai-Koshits (83). The glass structure is thought to compose of microcrystalline clusters, too small to give diffraction although for this condition to hold the actual crystallites would only occupy about 50% of the volume. Like the CRN theory, the fit with experimental work does not always hold, for example an overestimation of the oscillations in the radial distribution

function. However, there is stronger evidence for crystallites ~15Å across in amorphous metals (84).

Other possible models have been suggested, such as the ion theory of Bokris et al (85) and the strained mixed cluster by Goodman (86, 87). The latter, which relies on the polymorphism of materials, has the advantage that it is based on a phase diagram approach. Recent work however, such as the neutron diffraction studies of Sinclair et al (88), would appear to favour a structure related to the CRN model.

Several books deal with glass in greater detail (79, 89-95)

1.3.2 Glass Ceramics

Glass ceramics are made by carefully controlling the crystallization of a glass. For a fine grained microstructure this usually involves production of a large number of crystal nuclei by an appropriate heat treatment and controlling the rate of crystal growth. Nucleation within a supercooled melt has been extensively studied (96, 97), two different types being identified:

(a) Homogeneous nucleation. For this type of nucleation, nuclei form that are of the same chemical composition as the crystal phase that grows from them. They form through brief structural fluctuations within the melt. If the nucleus has a dimension less than some critical radius r* then the interfacial surface energy exceeds that of the reduction due to crystallization and the net free energy increase. At r* the two opposing free energies balance and further growth leads to a lowering in the net free energy since the crystallization energy dominates.

The nucleation rate, I, is given by the equation

$$I = A \exp(-\Delta G^*/kT) \exp(-\Delta Qn/kT) \qquad (1.6)$$

where ΔG^* is the Gibbs free energy for a nucleus of radius r^* and ΔQn is a kinetic barrier term for nucleation. A is related to the number of atoms per unit volume and may be taken as constant. Homogeneous nucleation is rarely observed in practice since a large degree of supercooling is generally required. More common is

(b) Heterogeneous nucleation. This occurs when a crystal phase grows on a nucleus that is chemically different and may include dust particles, scratches on the walls of the container or deliberate additions to the melt. Here the rate is given by

$$I = A'\exp((-\Delta G^* f(\Theta) + Q'n)/kT) \qquad (1.7)$$

where A' is a constant, Q'n the activation energy for diffusion and $f(\Theta)$ is a term relating to the wetting angle Θ of a spherical cap on the homogenity. At low temperatures the viscosity is high and Q'n dominates whilst at higher temperatures ΔG^* dominates.

Aspects of crystal growth have also been well studied (98-101), the basic kinetics of which are not too dissimilar to equation 1.7. The growth rate U, can be written

$$U = A_0 \nu \exp(-Qc/kT)(1-\exp(\Delta G/kT)) \qquad (1.8)$$

where Qc is the activation energy barrier to growth and ΔG the bulk free energy of crystallization. A_0 is roughly the interatomic spacing and ν is the thermal vibration frequency. Again at low temperatures Qc dominates and at higher temperatures, ΔG. The net variation of I and U with temperature is given in Fig.1.5.
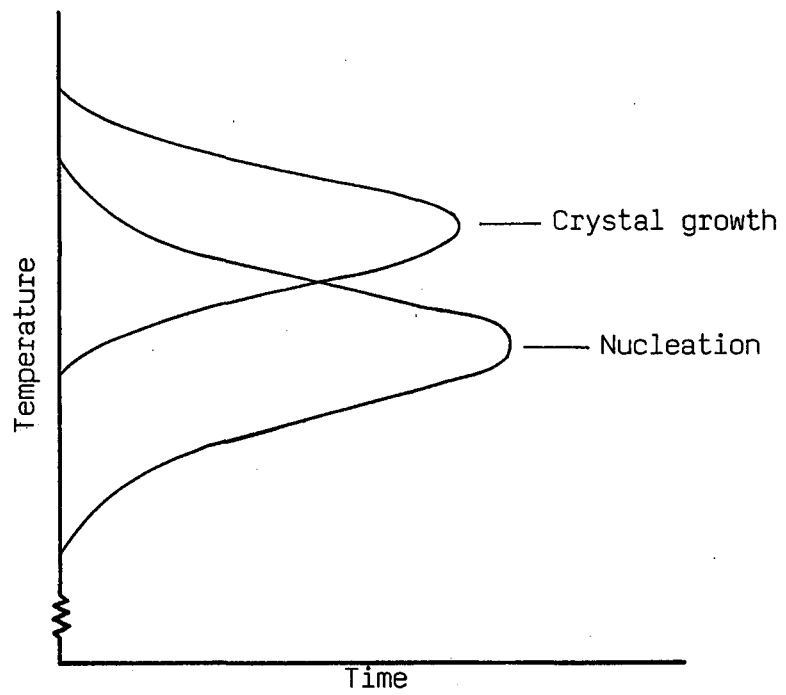
FIG.1.5 Variation of nucleation and crystal
growth rates with temperature
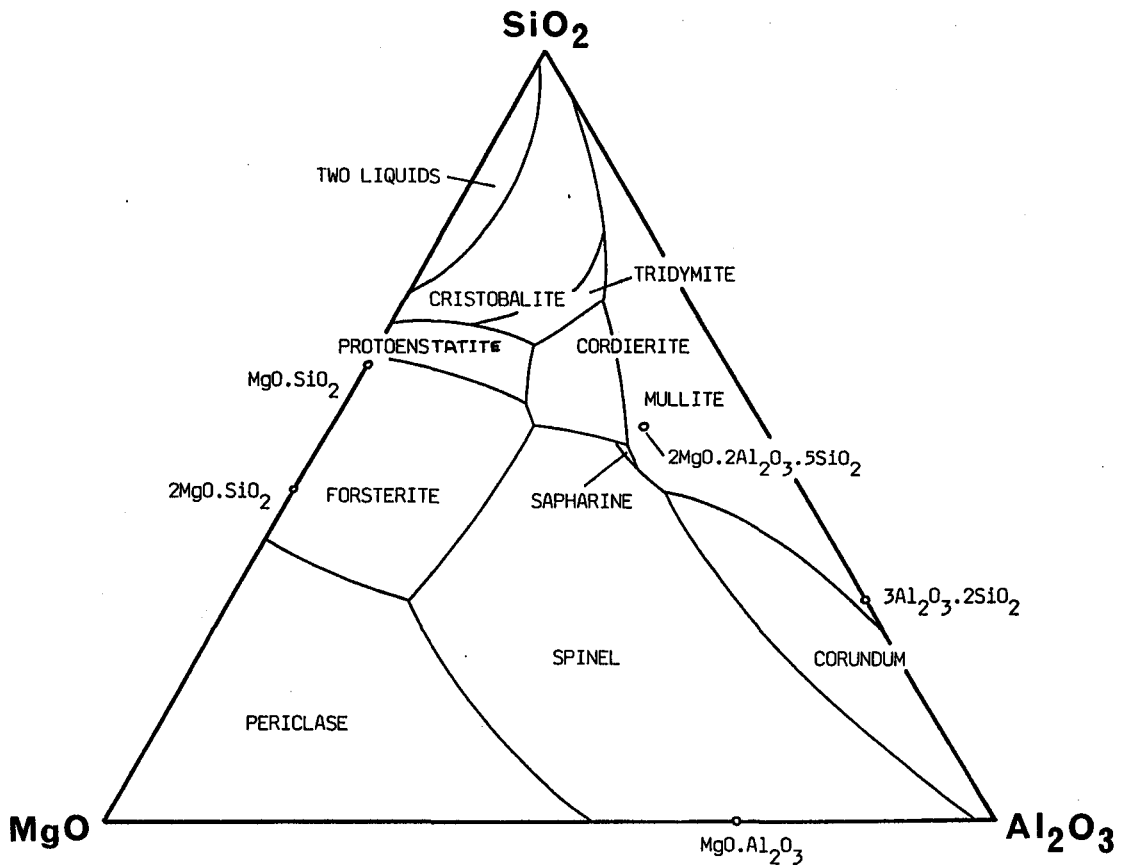
FIG.1.6 The MAS phase diagram

For a glass crystallized by a nucleation and growth mechanism the fraction transformed, f(t) at time t is expressed by the Johnson-Mehl-Avrami equation (102,103).

$$f(t) = 1-\exp(-\frac{\pi}{3} IU^3 t^4) \qquad (1.9)$$

where both I and U are assumed constant. Nucleation is also assumed to be random and in the form of spheres.

Classically three types of nucleation catalyst have been added to glass melts in order to improve nucleation a) Metals, in their elementary form, can be added as oxides and then reduced or irradiated (so called photosensitive glasses) to form colloidal dispersions. b) Halides, such as NaF or Na_2SiF_6, come out of solution when cooled, (if enough is added) so that a fine crystalline precipitate is formed. c) Metallic oxides (the most common case) such as TiO_2, P_2O_5 are added to induce a fine phase separated structure (see Appendix 1) which aids crystallization during subsequent heat treatments.

Glass ceramics are discussed in more detail in the books by McMillan (104) and Halvac (105).

1.4   CORDIERITE GLASS CERAMICS

The region in the $MgO-Al_2O_3-SiO_2$ (MAS) phase diagram which yields cordierite as the principal crystalline phase is shown in Fig.1.6 (106, 107). Note that the stoichiometric composition, $2MgO.2Al_2O_3.5SiO_2$, lies within the mullite phase field. Ceramic materials based on cordierite have been found to have good thermal shock resistance and low dielectric

constant. Consequently they have been used in such applications as catalytic converters in car exhausts (108-110) and missile radomes (99, 111, 112).

One of the earliest investigations in this ternary system was conducted by Rankin and Merwin (113) who identified two polymorphs, a metastable form (μ) and a more stable higher temperature form (α)to which it transformed. Both types were considerably affected by solid solution. The metastable form was later named μ cordierite by Karkhanavala and Hummel (114). This is not a particularly apt notation since the structure is related to β quartz (115, 116) and since it exhibits a range of solid solution between SiO_2 and $MgAl_2O_4$ (113, 117) it is sometimes referred to as a stuffed β quartz solid solution. Having noted this structural difference however, the term μ cordierite will be used hereafter.

Schreyer and Schairer (117) studied a large number of compositions within the ternary MAS system, particularly on the SiO_2-spinel line. They found that at least 58.7 weight percent (wt%) SiO_2 could be replaced by MgO and Al_2O_3. The high quartz structure is stabilized by the inclusion of Mg^{2+} and Al^{3+} ions within the structure. Above 92 wt% SiO_2 this stabilizing effect is reduced and the familiar α to β transition is seen but at much lower temperatures.

A third polymorph, designated β cordierite was obtained hydrothermally by Yoder (118). This stable low temperature modification could be obtained from the glass as well as from the μ and α forms. Upon heating in air the β polymorph transforms to α cordierite. Two less common phases have been identified by Schreyer and Schairer (119). One had a

structure similar to osumilite ($Na_2O.5MgO.12SiO_2$) whilst the other resembled the mineral petalite ($LiAlSi_4O_{10}$). Both were found to be capable of coexisting with μ cordierite.

The size of Mg^{2+} ions and Li^+ ions are very similar (0.66 and 0.68 Å respectively) and it would therefore not be unexpected for magnesium alumino-silicates and lithium alumino-silicates to have similar properties. This is indeed the case when one compares spodumene with cordierite (19). Indeed, work by Winkler (120) on the high temperature form of eucryptite ($LiAlSiO_4$) was the first to show the existence of stuffed β quartz solid solutions . Both β spodumene and μ cordierite form a complete series of solid solutions (114, 121) and the magnesium/lithium ion exchange within the quartz structure forms the basis of a strengthening mechanism for this material (122).

Formation of the μ phase is thought to occur by the precipitation of a silica rich solid solution into which isomorphous substitution of Al^{3+} and Mg^{2+} occurs (116) according to the relation

$$2Si^{4+} \rightleftharpoons Mg^{2+} + 2Al^{3+}$$
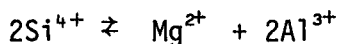
The Al^{3+} ions occupy tetrahedral (silicon) sites whilst the Mg^{2+} ions enter interstitially (123) into the helices of the quartz giving rise to a slightly larger unit cell (115, 116). It is thought that the instability of the phase is related to the unavailability of small coordination sites for the Mg^{2+} ions since in α cordierite they occupy fairly regular octahedral coordination.

The structural similarities between β quartz and μ cordierite have been further highlighted by Carpenter et al (124) who have shown from a thermodynamic viewpoint that the devitrification of the μ phase of

cordierite composition is energetically similar to that of β quartz from silica. They quoted 50 ± 6 KJmol^{-1} compared with 65 KJmol^{-1} (125) respectively. The μ form transforms to the α form in a sluggish manner (113, 114) between 950 and 1100°C. The transformation cannot be reversed once it has occured despite high temperature heat treatments for long periods of time (126). It would appear that μ cordierite is preferentially formed on powdered MAS glass and Karkhanavala and Hummel (114) were unable to recrystallize glasses greater than about 1.5mm.

Hexagonal α cordierite is synthesised from the μ or β phases or is the first phase to appear in larger glass specimens (127-129). It melts incongruently at 1460°C. Its structure has been well studied (130-134) and has been found to be isostructural with beryl (135). After an X-ray crystallographic study, Bragg (130) proposed the structural formula Al$_3^T$ Mg$_2^O$(Si$_5$Al)^{T}O$_{18}$. (T = tetrahedral, O = octahedral).

After many hours of heat treatment (e.g. 2000 at 1180°C) hexagonal cordierite approaches an orthorhombic form, which is the more thermodynamically stable state and is termed low cordierite (as opposed to hexagonal 'high' cordierite). This is of considerable mineralogical interest and work by many authors (124, 128, 134, 136-139) has shown that the high and low forms may be categorised by the degree or ordering of Al^{3+} and Si^{4+} within the 9 possible tetrahedral sites.

Low cordierite has Al^{3+} and Si^{4+} in ordered sites and has the structural formula Al$_2^T$Mg$_2^O$(Al$_2$Si$_4$)^{T}O$_{18}$ (132). The arrangement of Al and Si tetrahedra is such that the tetrahedra alternate in the hexagonal rings and linking chains except for two pairs of Si tetrahedra in the rings which share a common oxygen atom, Fig.1.7. This agrees with the

Si

Al
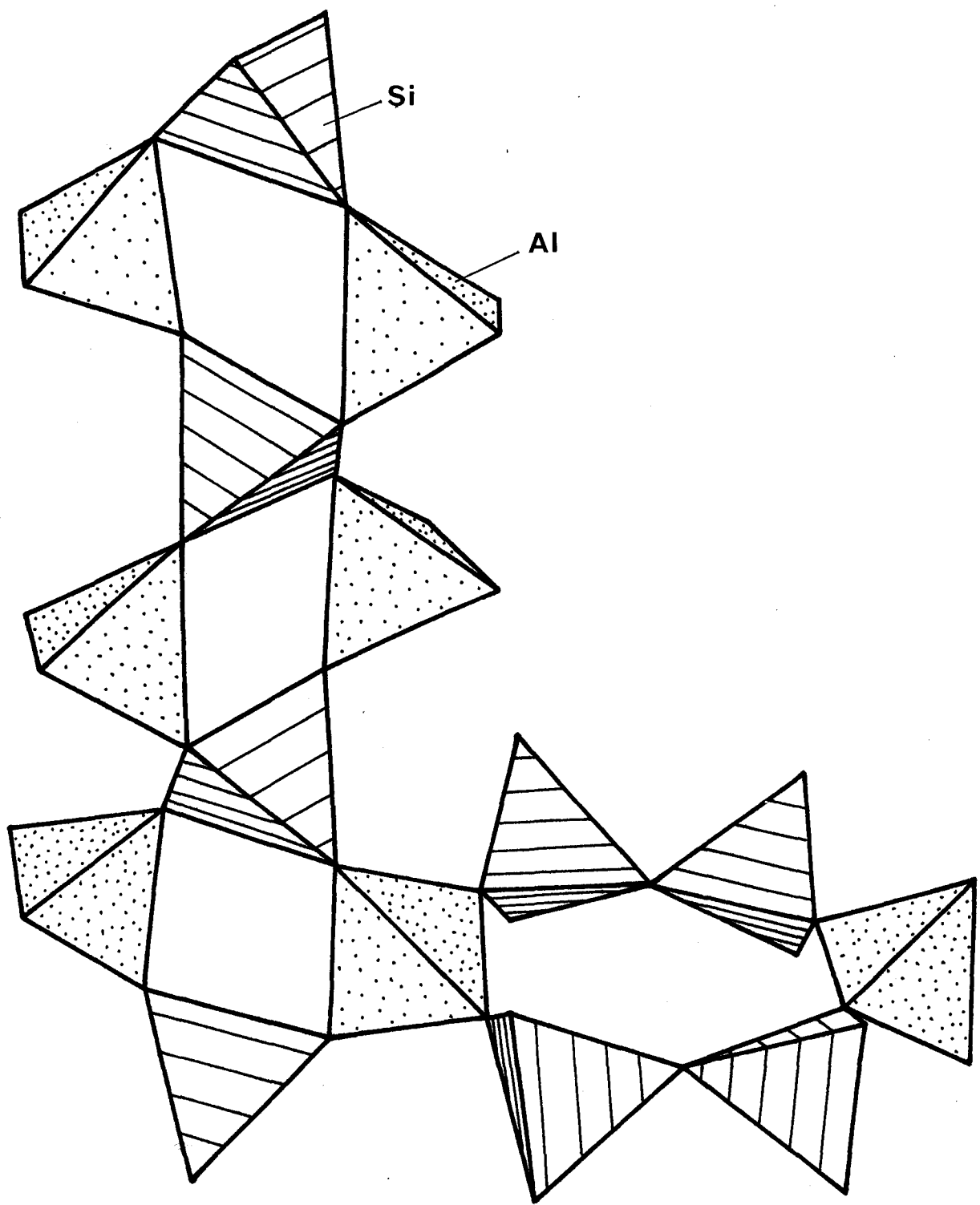
FIG.1.7 _Schematic arrangement of Al and Si tetrahedra in
low cordierite

aluminium avoidance rule proposed by Lowenstein (140).

The ordering in synthetic low cordierite was confirmed by Fyfe et al
(141) using Magic Angle Spinning Nuclear Magnetic Resonance (MAS NMR)
spectroscopy. Analysis of freshly crystallized synthetic hexagonal
cordierite however indicated that there was not a random distribution of
Si atoms as would be expected during the early stages of
crystallization. It was found that silicon exhibited a greater
preference for ring sites during the early stages than after many hours
of heat treatment, a chain to ring ratio of 0.122:0.878 being
quoted. They also found evidence that the aluminium tetrahedra were
somewhat distorted.

After an extensive crystallographic study by Miyashiro et al (142) on
both synthetic and natural cordierites, Miyashiro (143) concluded
that there exists a whole series of metastable states between disordered
high and ordered low cordierite. He also found that μ and α exhibit
hexagonal symmetry whilst all natural forms are orthorhombic except for
the fused clay shales from Vakaro, India. Consequently Miyashiro called
all α cordierites, Indialites.

In order to characterize these intermediate forms, Miyashiro proposed a
distortion index, Δ, which represents the degree of order within the
structure. Δ is related to the position of three adjacent peaks in the
cordierite X-ray diffraction pattern. For Indialite (hexagonal
cordierite) $\Delta = 0°$ and for ordered cordierites $\Delta = 0.29 - 0.31°$.
After this work however Schreyer and Yoder (144) were able to show that
the transition from high to low was due to compositional affects rather
than polymorphism. The cause was due to molecular water within the

structure and was shown to be so by plotting refractive index versus water content for cordierites with identical Δ values.

The possibility of ions within the open channels in the cordierite structure was first suggested by Folinsbee (145). After careful chemical analysis he found that certain ions were present that were too large to sit in either the three or six coordinated sites. The existence of molecular CO_2, Na^+, Cu^{2+} and Fe^{2+} besides molecular H_2O within the pseudo spherical cavities formed by the hexagonal rings ($r \sim 2.2\text{\AA}$ (146)) has also been reported (134, 147-150).

The possible presence of molecular water within a material for device packaging applications is a cause for concern as this can greatly speed up ion migration between conductors. The presence of water however, even in the hydrated minerals is less than 3% (151) and requires heating to 800°C for six hours in a hydrogen atmosphere before it is completely evolved.

So far discussion has been limited to pure MAS glasses. Stookey (152) however was able to show that considerable improvements to the crystallization kinetics and general properties was possible by inclusion in the melt of 2-20 wt% TiO_2. This helped form a fine, phase separated glass from which a bulk crystallized ceramic could be formed by appropriate heat treatments. Since this early discovery much work has been done on these titania and other bulk nucleated cordierites. The works by Gregory and Veasey (153), DeVekey and Majumdar (154), Barry et al (155, 156) and Todhunter (157) are referred to.

For this work, in which high surface area powders are employed, bulk

nucleation/crystallization is not required and thus TiO_2 was excluded. Instead P_2O_5 was added to promote surface nucleation and reduce melt viscosity whilst B_2O_3 was added to aid melting and sintering.

Rabinovich (158) examined the sintering of 40 cordierite based glasses containing various oxide additives. He found that those containing TiO_2 did not sinter well and consequently had poor strength. The converse was true for a glass containing P_2O_5 and concluded that glass intended for conversion into glass ceramic by way of powder technology must have crystallization originating from the surface.

However, both Helgessson (159) working on a glass of composition MgO 21, Al_2O_3 26 and SiO_2 53 wt% with 8 wt% $AlPO_4$ added to the melt and Morrel (160) working on a stoichiometric composition (MgO 13.7, Al_2O_3 34.9 and SiO_2 51.4 wt%) could not produce fully sintered materials due to premature surface crystallization. Morrel used certain alkali additions to improve final density but this was at the expense of some material properties. Helgesson suggested that this crystallization was nucleated by surface impurities and defects and found that dense bodies could be obtained by giving the powder a prior chemical treatment in an alkali solution. This had the effect of removing $0.05 - 0.1\mu m$ from the glass surface. Attention was also drawn to the fact that addition of 2.4 wt% CaF_2 (a flux) rather than $AlPO_4$ depressed formation of the μ phase.

A similar observation was noted by Miller (161) when $0.5 - 2.5\%$ K_2O and/or Cs_2O was added to the stoichiometric composition to improve sintering. Differential thermal analysis (DTA) was conducted on a glass containing only K_2O and showed two peaks (corresponding to the formation

of α and μ cordierite) whilst the DTA trace of the glass with Cs_2O only had one peak at the same temperature as the α cordierite peak in the first trace. He concluded that Cs_2O suppresses the formation of μ cordierite with crystallization occurring only at the higher temperatures.

It is interesting to compare the observations of Helgesson and Morrel with those of Stong (162). He worked on near stoichiometric compositions with minor oxide additions and found that sintering was limited to the viscosity range 10^6- 10^8 poises with excessive distortions occurring below 10^6 poises. Although recognising the problems of premature crystallization his glasses were sintered (in a vacuum) by only having a dwell time of 10 minutes within the lower viscosity range. Samples were then allowed to cool. A fine grained crystal structure resulted when nucleation was initiated in the range 750 - 950°C and crystallization between 1200 - 1245°C.

Several authors have suggested using sintered cordierite powders for substrate applications. Both Mussler and Shafer (163) and Rusconi et al (164) devised a cordierite/mullite composite. Although the properties were favourable in terms of MLC applications, processing temperatures were in excess of 1000°C thus making it unsuitable for the lower melting metals. Both Kumar et al (19) and Narken and Tummala (18) suggested cordierite based glasses with P_2O_5 and B_2O_3 additives. After sintering μ cordierite formed on the old glass particle boundaries, the resulting skeletal framework helping to prevent deformation at the elevated processing temperatures. The α cordierite phase had completely developed in some compositions between 950 and 970°C. See also Thompson (165). Thus it is of interest to see how μ and α cordierite develop and

what role P_2O_5 and B_2O_3 play in the sintering and crystallization kinetics.

CHAPTER TWO - EXPERIMENTAL TECHNIQUES

2.1   GLASS PREPARATION

The compositions covered in this work are listed in Table 2.1, the impurities for each component being given in Appendix 2. To reduce volatilization losses, it has been shown to be preferable to introduce the phosphate anions in the form of a phosphate of a metal whose oxide forms a major constituent of the glass (166, 167), $AlPO_4$ being used in this case. B_2O_3 was added in the form of boric acid (H_3BO_3). 200g of powder of the required composition was thoroughly mixed and then melted at 1500-1510°C in a zirconia grain stabilised 95% Pt 5% Au crucible. Crucibles containing rhodium were avoided since there is evidence that MAS based melts leach out Rh which can then act as crystal nuclei on cooling (155). It should also be pointed out that it only requires 100ppm Pt in the melt to give noticeable changes in the crystallization kinetics (127).

After five hours melting a glass frit was produced by pouring into demineralized water and then drying. The frit was then mixed and the procedure repeated. This ensured good homogenity of the melt. Production of a fine powder was achieved by crushing the frit in a ball mill jar, using alumina and magnesium silicate grinding media, for up to 36 hours. An equal weight of methanol (compared with the glass powder) was usually added. After milling the slurry was dried, recrushed in a vibratory mill using agate media and then sieved to 180μm Care was taken to avoid, in particular, metal contamination and to standardize the preparation procedure for all samples since cordierites

TABLE 2.1   COMPOSITIONS STUDIED (IN WT%)

	C1	C2	C3	C4	C5	C6	C7	C8	C9	C10
MgO	22.0	24.0	22.45	22.25	22.0	22.7	22.0	22.0	23.5	25.0
Al_2O_3	22.0	21.0	22.45	22.25	22.0	22.7	22.0	22.0	20.5	19.0
SiO_2	53.0	52.5	51.0	53.5	53.0	54.6	52.9	52.0	53.0	53.0
B_2O_3	1.0	0.5	1.0	-	1.0	-	1.0	1.0	1.0	1.0
P_2O_5	2.0	1.0	-	2.0	-	-	2.0	2.0	2.0	2.0
Fe_2O_3	-	-	-	-	-	-	0.1	1.0	-	-
TiO_2	-	-	-	-	2.0	-	-	-	-	-
ZnO	-	1.0	-	-	-	-	-	-	-	-

have been shown to be sensitive to preparative conditions (155, 168, 169).

2.2 SAMPLE PREPARATION

In the production of MLC's it is necessary to bind the glass powder together in order to form the thin pliable sheets used in the manufacturing process. Although material characterization was not performed on samples in this form, a binding mix was added to keep the pellets together and to hopefully give more realistic results. At first, paraffin wax dissolved in CCL_4 was tried but this was found to give unsatisfactory results. A more suitable mix consisted of 1wt% polyvinyl acetate dissolved in 5wt% ethyl ether and 25wt% acetone, the remainder being glass powder. After the solvents had evaporated, any agglomerates were broken up by remilling in a vibratory mill. The powder was again sieved.

Samples took the form of pellets, powder being pressed in a stainless steel mould. Since frictional forces between the compact and die wall lead to stress and density gradients within the compact (170-172) stearic acid was used as a mould lubricant. Pellets weighing ~1g and 16mm in diameter were prepared for X-ray, density and SEM analysis whilst ~1.5 and 2.5g samples about 25mm in diameter were used in electrical measurements. Strength, Young's Modulus and thermal expansion were measured on uniaxially pressed cylinders approximately 25mm in length and 5mm in diameter. Cylinders were pressed to ~300 MPa and the other specimens to~150MPa.

2.3 FIRING PROCEDURE

Using thermogravimetric analysis it was found that most of the binder burnt off in the region of 340°C. Sintering was found to occur in the region 825-875°C and consequently the following heat treatment was adopted. A heating/cooling rate of 3-3.5°C/min with holds at 340°C for 1.5 hours, 875°C for 2 hours and the final firing temperature for 2.5 hours. These hold times were lengthy in order to obtain maximum binder burn out and complete sintering although in industrial applications these times may be much reduced. All samples used for material characterization were fired in the same furnace. Grinding and polishing of surfaces after firing removed any effects of surface contamination.

2.4   NOMENCLATURE

The nomenclature used for fired samples comprises the composition, e.g. C2 refers to composition number 2 (Table 2.1), and sometimes the final firing temperature, e.g. C2,1025 refers to material of the same composition fired to a final firing temperature of 1025°C. In the sintering analysis reference is also given to the mode and duration of milling, i.e. M36 refers to milling in methanol for 36 hours whilst A24 refers to a powder dry (air) milled for 24 hours.

2.5   X-RAY DIFFRACTION

X-ray diffraction has been used for many years to obtain information on the structure of both crystalline and amorphous solids. Central to the technique is the Bragg equation

$$2d Sin\Theta = n\lambda \qquad (2.1)$$

which defines the condition for reflection. λ is the wavelength of the

incident beam and $2d\sin\Theta$ the path difference between adjacent planes within the crystal, d being the spacing between each plane. n gives the order of the reflection. The detailed theory behind X-ray diffraction (XRD) and various associated techniques have been discussed by Klug and Alexander (173).

2.5.1 Determination of Lattice Parameters

The d spacing for a hexagonal lattice is given as

$$d = \frac{a_o}{\sqrt{\frac{4}{3}(h^2 + hk + k^2) + (1/c_o)^2}} \qquad (2.2)$$

where a_o and c_o define the dimensions of the unit cell and hkl are the Miller indices for a particular plane. Comparison of equations 2.1 and 2.2 gives, for two reflections

$$\sin^2\Theta_1 = \frac{\lambda^2}{4}\left[\frac{4}{3}\left[\frac{h_1^2 + h_1k_1 + k_1^2}{a_o^2}\right] + \frac{l_1}{c_o^2}\right] \qquad (2.3)$$

$$\sin^2\Theta_2 = \frac{\lambda^2}{4}\left[\frac{4}{3}\left[\frac{h_2^2 + h_2k_2 + k_2^2}{a_o^2}\right] + \frac{l_2}{c_o^2}\right] \qquad (2.4)$$

where Θ_x refers to the angle of reflection due to plane $h_xk_xl_x$. Combination of equations 2.3 and 2.4 gives the following expression for a_o and c_o.

$$a_o = \lambda\sqrt{\frac{l_1(h_2^2 + h_2k_2 + k_2^2) - l_2^2(h_1^2 + h_1k_1 + k_1^2)}{3(l_1^2\sin^2\Theta_2 - l_2^2\sin^2\Theta_1)}} \qquad (2.5)$$

$$c_o = \frac{\lambda a_o l_x}{2}\sqrt{\frac{3}{3a_o^2\sin^2\Theta_x - \lambda^2(h_x^2 + h_xk_x + k_x^2)}} \qquad (2.6)$$

where x = 1 or 2 but not both in the same expression. Thus a₀ and c₀

where x = 1 or 2 but not both in the same expression. Thus a° and c°
can be determined for any two reflections. A computer programme was
written which calculated the average lattice parameters for cordierite
specimens for all the hkl lines determined from the corresponding XRD
pattern.

2.5.2 Determination of Mean Crystallite Size.

It has been shown (174) that small crystallites, of mean size D, within
a polycrystalline material give rise to a broadening, β, of the
diffracted peak such that

$$D = \frac{Ks.\lambda}{\beta Cos\theta} \qquad (2.7)$$

where Ks (the Shape Factor) is a constant and θ is the angle of the
diffracted line in question. For this work D is assumed to refer to
spherical crystals. As there is always some degree of line broadening
observed due to the instrument itself, b, this has to be subtracted from
the experimentally observed breadth, B.
i.e.

$$\beta = B - b \qquad (2.8)$$

Equation 2.8 was suggested by Scherrer (174) although different forms
have also been suggested (175-177). The natural broadening of the
spectrometer was determined by measuring the peaks produced by coarse
polycrystalline silica and alumina samples between 10 and 60° 2θ, which
enabled a correction curve for β to be plotted. β measured in radians,
is the full width at half maximum height. At larger angles two
convoluted peaks were visible due to the Kα_1 and Kα_2 radiation from the

Cu source. Where this was the case, b was taken as the full width of the two peaks, again at half maximum height.

The value of Ks depends on a number of factors such as crystal shape, the definition of β adopted (integral width or half width etc) and the particular hkl values of the reflecting planes. Several authors (174, 178-180) have shown however that Ks = 0.9 is a reasonable value. Chapter 9 of Klug and Alexander (173) covers crystal size determination in more detail. They point out that due to uncertainty in the exact shape of crystals and in their size distribution the above analysis yields only approximate values, an expected uncertainty of 25-30% being quoted. Nevertheless, relative values of crystallite size may be informative.

2.5.3 Experimental Procedure

XRD patterns were obtained from a standard Philips diffractometer, alignment of the system being checked against a silicon polycrystalline standard. Cu radiation was used from a tube operating at 40KV and 30mA. A mean $K\alpha_1$, $K\alpha_2$ wavelength of 1.54178Å was used in all calculations. Either solid or powder samples were mounted in aluminium holders (since this yields only two characteristic lines at 38.5 and 44.75° 2θ) and were scanned at rates between 0.5 and 2°2θ/min. depending upon the required peak resolution. After calculation of all the d spacings the various crystal phases present were identified and checked against those in the J.C.P.D.S. files.

In an attempt to gain some estimation of the amount of the various phases present in a particular sample the intensities of the diffracted

X-rays for a particular phase were taken, to a first approximation, as being representative of the total percentage of phase present. A calibration graph of experimentally determined contents against known contents for mixes of 'pure' μ and α cordierite enabled the results for the two phases to be adjusted accordingly.

2.6   DIFFERENTIAL THERMAL ANALYSIS

Differential thermal analysis (DTA) has become a standard analytical method for determining the nature of phase transformations within a range of ceramic, mineralogical and chemical applications. It has been discussed by many authors and the review by Gregory and Veasy (153) is suggested for further reading. DTA relies on the fact that there is generally a flow of heat, either into or out of a sample when a structural transformation occurs in it. To locate the temperatures at which these effects occur an inert reference material is placed in close proximity to the sample. The two are connected by thermocouples wired in opposition such that in the steady state the net emf from the thermocouples is zero. During heating and cooling however, transformations may occur in the sample which may be endo or exothermic. These heat fluctuations are detected by the sample thermocouple and give rise to a net emf. A plot of emf versus sample temperature usually exhibits gaussian curves in the region of the transformation, the peak of which corresponds to the maximum rate of reaction. The exact location of the peak temperature, Tp, depends on two factors, heating rate and powder particle size.

a) Heating rate has two effects. As the samples are usually mounted in an alumina block there exists a definite temperature gradient

between furnace and sample and has the effect that peaks appear to occur at higher temperatures than they would under isothermal conditions. If the rate is increased the shift is increased. The second effect is on peak profiles. A slow heating rate enables temperature differences between sample and reference to equalize out via conduction through the sample holder and a more flattened peak results. Higher heating rates thus give sharper peaks.

b) The effect of particle size has been studied by Thacker and Thiagarajan (100) during a study on the crystallization of glasses. If a glass is crushed and then separated into coarse and fine fractions and a DTA experiment performed, the fine glass produces an exothermic crystallization peak at a lower temperature than the coarse one, due to a decrease in activation energy. If nucleating agents are incorporated into the glass to enhance bulk nucleation/crystallization and the experiment is repeated then the two peaks occur at the same temperature. Thus DTA provides a rapid evaluation of the nature of crystallization occurring in a glass system.

2.6.1 Use of DTA in Studying Reaction Kinetics.

Two methods have been proposed for obtaining an estimate of the activation energy, E. One was essentially based on the peak profiles (181, 182) and the other on the variation of peak temperature, Tp, with heating rate, β, (183, 184). The latter, known as the Kissinger method has generally proved the more reliable. For a first order reaction, the total rate of reaction, dx/dt (where x is the fraction transformed) can be expressed as

$$dx/dt = K_T(1-x) \qquad (2.9)$$

where K_T is the rate constant and assumed to obey an Arrhenius temperature dependence i.e.

$$K_T = A \exp(-E/RT) \qquad (2.10)$$

where R is the gas constant and A is a measure of the probability that an atom with energy E will participate in a reaction and is again assumed constant. The derivative of (2.9) with respect to time is zero when the reaction rate is maximum. Thus combining equation 2.9 and 2.10 and assuming dx/dt occurs at Tp (185, 186) it is seen that

$$-E = R \frac{d(\ln \beta /Tp^2)}{d(1/Tp)} \qquad (2.11)$$

Thus a series of DTA experiments at different heating rates enables the activation energy for crystallization to be calculated. The application of the Kissinger method has been discussed in more detail by Henderson. (187).

2.6.2 Experimental

The DTA apparatus used is represented in Fig.2.1. Approximately 125mg of sample and reference material were placed in two Pt crucibles, the bottoms of which had a small recess in order to achieve good thermal contact with the thermocouples. Quartz was used as the reference material since the $\alpha \rightarrow \beta$ transition helps establish the exo/endothermic directions and the transformation occurs at a known temperature (573°C), thus giving an indication of the thermal response of the apparatus. Two Pt/Pt-13%Rh thermocouples were used, one for the

SAMPLE

FURNACE

LINEAR
THERMOMETER

AMPLIFIER

TO CHART
RECORDER
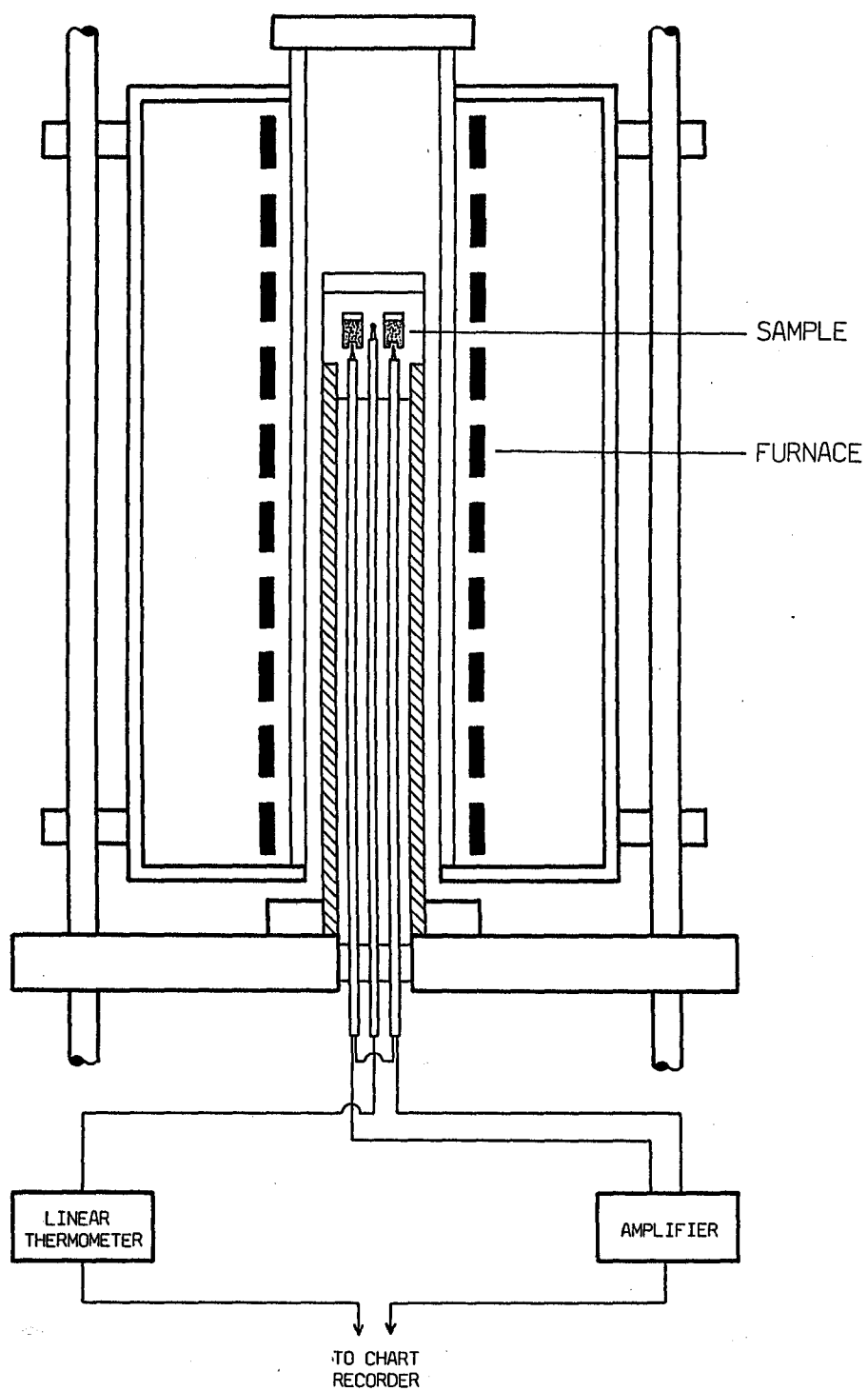
FIG.2.1   DTA apparatus

differential and the other to monitor sample temperature. A Stanton Redcroft controller allowed heating rates of 2-15°C/min. to be selected.

Problems were encountered with the DTA apparatus during later stages of the work, principally with noise at elevated temperatures and base line drift, the latter usually resulting in a loss in sensitivity. These problems only occurred during heating indicating an electrical rather than thermal cause. Improvements would probably occur if the sample holder held a screened Pt surround.

2.7   DIFFERENTIAL SCANNING CALORIMETRY

Due to the above mentioned problems differential scanning calorimetry (DSC) was also used to supplement DTA in the study of phase transformations. Like DTA, DSC is a comparative technique in that the output from a sample is balanced against that of some reference material. With DSC however, the measured magnitude is rate of change of heat, dH/dt rather than ΔT.

Thus, for a calibrated instrument, specific heat can be determined from which other thermodynamic properties can be calculated. The method of heat flow detection also lends itself to greater accuracy and sensitivity than that of DTA.

2.7.1 Application of DSC to Reaction Kinetics

Since the available range of heating rates was limited, determination of activation energy from peak profiles was found to be more applicable in this case. A general treatment has been done by Matusita and Sakka (188) using similar arguments to those outlined in section 2.6.1. The

relationship between volume fraction transformed, x, at temperature T was found to be

$$\log(-\ln(1-x)) = -n\log\beta - mE/2.3RT + \text{const} \qquad (2.12)$$

where β again equals dT/dt and n and m are numerical factors depending upon the mechanism of crystallization. The volume fraction of crystals can be obtained from the DSC curve by using $x = S/S_o$ where S and S_o are given in Fig.2.2

2.7.2 Experimental

Experiments were conducted on a Setaram High Temperature (1000°C) Calorimeter. Sensitivity was quoted as being 10μW (at constant temperature) although the large thermal mass of the system limited the range of heating rates to less than 1°C/min, 0.4°C/min being generally used in practice. About 1.2 g of sample and reference (quartz) were placed in Pt crucibles embedded in alumina powder inside 'identical' alumina holders, see Fig.2.3. These could then be introduced into the calorimeter whilst it was maintained at a lower holding temperature of 300°C.

2.8   SCANNING ELECTRON AND TRANSMISSION ELECTRON MICROSCOPY

Both SEM and TEM were used to study the effects of phase evolution on the morphology of cordierite glass ceramics. Due to the general macroscopic nature of the crystallization however, SEM was found to be a more useful technique for studying structural evolution with TEM only being used for analysing the initial stages of nucleation. A detailed account of both scanning and transmission microscopy is given in the
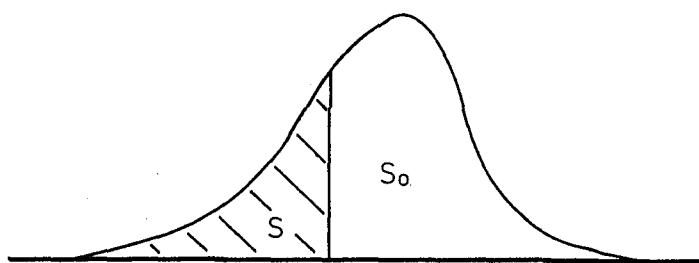
FIG.2.2 A typical DSC curve also showing S
          and So, the latter being the total
area under the curve

FIG.2.3 The DSC apparatus used
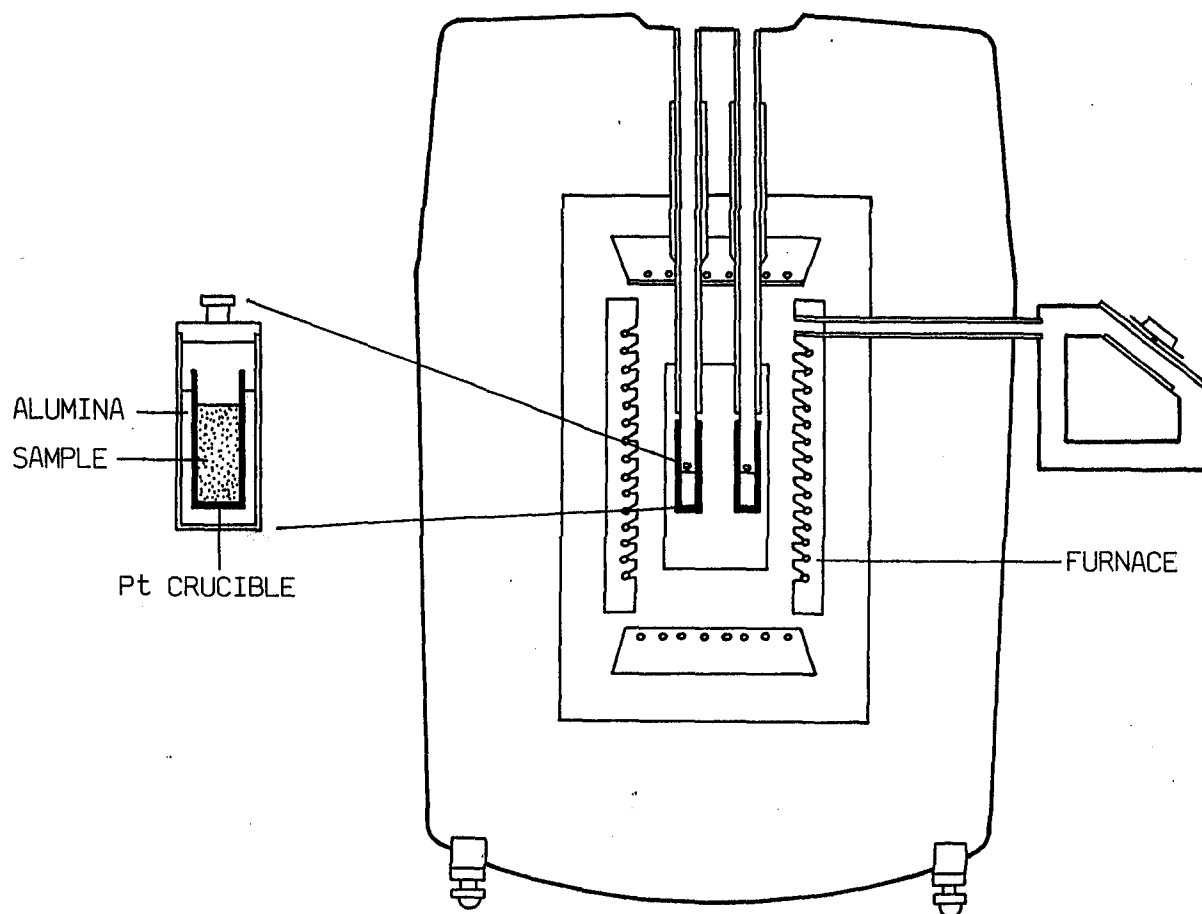
book by Bowen and Hall (189).

In conjunction with SEM, chemical analysis was made by means of Energy Dispersive Analysis of X-rays (EDAX) which allowed for a rapid check on both overall and more local variations in composition. To obtain quantitive results, the emitted X-ray intensity had to be corrected for i) Variations due to different atomic numbers (fluorescent yield, ionization cross-section (Z)) ii) Absorption within the bulk material (A) iii) Possibilities of secondary fluoresence (F). A Link 860 series computer coupled to the EDAX detector gave automatic ZAF corrections enabling oxide or elemental compositions to be determined either on an atomic or weight percent basis.

2.8.1 Experimental

For SEM, samples generally took the form of small flat surfaces which had been polished to $1\mu m$ diamond paste. Half the surface was then etched in a 5% HF soln. for periods of 10-30 seconds and then neutralised in a water ultrasonic bath.The rest of the polished surface was protected by a layer of Lacomit during etching. Although flat surfaces were required for EDAX analysis it was found that slight etching revealed far more topographical detail. Specimens were either carbon or gold coated prior to imaging to eliminate sample charging.

A Cambridge S250 MK.3 was used for the SEM work using an accelerating voltage of between 10-20KV and a LaB_6 source (to give enhanced resolution). EDAX analysis was of three different types i) large area, approximately $150\mu m$ square ii) spot, for small areas 400-200nm iii) line, for determining element variations across the specimen surface. Removal of the Be window on the EDAX detector head enabled lighter

elements (principally oxygen) to be analysed. Spectra were obtained over a period of 100s in order to obtain good statistics.

For transmission work, samples approximately 1-0.5mm thick were cut from bulk glass which had been appropriately heat treated. They were then polished to 1μm. Small brass rings were glued to the surface and the surrounding material cut away. Samples were finally thinned using an argon ion beam thinner, leaving electron transparent regions around the periphery of the hole, and carbon coated prior to imaging. This was done using a JEM-100C microscope with an accelerating voltage of 100KV.

2.9   INFRARED SPECTROSCOPY

This is a useful technique since the energy of most molecular vibrations corresponds to the infrared (IR) region of the electromagnetic spectrum. Furthermore, the vibrational frequencies of a functional group are characteristic of that functional group. Interaction occurs when the oscillating dipole moment, p, interacts with the oscillating electric vector of the IR beam. Such interactions only occur for specific vibrations i.e. where p at one extreme of the vibration is different to that at the other extreme (transverse antisymmetric optic modes). This is to be compared with Raman spectroscopy where spectra are independant of the presence of permanent molecular dipoles. For a linear diatomic chain (masses M and m) the classical angular frequency, ω, for the optical branch at zero wave vector is written as

$$\omega^2 = 2\alpha/\mu \qquad (2.13)$$

where α is the force constant and μ the reduced mass ($1/\mu = 1/M + 1/m$). Thus generally the stronger a bond and/or the lighter the atom

concerned, the higher the absorbed frequency.

In a crystalline solid, where bond lengths and angles are well defined, IR interaction gives rise to sharp absorption peaks. In liquids this is not the case and especially the rotational modes tend to get smeared out. Glasses have generated a great deal of interest due to the requirements of IR transmitting materials, particularly for communication purposes. The disordered nature of the glass structure (as compared to that for crystals) however, means that the interpretation of experimental results is more by inference and analogy as no rigorous theory can be applied. Greater detail on IR spectroscopy and its application to glasses may be obtained from the books by Wong and Angell (190) and Farmer (191) plus the paper by Simon (192). IR absorption in titania nucleated cordierites has been covered by Gregory and Veasey (153).

2.9.1 Experimental

IR studies concentrated mostly on bulk transmission spectra of pressed disks (193, 194). Samples were finely ground in acetone (195) and, after drying, added to crushed KBr roughly in the proportion 1:15. KBr was used since there is little absorbance until about ~230cm^{-1}. After mixing, thin transparent disks were pressed in a steel mould at ~500 MPa for five minutes. The KBr was stored at over 110°C and the disks used immediately due to the hydroscopic nature of the halide. Spectra were taken using a Perkin Elmer 983 spectrometer in the range 4000-230cm^{-1}. Double-beam scans were used in order to remove the absorptions due to atmospheric gases, spectra being stored and processed on a Perkin Elmer Data Station.

Reflection spectra (196, 197) were also taken using the technique of Multiple Attenuated Total Reflection. Here the IR beam is reflected from the surfaces of glass powder which is held in place on the opposite faces of a thallium prism. The method was mostly used to compare milled and unmilled glass powder but did not provide much useful information.

2.10 POWDER CHARACTERIZATION

Numerous methods exist for determining the average size and size distribution of a powder sample, the simplest (and most laborious) being those involving direct measurement. Three main methods are in use today. i) Sedimentation, whereby size is determined according to the settling velocities of particles in a fluid medium. Application of Stokes Law holds if the particles are spherical. ii) Electrical conductivity. Here the powder is suspended in an electrolyte and the suspension made to flow through a narrow orifice. Displacement of an equivalent volume of electrolyte by the particle causes the resistance measured across the orifice to drop. Thus once the system has been calibrated the mean size and size distribution can be measured. Dilution levels are kept low in order to ensure only one particle passes through the orifice at a time. iii) Optical Methods are perhaps the most widely used, either by obscuration (198) or by scattering, due to the speed and accuracy by which measurements can be made. Since a scattering technique was used here, this will be described in a little more detail.

If the size of powder is greater than $\lambda/10$ then light scattered from part of the surface will be out of phase from that of another giving

rise to interference and reduction in intensity. (For particles less than $\lambda/10$ then the scattered intensity is proportional to $1/\lambda^4$ and Rayleigh scattering holds (199)). Phase differences are small for small scattering angles and increase as the angle increases.
As the particle size increases the scattered light becomes more concentrated in the forward direction and is thus no longer symmetric with respect to solid angle as with Rayleigh scattering.

The theoretical analysis is due Mie (200). It is assumed that monochromatic light of cross sectional area A falls on a volume Ads containing N spherical particles of radius R. If Io is the incident intensity and I the scattered then

$$-I/Io = NAdsKc\,\pi R^2/A \qquad\qquad (2.14)$$

The minus indicates a reduction in intensity. Kc is the extinction factor and accounts for the fact that scattering occurs from a particle of section πR^2 as if its area was $Kc\,\pi R^2$.

2.10.1 Experimental

Initially a conductivity method was tried for powder characterization using a Coulter Counter. To obtain good resolution an orifice roughly comparable in size to that of the particles is required. It was found however that particles with a linear length greater than that of the orifice occurred which led to blocking unless this was made exceptionally large, which resulted in very poor resolution of finer particles.

Consequently a light scattering technique was used, the actual instrument being a Malvern 3600/D Particle Size Analyser, shown schmatically in Fig. 2.4. Before measurements were taken a background
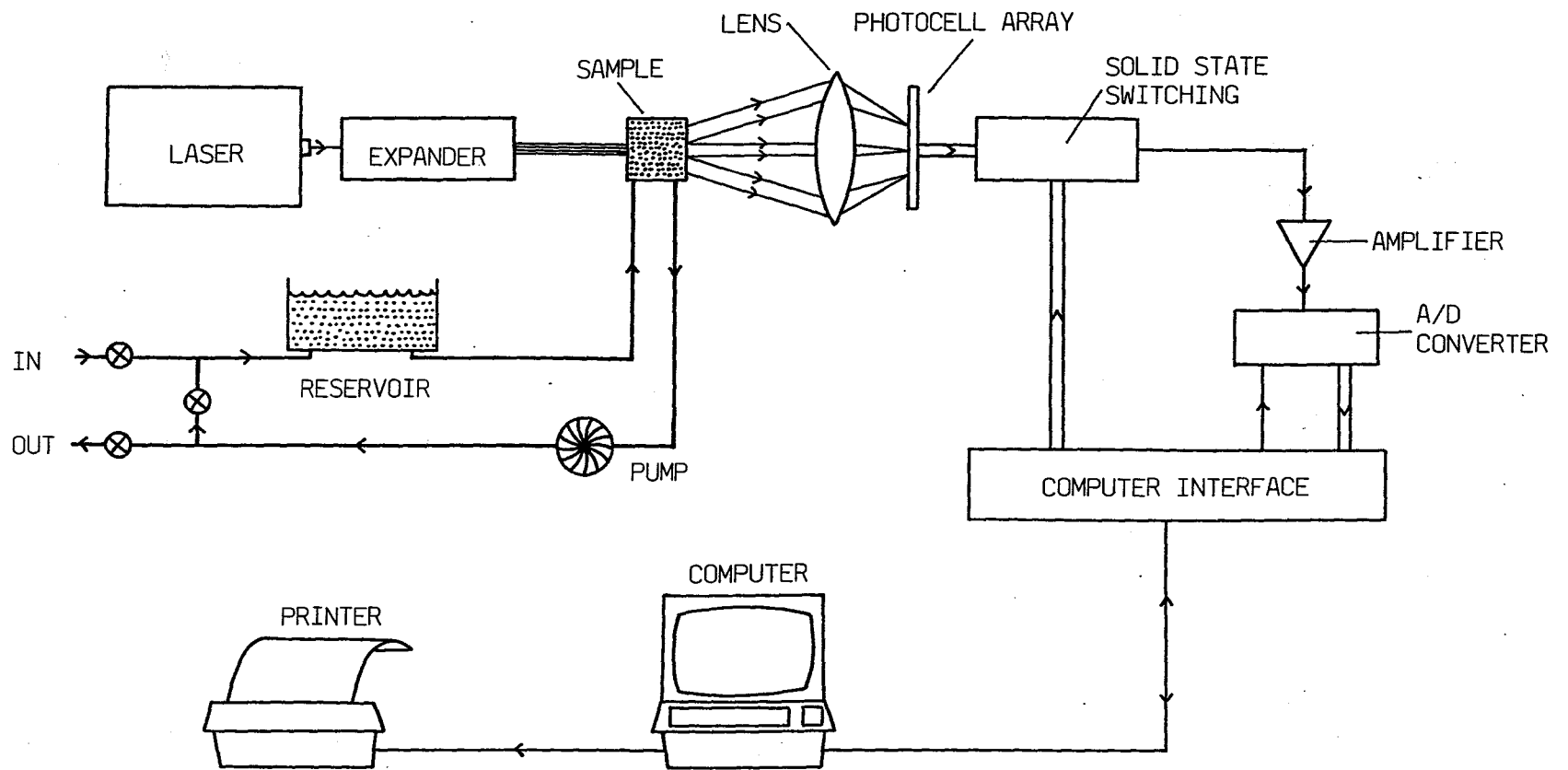
FIG.2.4 Schematic diagram of the 3600/D Particle Size Analyser

count was made in order to correct for impurities, dust, bubbles etc. Powder was then added to the reservoir until ~25% of the incident beam had been obscured. A wide angle lens was used to measure the large solid angle scattering caused by the fine powder. A computer scanned the output from the photo cells every 200μs for 20 seconds, iteratively fitted the results to a suitable model and printed the results out.

2.11 MAGIC ANGLE SPINNING NUCLEAR MAGNETIC RESONANCE

Although NMR is a relatively new technique (201,202) it has proved to be a useful tool in determining structure, particularly in the field of organic chemistry. It is based on the fact that nuclei with spin I can exist in 2I+1 different levels, the difference between them depending on the strength of the applied magnetic field, Ho. The orientation of the spin vector can be flipped from one state to another by absorption of a suitable quantum of energy, hv. It is found that if a magnetic field of a few Tesla is applied, the absorbed frequency corresponds to the radio frequency (RF) range, typically 10-100MHz. Structural information is gained because the local field, H, experienced by the nucleus will not correspond to the Ho since the nucleus will be screened by the electrons surrounding it. Thus the nucleus is sensitive to its chemical environment.

The sample, usually either a liquid or solid is placed within a strong magnetic field with RF coils at 90° to it, the signal being detected by a coil looped around the sample. Two methods of detection can be used i) In Continuous Wave NMR Ho is varied until the energy spacings are such to absorb the RF radiation, the resonance producing a signal in the detector coil. ii) For Fourier Transform NMR nuclei are excited by a single pulse of length tp. As they decay back to their equilibrium

state the decay of the magnetization takes the form of exponentially decaying sine waves (the Free Induction Decay) which can then be fourier transformed to give the normal NMR spectrum. For a more detailed account of NMR see the books by Slichter (203) or Abragham (204). The use of NMR in glasses has been dealt with by Bray and Silver(205).

For solids however the resonance profiles are generally not sharp due to several reasons. i) The magnetic fields of neighbouring nuclei give rise to dipolar broadening ii) Non cubic materials having crystallites of varying orientations to the magnetic field iii) Second order effects due to quadrupolar nuclei.

The problem of broadening has been reduced due to recent advances in hardware and techniques, giving rise to high resolution NMR (206-208), which includes the technique of Magic Angle Spinning (MAS) NMR (209,210). The technique relies upon the fact that for solids the dipolar term contains a factor $(3\mathrm{Cos}^2\Theta -1)$ where Θ is the angle to the magnetic field. Thus if the sample is tilted to 54° 44' (the 'magic angle') then $(3\mathrm{Cos}^2\Theta -1) = 0$ and the interaction vanishes. Furthermore, if the sample is rapidly spun then the time averaged value of Θ for all internuclear vectors is also 54° 44'. MAS NMR has recently been briefly reviewed by Klinowski and Thomas (211).

2.11.1 <u>Chemical Shifts</u>

The position, νs, of the sample resonance is measured relative to the position, νr, of a reference material which contains the same nuclei. The resonant frequency can be measured in Hz but is not universal since the exact frequency depends on the magnitude of the applied field.

Instead resonant positions are referred to by their chemical shift, δ defined as

$$\delta = (\nu_s - \nu_r) / \text{Operating frequency (MHz)} \quad (2.15)$$

Since $\nu_s - \nu_r$ is expressed in Hz, δ is given in parts per million (ppm).

2.11.2 Experimental

Spectra were taken of powdered samples on a either a Bruker WH-400 or MSL-360 spectrometer using spin rates of ~ 2.7 - 3.5 KHz (~150-200 Krpm). The resonances of both ^{27}Al and ^{29}Si were investigated. tp for both nuclei was of the order of a few μs but RD, the spin lattice relaxation time, (essentially the time between pulses) for ^{29}Si was long, of the order of several seconds. This required spectra to be collected over several hours to obtain good signal to noise. Because ^{27}Al has a quadrupolar nucleus it has additional relaxation mechanisms. This allowed for an RD of 0.5 seconds giving spectra with a good signal to noise ratio after only a few minutes. Due to limited machine time more aluminium spectra were obtained than silicon. Reference materials were tetramethylsilane for silicon and aluminium sulphate or aluminium hydroxide solution for aluminium.

2.12   VISCOSITY MEASUREMENTS

A knowledge of the dependence of viscosity with temperature is desirable when dealing with glass materials since the effectiveness of a particular heat treatment will be related to the viscosity at that temperature. This is particularly so when dealing with the sintering of glass powder since the sintering rate will be directly related to how

fast a glass particle boundary can deform. The theory behind glass viscosity has been well studied and is covered in many of the basic texts listed in section 1.3.1.

Viscosity measurements were made on 2-3mm thick disks using the Penetration Viscometer technique, outlined by Douglas et al (212). They found that viscosity, η , was related to the penetration depth, 1, of a sphere of radius r by the equation

$$\eta = \frac{9}{32} \quad \frac{Pt}{\sqrt{2R}} \quad \frac{1}{1^{3/2}} \qquad (2.16)$$

where P is the applied load. The experimental set up, shown in Fig .2.5, enabled viscosities in the region 10^{11} poises to be measured. The system was checked using a standard glass from the National Bureau of Standards.

2.13   THERMOGRAVIMETRIC ANALYSIS

Since a binder mix is used in the preparation of MLC's it is necessary to know at what temperature the various components are evolved so as to effect efficient burn-out during the heat treatment.

To this end thermogravimetric analysis (TGA) was performed by means of a Stanton Redcroft TG-750 thermobalance. A small amount of sample (~10mg) was placed on the pan of the sensitive electrobalance and the system itself was then balanced. A microfurnace was raised around the sample enabling rapid heating / cooling rates to be selected. Since the system was sealed, atmospheres other than air could be used (i.e. N_2). The output from the electrobalance was fed to a DTG unit which gave weight loss versus temperature as well as rate of weight loss versus

LOAD

L.V.D.T.

INDENTER
SAMPLE

FURNACE

THERMOCOUPLE
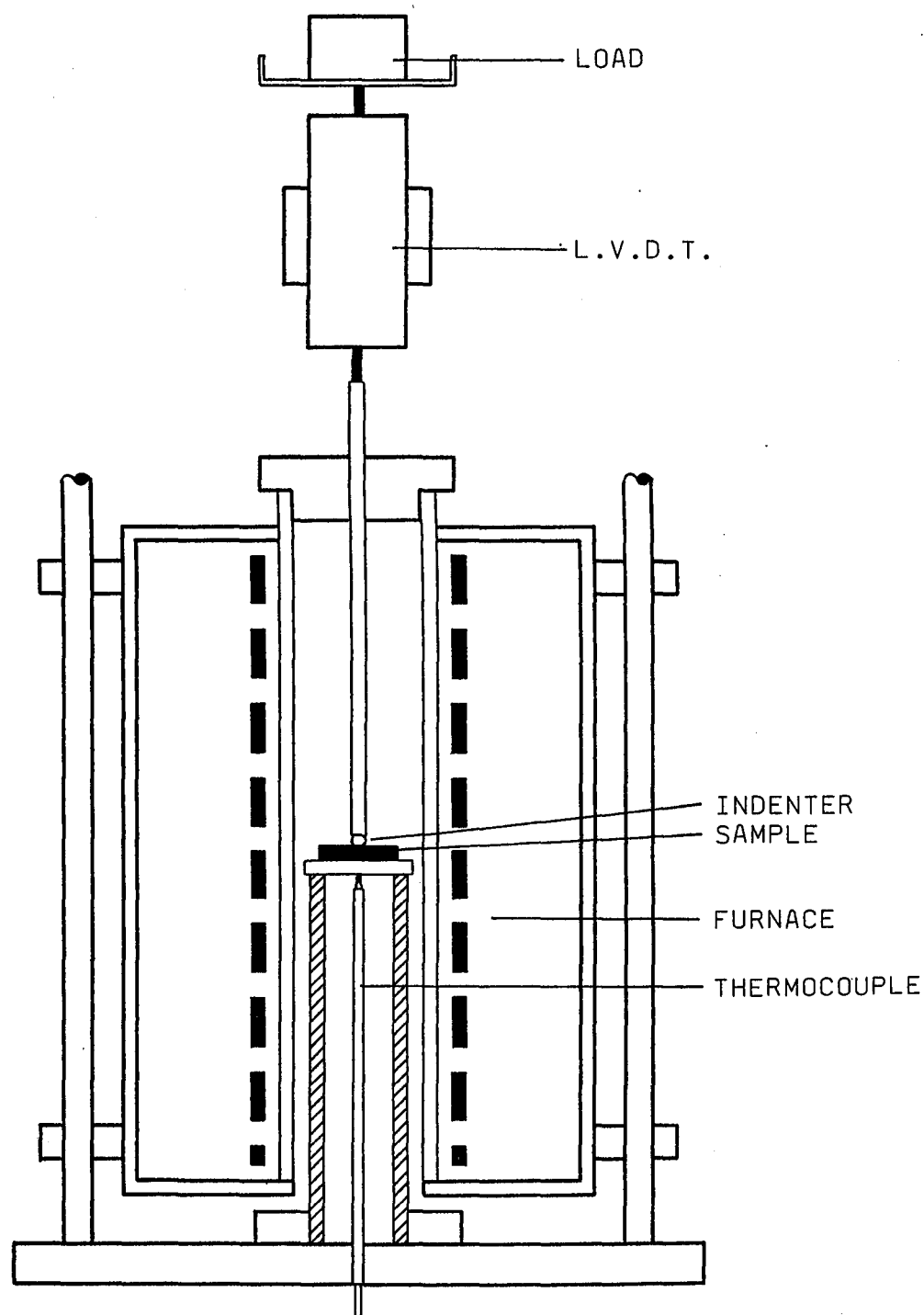
FIG.2.5 Penetration viscometer

temperature.

2.14   DENSITY MEASUREMENTS

The density, ρ, of both glass and fired specimens was determined by Archimedes' Principle, i.e.

$$\rho = \frac{W_A}{W_A - W_G} \cdot \rho a \qquad (2.17)$$

where W_A is the weight of sample in air and W_G the weight in the immersion fluid used (glycerol, $\rho a = 1.2575 \pm 2.5 \times 10^{-3}$ g/cc). Samples were suspended in the fluid using fine copper wire, measurements only being made after any air bubbles had been carefully removed.

2.15   THERMAL MEASUREMENTS

2.15.1 Thermal Expansion

Expansion coefficients (α) were measured in the range $\sim$20-200°C using a fused quartz dilatometer, Fig.2.6, with a sample heating rate of $\sim$ 2°C/min. The apparatus was calibrated using a Pt standard, extensions being monitored by a linear variable differential transducer (LVDT). α was calculated according to the equation

$$\alpha = \Delta L / L \Delta T \qquad (2.18)$$

where L was the original length and ΔL the change in length over the temperature range ΔT.

2.15.2 Thermal Conductivity

To obtain a measure of the thermal conductivity, K, of the cordierite glass ceramic, a determination was made for one sample using Lees Disks

L.V.D.T.

WATER   WATER

FURNACE
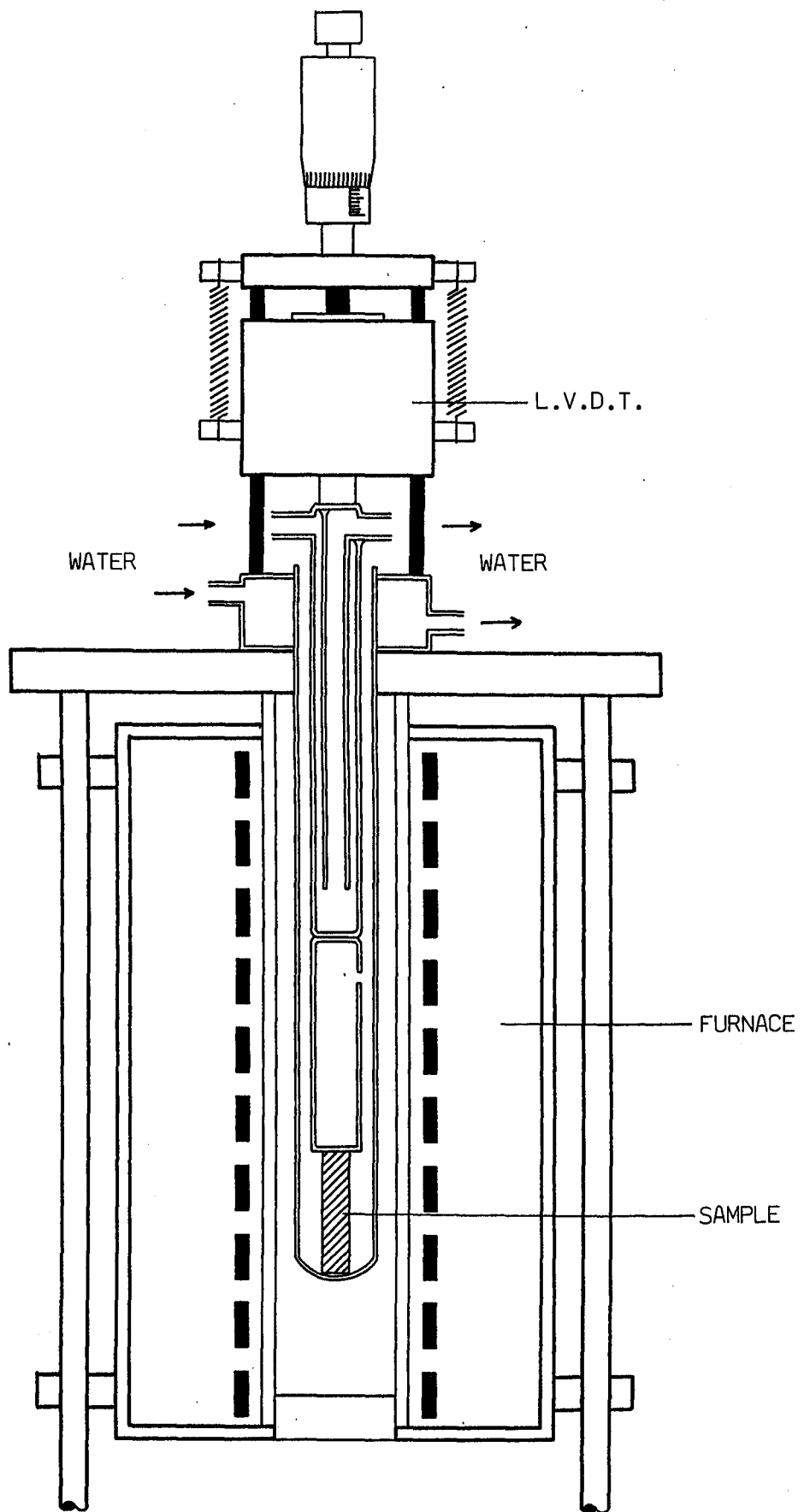
SAMPLE

FIG.2.6 Dilatometer

method (213). Steam was passed over the top surface of the specimen and the temperature gradient, $(\Theta_1-\Theta_2)/d$, through the sample measured by thermocouples, Fig 2.7. K was calculated according to the equation

$$K = \frac{4mS(d\Theta/dt)}{\pi D^2} \quad \frac{d}{(\Theta_1-\Theta_2)} \qquad (2.19)$$

where m is the mass of the lower brass block which has a specific heat S and a mean rate of heat loss $d\Theta/dt$. D is the diameter of the sample and t its thickness. A detailed account of the procedure may be found elsewhere (214).

2.16   MECHANICAL MEASUREMENTS

Both fracture strength, σ_f, and Young's modulus E, were measured on cylindrical specimens using a three point bend method in conjunction with an Instron Tensile Tester using a crosshead speed of 0.05 mm/min. σ_f of a bar of diameter D was determined using the formula

$$\sigma_f = PL/D^3\pi \qquad (2.20)$$

where P is the applied load at fracture and L the distance between the lower knife edge supports. E was calculated for the same specimens (radius R) by measuring the deflection, δ, as P increased, from which

$$E = PL^3/12\pi R\delta \qquad (2.21)$$

Both σ_f and E were measured on a number of samples (typically 5-10) so that an average value could be obtained.
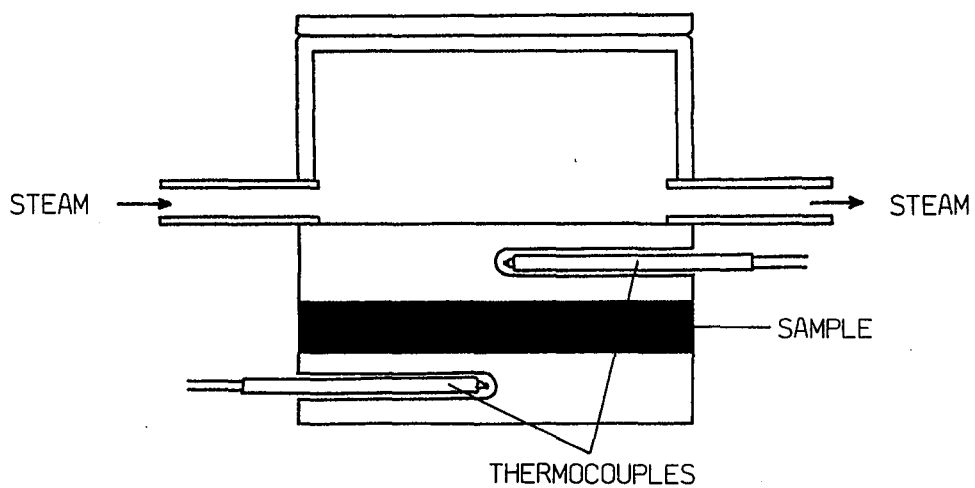
FIG.2.7   Thermocouple and sample arrangement
          for the measurement of thermal
conductivity
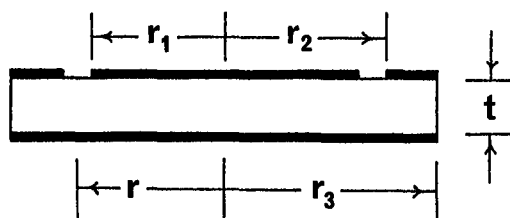
FIG.2.8   Electrode configuration used for
          electrical measurements

2.17 ELECTRICAL MEASUREMENTS

2.17.1 Dielectric Constant

When an insulator is placed within an electric field the electrons become polarised so that the large number of electric dipoles that result enhance the internal electric field. The dielectric constant, K, is then a ratio of the internal and external fields. Assuming a parallel plate configuration this is equivalent to

$$K = C_D/C_A \qquad (2.22)$$

where C_D is the capacitance of the dielectric and C_A the equivalent capacitance in air (assuming K for air is unity).

Gold electrodes were evaporated onto thin disk specimens, as was a guard ring. Care was taken in preparing the specimen surfaces prior to evaporation. First a paste consisting of glass powder of the same composition as the specimen and distilled H_2O was used to clean the surfaces which were then ultra sonically rinsed in more distilled H_2O.

After drying overnight at 100°C the specimens were allowed to cool in a desiccator. The radius r, and hence the effective area of the electrode was calculated according to the formula (215)

$$r = \frac{(r_1 + r_2)}{2} - \frac{2t}{\pi} \ln(\cosh(\pi \frac{(r_1 - r_2)}{4t})) \qquad (2.23)$$

where the different radii are shown in Fig.2.8. For good results it is required that $r_1 > 2t$ and $(r_3 - r_1) > 2t$. Using the equation 2.23 it was found that this gave a correction of $\sim 6\%$ compared to just using r_1. (See also Amery and Hamberger (216) and Field (217)).

Measurements were made using two Wayne Kerr Universal R.F. Bridges, one tuned to 1MHz and the other to just over 1KHz. The samples were contained in a specially constructed jig which supplied an earth to the guard ring and prevented interference from external fields. The system was tested using an alumina standard (K = 9.38) and this was measured to within 1%.

2.17.2 Loss Tangent

When an alternating field is applied to an insulator the time required for polarization shows up as a phase retardation of the charging current and is dependent upon the applied frequency. This is represented by the loss tangent (or Power Factor) $\mathrm{Tan}\delta$, where δ is the phase difference or loss angle. It is an important parameter since the product $\mathrm{KTan}\delta$ is equal to the dielectric energy loss, which usually appears as heat. The loss mechanisms within a glass have been outlined by Stevels (218), the most important of which are ion migration losses.

Measurements were made over the range 1KHz to 10MHz at 1V peak to peak on a Hewlett Packard 4192A Impedence Analyzer linked to a HP 9826 computer. At each measured frequency five readings were made and an average taken. As the equipment was a recent purchase no suitable sample holder had been made which lead to problems at the highest frequencies due to the effect of the probes and lack of screening.

2.17.3 Resistivity

The low ionic conductivity of cordierite ceramics requires special techniques in measuring the resistivity, ρ, of these materials. A

special amplifier was used which selected a peak to peak output square wave voltage (10V-10mV) and measured current for a given resistance scale. A 10Hz output from a single generator changed the polarity of the input voltage about once every six seconds. This allowed time for relaxation to occur within the sample whilst eliminating polarization effects. Measurements were made on a three electrode system for samples over the range 100-400°C on both heating and cooling, although results during cooling showed consideraly less scatter, presumedly due to a more homogeneous temperature distribution around the sample. Results were extrapolated·back to 80°C, a typical upper operating temperature for a VSLI chip. The system was tested using a Pilkington Float Glass specimen of known resistivity. Resistivity was calculated according to the equation 1.1.

CHAPTER THREE - POWDER PROCESSING

Many differing technologies have to be combined to produce functional
MLC'S, with the success of the entire manufacturing operation depending
on the success of each stage in the process. Thus it is important to be
fully aware of what is happening at each stage and to make suitable
adjustments where necessary eg. if a particular operation produces an
unacceptable level of residual contamination another processing step may
be needed to remove it. Since a MLC is essentially a dense ceramic
block or, as in this case, a glass ceramic block, an important factor is
the nature of the initial glass powder (shape, average size etc) and how
this influences the densification of the article at high temperatures.
This is one of the most critical stages since incomplete sintering will
yield a weak, porous product, inhomogeneous shrinkage will give rise to
distortions and, at these elevated temperatures, interdiffusion between
the metallization and surrounding dielectric is at a maximum.

3.1. POWDER PRODUCTION

3.1.1. Ball Mill Contamination

Although many comminution techniques exist, ball milling is the most
widely used for producing powders because of its relative simplicity and
low cost. Moreover, the powders so produced are fairly active, either
as a result of some surface modification or by the introduction of
strain energy into each particle. In the milling operation the coarse
powder (the "charge") is placed in a special jar which can have a
variety of inner linings (eg rubber, porcelain or alumina) and suitably

hard balls (the "grinding media") are added. These can be of hardened steel or magnesium silicate but are more usually made of alumina. The jar is then sealed and rotated on rollers until the powder is of the required size. Rotational speed is quite critical since a low speed leads to inefficient grinding and wear of the lining whilst too high a speed is also inefficient since media is pinned to the lining by centrifugal forces. Milling is dealt with in greater detail in the reviews by Mular (219), Somasundaron (220), Ryshkewitch (221) and the American Society For Metals (222).

The greatest problem with this technique is that contamination of the powder can occur by both the lining, and particularly the media, due to general abrasion and impaction with high energy fragments. This was noted by Francis et al (223) investigating 'white spots' in sintered 99%+ translucent alumina. These were caused by Si diffusing out of fragments originating from the 85.4% alumina media. Increasing the purity of the grinding media to 97.5% alumina noticeably decreased the effect and at 99.7% it had disappeared.

The effect of contamination in the milling of glass powder is important since it adds seed crystals which can alter the crystallization kinetics. That contamination occurs in the present system is evident from Fig. 3.1 which shows an alumina particle embedded within the glass ceramic. Not only does it effect crystal growth but it can also introduce strains and cracks into a material due to thermal expansion mismatch. Although contamination can be minimised by sieving out larger fragments, it is important to know both the quantity and nature of the impurity.
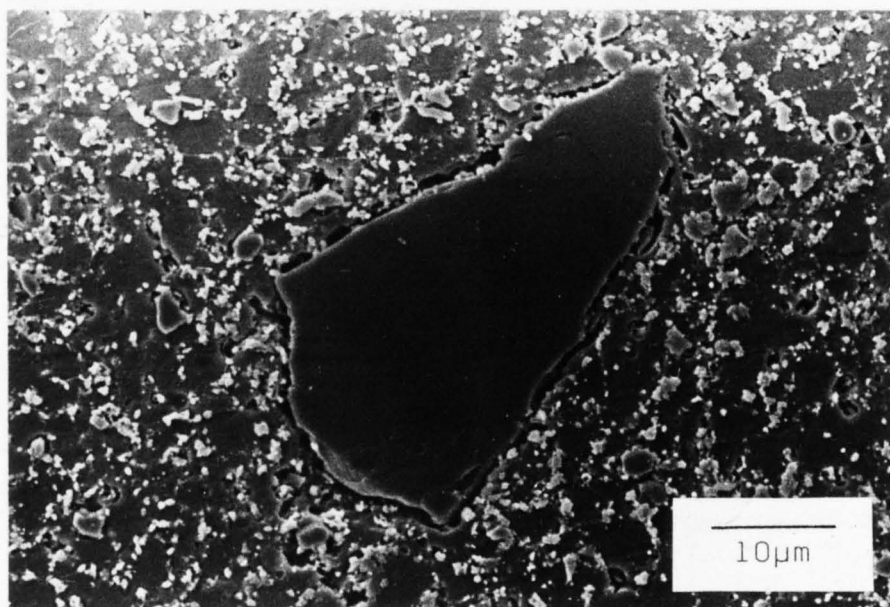
FIG.3.1 Fragment of alumina grinding media embedded
         within the glass ceramic

MAS NMR was used here to select, identify and quantify contamination by means of ^{27}Al and ^{29}Si resonances. The former is particulary suitable since its 100% natural abundance enables good spectra to be obtained quickly and since, under favourable conditions, its chemical shift can be resolved down to ~10 ppm, identification of different sources of Al can be made.

Usually ball milling of glass powder was performed with three sets of differently sized balls, the total mix being ~60% alumina, 40% magnesium silicate. This was so as to confine any impurities to elements already present within the system. For the contamination experiments however,alumina powder was milled with the magnesium silicate media (identified by XRD as being protoenstatite) and quartz powder with the alumina media. Milling was carried out for 48 hours using an equal weight of methanol to powder. For comparison, larger pieces of glass were hand crushed in an agate mortar and pestle.

The spectra for milled and crushed glass samples are shown in Fig.3.2. Comparison of the two for ^{27}Al clearly shows that contamination of the glass has occurred since the spectrum for the milled glass exhibits two peaks whereas there is only one for the crushed glass. Dupree at al (224) working on the MAS NMR resonances for various aluminas quote a value of ~13 ppm for α alumina although Muller et al (225) quote a value of 5ppm. Thus it is concluded that the peak occuring at δ = 12.1 ppm is due to octahedrally co-ordinated aluminium from the alumina balls and/or lining and is present at about 8%. Moreover, the narrow width of the line ($\Delta \delta \frac{1}{2}$ = ~12 ppm) suggests this is due to a crystalline phase
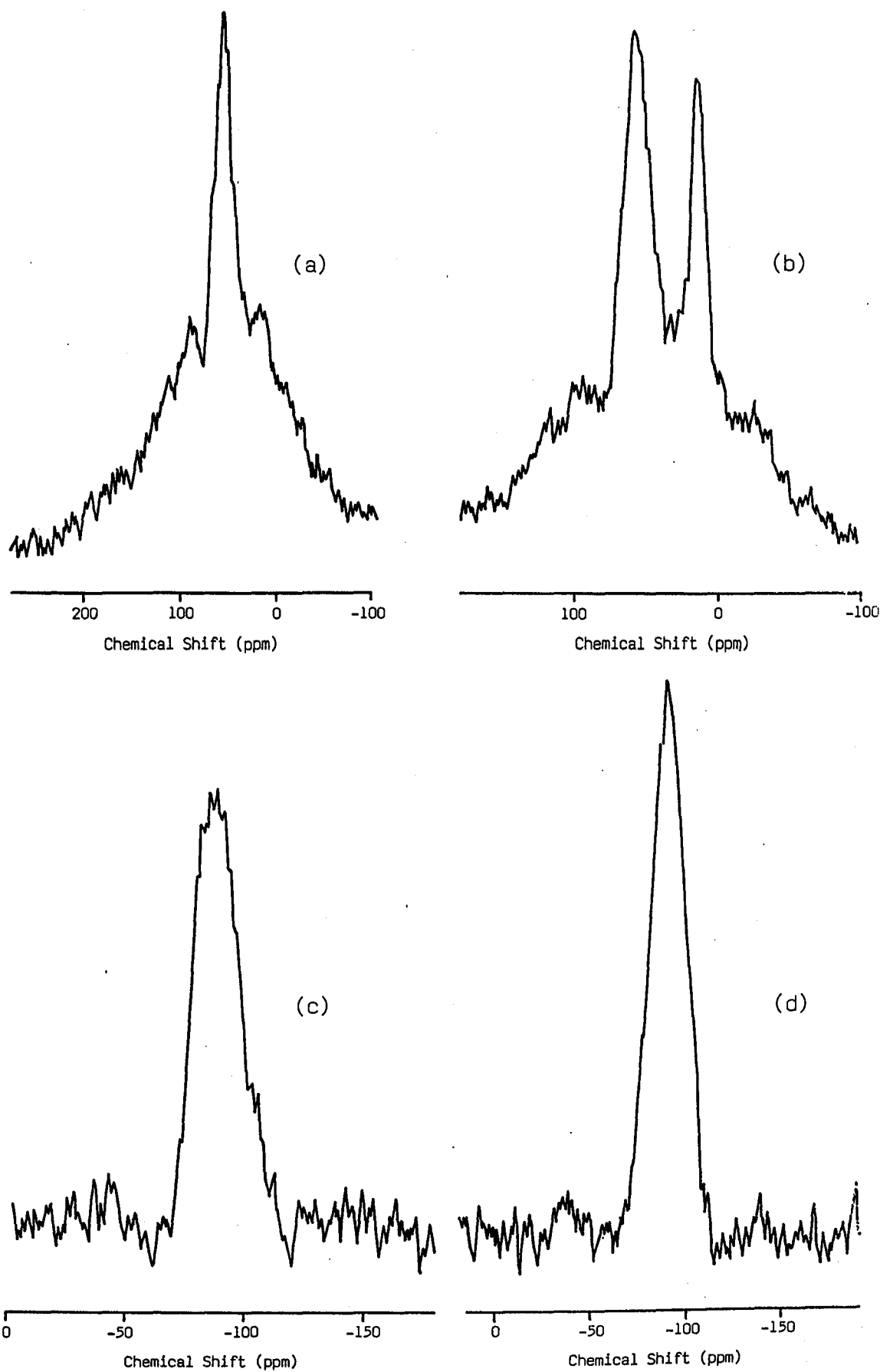
FIG.3.2   MAS NMR spectra for Cl glass (a) ^{27}Al resonance, crushed
sample (b) ^{27}Al resonance, milled sample (c) ^{29}Si resonance,
milled sample and (d) ^{29}Si resonance, crushed sample

whereas the line at δ = 54 ppm is broad ($\Delta\delta\frac{1}{2}$ = 20 ppm), as one would expect for a glass where there exists a wide range of Al environments ($\Delta\delta\frac{1}{2}$ refers to the full width at half maximum height). The small 'bumps' on either side of the peaks are called spinning side bands and occur at multiples of the spinning frequency. They are due to periodic modulations of the chemical shift by sample spinning and can be considered as being a mechanical echo in the time domain (226 - 228). They become less well resolved with higher spin rates or lower magnetic field strengths.

The possible amount of contamination was deduced for Al by comparing the MAS NMR signal strength from the milled quartz sample to that of an equal weight of pure α alumina since signal strength is directly proportional to the total number of Al atoms with in the sample (assuming that all the Al's are seen by the spectrometer). The spin rate was kept the same for both samples ($\sim$2.97 kHz). After a good spectrum had been obtained (ie. reasonable signal to noise ratio) the peak areas were integrated electronically on the MSL 360 and then corrections were made for the total number of pulses and sample weight. For alumina the ratio of the peak areas gave on Al contamination of quartz of 1.62 ± 0.05%. Richerdson (229) quotes a contamination rate of $\sim$0.1% per hour for Al_2O_3 by SiO_2 or porcelain media which, although being of the same order of magnitude, is about a factor of three greater than observed here. An interesting feature of Fig.3.2.b is the lack of crystalline peaks in the region δ = 50-80 ppm which is the resonance region for AlO_4 units (208). If the jar lining had contained mullite ($3Al_2O_3.2SiO_2$) and appreciable wear had occurred then peaks would have been apparent in this region since mullite contains aluminium in both

octahedral and tetrahedral coordination (230). As it happens the jar
lining was of aluminous porcelain.

The ^{29}Si MAS NMR spectra for the milled and crushed glass powder are
shown in Fig.3.2. c and d. Smith et al (231) have examined enstatite
and found that for ^{29}Si two peaks occured at $\delta = $ -81 and -83 ppm. In
this work examination of a crushed protoenstatite ball gave one shift at
~-85 ppm. As no evidence for peaks in this region above the background
noise could be found for the milled glass it was assumed that the wear
due to the magnesium silicate charge is much reduced. Indeed,
electronic subtraction of the two spectra gave, allowing for noise, a
straight line. However, it should be noted that a similar experiment to
that conducted above gave a contamination of 3.2 ± 0.6% for Si in Al_2O_3
powder from the $MgSiO_3$ media. The larger error was due to the increased
difficulty of processing spectra with a poor signal to noise ratio.
Finally, wear of the lining would appear to be less noticeable due to
the absence of quartz peaks in the region $\delta = $ -107 ppm (232).

3.1.2. Comminution

The difference between milling a powder in 'air' and in a liquid medium
as a function of time is shown in Fig.3.3 , which gives the resultant
average size and, Fig.3.4, the 90 and 80% cumulative weightings. (Here
average size corresponds to that point in the distribution where 50%
cumulative weight appears). The advantages of liquid milling can be
clearly seen in that size is reduced substantially faster than for dry
milling althought there is little reduction in average size or
cumulative weighting after about 24 hours. Greskovich (233) quotes a
lower limit of ~1-0.1 μm for ball milling under optimum conditions e.g.
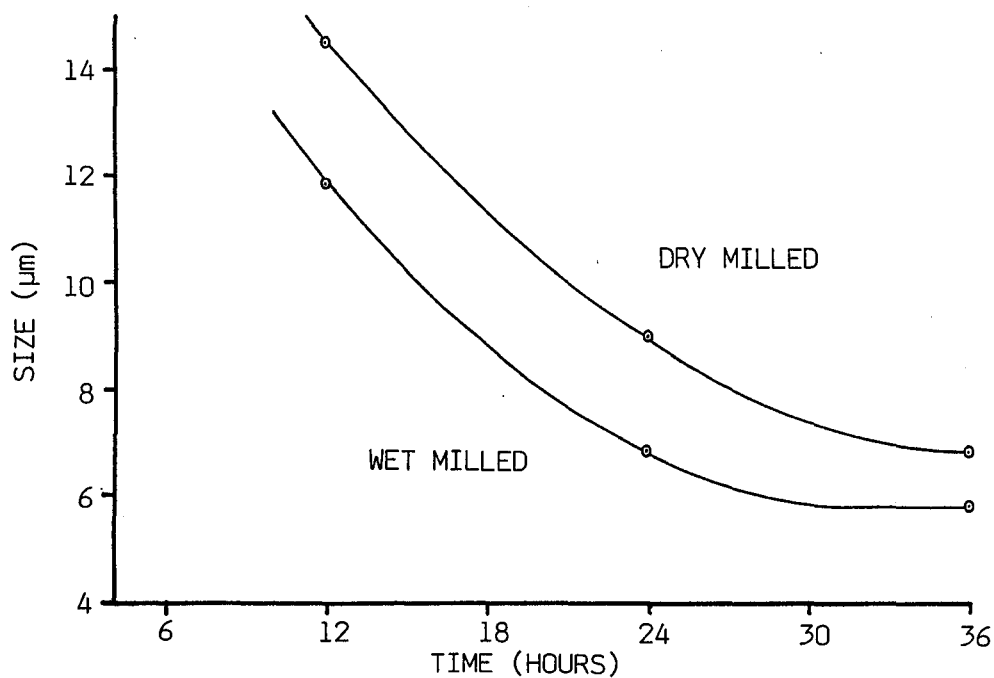
FIG.3.3 Size reduction as a function of time for dry
         and wet milled glass powders
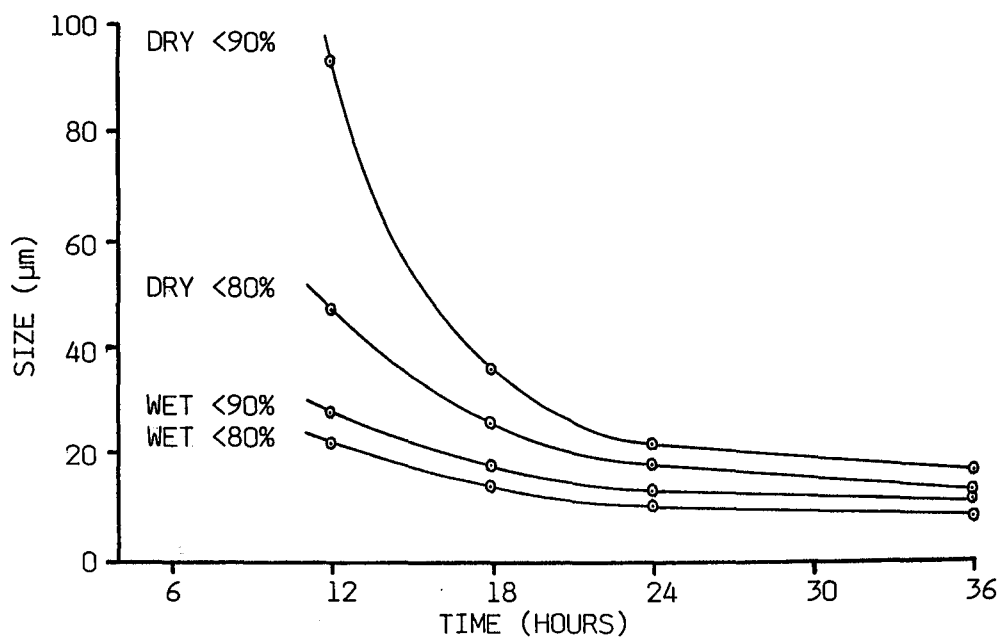
FIG.3.4 Cumulative weight percents versus milling time
         for dry and wet milled powders
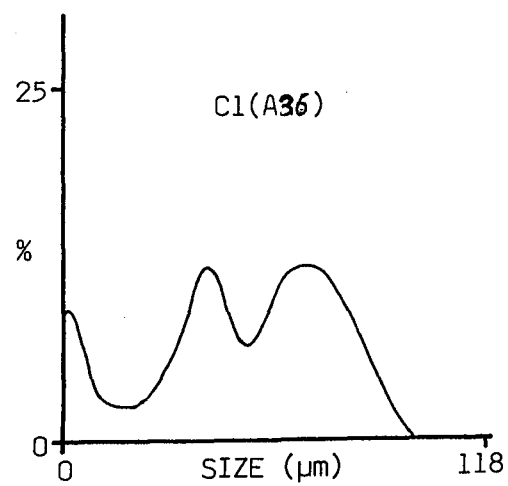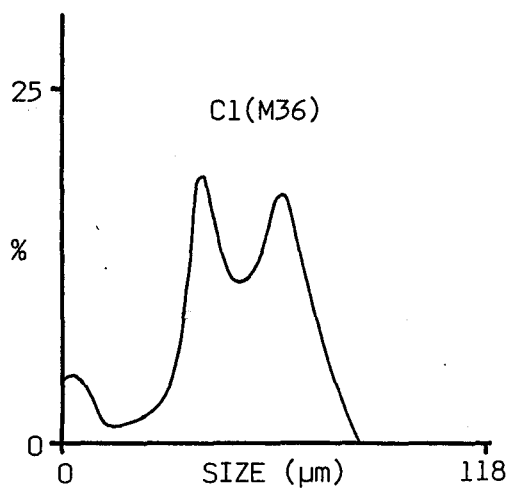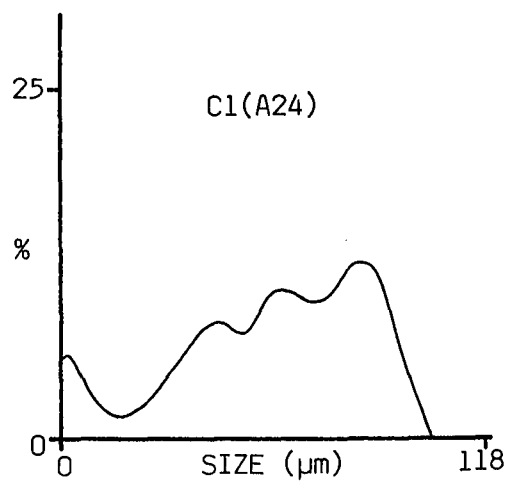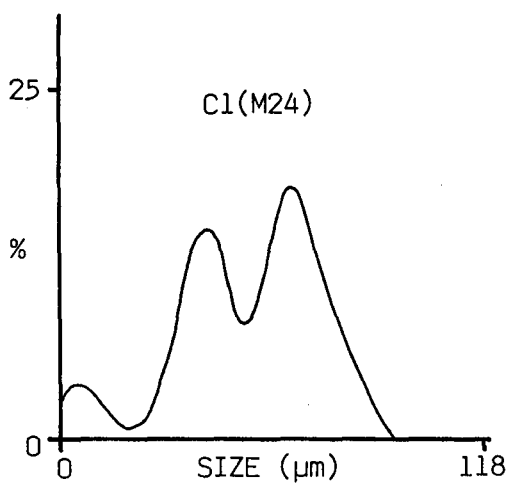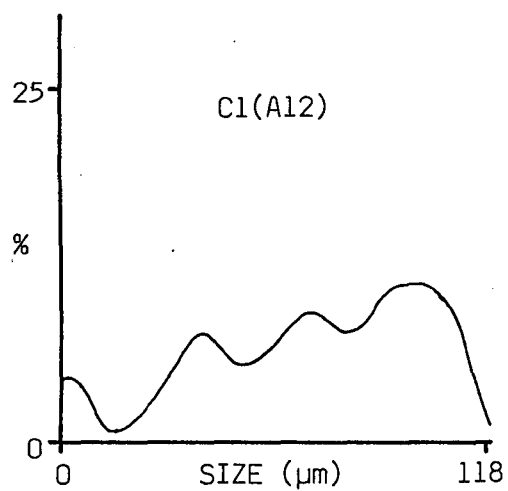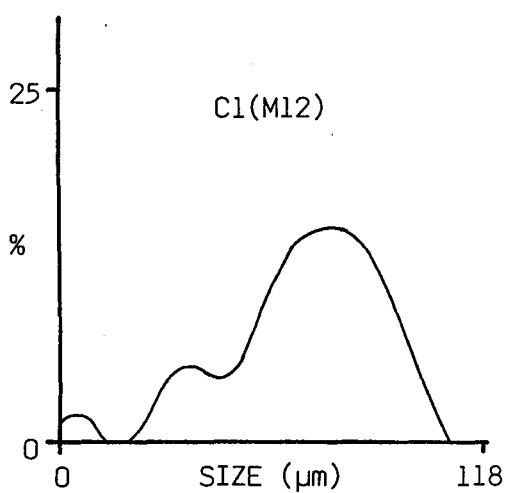
FIG.3.5 Size distributions for various glass powders
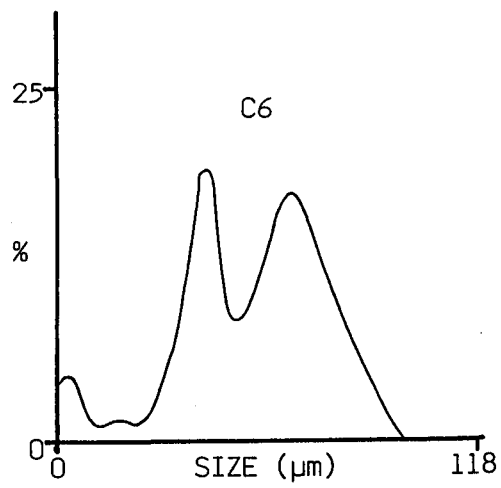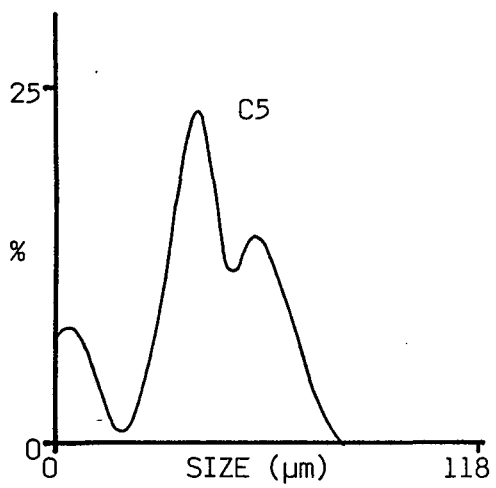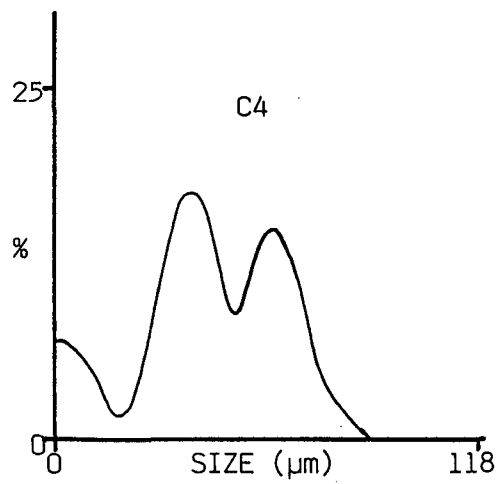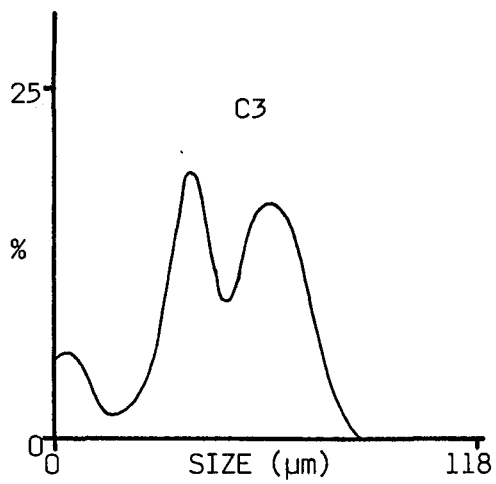
FIG.3.5 Continued

the addition of grinding aids (234). There are several reasons:-

I) Size reduction occurs either by tensile fracture through the focussing of shock waves within the particle or direct crack propagation. The strength of a glass particle is given by the Griffith equation (235) .

$$\sigma = (2E\nu/ \pi c)^{\frac{1}{2}} \qquad (3.1)$$

where ν is the fracture surface energy and c the critical flaw size. If one assumes that during fracture no new flaws appear, then as grinding progresses there is a gradual reduction in the number of critical flaws for a given stress and it becomes harder to break up smaller particles

II) Larger particles protect smaller ones and, as the number of particles increases, there is a general cushioning effect and the probability of a particle being involved in a comminution event is also reduced.

III) As the size decreases the volumetric capacity to store elastic stress energy is reduced.

IV) A balance is reached between rate of grinding and rate of agglomeration.

The size distributions of the various milled powders covered in this work are given in Fig.3.5 which gives the cumulative weighting against particle size. Again the advantage of milling in a liquid medium can be observed as it yields a narrower, more symmetric size distribution for a given time when compared to air milling. An interesting feature of these distributions is that they consist typically of three peaks, one

of which corresponds to very small sizes. The cause of this is unclear but is probably related to the different sized grinding media used. This could be easily verified experimentally.

The disadvantage of dry milling was readily apparent. As the glass frit reduced in size it started to pack around the jar walls, being held in place by the compressive action of the grinding media. This is clearly inefficient and may be reduced to some extent by the addition of a few wt% stearic or oleic acid. Dry milling does limit the number of agglomerates formed however. This can be a problem when wet milling, particularly when using water. For instance, alumina and water can form an aluminium monohydrate which acts as a cement between particles when the remainder of the water evaporates off (236). Reed et al (237) also noted that agglomerates formed by milling in water were noticeably stronger than those milled in propanol and Kiesskalt (238) reported a 12 fold increase in surface area was possible when a organic liquid was used as a milling medium rather than water. Consequently for this work methanol was used exclusively. After the resultant slurry had been dried any agglomerates were broken up using an agate vibratory mill where the 'ball to ball' contacts are greatly increased.

3.2 SINTERING THEORY

3.2.1. General

Sintering is an important step during the heat treatment of powders since it imparts strength to the article and leads to the removal of pores. The latter is desirable since residual porosity can have adverse effects on many bulk material propert.... Since sintering requires

relatively high temperatures, steps may need to be taken to improve sintering rates at such that a high final density is achievable as low a temperature as possible. This is particularly so for MLC applications where, for example copper forms a major constituent, since there is always increased risk of oxidation at elevated temperatures.

The theoretical basis for sintering of glass particles was proposed by Frenkel (239) who derived an expression for the expected decrease in size versus time for a compact of glass spheres. He assumed that densification would occur by viscous flow and that free energy would be reduced by decreasing the total surface area by the elimination of solid/vapour interfaces. The assumption that viscous flow is the predominant mechanism was later proved to be correct by the work of Kuczynski (240) and Kingery and Berg (241) and also shown to be valid for the closing of glass capillaries (242). During the initial stages of sintering, necks form between individual particles, the relationship between the contact area and time being given by (239)

$$\frac{x^2}{R^2} = \frac{3\nu t}{2\eta r} \qquad (3.2)$$

where ν is the surface energy and η the viscosity. R,r and x are shown in Fig.3.6.

During the initial stage little decrease in size occurs. Densification starts however when the pores, which at first exhibit a high degree of connectivity, become more isolated and start to close up. The approach between particle centres, and thus the overall densification during this stage is given as
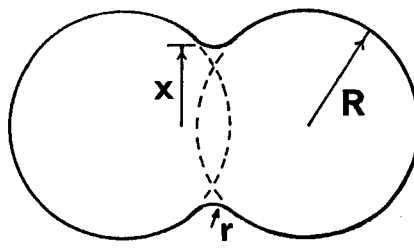
FIG.3.6 Two coalescing glass spheres
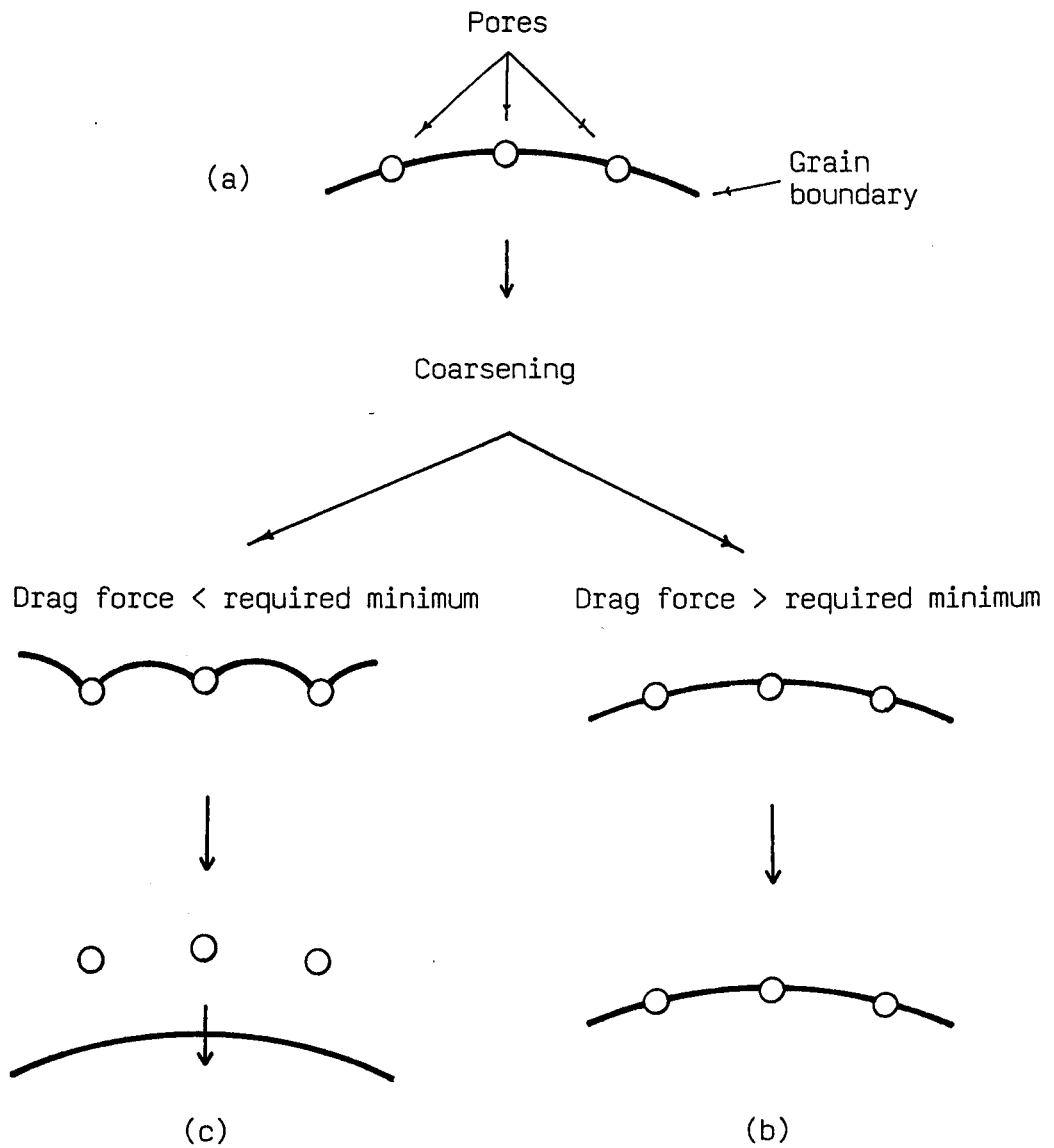
FIG.3.7 Possible movement of pores during coarsening

$$\frac{\Delta L}{L} = \frac{\nu t}{2R\eta} \qquad (3.3)$$

where L is the initial length and ΔL the change in length after time t. (Equation 3.3 is the correct version given by Eshelby (243) after a small numerical error in Frenkels original paper). After a certain length of time however the simple Frenkel model deviates from experimental results principally because it takes no account of the effects of closed pores. That this becomes important is readily seen when one considers that a pore 1µm in diameter, having $\nu = 1N/m^2$, can exert a pressure of ~41 MPa (about 40 atmospheres).

The sintering of a material containing closed, spherical pores has been investigated by Mackenzie and Shuttleworth (244). Assuming the number of pores, n, remains constant then the rate of change of relative density, ρ', is

$$\frac{d\rho'}{dt} = \frac{3}{2} \left[\frac{4\pi}{3}\right]^{\frac{1}{3}} \frac{n^{\frac{1}{3}}}{\eta} (1-\rho')^{\frac{2}{3}} \rho'^{\frac{1}{3}} \qquad (3.4)$$

The number of pores can be estimated from pore size and relative density (245) which simplifies equation 3.4 to

$$\frac{d\rho'}{dt} = \frac{3\nu}{2R\eta} (1-\rho') \qquad (3.5)$$

R being the initial radius of the particles.

In an attempt to improve upon the basic theory presented by Frenkel, Scherer (246) suggested, for low density glasses, a model for the sintering of spheres with open porosity by considering the contraction

of a cubic array of intersecting cylinders. These were of uniform length and radius and represented the strings of oxide particles within the material, the cylinder radius representing the average particle radius. When they had contracted to the extent that neighbours touched each other then closed porosity was assumed and the Mackenzie - Shuttleworth analysis became valid. The model fitted well to the experimental curve for fine soot particles (247) and was developed to take into account the effect of pore size distributions (248).

3.2.2. Powder Characteristics

It is very rare that the powder morphology corresponds to the idealized case assumed in the various models. Indeed, Exner et al (249) noted deviations even for loosely stacked spherical particles of uniform size. Thus it is of interest to see how the physical nature of real powders alters the expected sintering kinetics.

Sintering is greatly aided by pressing powders to high density before firing. Some powders, mostly metals, can actually be sintered at room temperature by the application of pressure somewhat greater than the yield stress (250,251). Pores are filled by plastic flow of the material due to the high shear stresses present during compaction. With most glasses and ceramics however, too high an applied pressure gives rise to brittle fracture rather than plastic deformation. The influence of green density upon sintering has been studied by Occhionero and Halloran (252) using alumina powder. He found the specimens which started with the highest initial density had a final pore size distribution which was quite narrow and centred on small sizes. For low starting densities the opposite was true. Moreover, it was noted that

the density at which grain coarsening occurred depended on the initial
green density, high initial values delaying the onset of grain growth.

As previously mentioned, reduction in surface free energy is the
principal driving force for sintering which makes particle size an
important parameter. Herring (253) investigated the effects of size on
sintering and concluded that "Simple scaling laws govern the time
required to produce, by sintering at a given temperature, geometrically
similar changes in two or more systems of solid particles which are of
identical geometry except for a difference in scale (size)". These
simple laws were found to have the form

$$\Delta t_2 = \lambda^n \Delta t_1 \hspace{3cm} (3.6)$$

where Δt_1 is the time required to sinter, to a certain point, particles
of radius r_1 and Δt_2 is the equivalent time for particles of radius
r_2. $\lambda = r_2/r_1$. n is dependant upon the transport mechanism present, 1 for
viscous flow, 2 for evaporation and condensation, 3 for volume diffusion
and 4 for surface migration.

Thus to a certain extent particle size governs sintering rate and
smaller particles are desirable for either fast rates or lower
processing temperatures. Sintering rate for glass powders can also be
increased by altering the composition so as to decrease the viscosity
but care has to be taken because of deformation problems. Deformation
can be reduced by using smaller sized powders of smaller size
distribution since the stresses due to surface tension are greater than
those due to gravity.

Particle shape is also an important parameter. Compact green strength is dependant on it since the strength is derived from the mechanical interlocking of particle surface irregularities. Irregular shaped particles produce compacts of higher green strength (254). It can also be important in sintering kinetics, pseudo spherical shapes being desirable for enhanced densification. This has been readily demonstrated by Chowdhry and Cannon (255) using β alumina. Powder of uniform shape, about 0.1μm in size, was sintered to~ 97% theoretical density at 900°C. Material fired to 1200°C yielded a β" phase with an aspect ratio of about 20. Final density here was less than 85%.

For glass powders the effect of particle shape has been examined by Cutler and Henrichsen (256). They found however that crushed glass of 'awkward' shape sintered over twice as fast as glass spheres of the same composition (and hence viscosity) at the same processing temperature. They concluded that points of contact for crushed glass had much smaller radii and hence sintered more rapidly. Later the Cahn and Heady (257) showed that contacts amongst jagged particles produce shears and torques (as opposed to the normal forces for spherical contacts) and that these would be important in particle re-arrangement during the early stages of sintering. Indeed, Nii (258) suggested that a certain degree of contraction was possible during the initial stages as large pores may be filled by moving particles driven by the forces within unsymmetrical neck growth.

The effect of particle size distribution is more upon final sintered density rather than sintering rate. From an initial packing point of view a fairly wide distribution is to be favoured since the numbers of large pores is greatly decreased. This leads to disadvantages during

the latter stages of sintering however, when coarsening (Ostwald ripening) may occur. For solid state sintering, the effect of size distribution may be derived from a consideration of pore separation from grain boundaries. During sintering pores decrease in size, grain boundaries acting as vacancy sinks and consequently there comes a time when pores are dispersed along the grain boundaries, Fig. 3.7a. Coarsening occurs during the latter stages of sintering, that is, large particles grow at the expense of smaller ones, driven by the reduction in interfacial energy. Coarsening requires the movement of grain boundaries which will obviously have an effect on the pores present on them. Either the pores will advance with the boundary, Fig. 3.7b or they stay put and the boundary moves without them, Fig.3.7c. In the latter case pores are left within grains and are only filled very slowly by lattice diffusion. Consequently there is a minimum solute drag force required to prevent pore separation.

It is shown analytically that the impurity concentration (which is usually attracted to grain boundaries so as to lower the surface energy) required to reach this minimum drag force is typically 14 times lower for a narrow distribution than for a large one (259). Moreover there is a critical density at which pore separation will occur if the drag force is below the required minimum. This density is 90.6% for a non uniform distribution but 99.3% for a narrow distribution (259).

Finally there is an important consideration to be taken into account during powder preparation which can have an adverse effect during sintering, that is the formation of aggregates and agglomerates. Aggregates are groups of particles held together by strong forces, typically due to diffusional mechanisms whilst agglomerates, usually the

more prolific, are held together by weaker forces.

During milling there are many particle - particle contacts and bonding may occur if there is a net attractive force, usually Van de Waals. Obviously this must be greater than any repulsive forces that may exist, such as electrostatic which arises through charges residing on the particle surface. As the slurry is dried liquid bridges form between particles which are then attracted to each other due to capillary pressure. The presence of such clusters is detrimental to sintering because the packing within an agglomerate is generally greater than the surrounding powder. Thus it sinters more quickly leaving larger pores around the periphery which are more difficult to remove and may even grow (260). The possibility of forming agglomerates can be reduced by the addition of a deflocculent to the milling liquid.

3.2.3. Viscosity Measurements

In order to compare the theoretical and experimental results of sintering, information is required on the viscosity of the glass under investigation, particularly the dependance of viscosity with temperature. (The various aspects of glass related viscosity are dealt with more fully in many of the general texts cited in section 1.3.1). The dependance of viscosity upon temperature is important not just in sintering but in glass manufacturing generally and has prompted much work. The most widely accepted relationship between the two is due to Fulcher (261) and takes the form

$$\log \eta = -A + \frac{B}{T-T_0} \qquad (3.7)$$

where A, B and T_0 are constants and are usually obtained by a least squares fit to the experimental data. Thus once these constants are known for a specific composition the viscosity at any temperature can be readily calculated.

As mentioned in section 1.3.1 the effect of the addition of modifier and intermediate oxides to silica alters the structure and thus the viscosity is consequently related to composition. Again the relationship between viscosity and composition has been widely studied by many authors. Lakatos et al (262) derived an expression to calculate A, B and To from the experimental data from 30 glasses composed of varying amounts of Na_2O, K_2O, CaO, MgO, Al_2O_3 and SiO_2. Lyon (263) also included the effects of BaO, Li_2O and B_2O_3 and derived an expression for $\log\eta$ directly at specific temperatures by using tabulated multiplication factors. Three calculations at different temperatures enabled the Fulcher constants to be deduced.

More recently Giess and Knickerbocker (264) have determined the viscosity relationship for cordierite glasses with B_2O_3 and P_2O_5 additions which had the form

$$\log\eta = C + \frac{37276}{T} \tag{3.8}$$

with T in °K. C was computed using the composition in wt% and previously determined coefficients. They also showed that MgO and P_2O_5 lowered the viscosity whilst B_2O_3, Al_2O_3 and SiO_2 increased it.

The theoretical viscosities from equation 3.8 are shown in Fig.3.8 for compositions C1, C3, C4, C6 and C10. Also shown are the experimental points, determined by the indentation method outlined in section 2.12,
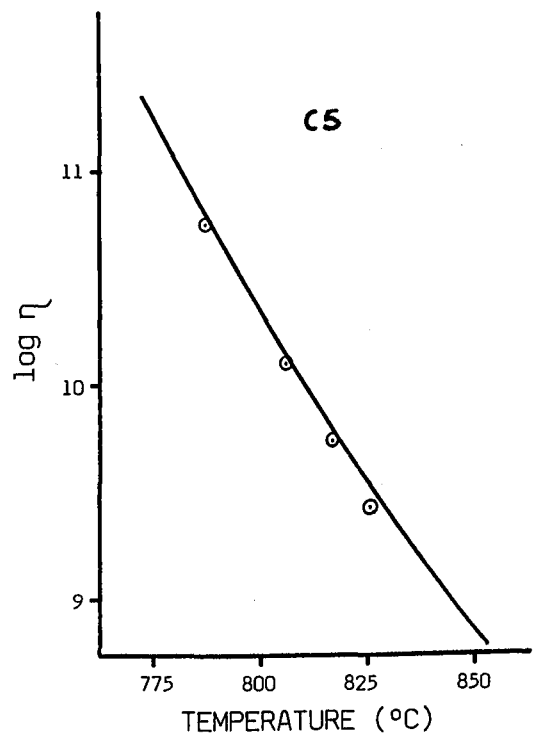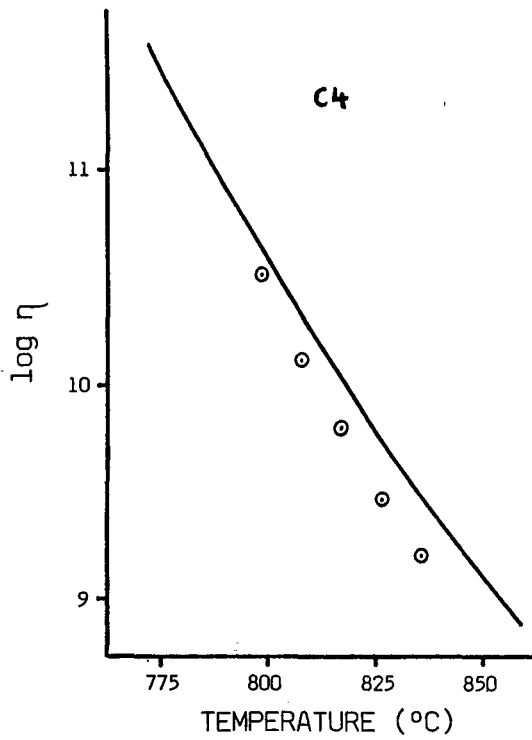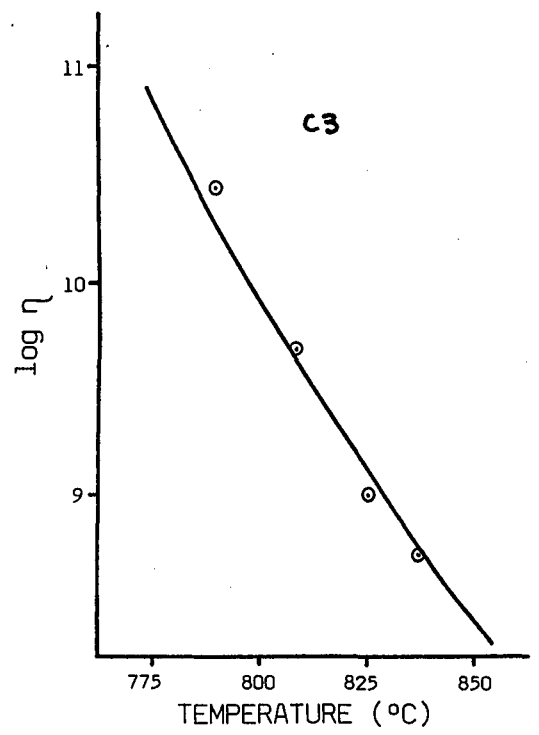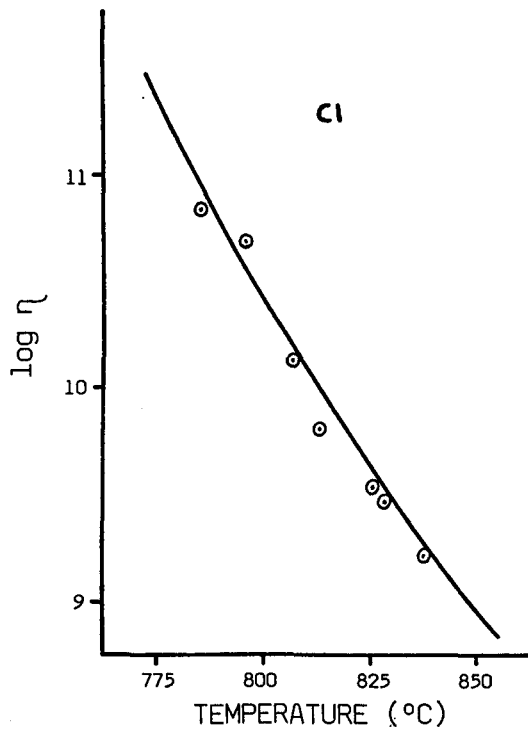
FIG.3.8 Theoretical viscosity curves for various glass
         compositions. Also shown are the experimentally
determined points.

C6

log η

TEMPERATURE (°C)
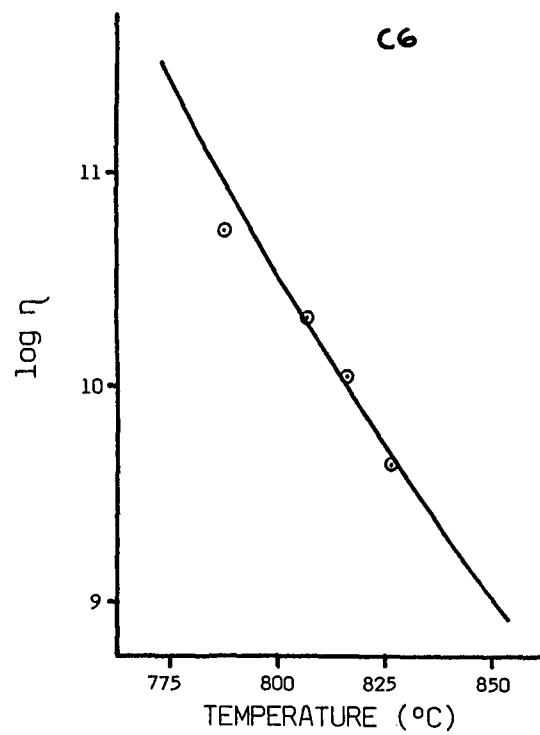
FIG.3.8 Continued

and it can be seen that there is reasonable agreement between the two although the results for C3 are noticeably lower than expected. Glass C10 had a lower viscosity compared to the other compositions ($\Delta \log_{10} \eta \sim 0.5$) and reflects the addition of MgO in breaking up the silicate network and creating NBO's. As expected the other compositions were all fairly similar due to the small amount and equal and opposite effects of B_2O_3 and P_2O_5.

Table 3.1 shows the predicted viscosity for glass of C6 composition, determined by the methods outlined by the three above mentioned authors, compared with the experimental result obtained at 800°C. Clearly the predicted values by Lyon and Lakatos et al are in considerable error. This is because the composition of C6 is quite different from those from which the two authors base their equations and thus viscosities should not be predicted using these methods if a large degree of extrapolation is required.

TABLE 3.1   Viscosity of C6 glass at 800°C

Lakatos et al (262)	Lyon (263)	Giess & Knickerbocker (264)	Experimental
8.790	13.279	10.543	10.48±0.05

3.3   SINTERING RESULTS AND DISCUSSION

For the sintering measurements, powder, with a small amount of binder, was pressed to form pellets 10-15mm in length and 5mm in diameter.

After scraping clean the surfaces of any contamination, the precise
dimensions were measured with a micrometer. Each pellet was placed in a
small alumina tube and then had nichrome wire wrapped around the ends in
order to prevent the pellet from dislodging. Seven samples were placed
simultaneously in a horizontal tube furnace by means of stouter pieces
of nichrome wire attached to the front of each small tube. A cross
sectional view is given in Fig.3.9. Time t=0 was taken when the sample
temperature was back to within 5% of the set temperature which usually
took about 30 seconds. After the desired length of time individual
pellets were removed and, after cooling, remeasured. This enabled a
shrinkage versus time curve to be plotted for each set of specimens at
different temperatures.

Such plots are shown in Fig.3.10 for M and A12 and M and A36 of C1
composition for sintering temperatures of 820, 850 and 875°C. The
dependance of sintering rate on temperature, and hence viscosity, can be
clearly seen. From these curves the exponent n in equation 3.6 can be
calculated and was found to be 0.9 ± 0.15 indicating that, as expected,
viscous flow is the predominant mechanism during sintering. The
applicability of Herrings scaling laws have been discussed by Song et al
(265). They found that for alumina powders the exponent was generally
greater for materials with a narrow size distribution however comparing
the plots of the dry and wet milled powders there was no perceptible
difference within experimental errors. They also showed that for

FURNACE WALL

THERMOCOUPLES

SAMPLE

NICHROME WIRE
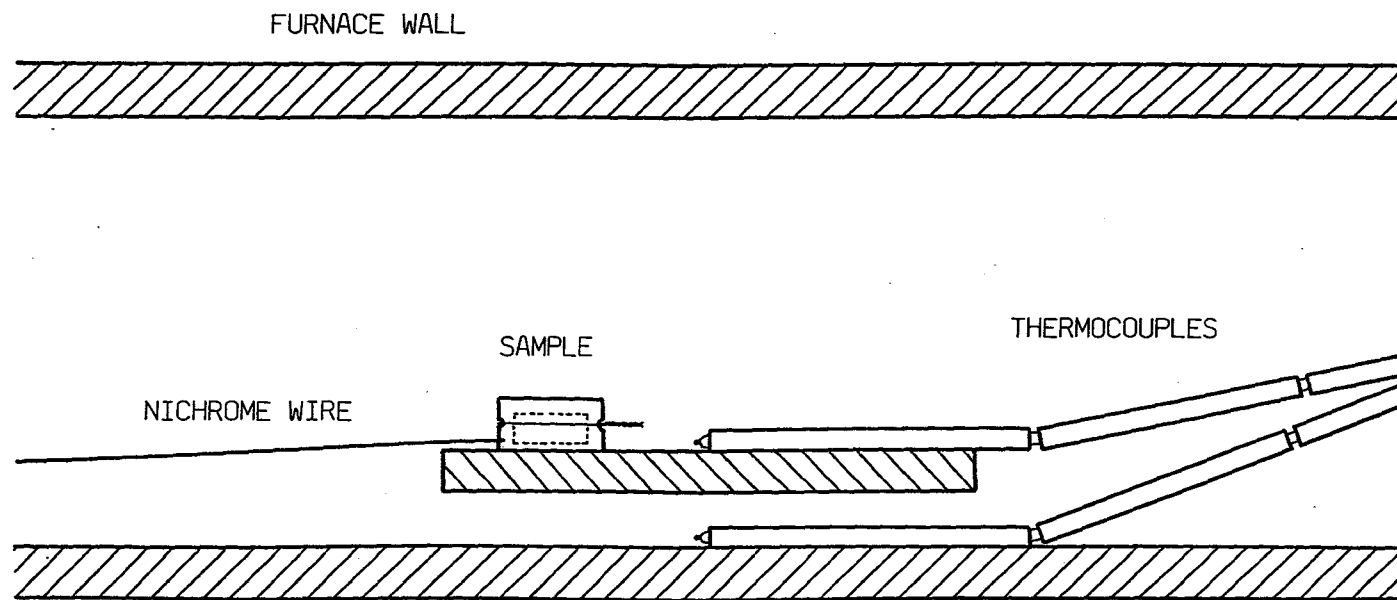
FIG.3.9 Sectional view of sintering furnace

irregularly shaped powders the value of the exponent tended to increase with time. This was found to be true here. Comparing A12 and A36 at 825°C n increased by 0.19 between t=0 and t=400 minutes.

Coefficients exist whereby the surface tension can be calculated for a glass as a function of composition (266) and for cordierite glass Giess et al quote a value of 0.36 N/m in this temperature range. This enables the expected curves from the Frenkel equation to be plotted and are shown as the heavier dashed lines in Fig.3.10. (The viscosity values used are those determined by equations 3.8 whilst r was taken as the average obtained from the particle size measurement).

It is seen from Fig.3.10 that although the initial shrinkage for all samples appears linear with time there is only good agreement for the compacts sintered at 850°C. This is to be compared to the sintering curves presented by Giess et al (267) where a good fit was obtained at four different temperatures for a milled cordierite glass. A possible contributing factor to this lack of fit is likely to be due to the sensitivity of viscosity to temperature, a change of 10°C giving a change in $\log_{10} \eta$ of ~0.35. Comparison of the theoretical and experimental curves at 820°C gives a ΔT of 14±4°C, thus variation in furnace temperature may in part explain the deviation. One also has to consider how the average particle size is defined/measured since the different methods outlined in section 2.10 can yield quite different values (268). Thus an inaccurate particle size will also alter the expected theoretical curve. For instance, a much improved fit is
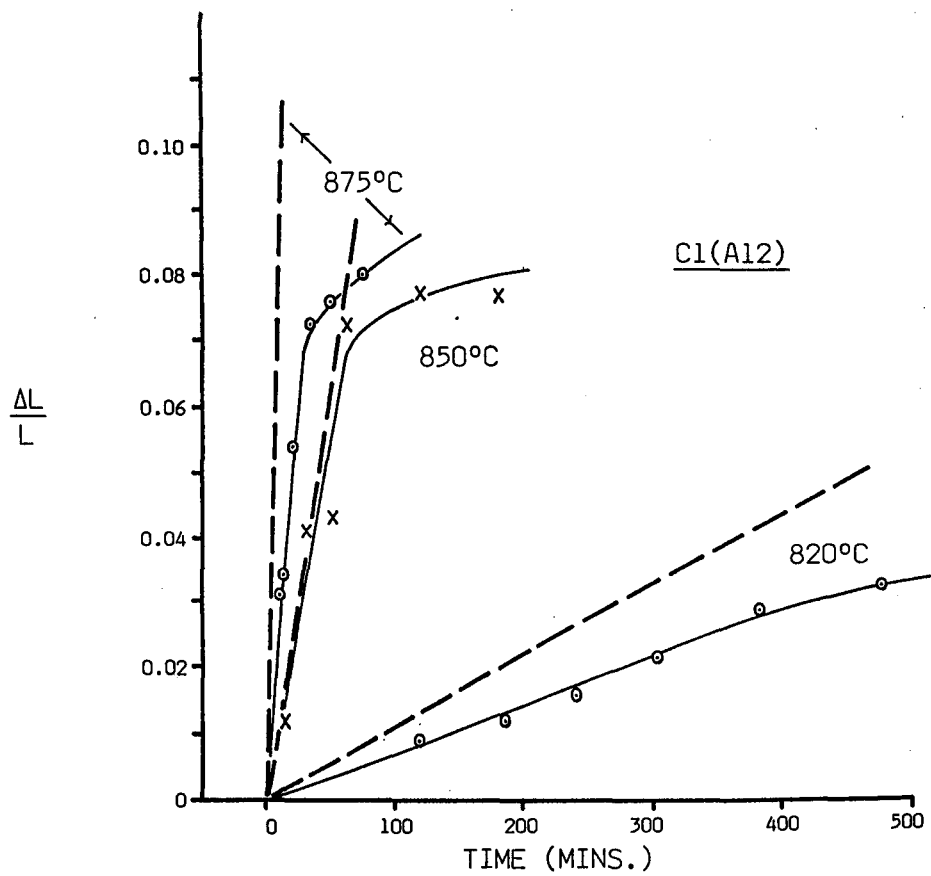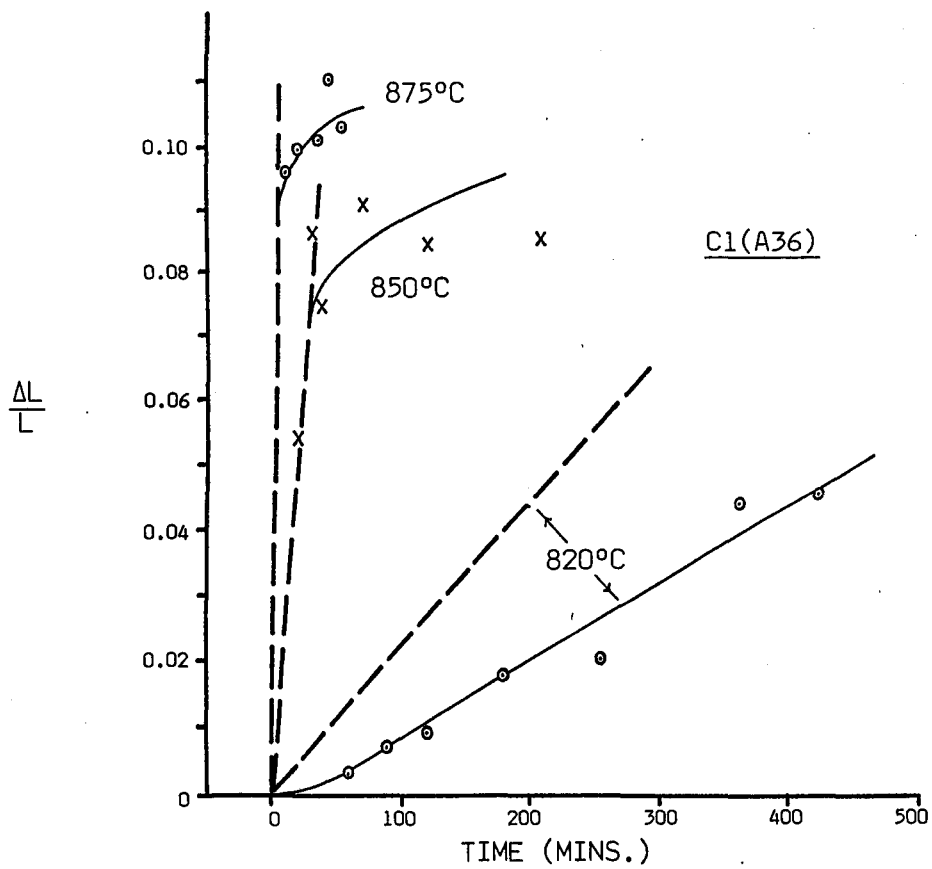
FIG.3.10   Sintering curves for the lengths of
          glass powder compacts
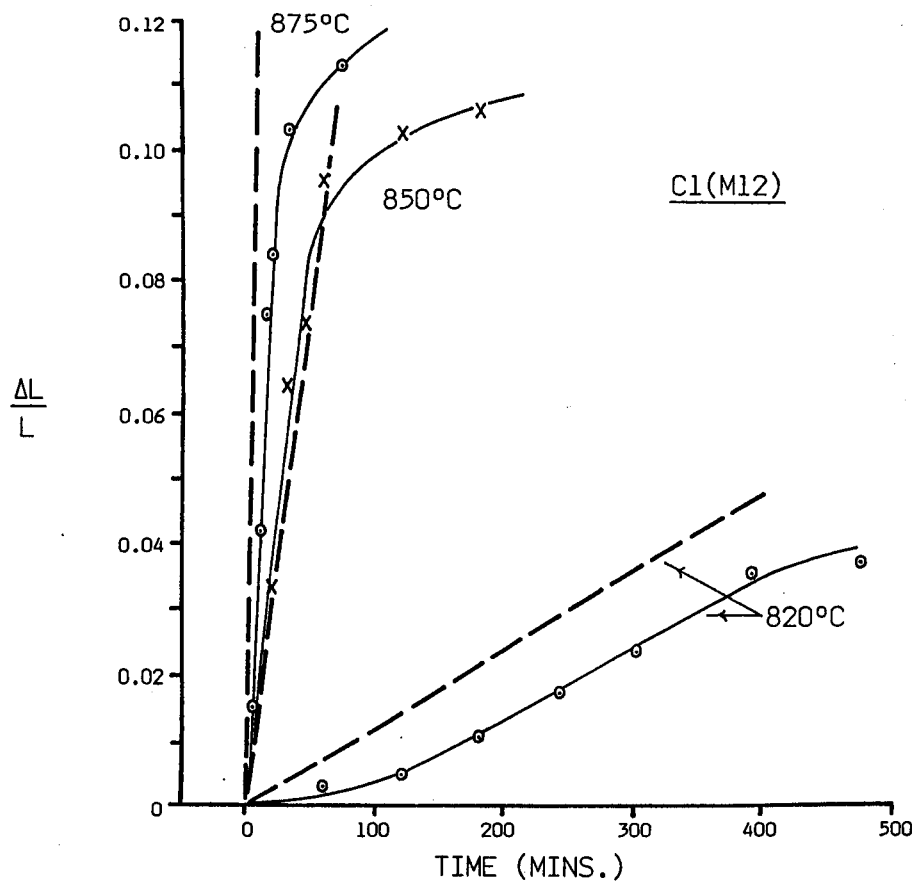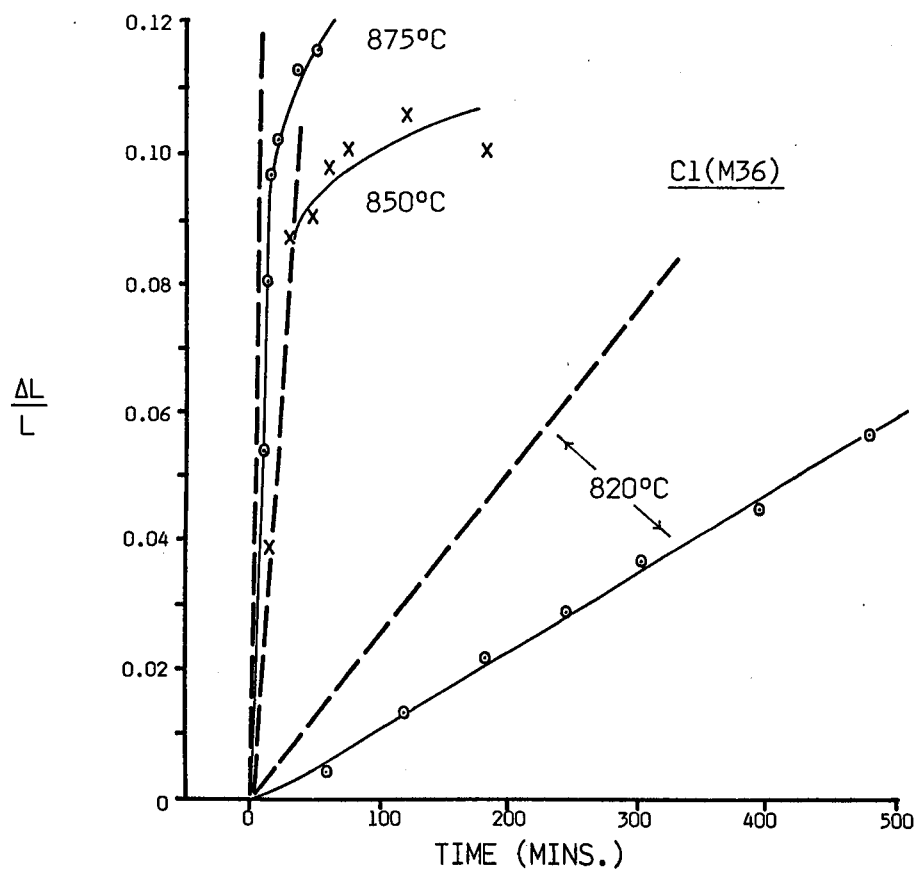
FIG.3.10   Continued

obtained for A36 using an assumed radius of 5μm instead of 3.4μm.

That these are the only factors is unlikely however, especially when one considers the shrinkage of compact diameters rather than lengths, as depicted in Fig.3.11. Here it can be seen that a much better fit is obtained, diameters shrinking faster than lengths. Also the trends of the curves would suggest a final sintered density some 25% greater than for lengths. Thus it would appear that the packing within a uniaxially pressed powder plays an important role during sintering. Giess et al (267) also noticed this anisotropy and suggested that it was due to alignment of angular particles perpendicular, rather than parallel to, the compression axis. Later work however on milled glass spheroidized before sintering gave rise to the same anisotropy although the sintering rate was reduced (269). It was thus concluded that the difference was possibly due to axial and radial distributions of particle sizes present within the compacts. Exner and Petzow also pointed out that slower rates of sintering could be expected for glass spheres where multiple contacts give rise to particle rearrangements leading to the creation of larger pores (270).

Examination of Figures 3.10 and 3.11 shows that many of the individual curves start to deviate after a certain length of time and this represents the transition from the Frenkel to the Mackenzie – Shuttleworth mechanism of sintering. Also particles are beginning to loose their individual identity as densification progresses and the assumed value of r is no longer applicable. Indeed, as grain growth occurs the average r increases and thus the rate decreases. During the final stages of sintering at 875°C there was also evidence from XRD that
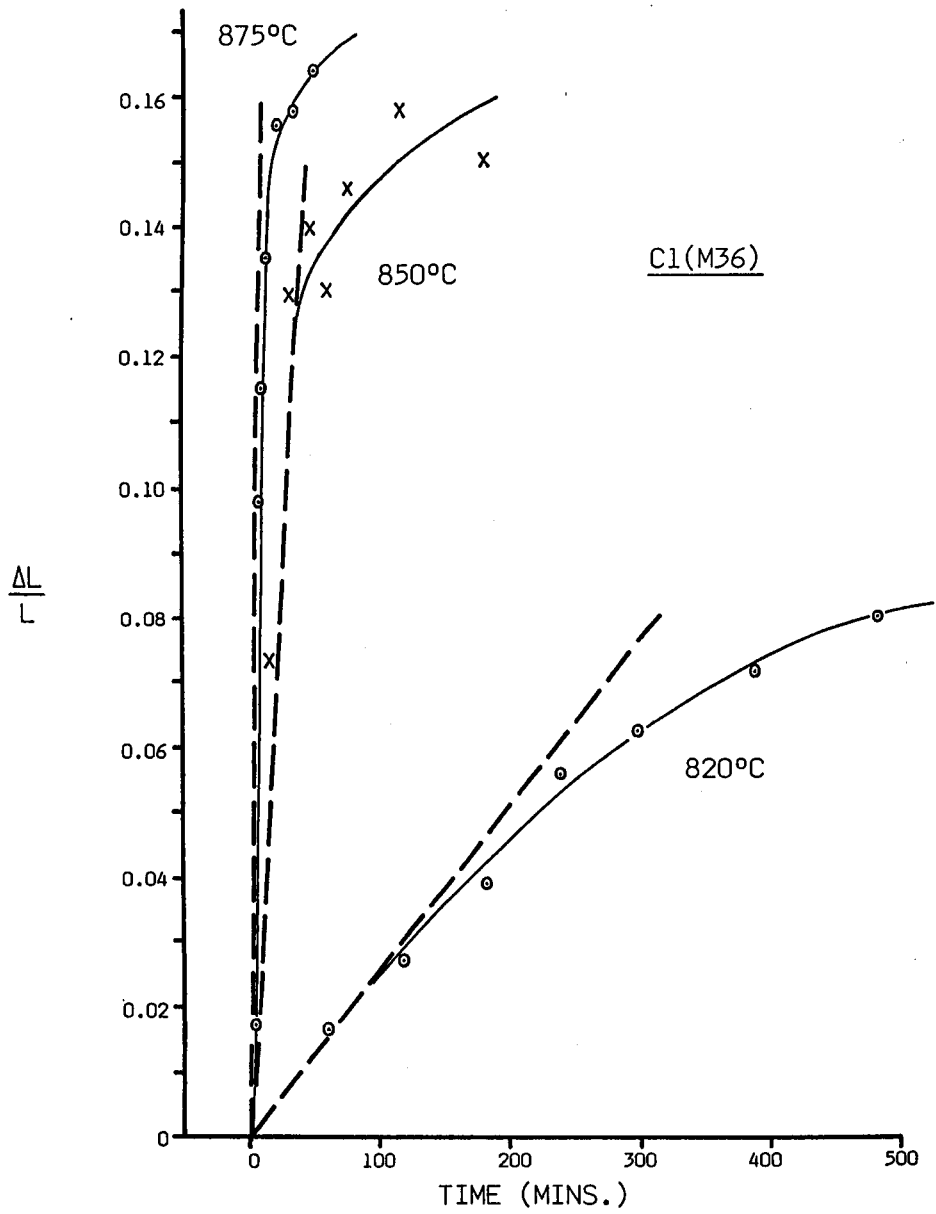
FIG.3.11 Sintering curves for the diameters of
glass powder compacts

crystallization was starting to occur. This introduces additional diffusional mechanisms associated with glass-solid interfaces rather than glass-glass interfaces although viscous flow is still likely to be dominant. Finally the presence of a range of particle sizes would be expected to have an influence since larger particles will sinter more slowly (see Wilder and Fitzsimmons (271) and Norton et al (272)) and thus powders with wider size distributions would be expected to exhibit a decrease in sintering rate.

Fig.3.12 represents plots of relative density against time for M12 and M36 (lengths) and M36 (diameters). Superimposed on these curves are the theoretical lines derived from the Mackenzie-Shuttleworth equation (3.5). It can be seen that this approach describes the overall sintering curves more accurately although the fit, especially for C1 A12, is not completely accurate. Again there is better agreement for diameters than for lengths. The poorer fit for A12 is not unsurprising since the Mackenzie-Shuttleworth theory is based on the closure of a constant number of equally sized pores. For powders with a wide size distribution, as in A12, then there is a correspondingly larger distribution in pore sizes and thus pores will not contract at equal rates. There is also evidence that the number of pores fluctuates during sintering (267,271).

Closer examination of the curves in Fig.3.10 suggests an influence of average size and size distribution in the sintering rate and final sintered density. League tables were drawn up for the four powders at the three different temperatures, categorized into sintering rate (highest first) and final density (highest ΔL/L first , averaged for the
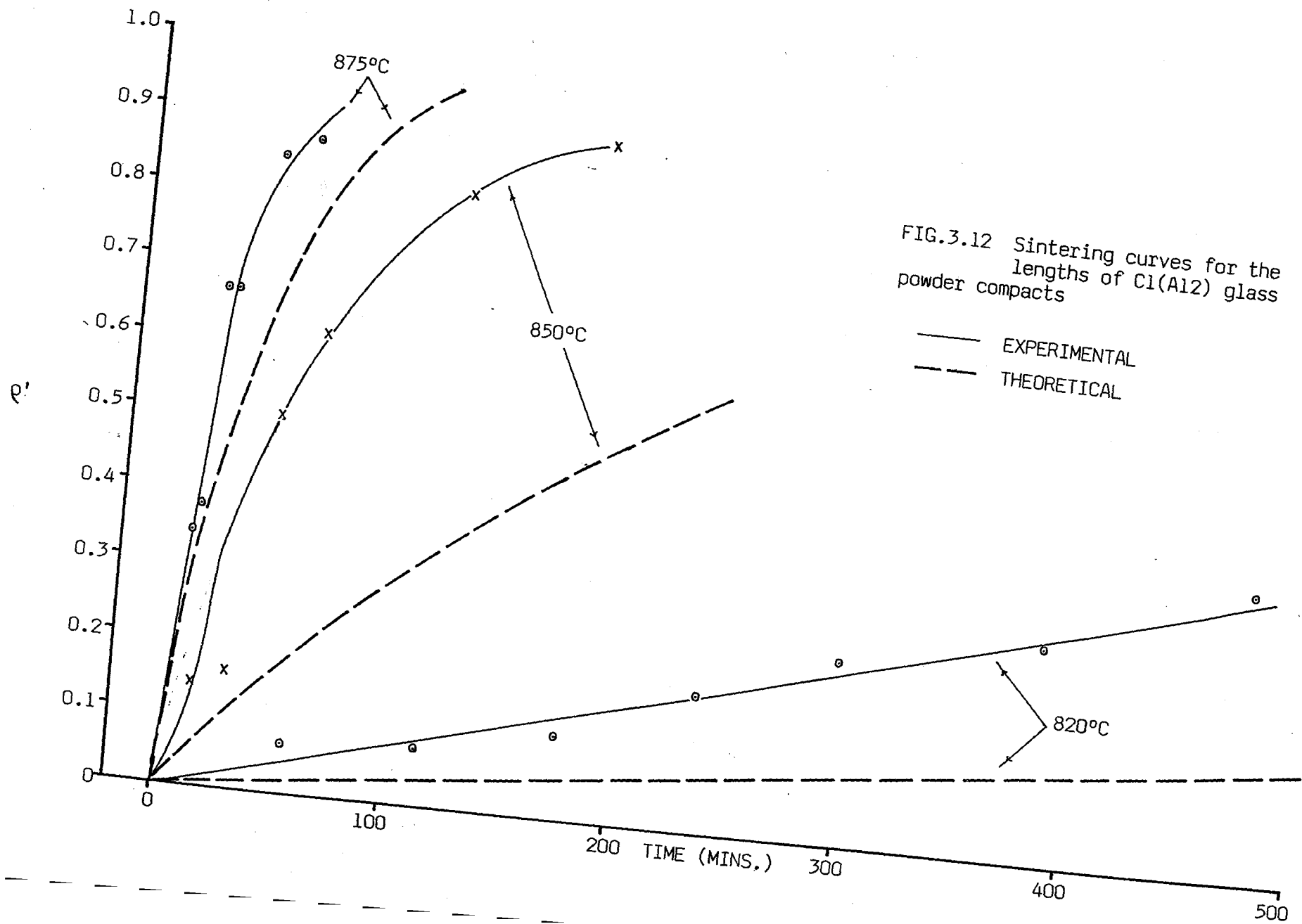
FIG.3.12 Sintering curves for the lengths of Cl(Al2) glass powder compacts

—————— EXPERIMENTAL
— — — — THEORETICAL

FIG.3.12 (Continued). Sintering curves for
the lengths of Cl(M36) glass
powder compacts
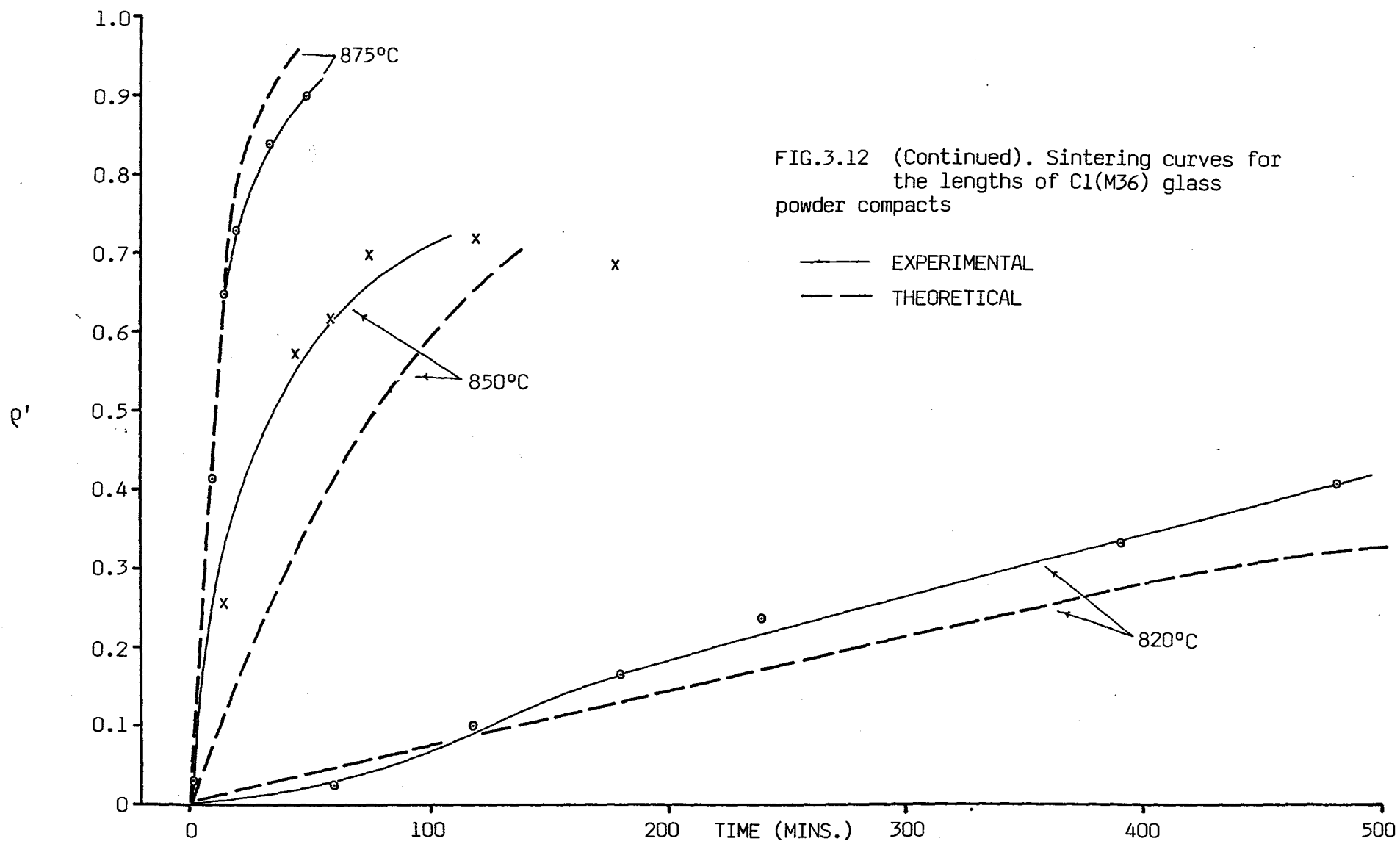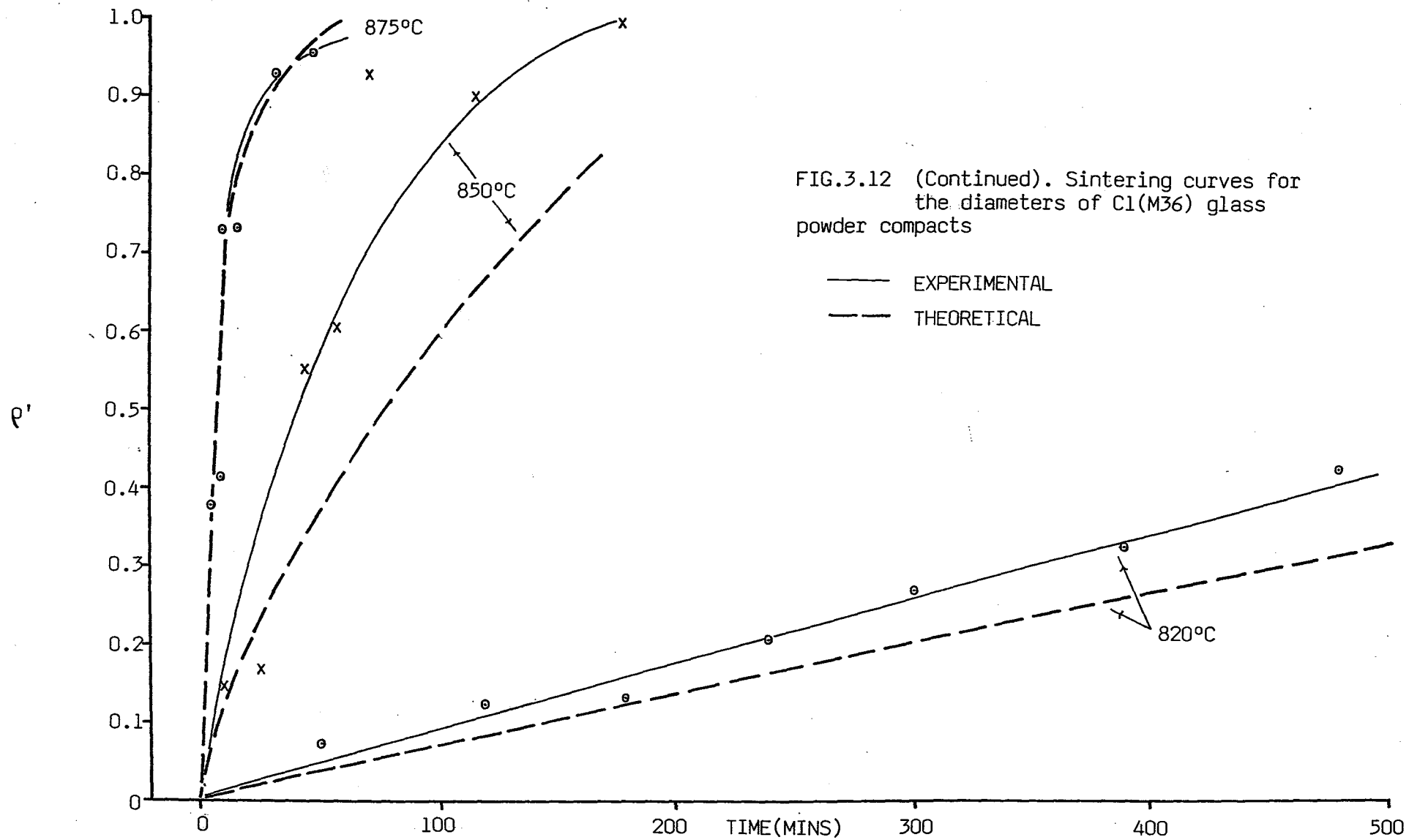
FIG.3.12 (Continued). Sintering curves for the diameters of Cl(M36) glass powder compacts

EXPERIMENTAL
—— —— THEORETICAL

TABLE 3.2.a <u>'League tables'</u> for the sintering of Cl A12, M12, A36
and M36

	Sintering Rate	ΔL/L	Calculated Density	Average particle size (μm)	
820°C	M36	M36	A36	M36	5.8
	M12	A36	M36	A36	6.8
	A36	M12	A12	M12	11.8
	A12	A12	M12	A12	14.6
850°C	A35/M36	M12	M12		
		M36	M36		
	M12	A36	A12		
	A12	A12	A36		
875°C	A36/M36	M36	M36		
		M12	M12		
	M12	A36	A36		
	A12	A12	A12		

TABLE 3.2.b 'League tables' for the sintering of C1 M24, A36, M36*, C3, C4 and C5

	Sintering Rate	ΔL/L	Calculated Density	Average Particle size (μm)	
820°C	C5	C5	C5	C5	4.5
	C1(M24)	C3/C1(M24)	C3	C3/C1(M36)	5.8
	C3	C1(A36)	C1(A36)	C4	6.4
	C1(A36)	C1(A36)	C4		
	C4	C4	C1(M24)	C1(A36)	6.8
	C1(M36)	C1(M36)	C1(M36)	C1(M24)	7.0
850°C	C3	C5	C5		
	C5	C3	C4		
	C1(M24)	C4	C3		
	C1(M36)/(A36)	C1(M36)	C1(M36)		
	C4	C1(A24)	C1(A36)		
		C1(M24)	C1(M24)		
875°C	C4	C5	C1(A36)		
	C5	C4	C4		
	C1(A36)	C1(M36)	C5		
	C1(M36)	C1(A36)	C3		
	C1(M24)	C1(M24)	C1(M36)		
	C3	C3	C1(M24)		

* No binder added to C1(M36) before the pellets were pressed

last two pellets for each run). The latter was compared to the measured density, equation 2.17, again averaged for the last two pellets. This is shown in Table 3.2a. It is interesting to note that M36 (smallest average size and narrowest distribution) did consistently well while A12 did consistantly badly. For the higher two temperatures the role of size and size distribution appears to be that smaller sizes lead to faster sintering rates whilst narrower size distributions give greater sintered densities, confirming the predictions of theory. For the low temperature sintering (820°C) the position appears less clear, suggesting that for low sintering temperatures the effects of the two variables become less noticeable.

A similar series of experiments was conducted on C1(A36), C1(M36) with no added binder, C3(M36), C4(M36) and C5(M36), again at temperatures of 820, 850 and 875°C. League tables were again drawn up from the results of the sintering curves, as shown in Table 3.2b. The trends for this set of experiments were unclear however, as exhibited in the performance of C3 and C4 for example. This is probably due to the fact there was little variation in particle size (4.5 - 7.0μm) or in distribution. Although the glasses were of differing composition the changes were fairly subtle and thus the difference in viscosity at a certain temperature is also likely to be fairly small. Despite the lack of trends some observations can be made.

Firstly C5, which had the smallest average particle size, did consistently well. This is a little surprising since TiO_2 is known to promote bulk nucleation and Rabinovich (158) from his sintering

experiments states that "Glasses which show significant (bulk) nucleation cannot be well sintered in the powder form." One glass containing TiO_2 however that did sinter successfully also contained 2.2 wt% Na_2O and it may be that B_2O_3 exerts a similar effect. It is also possible that the small amount of TiO_2 in this composition (2.0 wt%) is insufficient to have any real influence. Secondly, M36 without binder did not do as well as expected. Again this is at first surprising since one would assume that any binder burning off would leave a more porous material. At the low levels used here however this may be offset by improved compaction when a small amount of binder is present, individual particles being able to slide more easily once they are covered in a thin film.

Finally, Rabinovich suggested that more rapid heating provided better sintering than did a slow rate which consequently lead to an improved strength. This claim was briefly studied. Fig.3.13a is for a material of composition C1 heated at 3.5°C/min. up to 800°C and then at 1°C/min. between to 800°C and 875°C before being air quenched. Fig.3.13b is for the same composition but heated at 3.5°C/min. up to 850°C. Quite clearly the material sintered at the faster rate has sintered more successfully.
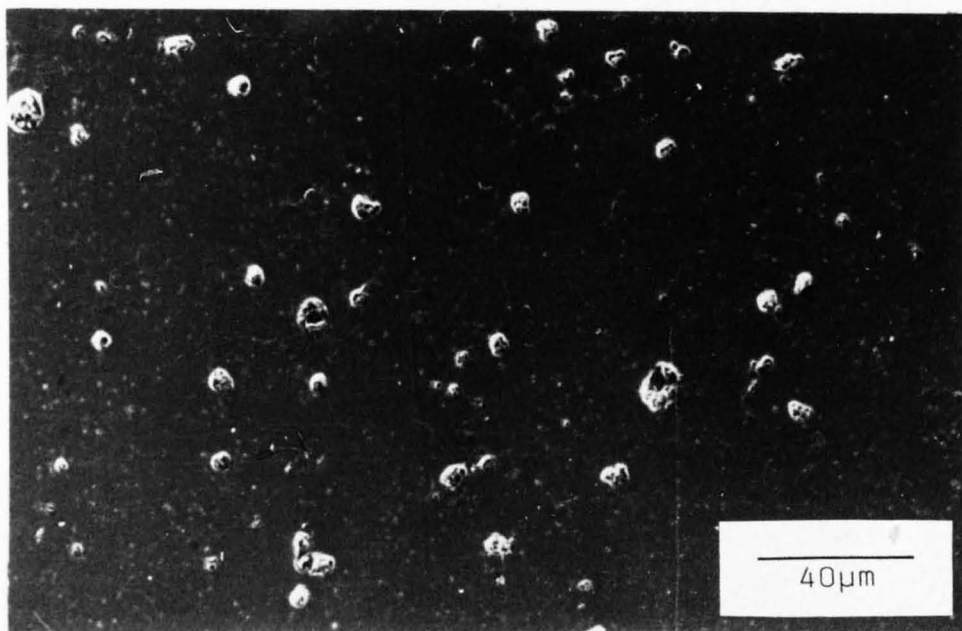
(a)
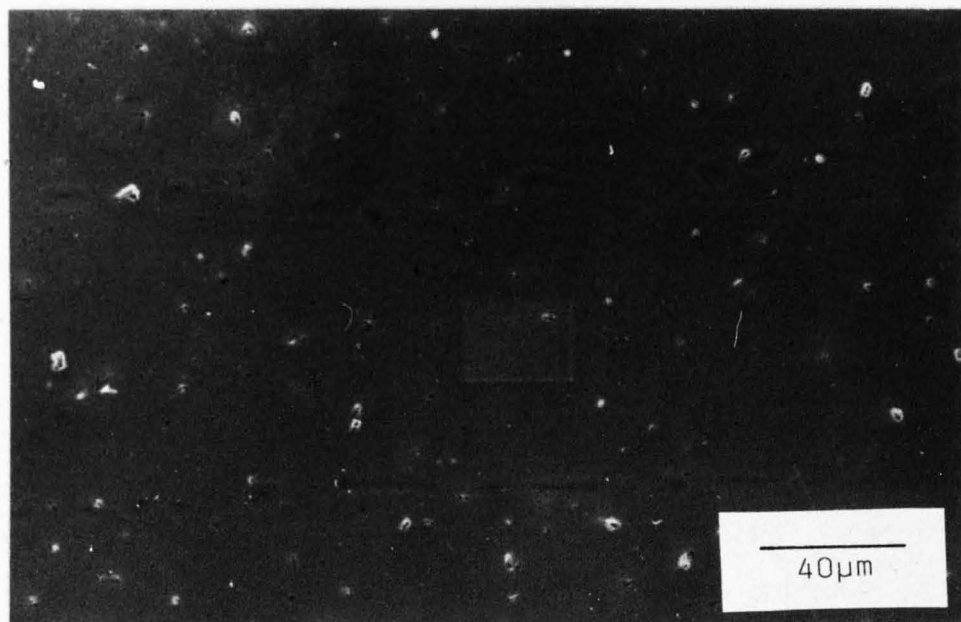
(b)

FIG.3.13 C1 glass ceramic fired at different heating
         rates (a) 3·5°C/min to 800°C and then 1°C/min
to 875°C (b) 3·5°C/min to 850°C

CHAPTER FOUR - PHASE DEVELOPMENT

The analysis of crystallization in the cordierite glass studied here is beneficial since microscopic variations within any glass ceramic system can give rise to measurable macroscopic changes. The phase evolution from glass, to μ cordierite through to α cordierite dictates the properties of the material, as discussed further in Chapter Five, and thus a close understanding of them can enable subtle alterations to be made in order to improve the final material. Furthermore, investigation of the interactions that occur within the system (e.g. anticipated thermal expansion mismatch between various phases) enables causes of inadequate material properties to be readily identified and again, where possible, changes can be made. A variety of techniques are used in order to investigate the crystallization process as are a range of slightly differing compositions which gives insight to the roles of differing chemical components.

4.1   PHASE AND MICROSTRUCTURE DEVELOPMENT FOR COMPOSITION C1

4.1.1   DTA and DSC Results

The application of DTA and DSC to Tg determination in C1 glass is shown in Table 4.1 which also gives the refractive index of the as melted glass and glass fired to 850°C. For comparative purposes the results for other compositions are also shown in the table. The difference between the two sets of figures for Tg is probably due to the differing heating rates ex ɪloyed, 8°C/min. for the DTA and 0.4°C/min. for the DSC.

TABLE 4.1   SOME BULK GLASS PROPERTIES

| Composition | Tg | | Refractive Index | |
	DTA	DSC	As Melted	Fired to 850°C
C1	756	739	1.5621	1.5619
C3	758	740	1.5644	1.5632
C4	767	749	1.5672	1.5646
C6	-	748	1.5636	1.5650
C10	760	736	1.5683	1.5692

(The DTA measurements given in this table were made on a commercial piece of apparatus at Sheffield University and the refractive indices on a Abbe Refractometer).

As mentioned in section 2.6.2 problems were encountered with the DTA apparatus during the latter period of the work due to noise and base line drift. Furthermore glass material that before gave two distinguishable peaks later only gave one which had a noticeable shoulder. XRD analysis of the glass ceramic showed that the first peak or shoulder was due to the formation of μ cordierite whilst the second was due to α cordierite. Amoto and Negro (273) have shown that increased additions of Fe_2O_3 to a cordierite based glass both increases the resolution of the two peaks and lowers the temperature at which they occur. On some runs for compositions C9 and C10 a small peak was just discernible at about 930°C. This may be due to the formation of a magnesium silicate phase.

During the initial period of the work, when the DTA was yielding two well resolved peaks, one at $\sim$ 890°C, the other at $\sim$ 950°C, a series of experiments was conducted on C1 using different heating rates. This enabled a Kissinger plot, equation 2.9, to be drawn. A linear plot was not obtained for the first peak, thus it was concluded that the initial formation of μ cordierite was not a first order reaction. A linear plot was obtained for the α phase however and this is shown in Fig.4.1. The activation energy was determined to be 430±15 KJmol^{-1}. This to be compared to values around 400 KJmol^{-1} reported by Todhunter (274) for bulk titania nucleated cordierites.
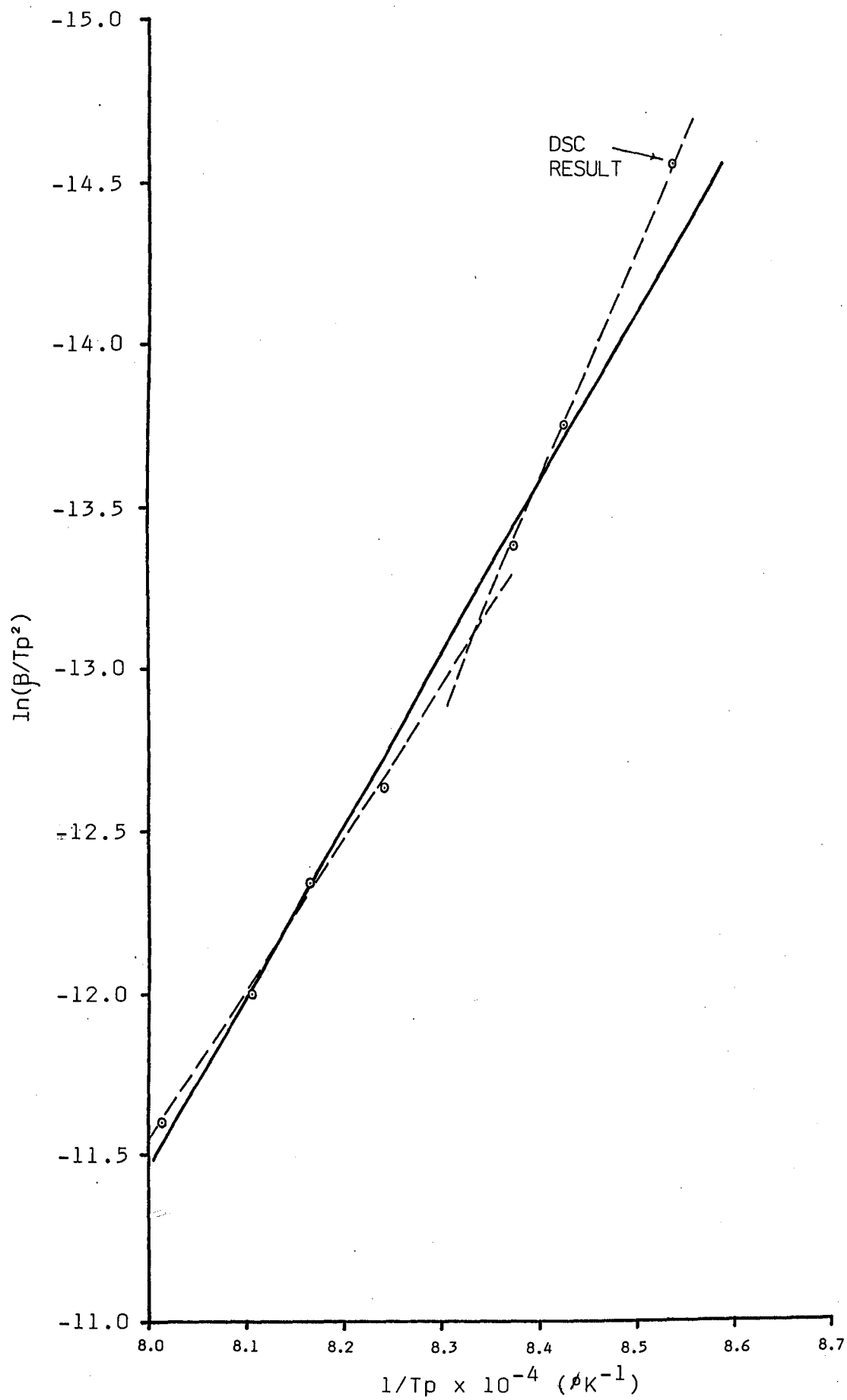
FIG.4.1 Kissinger plot for Cl glass ceramic

The study of crystallization kinetics by DTA has been examined by Matusita et al (275) and Matusita and Sakka (276,277), particularly for lithium silicate glasses. They found that if a phase that was of a similar composition to that of the base glass nucleated and grew on the surface then the activation energy for crystallization was similar to that for viscous flow. If the phase nucleated internally and then grew three dimensionally then the expected activation energy was about half that for viscous flow. The latter can be readily calculated for these glasses by plotting $\log\eta$ (from equation 3.8) versus $1/T$. The activation energy was found to be 713 ± 10 KJmol^{-1} for composition C1.

Thus it would appear that α cordierite, which transforms via a nucleation and growth process, is bulk nucleated. Although this cannot be observed directly, μ cordierite is clearly seen to grow from old glass particle surfaces Fig.4.2. Watanabe and Giess (278) have conducted a similar experiment on a cordierite glass (no composition given but it had an excess MgO and SiO$_2$ content with other minor additions). Their quoted activation energies were 272 and 585 KJmol^{-1} for crystallization and viscosity respectively. As their material also underwent surface crystallization they expected the values to be the same and concluded that possibly their DTA results were in error. Consequently it would appear that for cordierite glasses either the observations shown to hold for lithium silicate glasses do not hold here or that bulk nucleation is dominant despite surface crystallization occurring.

Matusita and Sakka (188) have also investigated crystallization kinetics by means of DSC (equation 2.12). The value of m in this equation was
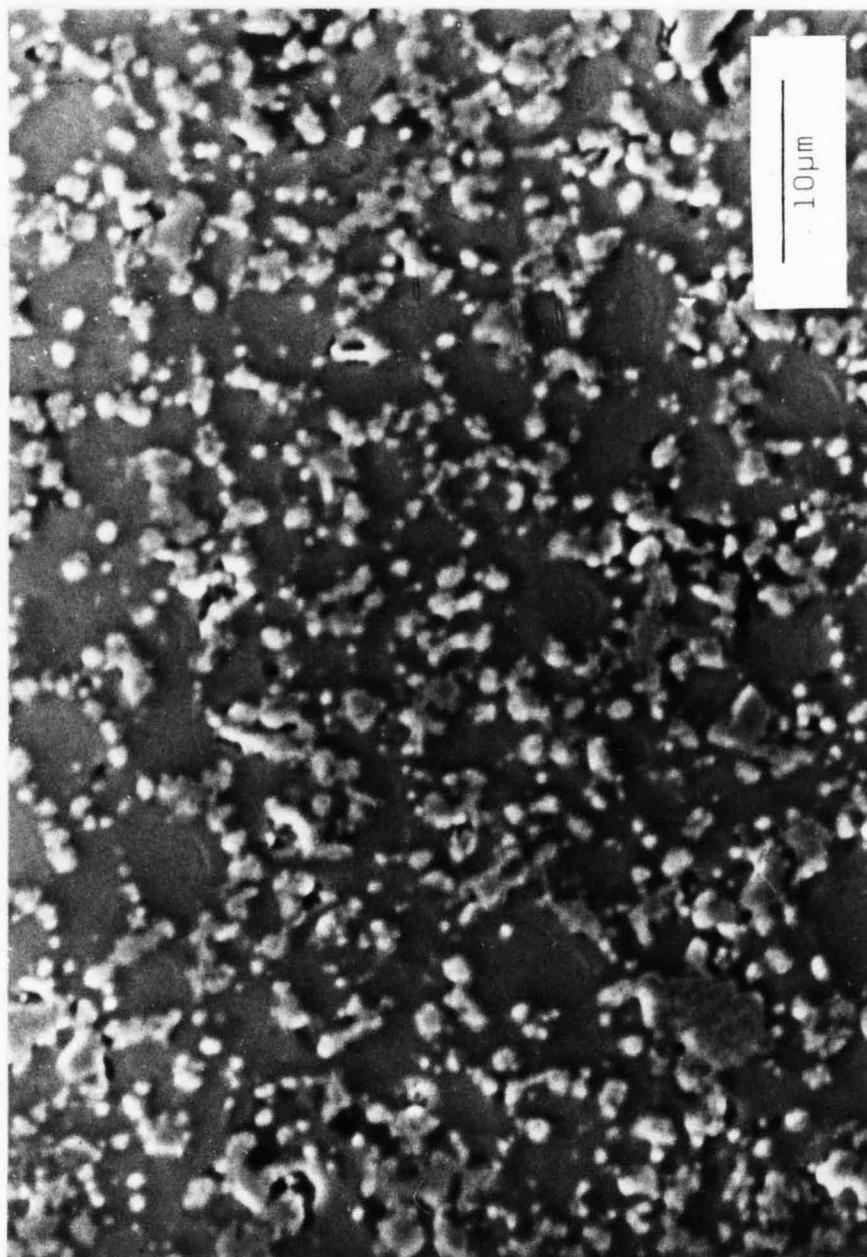
FIG.4.2 Initial stages of surface crystallization in C1 material

found to vary between one, for surface nucleation and growth into the centre, to four for three dimensional bulk nucleation and growth. The appropriate plot for Cl is shown in Fig.4.3 and gives a value of mE=860 ± 28 KJmol^{-1} for the as milled powder and mE=594±34 KJmol^{-1} for coarser powder (150-500 μm). (It should be pointed out that the latter figure was derived from a plot which showed a degree of departure from linearity, the tangent being drawn in the region of the peak temperature, 938°C). Comparing these results with the other values obtained it does not seem unreasonable that m is of the order one or two.

Thus it would appear that for slow heating rates (e.g.~ 0.4°C/min.) surface, or near surface growth, is dominant, possibly aided by more efficient nucleation conditions (see Barry et al (155)) whilst for higher rates there are two mechanisms present, a readily observed surface growth plus a submicron bulk crystallization which occurs at about the same temperature. Indeed, if one adds the peak temperature obtained by DSC to Fig. 4.1 then it is possible to draw two lines of differing gradients (shown dashed) with an intercept with each other corresponding to a heating rate of 2.9°C/min. For higher rates E is 385±15 KJmol^{-1}, very nearly half that of viscosity whilst for rates below 2.9°C/min. E is ~600±28 KJmol^{-1}. This dual mechanism for powder heated at higher heating rates appears to be confirmed by XRD. The specimen shown in Fig.4.2 would be expected to exhibit a broad glassy peak if the observed crystal phase was the only one present. This is not the case. The glassy peak is much smaller than expected, the majority of the material being μ cordierite. This also agrees with the
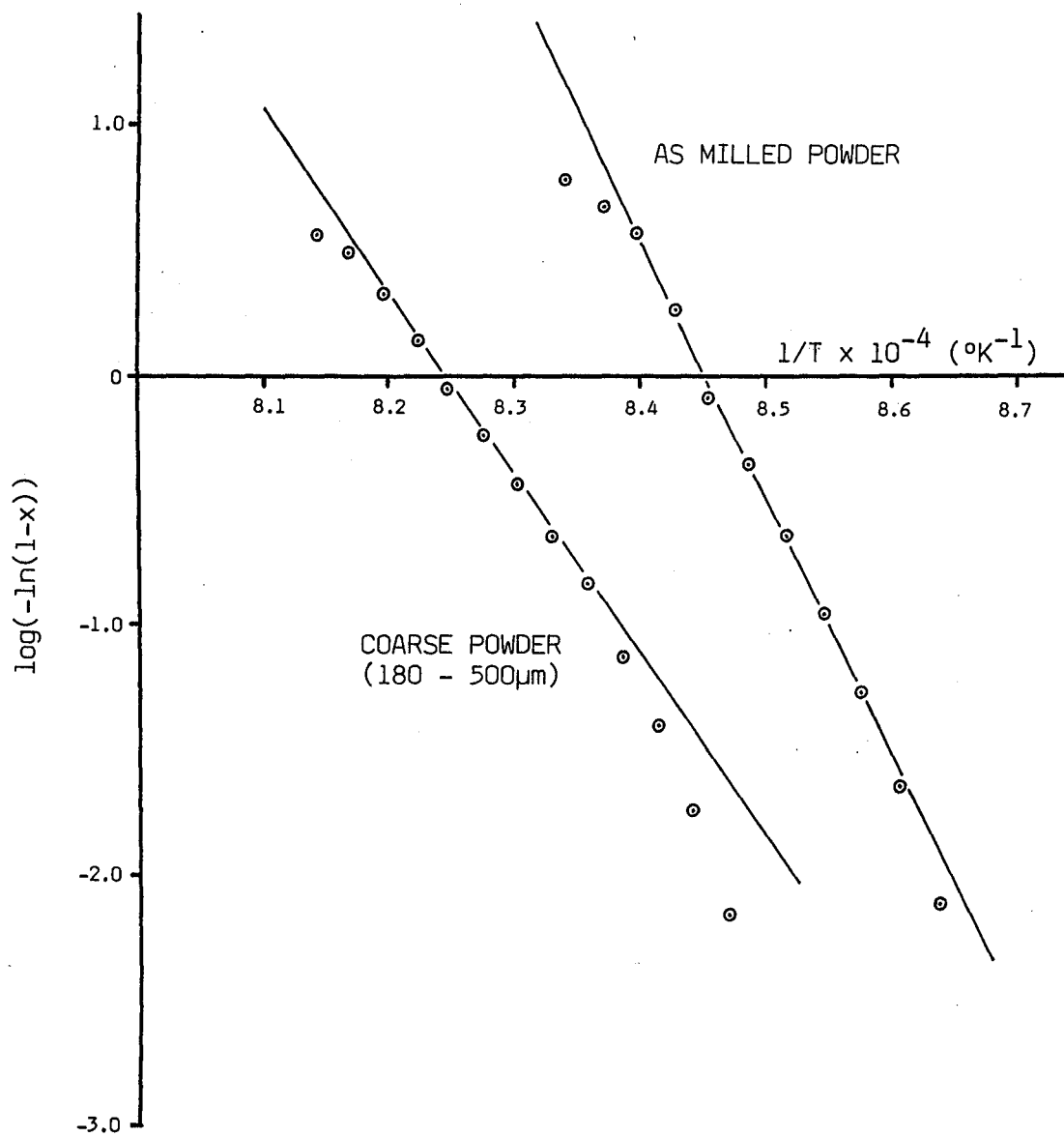
FIG.4.3 Crystallization activation energy plot as determined
from DSC results for Cl glass powder
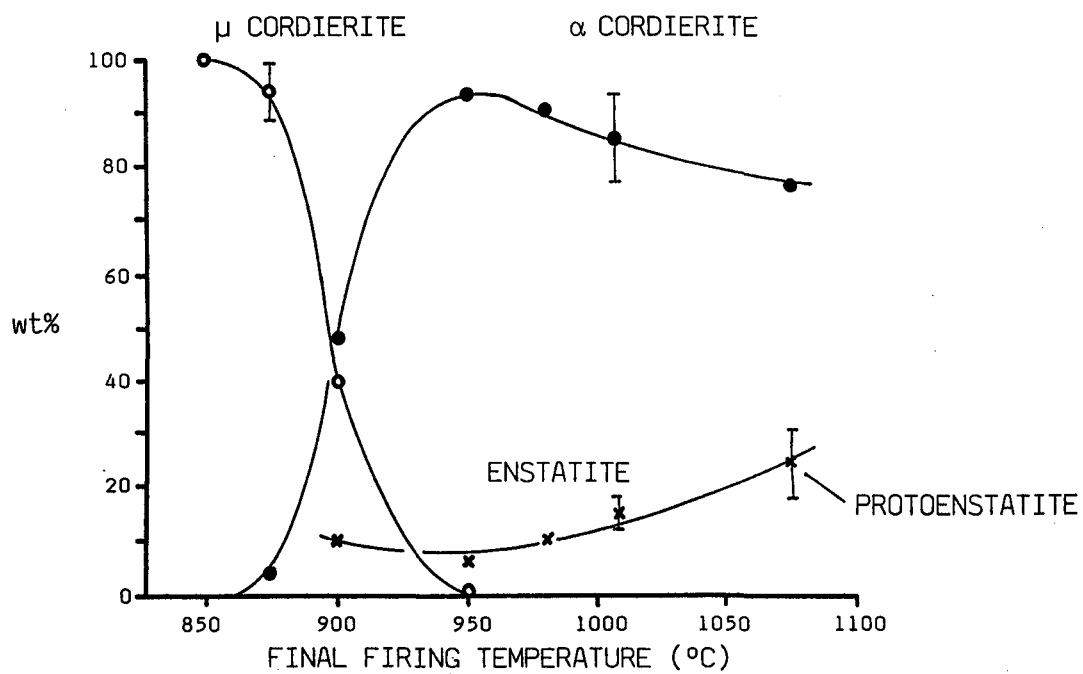
FIG.4.4 Phase evolution for C1 glass ceramic as a function
        of final firing temperature
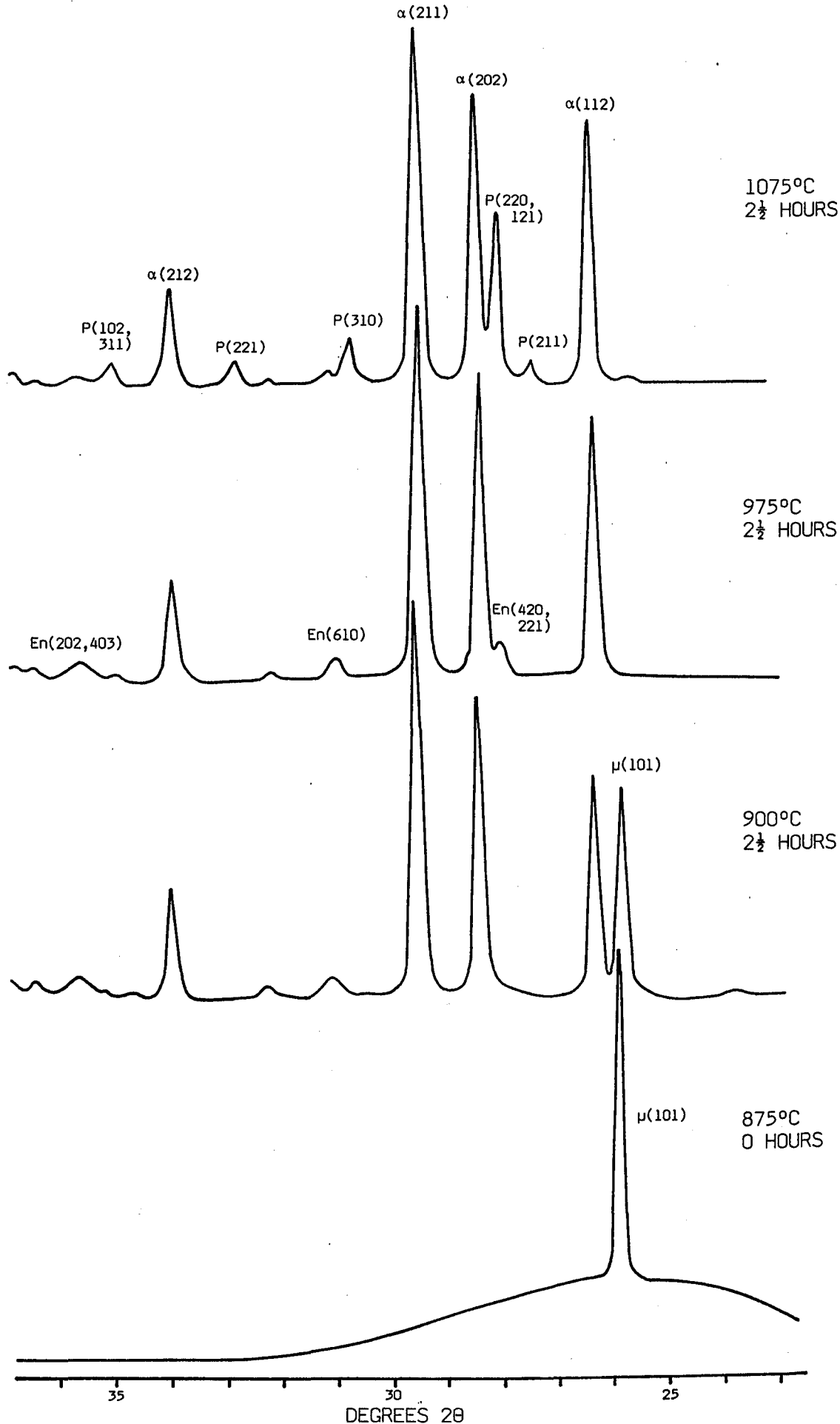
FIG.4.5 Change in some of the more intense peaks of the XRD spectra
as a function of phase content for Cl glass ceramic (En =
Enstatite, P = Protoenstatite)

observations made by Kumar et al (19) who describe a highly crystalline network around glassy domains which crystallize internally at a slightly higher temperature.

4.1.2 Phase and Microstructure Development Versus Final Firing Temperature

Phase evolution for composition C1 is shown in Fig.4.4 which gives the results determined from XRD studies. (Firing in N_2 resulted in an equivalent shift of the phase pattern by ~15°C to higher temperatures). Enstatite ($MgO.SiO_2$) was present as a minor phase, converting to the high temperature stable form, protoenstatite, in the region 1050°C. It should be noted that no residual glass phase could be detected by XRD on samples prepared at temperatures in excess of 900°C. Development of μ cordierite at low temperatures can clearly be seen, transformation to the stable α form occurring rapidly in the region 875-925°C. This is in contrast to MAS glasses with no additives where generally high heat treatment temperatures are required to initiate the transformation and the transformation itself is fairly sluggish (113, 114). At temperatures above ~960°C the amount of magnesium silicate phase appears to increase at the expense of α cordierite. This can also be seen in Fig.4.5 which shows the XRD patterns in the region of 20-30°2θ. μ cordierite is identified by the major peak at 25.8°2θ plus minor subsidiary peaks.

Combining XRD with TEM and SEM analysis, a clearer picture of phase development within the material is obtained. No apparent changes within

the melt occur with increased temperature but glasses quenched after heating to 850°C are clearly phase separated, as shown in Fig.4.6a. The short wavelength of the structure, ~100-150Å, the high degree of connectivity and diffuse boundaries are indicative of spinodal decomposition i.e. no nucleation of the second phase is required and the two immiscible phases separate out spontaneously (see Appendix I).

MAS glasses containing TiO_2 have been observed to phase separate readily (279), if heat treated just above Tg, into a high silicate phase and a magnesium/aluminium silicate phase, perhaps of metasilicate composition (280) and probably also rich in titania. The latter does not seem too unreasonable since magnesium dititanate is usually one of the first phases to appear (157). It is interesting to note that Zdaniewski (279) reports a nucleation and growth phase separation i.e. rounded droplets of one phase dispersed within a second, the boundary being fairly sharp.

Seifert et al (281) have investigated the possible structure of MAS based melts using Raman Spectroscopy. They postulated that the melt consisted of "Mixtures of three dimensionally interconnected rings with no Al^{3+} (i.e. 6 membered SiO_2 rings), rings with Al/Si = 1 (4 membered $Al_2Si_2O_8^{2-}$ rings) and rings with no Si^{4+} (6 membered AlO_2 rings)". The proportion of ring types was found to depend on the Al/Si ratio. Taking this into account, plus the observations made for the titania nucleated glasses, it would appear likely that the phase separated structure for these glasses consist of a silicon rich phase and a Mg/Al rich phase. It is possible that during the phase separation process some degree of ordering occurs within the individual phases. This may explain why the

(a)

150nm

(b)

150nm
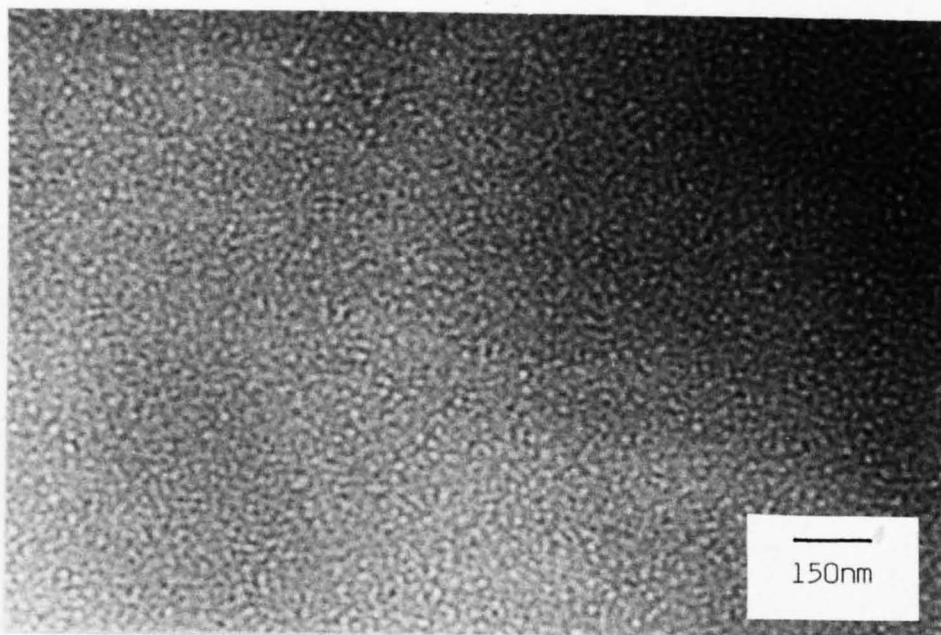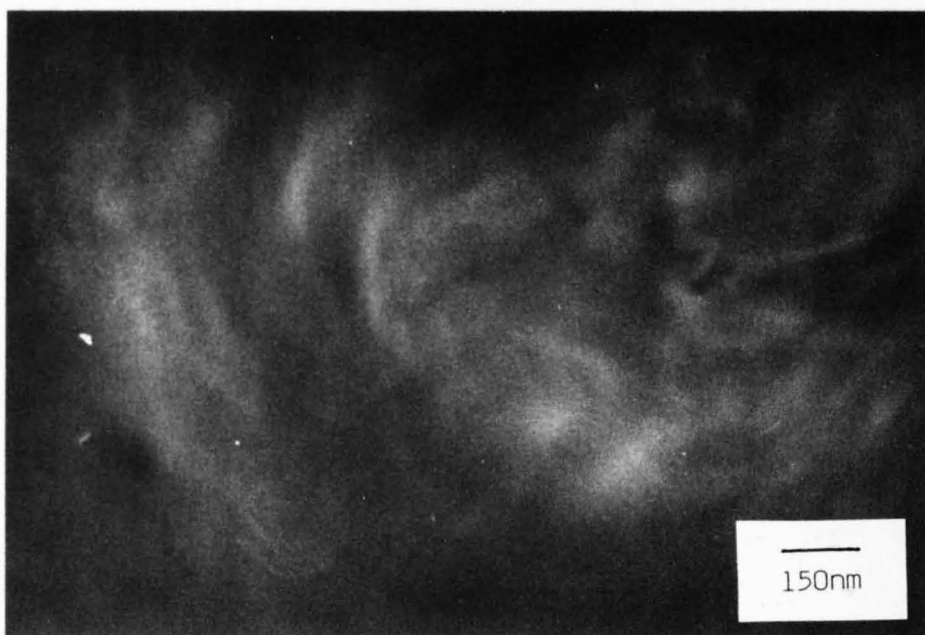
FIG.4.6 Cl glass (a) fired to 850°C and then
quenched (b) no heat treatment

enthalpy of crystallization for μ cordierite (50 ± 7 KJmol^{-1}), as reported by Carpenter et al (124), is low compared to that for the most disordered hexagonal cordierite (168 ± 6 KJmol^{-1}). The influence of phase separation on refractive index, n, has been investigated by Simmons (282) who found that for a borosilicate glass n decreased with increased heat treatment time. For the first ~30 minutes n increased however due to volume relaxation and this may account for why not all the heat treated specimens in Table 4.1 show a decrease, if indeed they all phase separate, compared to the unfired glasses.

That phase separation only occurs during heat treatment is readily shown in Fig.4.6.b which is of a material cut from a piece of bulk glass, from the same batch, but annealed at ~700°C for three hours. Therefore phase separation must occur at a temperature above this. That it is not an artefact of the carbon coating process is also shown, both specimens being coated under similar conditions, i.e. high vacuum and short coating time.

Either after or during phase separation the glass powder starts to sinter until a point is reached where the porosity is less than ~5% but the material is still glassy, Fig.3.13.b. Light etching of the surface at this point clearly shows the cohesion of the glass grains that has occurred during the sintering process. During the final stages of sintering crystallization of the μ phase takes the form of roughly spherical crystals, a few μm in diameter, around the old glass particle boundaries, Fig.4.2. (Takher et al (283) reported the two processes, sintering and crystallization, occurring concurrently for cordierite

based glass powders). This would indicate that nucleation has occurred on the particle surfaces prior to sintering.

As heat treatment continues the μ cordierite forms a continuous layer around the glass particles. Formation of this interconnected network helps prevent deformation through viscous flow of the remaining glass phase and is a necessary requirement in the firing of MLC's where close tolerances are required. Shortly after this the glassy domains crystallize to give μ cordierite but on a scale too fine to be observed directly by SEM. At about 875°C α cordierite starts to appear, followed shortly afterwards by enstatite. By 950°C the μ phase has all but disappeared and the α cordierite content is nearing a maximum.

The microstructural development as a function of final firing temperature is shown in Fig.4.7 for specimens fired to 875, 925 and 975°C. For the lower two temperatures the structure exhibits areas of quite dense crystal growth with clearer areas covered in a dendritic like growth. Although in some cases the dendrites appeared to be directed towards a central point (possibly a glass particle centre) most of the time the growth was more of a random nature. Material fired to 975°C yielded extensive crystallization although the crystallites had a more isolated appearance. Up to this firing temperature the overall density of the material had been steadily decreasing due to the formation of α cordierite (ρ= 2.51 g/cc). For samples fired above this temperature the density remained fairly constant, Fig.4.8.

Another interesting feature of the microstructure development is the
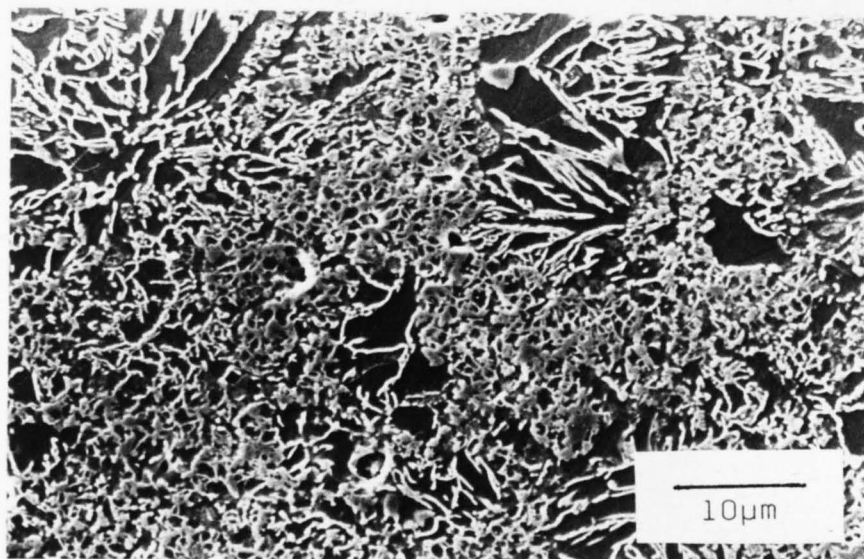
(a)
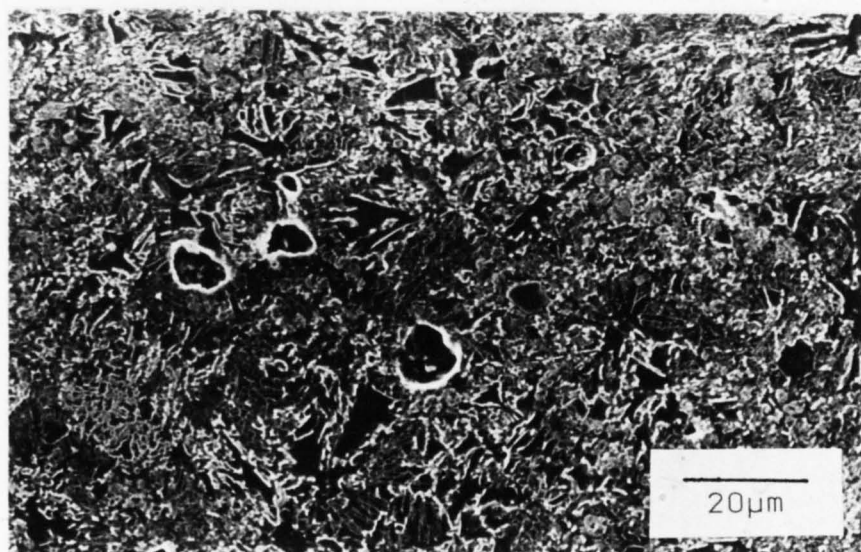
(b)
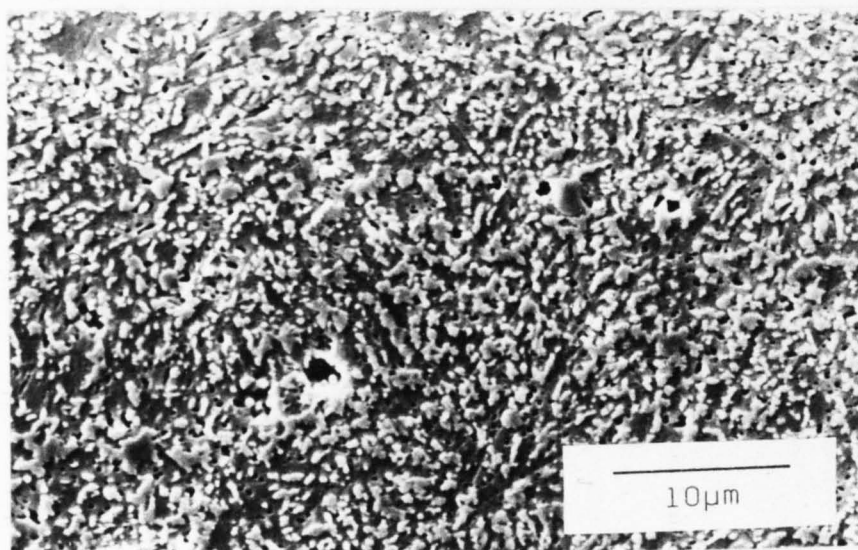
(c)

FIG.4.7 Microstructure of C1 (a) fired to 875°C (b) fired to 925°C (c) fired to 975°C
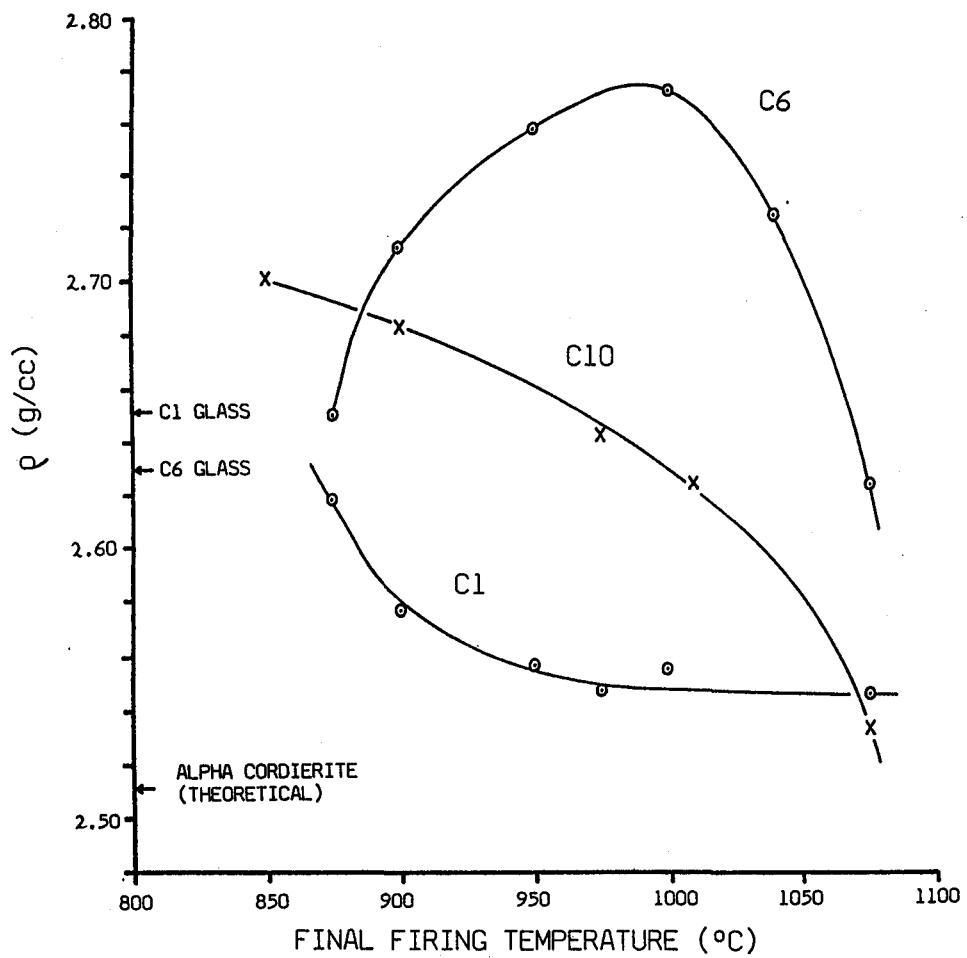
FIG.4.8 Change in density as a function of final firing
        temperature for three glass ceramic compositions
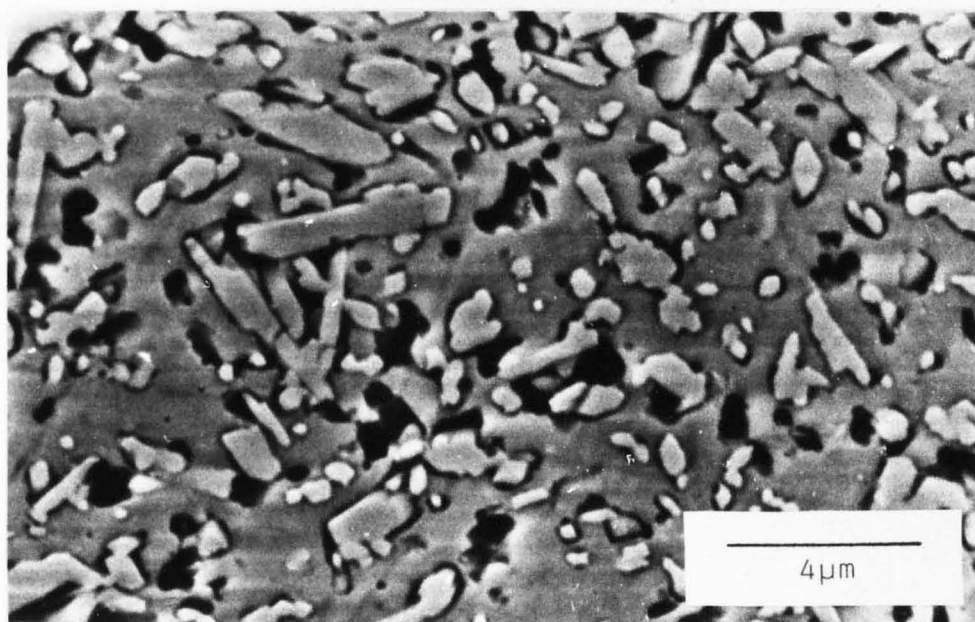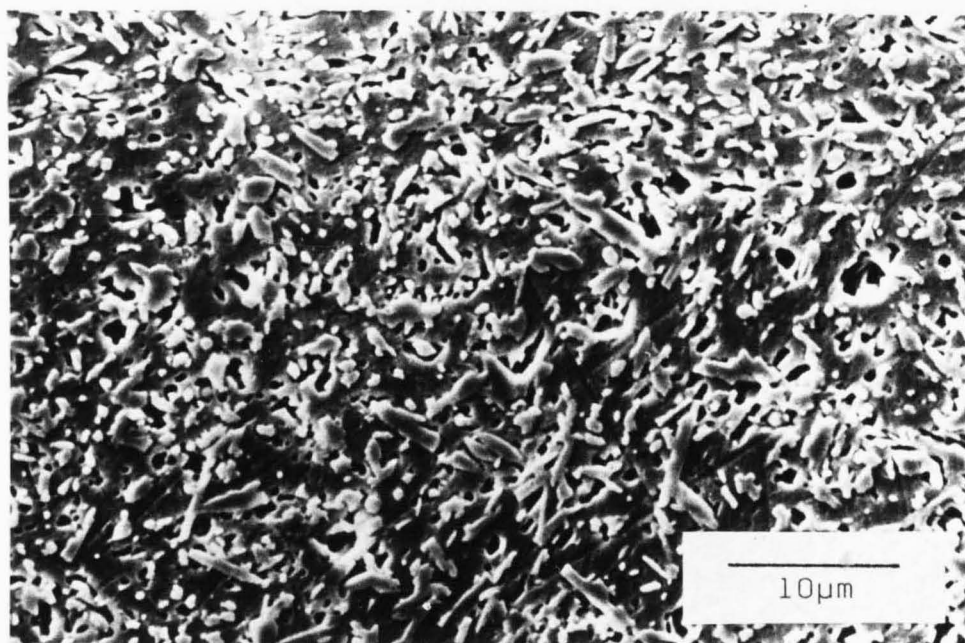
FIG.4.9 Microstructure of C1 fired to 1075°C

residual porosity which can be divided into two groups.

(a) Pores of a fairly coarse nature, typically 2-4 μm in diameter but generally less than 10 μm. These are probably the result of incomplete sintering and appeared to decrease in size and number as the heat treatment temperature was increased.

(b) Small pores, ~500nm in diameter that only seemed to appear during etching and were not present for material fired to 875°C. In an attempt to identify whether one particular phase was being preferentially removed or if it was just enhanced etching due to surface defects, a heat treated powder (975°C - 2½ hours) was X-rayed and then etched in a 2.5% HF solution for 30-45 seconds. After several washes in distilled water the powder was dried and another XRD pattern obtained. Comparison of the two spectra showed them to be 'identical' suggesting preferential etching of surface defects.

Firing the material to 1075°C had a marked influence on crystal morphology, as shown in Fig.4.9, the cordierite crystals growing and taking on a more facetted appearance. This facetting represents a change in the growth mechanism due to the lesser degree of undercooling at these higher processing temperatures. Watanabe et al (129) have examined the crystallization mechanism of cordierite from bulk glass, as a function of undercooling from the melting point (1370°C, for a composition very similar to that of C1). For large degrees of undercooling (~480°, i.e. fired to 890°C) cordierite crystals "had an irregular form having a cellular structure' and were formed by a continuous

growth mechanism. At about 280° undercooling (i.e. fired to 1090°C) they noticed a transition from a continuous to layer growth as the crystals took on a more prismatic form.

At these higher firing temperatures there is also an increase in porosity of the material and this would explain why the density does not increase (Fig.4.8) as one would expect for an increased protoenstatite content (ρ = 3.1 g/cc). The required porosity to give a net density of ~ 2.55 g/cc at 1075°C is ~5%, assuming the phase contents given in Fig. 4.4 are correct. This agrees with the experimentally measured porosity. The cause of this porosity may be attributable to density changes during the μ or enstatite inversions. It may also be due to thermal expansion mismatch between the low expansion cordierite phase and the high expansion protoenstatite (α = 98x10^{-7}°C^{-1} (284)) and/or residual glass phase.

The change in crystal sizes, as a function of final firing temperature, for all three phases is shown in Fig.4.10. The dimensions have been obtained for XRD line broadening. Clearly the measured size during crystallization and phase development is less than that depicted in Fig. 4.7 and the average size for μ cordierite is seen to decrease. This would agree with the idea of smaller crystallites forming in the glass after the initial surface crystallization. α cordierite crystals start very small, less than 100nm, which is unusual as one would expect them to be roughly the same size as the μ cordierite crystals if it is from
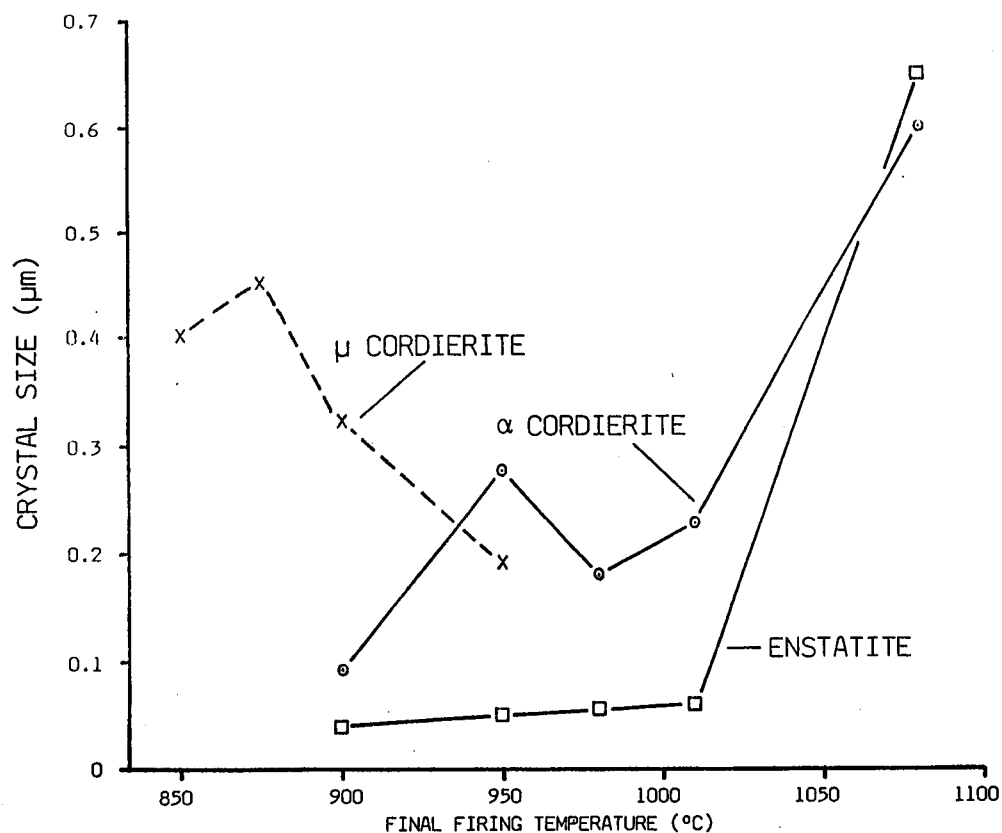
FIG.4.10   Variation in crystal size with final firing temperature
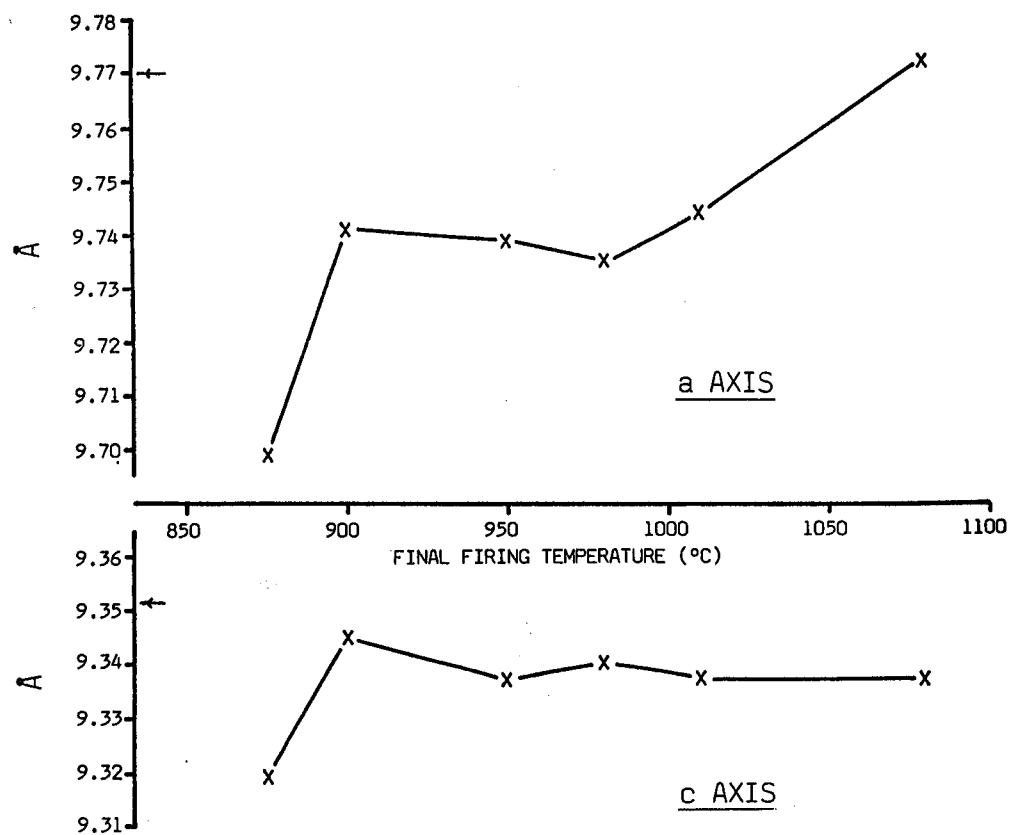
FIG.4.11   Change in lattice parameters as a function of final firing
temperature for Cl glass ceramic (alpha cordierite phase
only). ← Represent the J.C.P.D.S. quoted values (288)

these that they are transforming. It may be that the smaller crystallites transform first due to the higher energy associated with these particles and/or the difference in crystal morphology gives rise to a quite different shape factor, Ks (see equation 2.7). Enstatite crystals are also small and grow only slowly up to ~1000°C. Above this temperature the average size of both the α cordierite and enstatite/protoenstatite crystals increases rapidly. It could be that above 1000°C residual glass has become sufficiently viscous so as to act as an efficient diffusion path, thereby facilitating growth.

Careful examination of the XRD patterns shows that for μ cordierite the peaks are shifted to higher 2θ values (typically 0.1 - 0.2°) when compared to the pattern for stoichiometric cordierite. This may indicate that substitutional solid solution has occurred. Gossner (285) working on natural cordierites attributed the solid solution which gave rise to shifts to higher angles as being the substitution of Mg and Si for 2Al within the cordierite structure. Work by Iiyama has supported this idea (286). Thus shifts to higher 2θ values are not unexpected since C1 is rich in MgO and SiO_2 compared with the stoichiometric composition. For α cordierite, although there was an initial shift of 0.1° to higher angles, by 900°C and above the shift is in the region 0-0.05° which is within experimental errors. Consequently it would appear that during transformation there is a certain degree of exsolution, from the μ phase, of Mg and Si ions. This process would also aid the formation of enstatite. If one assumes that the maximum possible amount of stoichiometric cordierite forms from C1 then the ratio of excess SiO_2 to MgO is 1.53:1, the ratio required for the

formation of enstatite is 1.49:1. As an aside Toropov and Barazokovski (126) reported that irreversible breakdown of solid solution occurred above 1300°C yielding stoichiometric cordierite as one of the phases.

Fig.4.11 shows the variation in lattice parameter with final firing temperature for α cordierite (insufficient peaks being fully resolved for μ cordierite to accurately follow the trends). The change in lattice parameters for various isomorphous substitutions in α cordierite of stoichiometric composition has been investigated by Ikawa et al (287). They found that for Fe and Mn substitution for Mg, a_o increases but c_o decreases. For Ge substitution for Si and Ga for Al the effect was to make both a_o and c_o decrease. It can be seen that as the firing temperature increases, both a_o and c_o increase although by 1075°C c_o is still below the expected value of 9.352Å (288). This increase in lattice parameters indicates that changes are occurring within the α cordierite structure although Langer and Schreyer (289), heating a cordierite of stoichiometric composition, reported that the lattice parameters for both phases remained constant over the whole period of their existence.

4.1.3 Infrared Analysis

The IR spectra for these materials are shown in Fig.4.12 and depict the changes that occur as phase evolution progresses. Several observations can be made. The glass, as milled, exhibits a spectrum typical of silicate glasses which have strong absorptions in the region 1000 and 500 cm^{-1}, in this case the 1000 cm^{-1} peak being split into two components, one at 1070 and the other at 950 cm^{-1}. On phase separation the spectrum is similar except the 1070cm^{-1} peak is shifted to 1086cm^{-1}
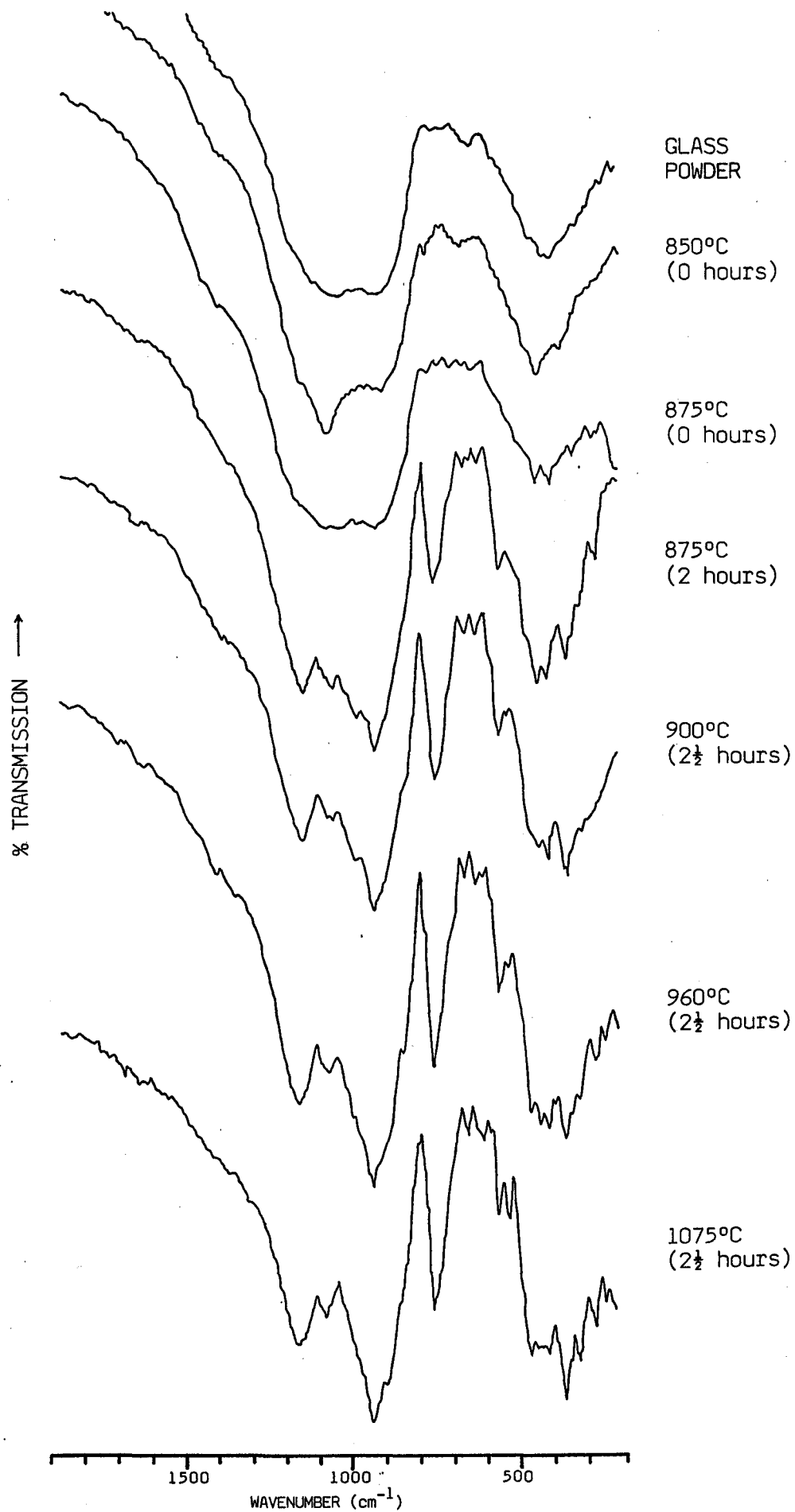
FIG.4.12   Change in IR spectra as a function of final
heat treatment temperature and time for Cl

and a shoulder appears at $1162 cm^{-1}$. Marked changes occur on crystallization including the appearance of peaks at 1160, 770 and $375 cm^{-1}$ and also a general sharpening and splitting of peaks.

This peak splitting has been examined by Langer and Schreyer (289) who found that it occurred for only up to about 10 hours at 1400°C but was not accompanied by a corresponding splitting in the XRD pattern, as confirmed in this case. They concluded that the IR splitting was caused by the first stages of the high to low cordierite transition and that the two techniques were measuring differing degrees of Al/Si ordering. IR is sensitive to short range order whilst XRD is more sensitive to long range and it is this long range ordering process which enables the latter method to account for the final increase in distortion index.

For the spectra collected for C1 there appears to be some confusion in assigning some of the peaks. For instance Langer and Schreyer (289) calculate the expected stretching modes for SiO_4 and AlO_4 to occur at 1085 and $960 cm^{-1}$ respectively, this calculation being based on empirical relationship by Dachille and Roy (290). The band at $1180 cm^{-1}$ was assumed to be sufficiently close to $1085 cm^{-1}$ to be due to SiO_4. This assignment seems a little strange since Al is a lighter atom (albeit only just) and one would expect the force constant to be greater (e.g. higher melting point) thus giving rise to a stretching mode at higher frequencies (equation 2.13). Indeed, the work by Tarte (291) on the $Al_2 SiO_5$ polymorphs clearly shows a strong absorption at $1200 cm^{-1}$ for sillimanite (which contains tetrahedrally co-ordinated Al) which is not

present either for andalusite (six fold) or kyanite (six and five fold
co-ordination). Farmer (292) attributes this vibration to the almost
linear Si-O-Al bond which occurs in silliminite. The occurence of this
peak even in the material containing μ cordierite may suggest why it is
shifted to the lower frequency of 1160cm^{-1}. Such linear linkages are
present in the hexagonal rings of the α cordierite structure but
initially the distribution of Al in ring sites is small (141).

Hutton and Thorpe (280), citing the work of Crozier and Douglas (293),
claimed that a shoulder at ~1200cm^{-1} on the 1080cm^{-1} peak is indicative
of a high silica phase in a phase separated glass, whilst one at ~950cm^{-1}
is due to a metasilicate phase. The sample in Fig. 4.12, which has been
heated to induce phase separation, indeed shows these two features,
although the peak at 1162cm^{-1} may be the precursor to the Si-O-Al
vibration. The peak at ~950cm^{-1} is associated with the Si-O vibration
within the SiO$_4$ tetrahedron (294). In alkali silicate glass systems the
normally triply degenerate F$_2$ vibration is resolved into a Si-NBO
stretching vibration at ~950cm^{-1} and a Si-O-Si vibration in the
environment of the modifier occurring at ~1050cm^{-1} (295). Careful
analysis of Fig.4.12 would suggest that for μ cordierite this F$_2$
vibration is actually resolved into its three components, a small peak
at ~1000cm^{-1} also being visible. It is interesting to note that in
enstatite, Estep et al (296) noted three peaks in the region 850-1050cm^{-1}
which they also assigned to the splitting of the Si-O stretching
vibration.

The peak at 770cm^{-1} has also caused some confusion as to its origin

(289, 297) since it is usually associated with ring silicates (298) of which cordierite is one but β quartz is not. The explanation would appear to be that it is due again to a Si stretching mode, activated in the β quartz solid solution phase due to a certain degree of deviation from cubic symmetry of the Si tetrahedra (299). The vibration of the Mg octahedra is described by Langer and Schreyer (289) as occurring at 580cm⁻¹ for α cordierite. The peak is also present in the spectra in which μ cordierite is dominant where it is thought that the Mg ion sits in a roughly six fold co-ordination within the spirals of the structure. Bachiorrini (300) however ascribes this vibration to ~420cm⁻¹ in cordierite where the Si-O-Si bending vibrations also occur. Finally the contribution from the magnesium silicate phase yields peaks roughly corresponding to that of the magnesium alumino silicate except for the peaks at 1180 and 770cm⁻¹ which are absent.

4.1.4 MAS NMR Results

MAS NMR has already proved to be a useful technique in investigating Al/Si ordering in zeolites (301-303) and has been used by Fyfe et al (141, 304), mainly examining the ^{29}Si resonance, in the study of the high to low transition in cordierite. Although they did examine freshly crystallized α cordierite (obtained from glass heated to 1185°C), see Fig.4.13a, the initial development of the μ phase and its transition to α cordierite is examined here in more detail. For convenience the (SiO$_4$) unit, where n = 0 to 4, is referred to as Q^n where Q^4 represents SiO$_4$ with no NBO's, Q^3 with one NBO etc. (232). Furthermore, A refers to a Si atom with one of the bonds linking, via oxygen, to an Al atom (the

CHAIN
SITES

RING
SITES

Si(3Al)

Si(2Al)

Si(3Al)

Si(4Al)

Si(1Al)

Si(4Al)

-70   -80   -90   -100   -110   -120
CHEMICAL SHIFT (ppm)

(a)

-30   -50   -70   -90   -110   -130   -150
CHEMICAL SHIFT (ppm)

(b)
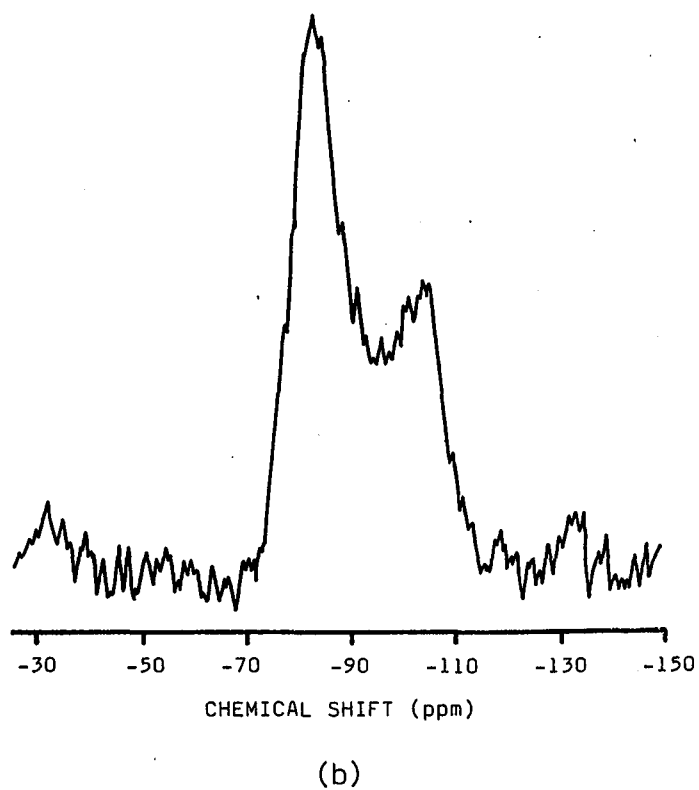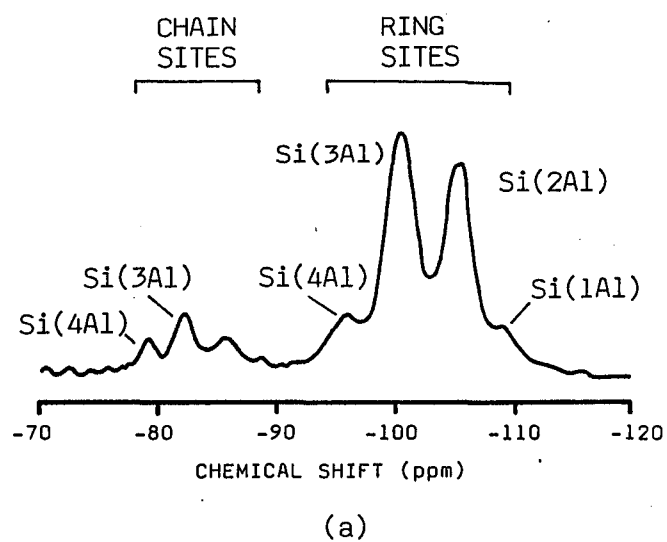
FIG.4.13 ^{29}Si MAS NMR specra for cordierite glass ceramic
(a) alpha phase after (141) (b) mostly μ phase

remainder via oxygen to other Si atoms or NBO's) and 2A is a Si atom with bonds to two Al atoms etc.

If for convenience one approximates the composition for Cl as 33 mole % MgO, 13% Al_2O_3 and 53% SiO_2 then the theoretical distribution of Q units can be calculated, assuming a binary type model. (This assumes that addition of a modifier to a silicate network gives rise to a Q^n/Q^{n-1} distribution, as opposed to a clustering of Q units or a random model, i.e. more than two Q units present at any one time, see Dupree et al (305, 306)). The distribution for the 53 silicons is calculated as $13Q^4$ (2A), $38Q^3$(2A) and $2Q^3$(A). The ^{29}Si resonance for the Cl glass is shown in Fig.3.2 and gives a broad peak centred at ~ -90ppm. Whether deconvolution yields any Q^4 contribution is highly questionable, especially since other factors such as 'phasing' during the Fourier transform can also affect the peak profile. A longer experiment yielding a spectrum of higher signal to noise ratio may help answer this question.

On crystallization of the μ phase the ^{29}Si resonance is not much changed from that of the glass, i.e. a broad peak ($\Delta\delta\frac{1}{2}$= 25ppm) centred around -90ppm. Material heat treated to give a cordierite content of $\frac{2}{3}\mu$, $\frac{1}{3}\alpha$ plus some enstatite shows a splitting of this peak to a relatively narrow one ($\Delta\delta\frac{1}{2}$ ~ 11ppm) centred around ~-82ppm plus a broader one at -105ppm, Fig.4.13b. Further heat treatment to give an approximate 90%α, 10% enstatite material shows a clear resolution of the second peak into two, as shown in Fig.4.14a, one at ~-101ppm and the other at ~-106ppm. This agrees with the spectra given by Fyfe et al (141,304) who assigned
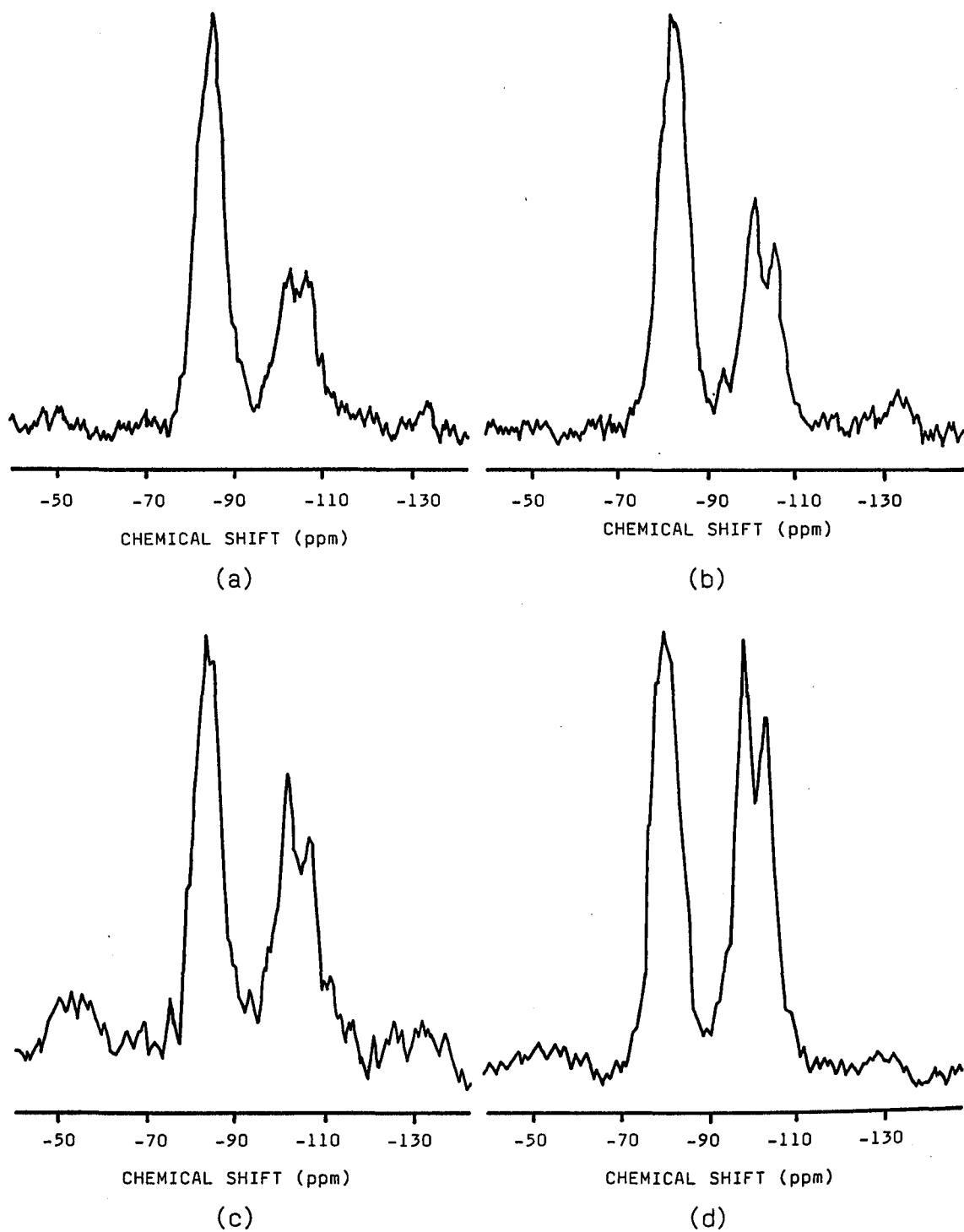
FIG.4.14 ^{29}Si MAS NMR spectra for alpha cordierite as a function of spin lattice relaxation time (a) RD=1 second (b) RD=3 seconds (c) RD=10 seconds (d) RD=30 seconds

GLASS
POWDER

850°C
(0 hours)

875°C
(0 hours)

895°C
(2½ hours)

950°C
(0 hours)

975°C
(0 hours)

975°C
(2½ hours)

300   200   100   0   −100   −200
CHEMICAL SHIFT (ppm)
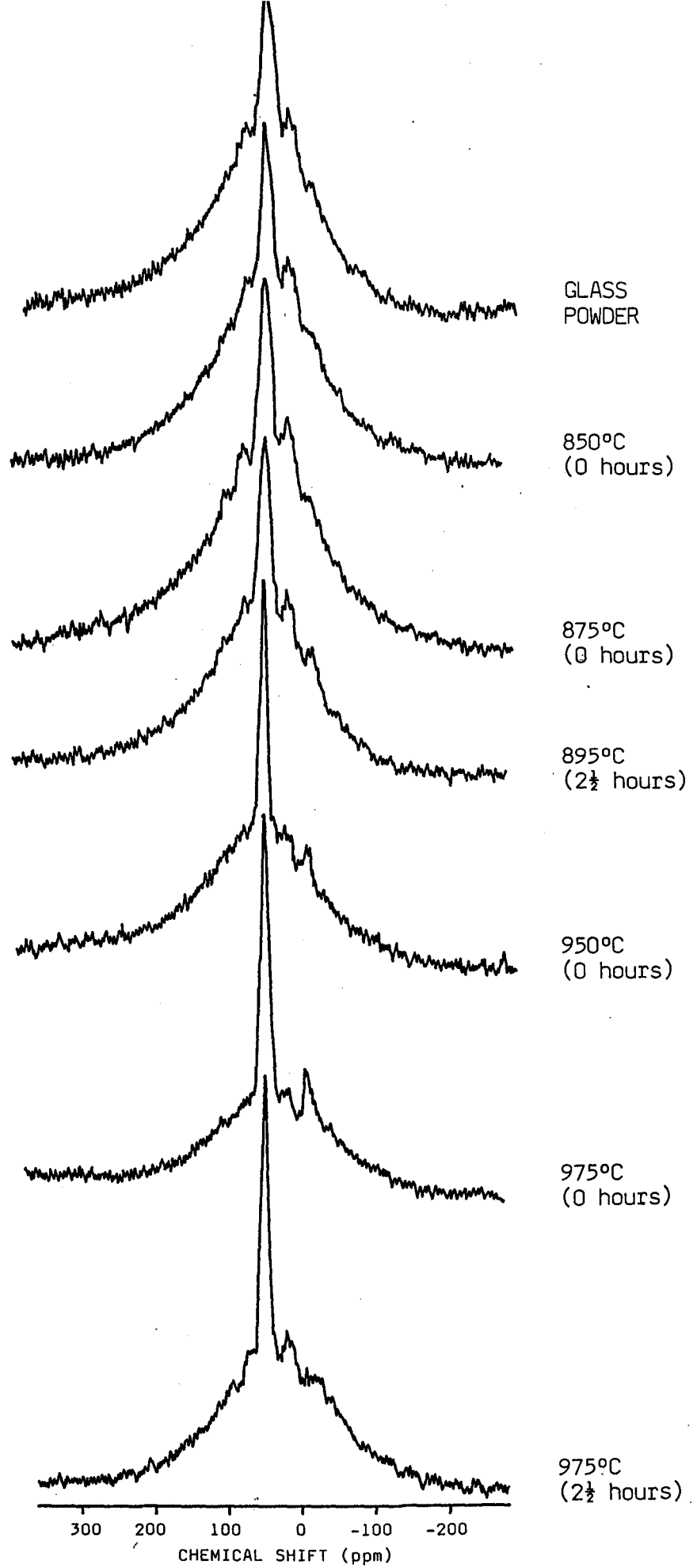
FIG.4.15 ^{27}Al MAS NMR spectra for Cl as a function of
heat treatment temperature and time

the resonances to Si bonding to 3 and 2 Al's respectively. The
exception is the large peak at ~-82ppm which is probably due to
enstatite (231).

The ratio of the enstatite peak to the two others however would suggest
that the material was composed of ~70% enstatite, contrary to other
results. Consequently more runs were done with varying times between
pulses (RD) from RD = 1 to RD = 30s and these are shown in Fig.4.14a to
d. As can be seen there is a gradual increase in the double peak, a
further indication that the Si giving rise to the peak at -82 ppm is in
a different environment to that in cordierite. A plot of RD versus peak
ratios was almost linear, indicating that very long spin-lattice
relaxation times would be required in order to give an accurate picture
of the system. Nevertheless, absence of other large peaks in the range
-80 - -90 ppm agrees with Fyfe et al that Si favours ring sites during
the initial stages of crystallization.

The development of the ^{27}Al spectra as a function of μ and α content is
shown in Fig.4.15. Several observations can be made: i) There is
little environmental change for Al in the phase separated glass ii) As
with Si, the Al environment in μ cordierite is rather distorted giving Δ
$\delta\frac{1}{2}$=17ppm, a noticeable narrowing occurring during the development of α
cordierite where $\Delta\delta\frac{1}{2}$ ~12ppm (the broad area below the peaks is also
thought to be due to a general distortion in Al sites giving an
incompletely averaged second order quadrupole interaction). iii) During
the initial period of α cordierite development a second peak appears
at 0 ppm. There is evidence for a 'feature' here even for the
glass but this is more likely

to be a result of a spinning side band and phase shifting during the data processing. iv) There is little shift of the main peak from around 58ppm.

Muller et al (307) have ascribed chemical shifts near 0ppm as corresponding to octahedral co-ordination while those from 50-80ppm are characteristic of Al tetrahedra. Thus it would appear that during the initial crystallization of α cordierite there is evidence that some Al is entering into octahedral co-ordination i.e. replacing MgO_6 either in the cordierite chain framework (as in Beryl) or in the enstatite. Fyfe et al (141) also reported a small amount of Al in octahedral co-ordination in their stoichiometric material (suggesting it is not substitution in enstatite) but they dismissed it as a trace impurity. This would seem to be an unlikely explanation, despite the sensitivity of the MSL 360 to Al, as there is no real evidence of a peak in the upper traces of Fig.4.15 and it is not in the expected position of a sideband. It is also possible then that some Al may assume a similar environment to Mg in the μ cordierite structure i.e. in a pseudo six fold co-ordination within the spirals, an observation also made by Beall et al (122) working on stuffed β quartz structures generally. If this were so however, it is likely that the site would be so distorted as not to show up in the resonance spectrum. Finally Selkregg and Bloss (146) have demonstrated the sensitivity of lattice parameter to the radius of the ion, Ra, in the octahedral site (a_0 increasing and c_0 decreasing to a point with increasing Ra). Thus variations of ions, other than Mg, in the octahedral sites may account for some of the perturbations in Fig.4.11.

4.2   <u>MAGNESIUM SILICATE AND ITS PHASE DEVELOPMENT</u>

Three polymorphs of $MgSiO_3$ are known to exist. Enstatite, the low temperature stable form, protoenstatite, the high temperature form and clinoenstatite, an unstable intermediate. The first two are orthorhombic whilst the latter is monoclinic. Their structures have been studied by several authors (308-311) and it is seen that all the atoms in the three polymorphs have practically the same x and y co-ordinates, their differences essentially lying in the z position of the Mg atoms. Foster (308) found that enstatite converted very slowly to protoenstatite at 1260°C. On cooling slowly this converted to clinoenstatite or, in the presence of mineralizers such as LiF or MgF_2, to enstatite. Rapid cooling resulted in protoenstatite at room temperature although it was not particularly stable, grinding being sufficient to convert it to clinoenstatite. Sarver and Hummel (284) found that in the presence of mineralizers enstatite converted to protoenstatite at 1042±3°C.

Due to the small crystal sizes and the relative similarity in atomic number of the elements involved, it was difficult to ascertain the location of the enstatite crystals within the overall material using back scattered SEM imaging. Knowledge of the cordierite development can, however, help to infer some details. For instance some enstatite is expected to be associated with the region of the initial growth of the cordierite crystal phase since the growing solid/liquid interface will have associated with it a liquid phase rich in rejected magnesia

and silica, the exact composition depending upon the composition of the cordierite. This would appear to be confirmed from EDAX results with regions around the edges of the old glass particles having an excess MgO content compared with the centre. There was little difference in SiO_2 content.

During the bulk crystallization of cordierite the enstatite can be assumed to be more intimately mixed with the other phase. That this is probable can be clearly seen in Fig.4.16. It shows the microstructure for glass of composition C2 fired to 1300°C for 5 minutes. The large, faceted crystals are α cordierite and the enstatite (as inferred from EDAX analysis) can be seen as smaller crystals within them. Also quite noticeable is the large degree of porosity, associated with poor sintering and rapid growth, both around and within the cordierite. This morphology agrees with that found by Watanabe and Giess (278).

4.3   CRYSTALLIZATION OF BULK GLASS

Work on bulk glass of composition C1 yielded some different trends compared to those of the powder. The initial stages of crystallization were examined by firing polished glass sections introduced into a furnace at 850°C for one, two and three hours.

SEM examination of glass fired for one hour shows small ($\sim$2µm), isolated leaf like crystals on the glass surface, Fig.4.17a. Subsequent polishing removed these crystals, proving it to be a surface phenomenon, whilst polishing perpendicular to the surface showed negligible
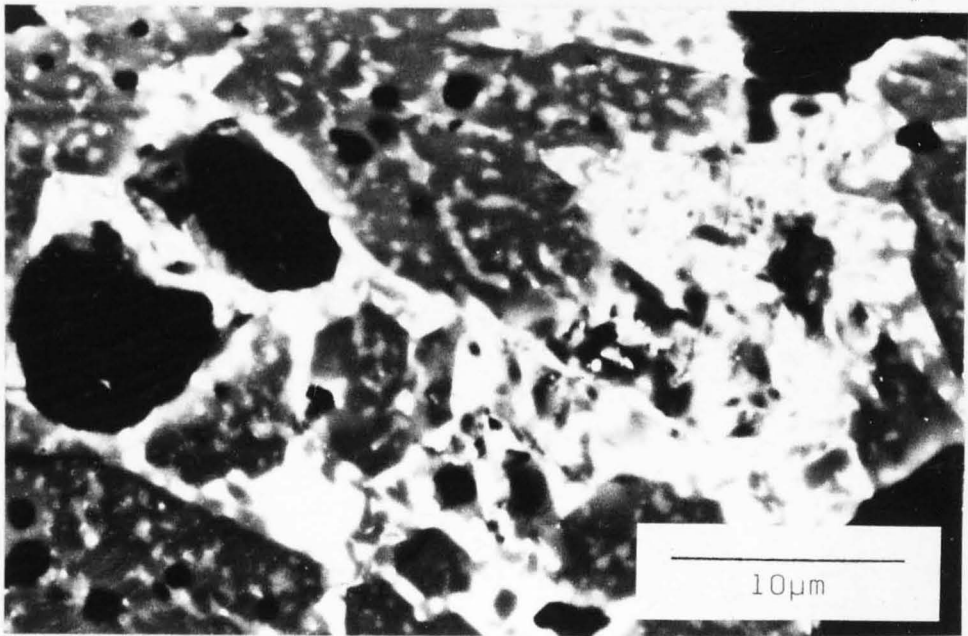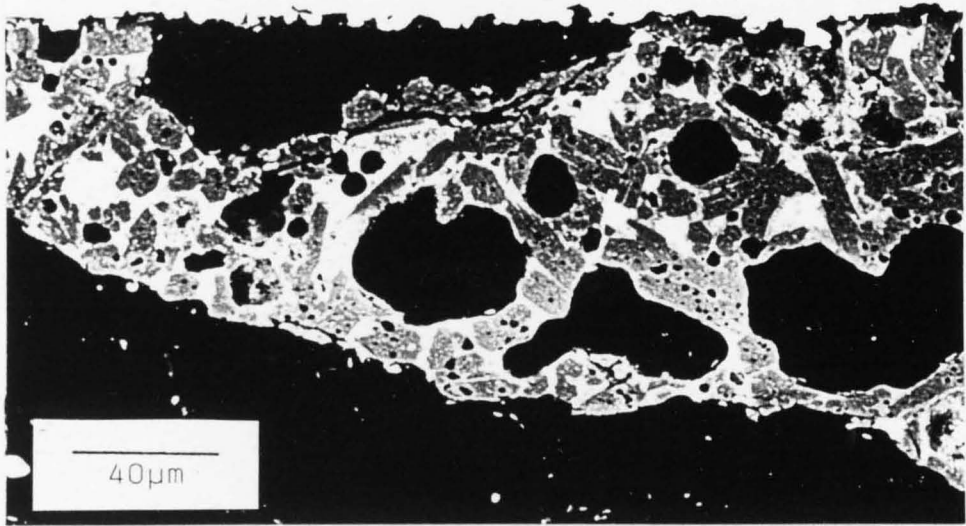
FIG.4.16   Microstructure of C2 glass ceramic fired
to 1300°C for 5 minutes
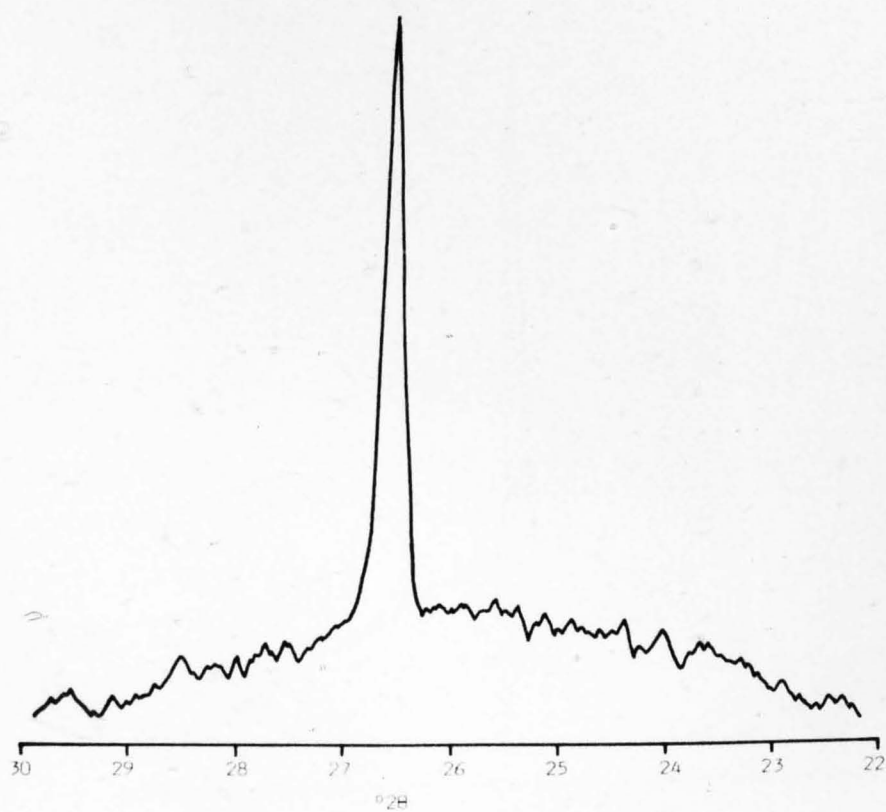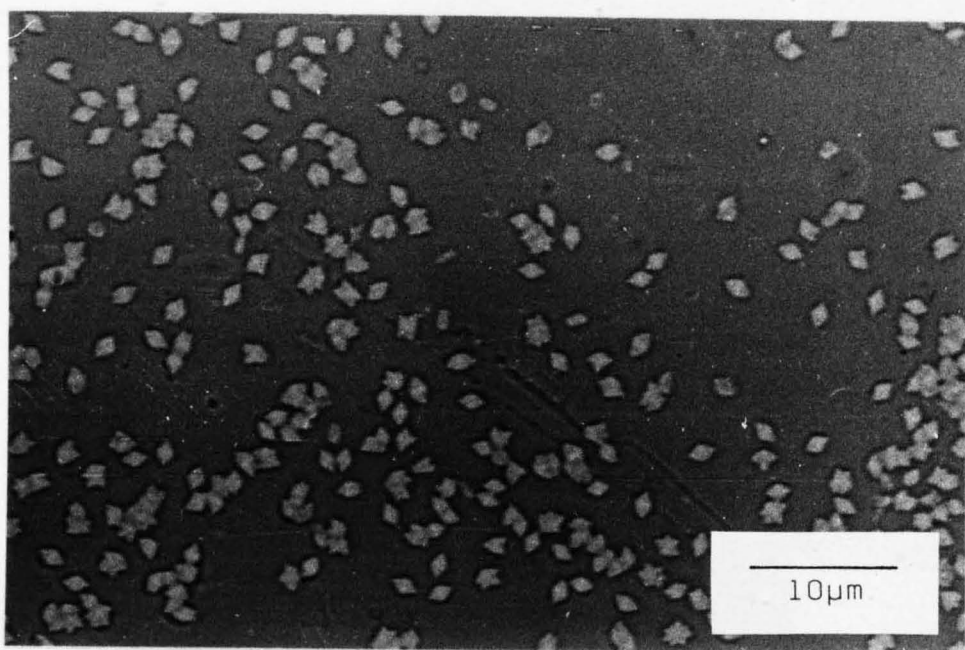
FIG.4.17a Crystallization on the surface of C1 glass
            fired to 850°C for one hour and the
corresponding XRD pattern
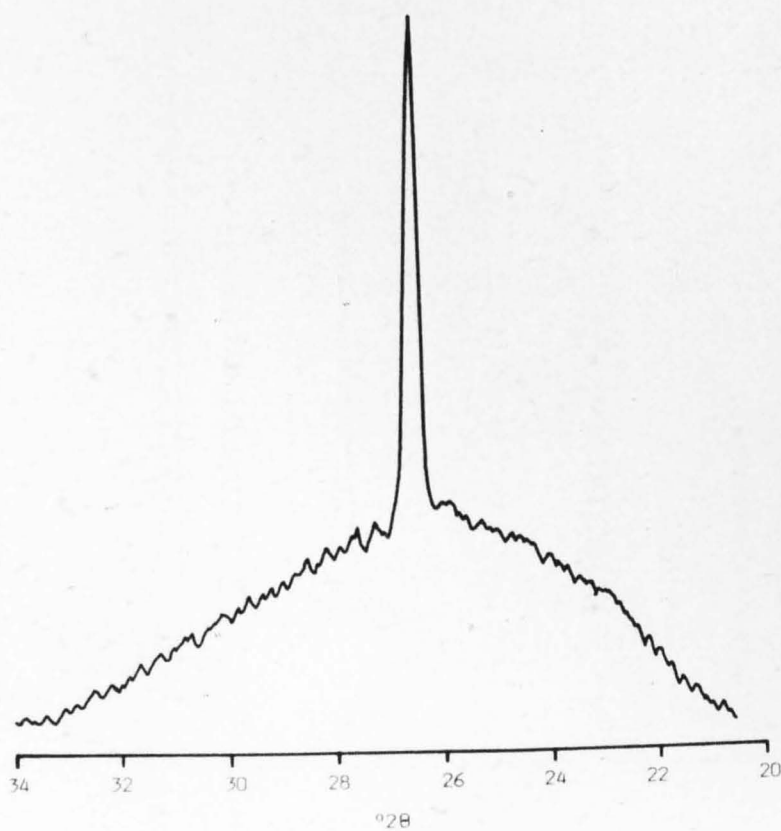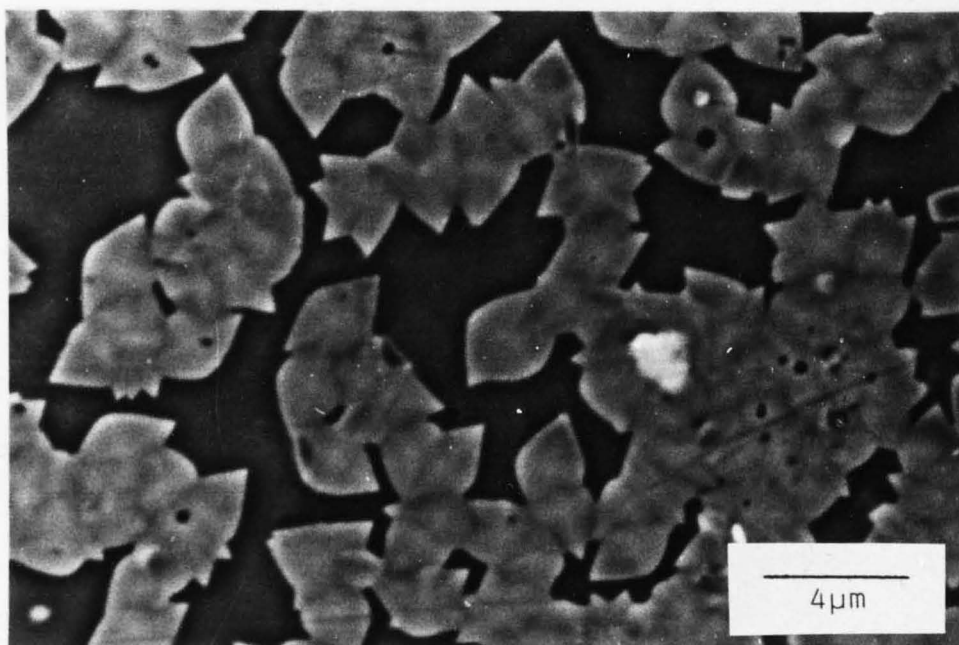
FIG.4.17b Crystallization on the surface of Cl glass
fired to 850°C for two hours and the
corresponding XRD pattern
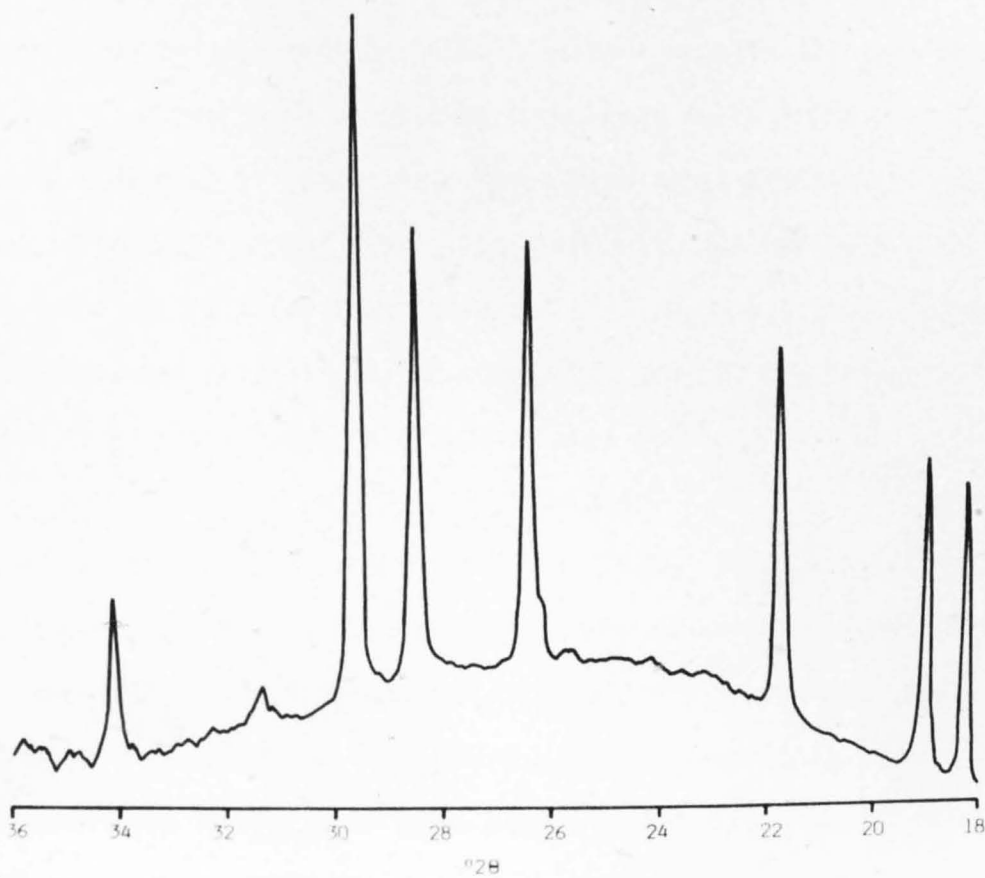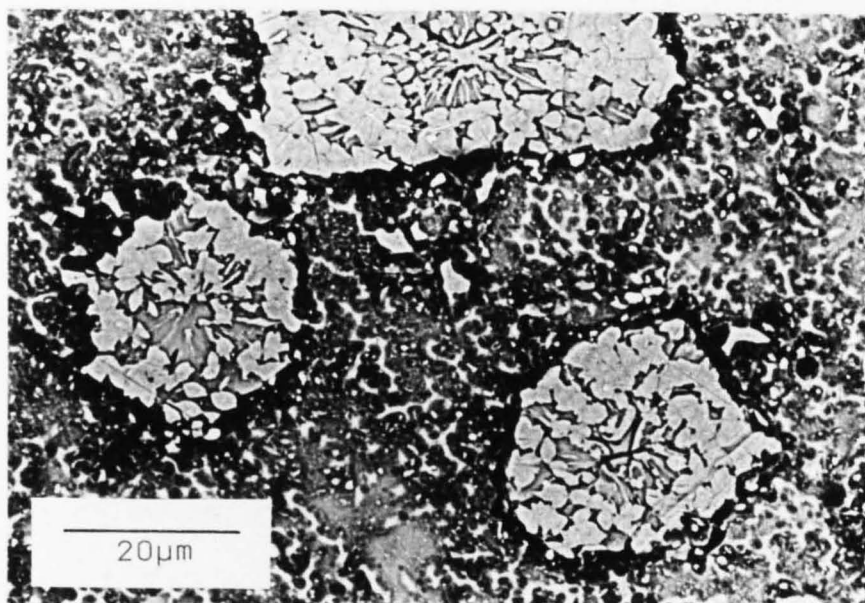
FIG.4.17c Crystallization on the surface of Cl glass
fired to 850°C for three hours and the
corresponding XRD pattern

penetration of crystallization into the bulk glass. The surface XRD
pattern is also shown for this material. The solitary peak at 26.5°2θ
(d = 3.363Å) could have two origins. Either it is due to preferred
orientation of the μ phase (no other peaks being visible) or it is
another phase. The first explanation would appear unlikely since the
main (101) peak for μ cordierite occurs at 25.8°2θ. For similar reasons
the phase is also unlikely to be 'pure' β quartz (main peak at 26.2°2θ)
or α quartz (26.6°2θ). Because of the peak location however this phase
will, for convenience, be referred to as a quartz like phase.

Glass fired at 850°C for two hours shows a similar surface covering,
Fig.4.17b, although the covering is a little more extensive. Again the
XRD pattern shows a large peak at 26.65°2θ plus a much smaller one at
37.95°2θ. It is interesting to observe from these micrographs that the
crystals all appear to be of the same size. Application of equation 2.7
however would indicate a mean crystal size somewhat smaller than that
observed visually, 389 Å for Fig. 4.17a and 724Å for Fig.4.17b. It may
be that the observed crystals may be composites and not single crystals
or that the shape factor used is inappropriate.

Glass fired for three hours at 850°C still exhibited the quartz like
growth but also yielded a large number of larger equisized prismatic
crystals, generally either rectangular or hexagonal in section. Again
polishing confirmed that this was a solely surface phenomena. XRD
showed however that both crystal types were α cordierite although there
was a remnant of the 26.6°2θ peak plus some enstatite. (Careful
re-examination of the one hour heat treated material showed that only

one larger 'faceted' crystal was present and a few were discernable for the two hour material. In both cases the crystals were poorly defined.) Analysis of the XRD pattern showed that the α cordierite exhibited preferred orientation. The degree of orientation can be defined by an XRD intensity ratio (312)

$$I = \frac{I(110)}{I(110) + I(002)} \qquad (4.1)$$

Where I(110) and I(002) are the peak heights from the reflections of the (110) and (002) planes which are respectively parallel and perpendicular to the c axis. The higher the concentration of crystalline c axes in the direction normal to the surface the greater the I ratio and vice versa. For a powder with a random crystalline orientation I was found to be 0.65. For the three hour material I was 0.49 ± 0.005. A polished section fired to 975°C for 2½ hours gave I = 0.66

Further examination of the XRD pattern shows a shift of ~0.15° to higher 2θ values for the three hour glass. Firing for 16 hours at the same temperature had little effect on the shift but the 975°C, 2½ hours glass exhibited a shift nearer to 0.1°. The shift of 0.15° represents a contraction of the c axis from 9.352Å (stoichiometric value) to 9.24± 0.09 Å, the a axis appearing unchanged. EDAX analysis of the quartz like crystals, Table 4.2, shows an increased incorporation of Mg at the expense of Al. Analysis of the larger crystals in Fig.4.17c gives a composition similar to that of the smaller crystallites but this is misleading since these occur on the crystal surface. Careful probing of

TABLE 4.2 EDAX ANALYSIS OF BULK C1 GLASS (IN WT%)

	NOMINAL COMPOSITION	EDAX GLASS COMPOSITION	QUARTZ LIKE PHASE 1 HR	QUARTZ LIKE PHASE 2 HRS	QUARTZ LIKE PHASE 3 HRS	FACETED α CORD. CRYSTALS
MgO	22.0	22.3±0.2	25.1±0.1	23.5±0.3	28.8±0.3	14.2±0.2
Al_2O_3	22.0	21.8±0.15	20.7±0.2	20.7±0.2	17.9±0.5	27.8±0.35
SiO_2	53.0	53.4±0.2	51.6±0.1	53.1±0.2	50.4±0.3	56.65±0.35
P_2O_5	2.0	2.5±0.05	2.6±0.05	2.8±0.1	2.9±0.1	1.3±0.15
B_2O_3	1.0					

the actual surface of the larger crystals, many of which appeared cracked, showed a composition nearer to that of the stoichiometric composition. (The calculated electron beam penetration depth using an accelerating voltage of 10KV was found to be a little over 1 µm (313)).

Thus for the bulk glass it would appear that an unidentified quartz like phase is the precursor to the formation of α cordierite and that the smaller crystals may, possibly through a match in lattice parameters, stimulate the growth of the larger hexagonal crystals. Deviation from stoichiometry may explain the contraction of the c axis but this is not matched by a change in the a axis.

4.4   PHASE DEVELOPMENT FOR COMPOSITIONS C3, C4, C5 and C6

In an attempt to understand the role played by the minor constituents in the base C1 glass four further compositions were examined. C3 had no added P_2O_5, C4 no B_2O_3, C5 had P_2O_5 replaced by TiO_2 and C6 had no additives, see Table 2.1. In all cases the ratio of $MgO:Al_2O_3:SiO_2$ was kept constant.

Phase evolution and approximate content as a function of final firing temperature for the four glass ceramics is shown in Fig.4.18. Several observations can be made. In all materials enstatite was found to be present in generally larger quantities and was of two types. The first to crystallize corresponded to the synthetic form (314), represented by the dashed line in Fig.4.18, this later transforming to the more ordered variety, as present in the C1 material (315). Again there was a shift
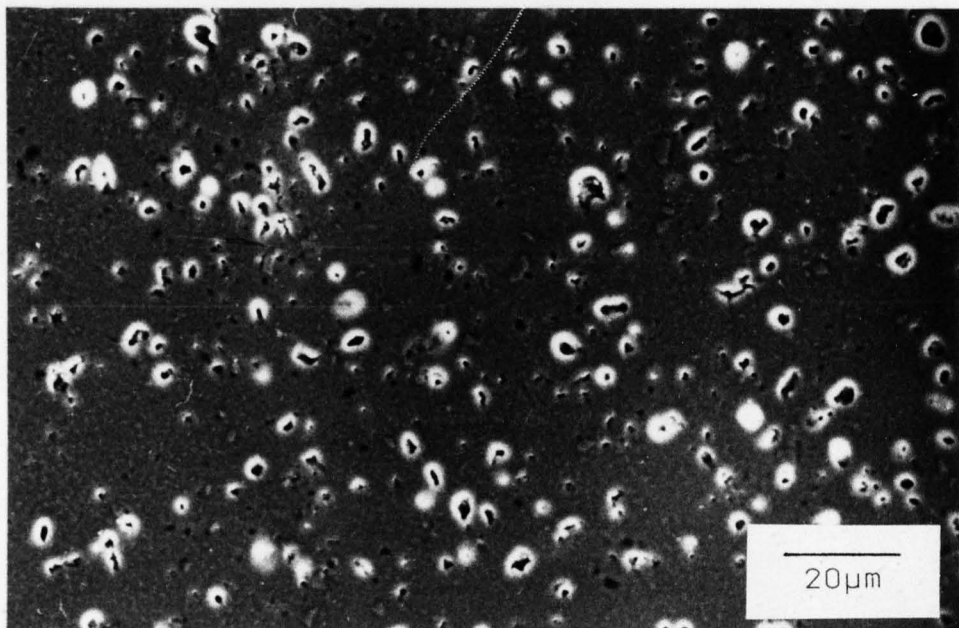
FIG.4.19 Microstructure of C5 fired to 975°C
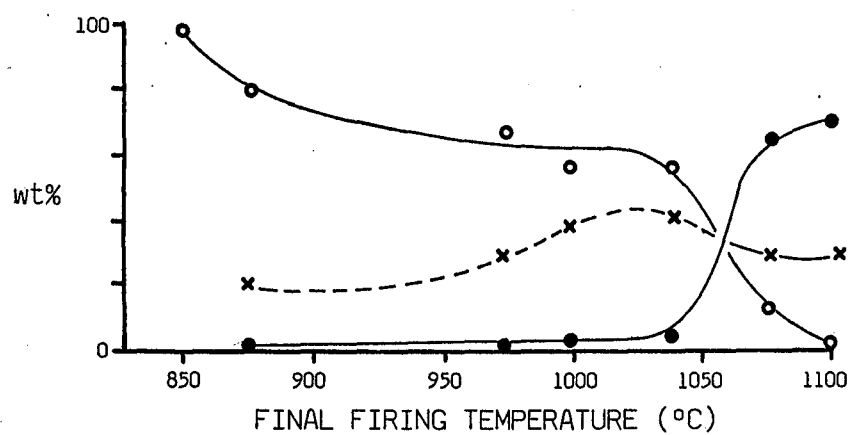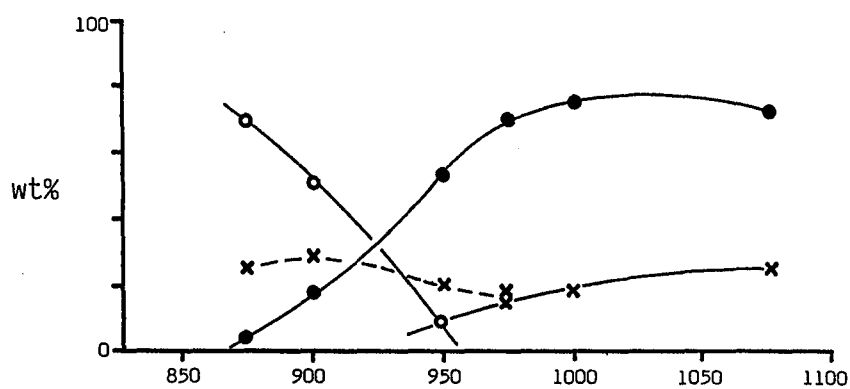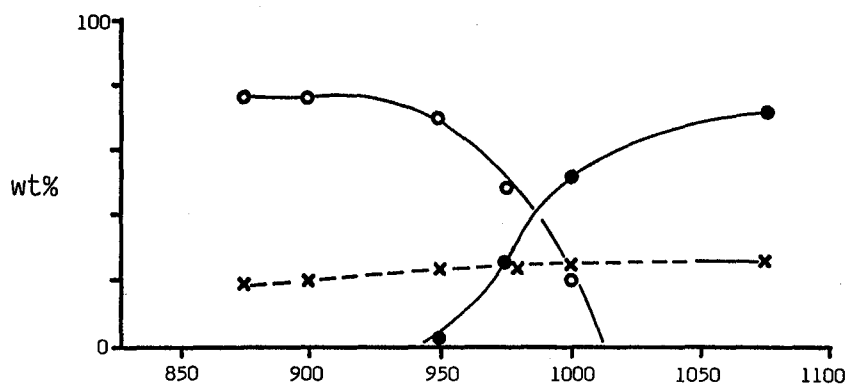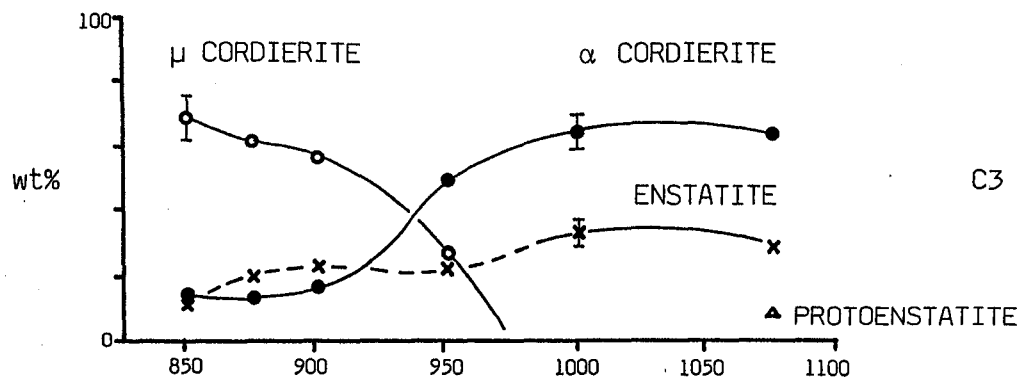
FIG.4.18 Phase evolution for four glass ceramic compositions

to higher 2θ values for the XRD peaks, especially for C4. Here, for μ cordierite the shift was 0.15° at 875°C and 0.35-0.4° at 1000°C. In all cases the shift for α cordierite at 1075°C was much reduced. All four materials had the μ to α transition shifted to higher temperatures, especially for C6, although for C3 and C6 some α cordierite was found to be present at low temperatures, ~850°C. In all cases the transformation itself was fairly sluggish and C6 had residual glass phase present, as discerned from the XRD pattern, up to 1100°C.

The microstructural developments were not too dissimilar to that for C1 except that at all temperatures quite large pores, typically 5 μm across, were present. This was particularly so for C5, Fig.4.19 and could be due either to failure to sinter or to thermal expansion mismatch between the high expansion enstatite and the lower expansion cordierites. The nature of the pores, i.e. roughly spherical, would imply that the former was more likely. That C5 is quite porous and yet still gave a higher final density compared with other materials (Table 3.2b) is a reflection of the increased enstatite content since enstatite has a higher density compared with cordierite (3.19 g/cc to 2.51 g/cc). TEM analysis of C6 showed that the heat treatment process also gave rise to phase separation although firing to 850°C and then quenching showed that the size of the separation was on a finer scale compared with C1.

Since C6 material has no added minor constituents and μ cordierite is present to higher temperatures it was decided to examine this material in a little more detail. The crystallization activation energy was calculated from the DSC curve and came out to be mE=875±30KJmol^{-1}. This is to be compared with a viscosity activation energy of 712±10KJmol^{-1}.

(As expected the latter is similar to that of C1 since B_2O_3 and P_2O_5 have roughly equal and opposite effects.)

The change in lattice parameters for both μ and α cordierite are shown in Fig. 4.20 as a function of final firing temperature. As can be seen, on the initial crystallization of the μ phase there is a rapid decrease in a_o and increase in c_o. For their materials, Barry et al (156) ascribed this to exsolution of Mg and Al with the corresponding formation of spinel, the exsolution rate being found to depend on heating rate and nucleation catalyst. Above 875°C the trend of the cell parameters is reversed, suggesting some sort of back reaction, ultimately aiding the formation of α cordierite. To suggest that changes in lattice parameter wholly describes exsolution or dissolution is not correct however, since it is likely that order/disorder effects within the lattice will also alter the values for a given solid solution (316, 317). For α cordierite there is a small increase in a_o and a decrease in c_o as the firing temperature increases except above ~1050°C where both decrease more sharply. This temperature corresponds to the rapid evolution of α cordierite and is opposite to that found for the C1 material.

A study of the IR spectra as a function of final firing temperature yielded similar results to those of C1 although some of the peak intensities were different. Also the amount of peak splitting by 1075°C for the α cordierite was, as expected, much less than that found in the corresponding spectra for C1. Finally the 27Al MAS NMR spectra was also found to be similar to that of C1, Fig.4.21. The peak at ~13ppm is due
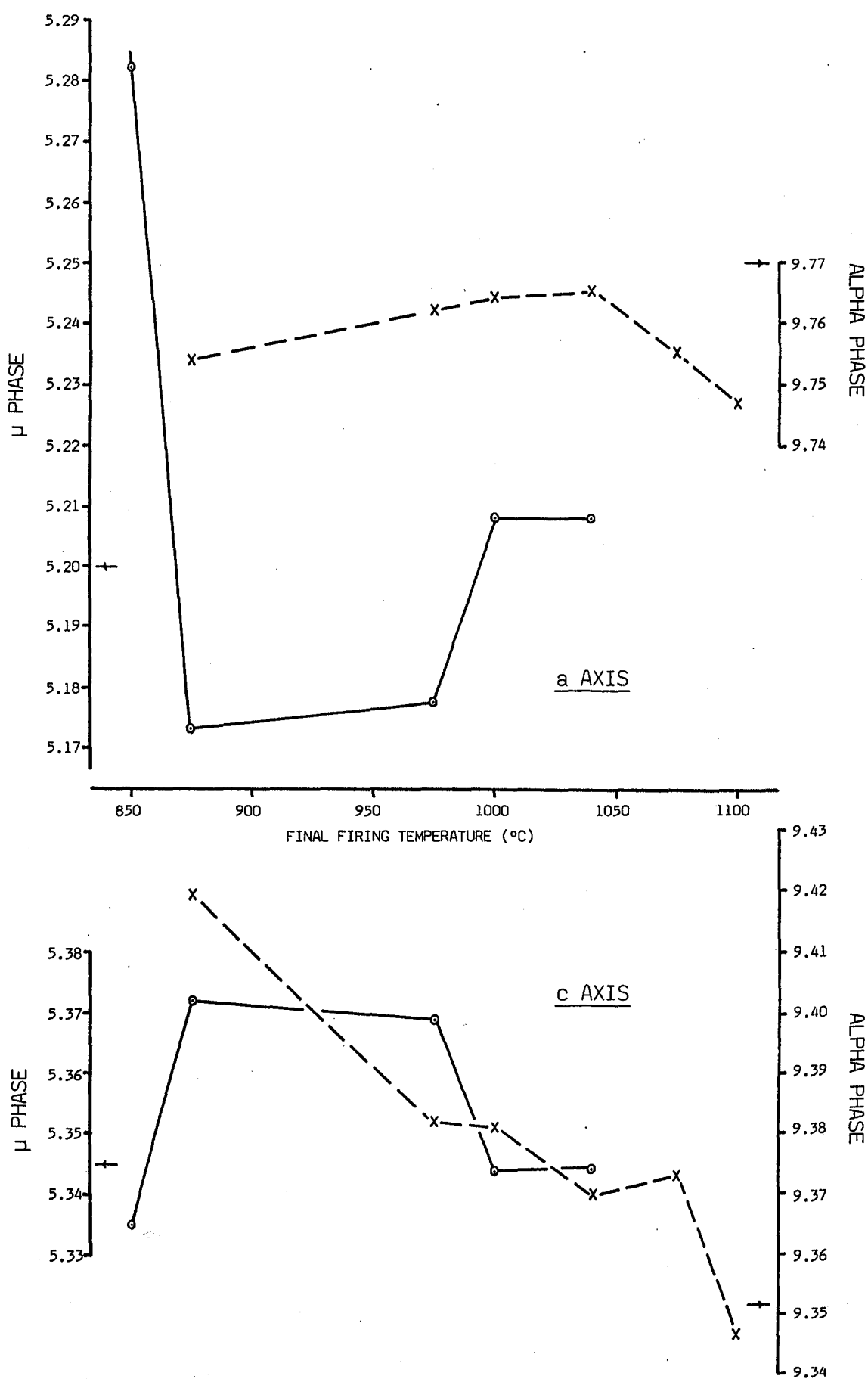
FIG.4.20 Change in lattice parameters of both cordierite phases for C6 glass ceramic. ← Represent the J.C.P.D.S. quoted values

MILLED
GLASS

900°C
2½ HOURS

1100°C
2½ HOURS

CHEMICAL SHIFT (ppm)
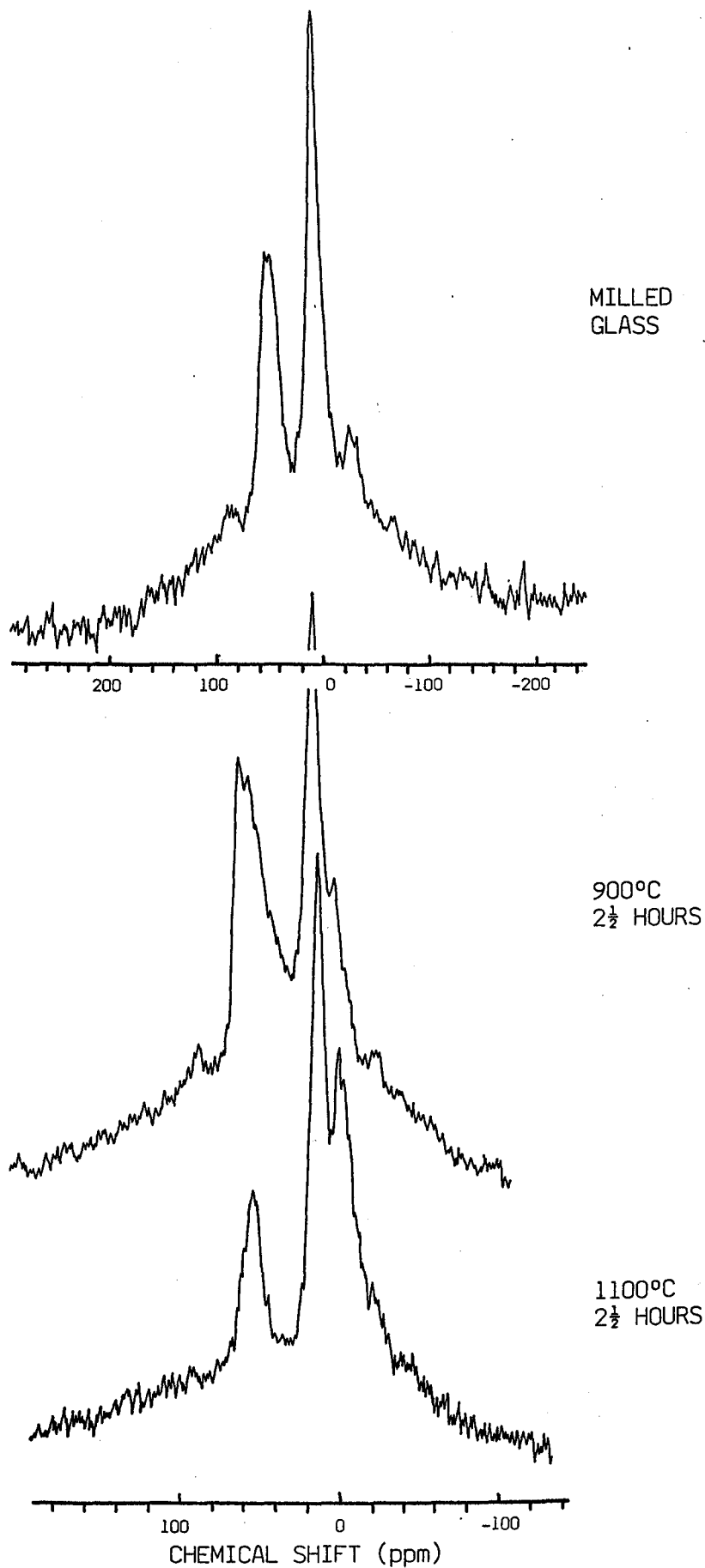
FIG.4.21 ^{27}Al MAS NMR spectra for composition C6

to the Al from the grinding media. The peak at ~52ppm for the mainly α cordierite material is still quite broad, $\Delta\delta_{\frac{1}{2}}=22$ ppm, suggesting a wider range of Al environments and again a small peak at ~0 ppm is present, suggesting some Al's are in an octahedral environment.

4.5 THE ROLE OF B_2O_3 AND P_2O_5

For this work B_2O_3 was added to aid melting and P_2O_5 to lower the viscosity and to act as a nucleation catalyst. Dietzel (318) has shown that as little as 0.1% B_2O_3 added to a batch can lower the melting temperature by 10%. There are several mechanisms by which this action works (319): i) Liberation of H_2O from the boric acid pulls grains closer together through surface tension effects. ii) B_2O_3 itself reduces surface tension and hence improves wetting of the other components iii) A flux forms at ~500°C accelerating the reaction between the other components. The role of B_2O_3 and its effect on the silicate network is uncertain since it is known to exist in several co-ordinations (see Konijnendizk (320)) although in the small concentration used here it probably resides in tetrahedral co-ordination and has associated with it a charge compensating ion.

P_2O_5 has been found to be an efficient nucleation catalyst, only a few wt% being required to nucleate a whole range of compositions. Just how this is achieved is uncertain but it is probable that prior phase separation plays an important role. The instability of P_2O_5 within the silicate network results from the strong P=O bond, large deviation in symmetry of its tetrahedra and difference in charge for the Si ion. In

the presence of Al_2O_3 the picture becomes more complicated since Al_2O_3 tends to stabilize the P ion (321). This is because the average ionic charge of Al plus P is equal to that of Si i.e. $(3^+ + 5^+)/2 = 4^+$ and the average size of an Al-P tetrahedral unit is similar to that of the surrounding silica network i.e. 0.50Å (Al) + 0.34Å(P) = 0.84Å compared with 2 x 0.41Å (Si) = 0.82Å. That P_2O_5 alone is a prerequisite for phase separation however is not true since as it has been observed in certain unadulterated compositions of lithium silicates and MAS based glasses (280) plus the direct observation for the C6 glass.

From Table 4.1 it can be seen that absence of B_2O_3 and P_2O_5 from the melt (composition C6) increases the onset of Tg although overall there is little variation in refractive index. The influence of both B_2O_3 and P_2O_5 on the crystallization kinetics can be best examined by comparing the DSC curves for the relevant compositions, Fig.4.22. Clearly, even at the low concentrations that each was added, there is a noticeable difference in the onset of crystallization. (Onset being taken to be that temperature at which the signal deviates significantly from the base line.) This is particularly so for materials where P_2O_5 has been excluded, i.e. C3, C5 and C6, where there is a noticeable shift to lower temperatures compared with C1. Observations made by Kumar et al (19) suggested that the action of B_2O_3 in MAS based glasses was to delay the onset of crystallization until sintering was near completion. The DSC results however would indicate that this is the role played by P_2O_5. Crystallization does appear to start at a lower temperature where B_2O_3 is excluded (C4) but the rate of crystal growth is slower such that the peak occurs at the same temperature as for C1. The low onset
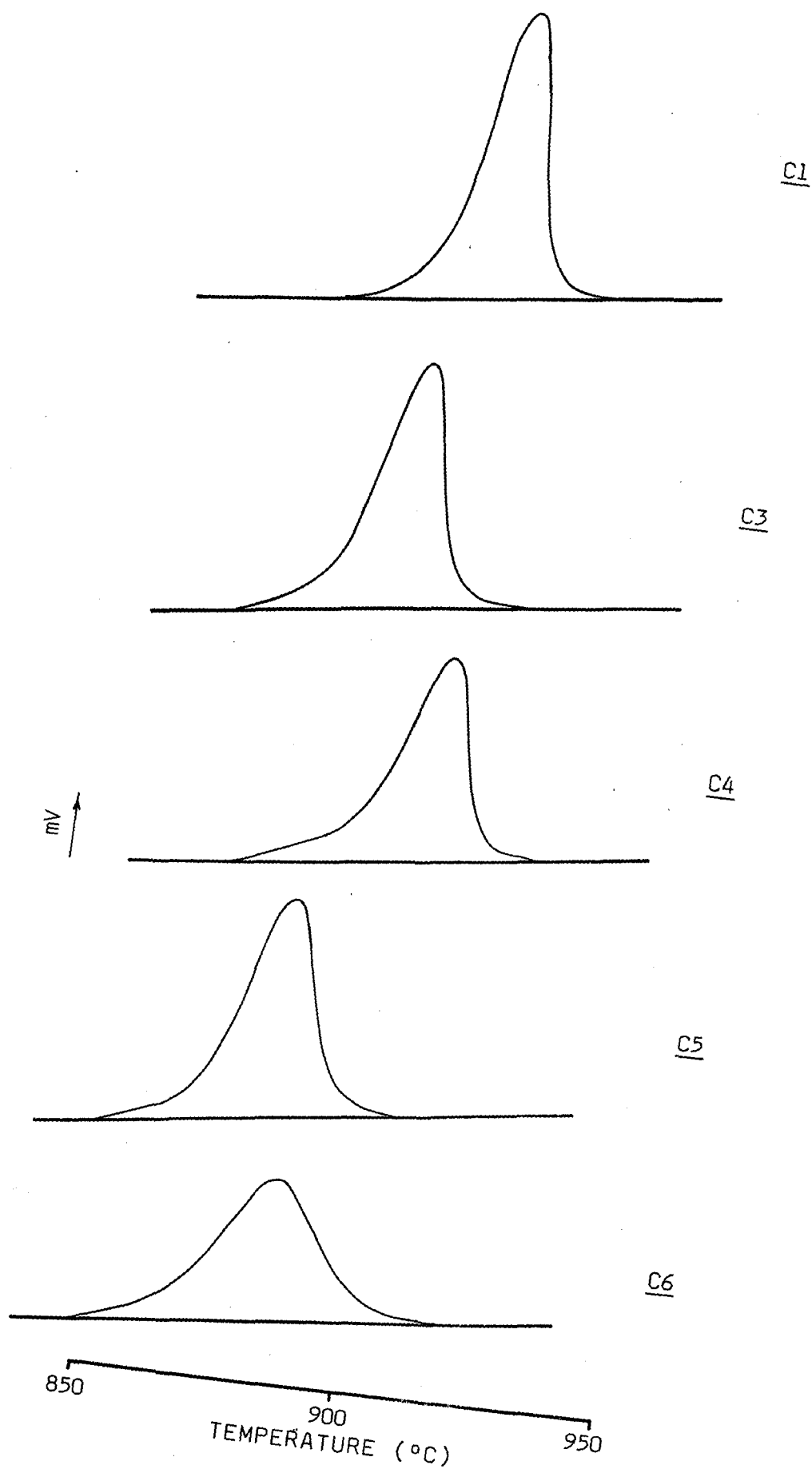
FIG.4.22 DSC curves for various compositions

temperature for C5 explains why this material was found to be quite porous, crystal growth initiating around 850°C inhibiting complete densification.

That both B_2O_3 and P_2O_5 play an important role in crystallization kinetics can be clearly seen in the comparison of Fig.4.4 with Fig.4.18. It is especially noticeable when comparing C1 with C6 where both oxides are excluded. The μ to α transformation has been examined by Topping and Murphey (322). They found that the α cordierite structure could accommodate up to 20 wt% $AlPO_4$ although for μ cordierite it was slightly less. The substitution is presumably $2Si^{4+} \rightleftharpoons Al^{3+} + P^{5+}$. Inclusion of P in the tetrahedral sites in the cordierite structure would be expected to have a marked effect and this may account in part for the observed distortion of the Al tetrahedra as seen in the ^{27}Al MAS NMR spectra. Topping and Murphey also found that addition of $AlPO_4$ to μ cordierite reduced the μ to α transition temperature,~20wt% giving a reduction of 75°C. Thus it would seem that the high field strength of P^{5+}, (43.0), lends itself to greater instability of the μ cordierite structure. 2wt% alone could not account for the observed difference between the transition in C1 (~900°C) and in C6 (~1050°C) and consequently B_2O_3 must also play an important role. It is interesting to note that B^{3+} has a very high field strength (75.0) compared with that of Si^{4+} (23.8).

CHAPTER FIVE - MATERIAL PROPERTIES

5.1   PROPERTIES OF C1

A resume of material properties which were measured for C1 material

fired to 975°C is given in Table 5.1. For comparison typical values are

also given for a cordierite refractory, a commercially available titania

nucleated cordierite (Corning 9606 selling under the trademark

"Pyroceram") and alumina.   Data was taken from a number of sources (10,

42, 99, 323). As can be seen, from a device substrate point of view,

the C1 glass ceramic offers improved properties compared with those of

alumina. The derivation of some of these properties will now be

discussed in a little more detail.

5.1.1 Thermal Characteristics

Thermal expansion measurements on cordierite have been made by a number

of authors (312, 324-329) since the primary advantage of this phase is

as a low expansion material. Not surprisingly the expansion

characteristics are not to dissimilar to those of Beryl (330). Lachman

et al (312) measured an expansion of $7-10 \times 10^{-7}°C^{-1}$ over the range

25-1000°C in the extruded direction for an extruded stoichiometric α

cordierite honeycomb structure. Roy and Agrawal (331) were able to

lower the expansion further by substituting GeO_2 for SiO_2 (i.e. $2MgO.2Al_2$

$O_3.(5-x)SiO_2.xGeO_2$), the lowest expansion occurring for x = 1-0.8. A

TABLE 5.1 MATERIAL PROPERTIES OF C1,975 COMPARED WITH OTHER MATERIALS

	CORDIERITE REFRACTORY	CORNING 9606	ALUMINA	C1,975
RESISTIVITY (Ωcm)	10^{12}-10^{14}	10^{10}(250°C)	10^{14}	$3\pm1\times10^{15}$
THERMAL EXPANSION($\times10^{-7}$°C^{-1})	25-30	57	73	15.5 ± 1.5
DIELECTRIC CONSTANT (1MHz)	60-70	5.6	9.6	5.35 ± 0.15
Tanδ (1MHz) ($\times10^{-3}$)	4-10	9	2.6	0.47 ± 0.05
DIELECTRIC LOSS (1MHz)	0.045	0.05	0.025	2.1×10^{-3}
THERMAL CONDUCTIVITY (Wm^{-1}K^{-1})	2.0-2.6	-	29	1.9 ± 0.4
YOUNGS MODULUS (GPa)	14-34	119	365	84 ± 5
STRENGTH (MPa)	7.24	130	345	133 ± 10
DENSITY (g/cc)	1.6-2.1	2.6	3.6	2.50

value of $5 \times 10^{-7} °C^{-1}$ was quoted althouth it was zero for some
compositions in certain temperature ranges. Clearly such a property is
highly desirable for applications where thermal shock is likely.
Generally the thermal expansion for equivalent mineralogical specimens
is two to three times greater due to contamination by other elements,
both within the structure and within the open channels (332). This has
been readily demonstrated by Evans et al (333) working on single phase
cordierite materials. With K^+ occupying the cavity there was little
change in the overall expansion but when the larger Cs^+ was introduced
there was a dramatic change with $\Delta c/c$ (which is usually negative)
becoming positive at all temperatures.

The low expansion of cordierite is attributable to a highly anisotropic
behaviour of the framework when heated, the direction parrell to c
exhibiting an initial contraction whilst the perpendicular direction has
a positive expansion. This behaviour has been carefully examined by
Hochella and Brown (332) who found that the anisotropy was caused by the
expanding Mg octahedra, which has a mean Mg-O bond expansion of 126×10^{-7}
$°C^{-1}$ (150). Its effect is limited however by the more rigid surrounding
tetrahedral framework and leads to a contraction in the c direction, the
hexagonal rings alternately rotating in opposite directions to
accommodate the various changes in bond angles. Thus the nature of the
octahedrally co-ordinating ion would be expected to have a strong
influence on the net expansion, an observation which has been made by
Selkregg and Bloss (146). The effect of Si/Al ordering on the expansion
of cordierite is minimal. Lee and Pentecost (327) working on single
crystals found that thermal contraction of the c axis increased slightly

during the hexagonal to orthorhombic transition. Finally Beals and Cook (326) made measurements on a number of compositions within the MAS system. They found that the overall expansion of a material was dependant on the amount of cordierite phase contained within it, the larger the amount the smaller the expansion. This observation is developed further in section 5.3.

Although glass ceramics generally have improved thermal conductivities compared to those of glasses they are inferior to pure oxide ceramics as can be readily seen when comparing the value obtained for cordierite to that of alumina in Table 5.1. A contributing factor to this is the amount of residual glass phase within the microstructure and thus it is beneficial, from a conductivity point of view, to reduce this as much as possible.

Thermal conductivity in both glasses and ceramics has been extensively studied by Kingery (334). He pointed out that at temperatures near room temperature and above "The major process giving rise to a finite thermal conductivity and energy dissipation from thermal elastic waves are phonon-phonon interactions corresponding to phonon scattering" - so called 'Umklapp' processes. These result particularly from lattice imperfections. Since K is related directly to the phonon mean free path the more complex or disordered the structure the lower the K value. This is why glasses are found to have a phonon mean free path that is limited to the order of interatomic distances within the near random structure (335) and leads to a narrower range of K values observed in glass systems. In ceramics, lattice anharmonicity and impurity atoms in

solid solution also lower K but it should be noted that above room temperature the mean free path is much less than 100Å which leads to negligible effects due to grain boundaries, although fine scale residual porosity can disrupt heat flow. Thus it would appear that there is little scope for radically increasing K in this material system if one just relies on the various crystalline phases present.

5.1.2 Mechanical Properties

The conversion of a glass to a glass ceramic, amongst other things, generally leads to an increase in strength. (Baskaran et al (336) noted for Corning 9606 that the rate of crack growth required a stress intensity factor for the fully crystallized glass ceramic about three times higher than that for the original glass). There are several contributing factors to this which include:-

i)   Reduction in the stress concentration associated with Griffith flaws as the glass is heated above the annealing point.

ii)   Reduction in the possible size of critical flaws within the intercrystalline glass phase.

iii) Increase in fracture toughness through crack deflection, segmentation etc.

iv)   Enhanced resistance to surface damage - see Watanabe et al(337).

With regard to the second point this has been investigated by Hing (338) and Hing and McMillan (339) who found for a lithium silicate material that the strength was inversely proportional to the square root of the distance between crystalline particles, i.e. critical microcracks exist only in the glass and are terminated by the crystalline boundaries.

It is interesting to note that the fracture strength of C1,975 was found to be ~10% lower than that for the bulk glass which was measured at 147± 13 MPa. Thermal expansion differences between the various phases present may introduce stress and even microcracking within the material which may account for this difference. These are more likely to occur between the cordierite/residual glass phase and enstatite, $\alpha = 120 \times 10^{-7}$ $°C^{-1}$ (284). The comparison between the strengths of glass and glass ceramics however assumed that crystallization was via bulk nucleation yielding a relatively fine grained, pore free microstructure. Clearly this is not the case here where strength is also dictated by ability to attain complete densification.

An empirical relationship between strength and porosity has been observed by Duckworth(340) which has the form

$$\sigma = \sigma_0 \exp(-nVp) \qquad (5.1)$$

Where σ_0 is the strength when the volume fraction of porosity, Vp, is zero. n is a constant, usually about 7. The exponential behaviour is because pores not only reduce the cross-sectional area but they also increase the local stress concentration - see Evans (341). Thus it can

be seen from equation 5.1 that a porosity of ~1.5% would be sufficient to account for the reduction in strength. (It should be noted however that for Corning 9606, Pletka and Wiederhorn (342) found that the absolute value of various crack growth parameters was dependant on the method of measurement, attributing this to the intimate relationship between crack tip and microstructure. Also three point bend tests give strength values some 15-20% higher than for four point (343), due to different stress distributions through the specimen whilst under load.

In the C1 glass the critical flaw occurred mostly at the surface, some specimens exhibiting the classical fracture pattern for glasses, Fig. 5.1.a. In the glass ceramic however two modes of fracture were evident, those originating from surface flaws, Fig.5.1.c and those originating from interior defects, e.g. foreign inclusions and pores Fig.5.1.b. A similar observation was made on Corning 9606 by Bansal et al (344) who also noted that fracture stresses were higher by a factor ~1.3 for specimens exhibiting a surface originating failure. Later Lewis (345), working on the same material, suggested that the variation in absolute sample to sample strength values was due to subtle microstructural variations since they were not accompanied by measurable changes in other physical properties or by gross changes in microstructure.

During measurements of Young's modulus it was noticed that the values obtained were typically an order of magnitude less thanthe expected value (~120 GPa). To investigate this further a series of measurements were made on a large number of similar sized porcelain cylinders, E being measured as a function of the intersupport distance, L (see
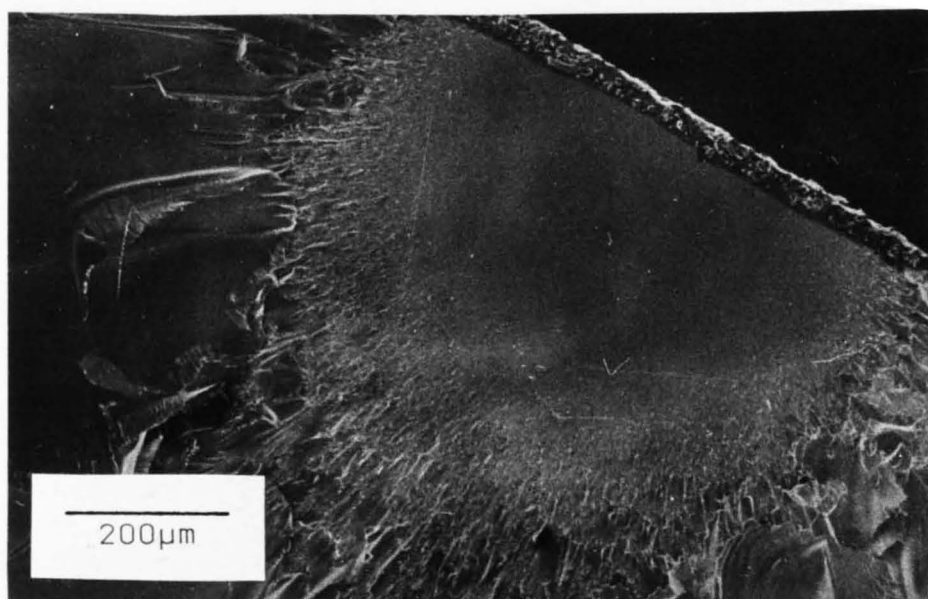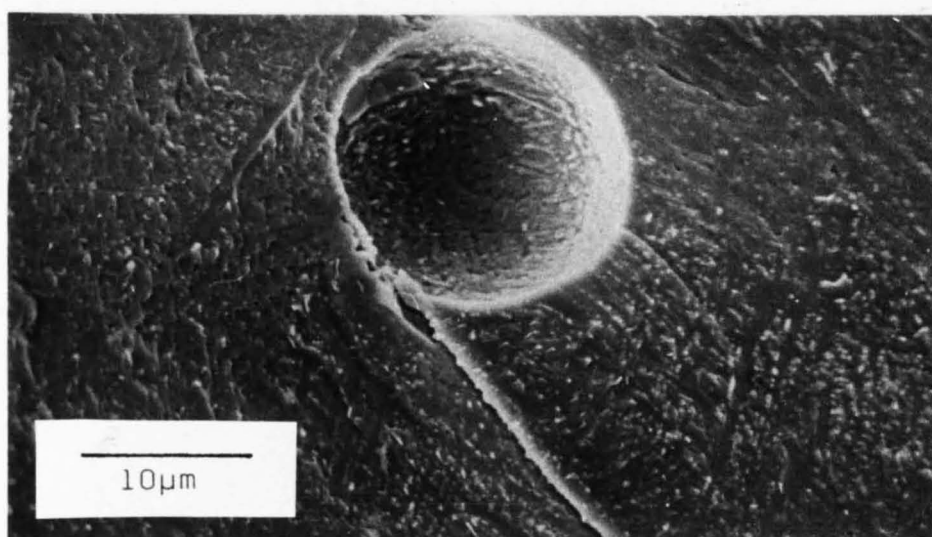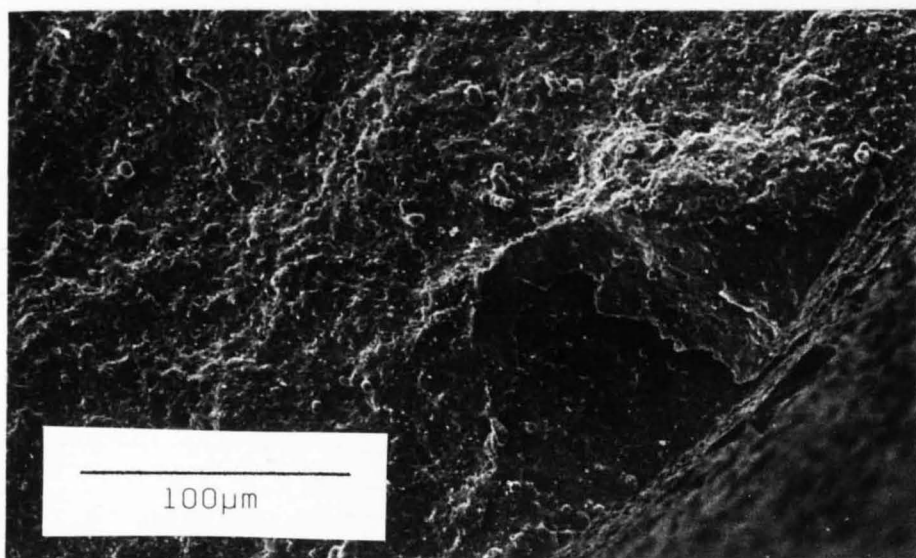
FIG.5.1 Fracture surfaces showing critical flaws
         originating from (a) the surface for the
glass (b) internal defects for the glass ceramic
(c) surface defects for the glass ceramic
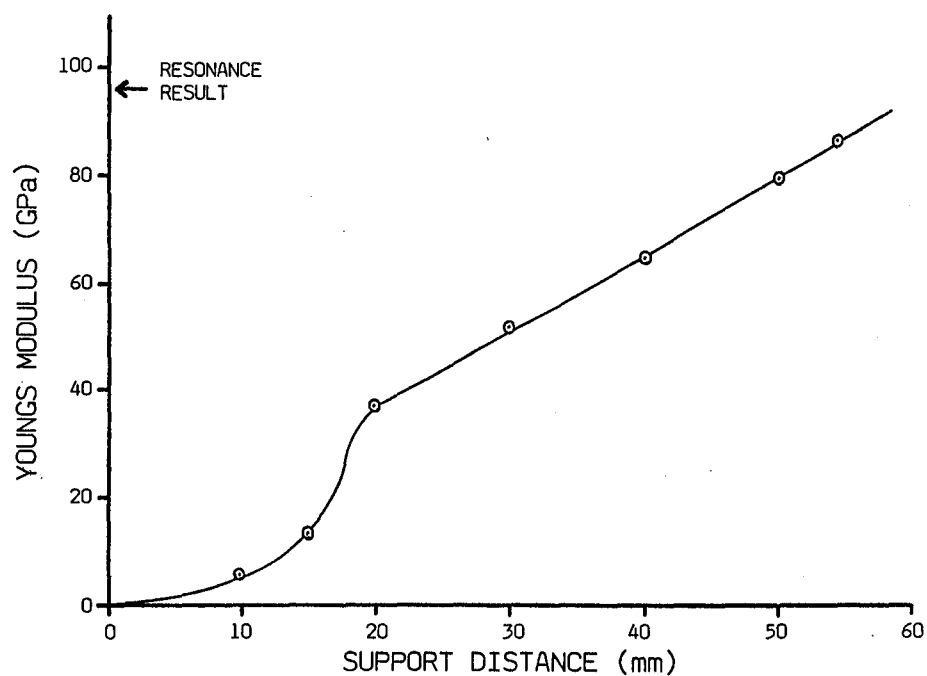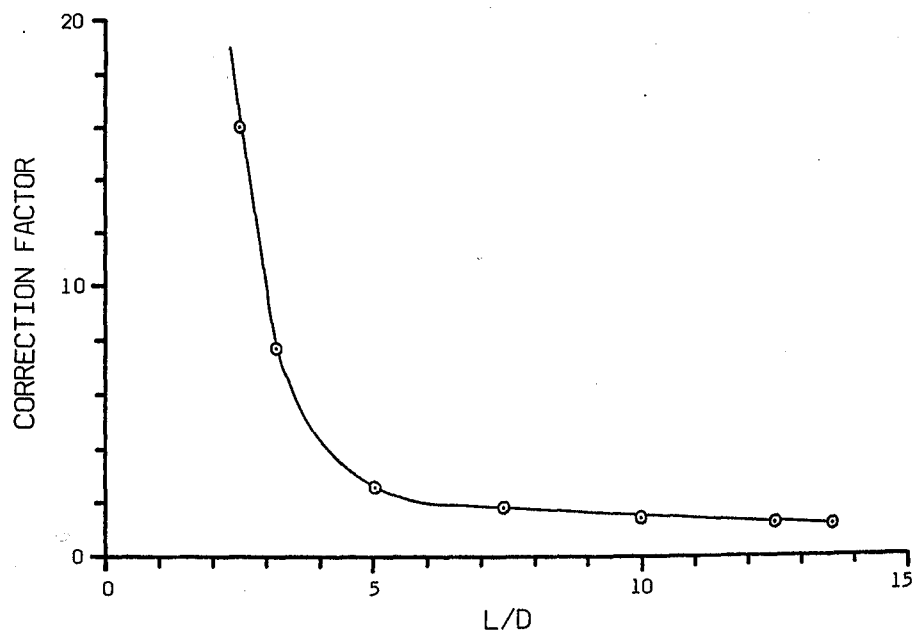
FIG.5.2 Variation of Youngs Modulus as a function of specimen dimension for porcelain cylinders

equation 2.21). The results are shown in Fig.5.2.a. Also marked is the value obtained using a resonance technique, see Pickett (346). Clearly there is a strong dependance on L or, more correctly, L/D, D being the diameter. The stress distribution in specimens with low L/D values have been investigated by a number of authors (347-349) all of whom showed that for 'deep beams' there is considerable deviation from the simple theory of flexure (which assumes a parabolic shear stress distribution along the specimen) with the result that the neutral axis is no longer at the specimen centre. This is principally due to the effects of loading plus reactions and friction at the supports. Causes of errors in bend tests are discussed more fully by Duckworth (350) and Hoagland et al (351).

The deviation from the simple theory depends on both E and G (the shear modulus). In timber for example, where G~E/6, Roark and Young (352) suggest corrections should be made where L/D is less than 24. For this work the L/D ratio used was either 4.6 or 2.7. Thus it would appear that the experimentally derived values for E needed to be adjusted according to the L value used in making the measurements. The correction factors as a function of L are given in Fig.5.2.b for the porcelain specimens where it is assumed that E measured by the resonance technique (i.e. 96 GPa) is the correct one. Consequently the E value quoted in Table 5.1 has been multiplied by the appropriate factor given in Fig.5.2.b on the assumptions that the nature of the procelain and cordierite cylinders is similar.

Strength values were also investigated as a function of L/D and showed little variation, values being ~15% higher for L/D just less than 5

compared with L/D greater than 7.5. The reason for this small amount of deviation may be that although the stress concentrations are higher for deep beams the regions of high stress are also more localized and are thus less likely to encounter a critical flaw. Consequently strength values were not corrected.

5.1.3 Electrical Properties

On conversion of a glass to a glass ceramic the resistivity generally increases since the average activation energy is lower in a glass and also the presence of phase boundaries hinders the mobility of charge carriers. In both glasses and ceramics it tends to be the more mobile alkali metal cations (K^+, Na^+ and Li^+) that contribute most to the conductivity. Thus the high resistivity values obtained for the cordierite glass ceramic are a result of minimising the amount of residual glass phase and using high purity oxides to reduce alkali metal contamination.

The low dielectric constant of the material is directly attributable to the ions making up the cordierite structure. Dielectric constant is proportional to the polarizability, there being direct contributions from both electric and ionic polarizations. Consequently low dielectric materials derive from the use of low atomic number elements, (since the electron density is smaller) and strong ionic bonds. (For a comparison of Mg^{2+}, Al^{3+} and Si^{4+} with other ions see table 1 on page 371 of Kittel (353)).

As previously mentioned, if a material is to be used for insulatation at high frequencies then a low power factor is required as well as a low dielectric constant. The main contribution to dielectric losses is ion migration and thus again the cordierite glass ceramic is favoured by the absence of the more mobile alkali ions and reduction in the amount of residual glass phase which could be a major contributor. The effect of composition on Tanδ for MAS glasses has been examined by Mashkovich and Udovenko (354). They found that Tanδ was linearly proportional to the MgO content at a fixed alumina concentration, a typical value being $80-90 \times 10^{-4}$ for a composition in the region of C1.

3.1.4 Iron Oxide Contamination

In any manufacturing process a certain degree of contamination is inevitable and a likely contender, apart from airbourne particulate matter, is iron oxide which is also present in the initial starting materials (Appendix II). Consequently it was decided to investigate the effect of adding 0.1 wt% Fe_2O_3 to the glass melt (composition C7, table 2.1). Phase development as a function of final firing temperature is shown in Fig.5.3.a and is noticeably different to that of the C1 material. Clearly the addition of Fe_2O_3 favours the development of α cordierite at lower temperatures and slightly more enstatite appears to be present which is reflected in a slightly higher expansion coefficient (α for C7, 975 in $17.5 \pm 2 \times 10^{-7} °C^{-1}$, 20-100°C). This alteration in phase kinetics could be due to the influence of iron within the cordierite structure. Fe^{2+} ions are known to exist either in the open
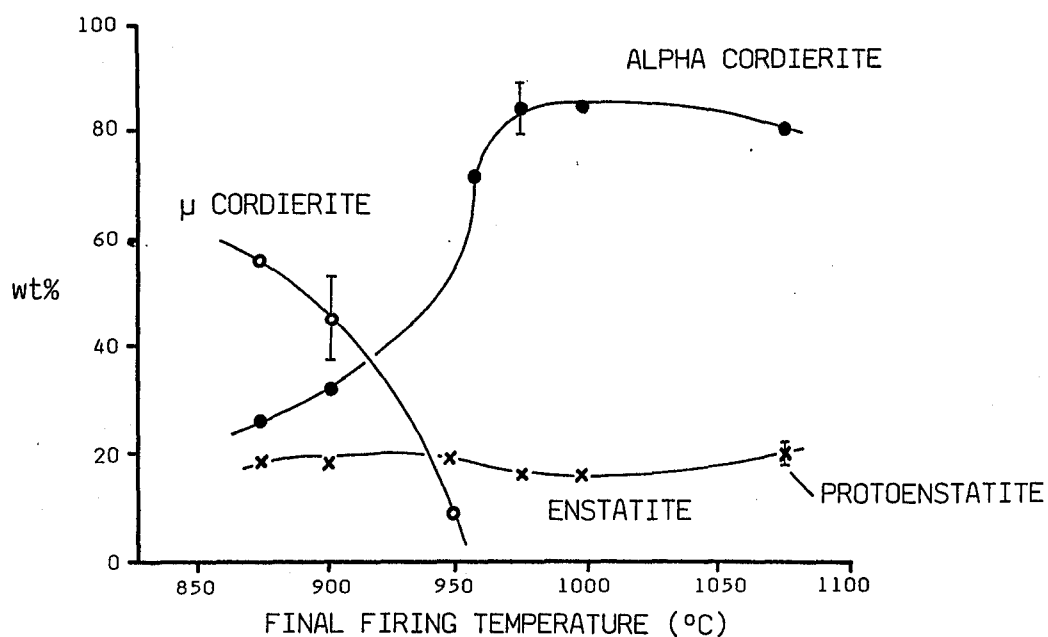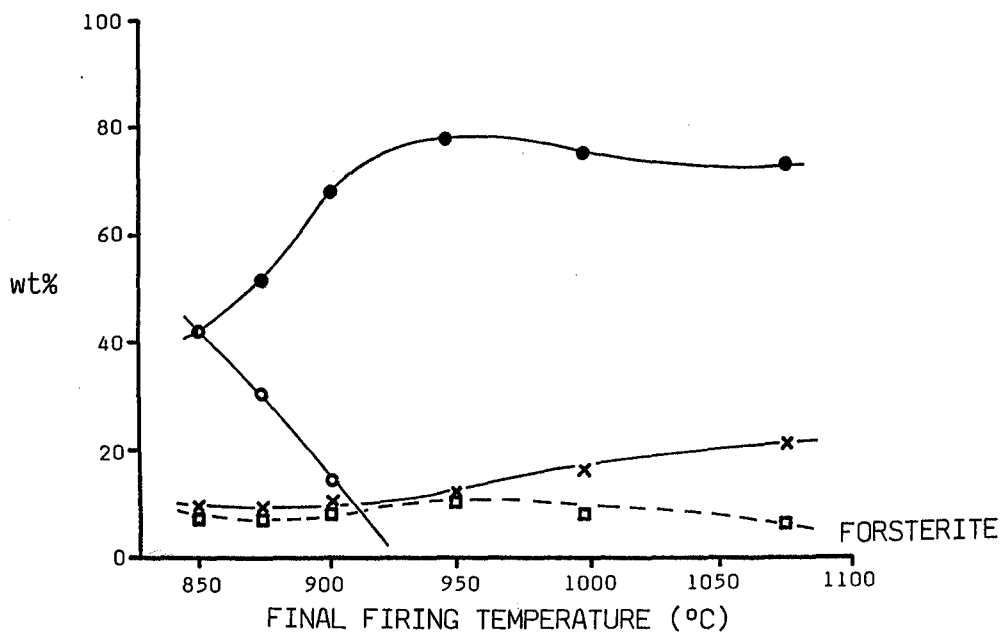
FIG.5.3 Phase evolution as a function of final firing temperature
for compositions (a) C7 and (b) C8

channels or to replace the Mg^{2+} octahedra, iron cordierite ($2FeO.2Al_2O_3.$
$5SiO_2$) being found to occur naturally. Presumably Fe^{3+} ($r=0.64$ Å) may
also occupy the open channels if the ionic charge can be balanced.

Addition of 1wt% Fe_2O_3 (composition C8) is further beneficial to the
phase transformation between μ and α cordierite as shown in Fig.5.3.b
and also enhances the formation of forsterite. This seems to confirm
that Fe^{3+}, along with B^{3+} and P^{5+}, exerts a strong influence on the
crystallization kinetics. McMillan (355) noted that Pt also had a
similar effect on the μ to α transition and it may be that these ions,
whilst promoting nucleation at lower temperatures, also disrupt the
stability of the μ phase causing a transformation to occur at a lower
temperature. (This would appear to contradict the findings of
Fekaldjiev and Andreeva (356) who found that the presence of iron oxide
impurities in the original starting materials did not effect the glass
ceramic properties. They used 20-40% serpentinite with an Fe_2O_3
concentration of 3.14%). Unfortunately, despite the formation of α
cordierite at low temperatures, C8 950 had a dielectric constant of 14.7
±1.3 making this material unsuitable for packaging applications.

5.1.5 Material Properties of C3, C4, C5 and C6

Representative material properties for the compositions based on C1 but
with various alterations to the minor oxide additives are given in Table
5.2. Clearly C3 (no added P_2O_5) is not too dissimilar to C1 although
the expansion coefficient is higher, attributable to a greater enstatite
content. Both C3 and C5 have enstatite contents in the region 20-25

TABLE 5.2   Some material properties for other compositions fired to 975°C

SPECIMEN	STRENGTH (MPa)	YOUNGS MODULUS (GPa)	THERMAL EXPANSION $(10^{-7}°C^{-1})$	
C3	137±2	90±6	30-100°C	21.6±1.9
			30-200°C	25.3±1.5
C4	91±4	82±6		31.0±3.0
				34.0±3.0
C5	114±4	96±4		23.0±2.0
				28.2±2.2
C6	124±14	103±8		67.3±2.5
				69.8±1.9
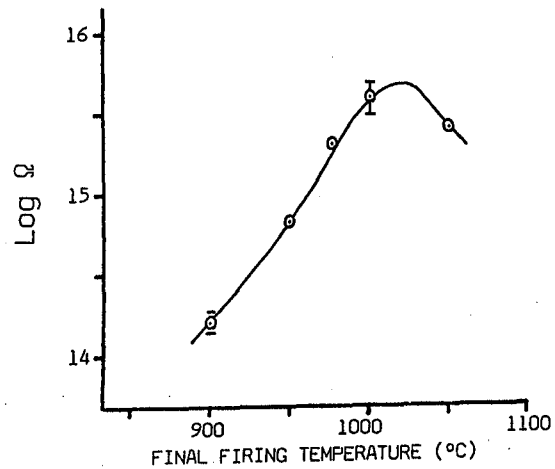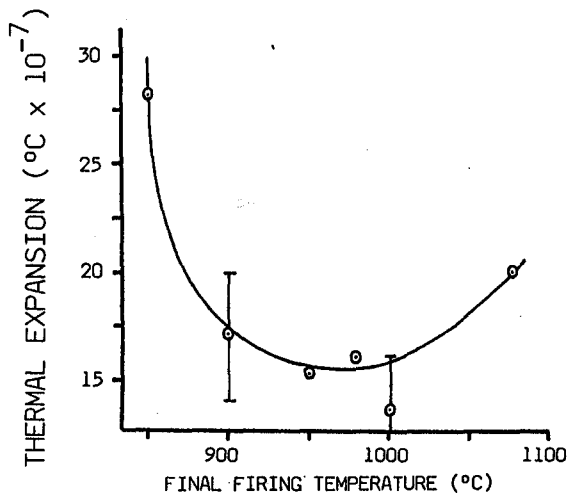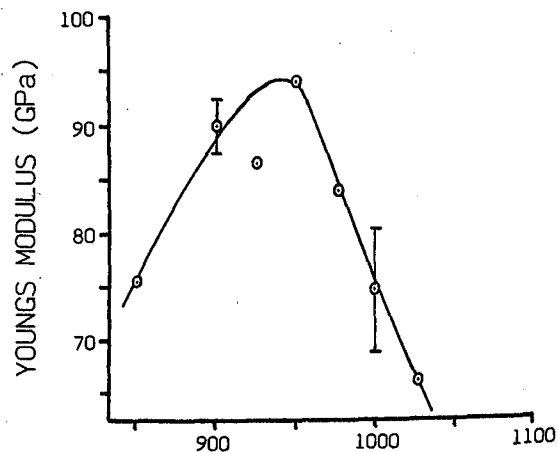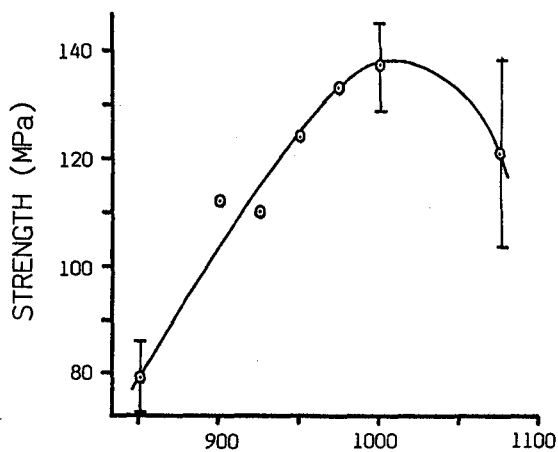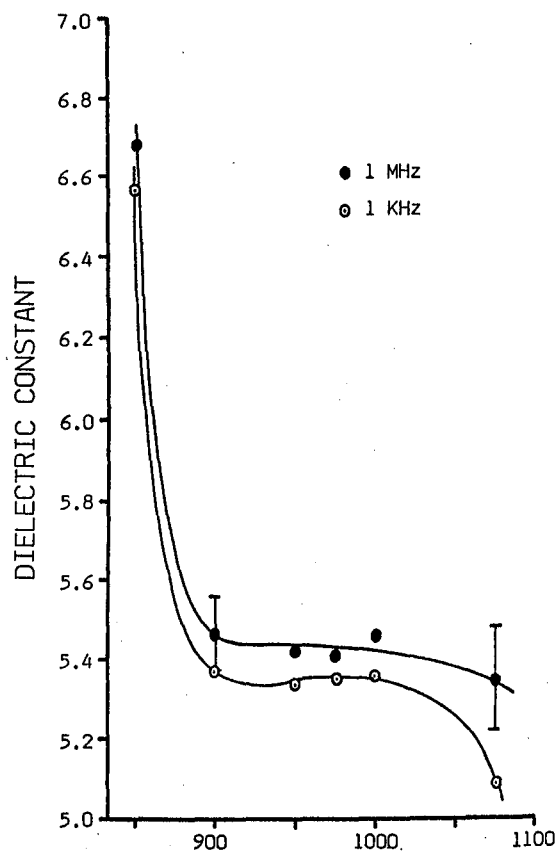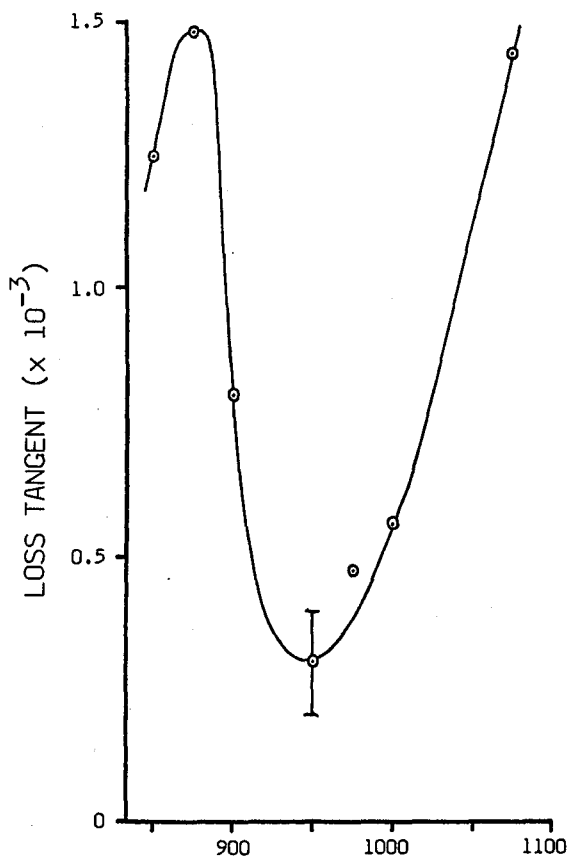
FIG.5.4 Variation in material properties with final firing temperature
for Cl glass ceramic

wt%. The expected expansion coefficient for this αcordierite/enstatite

composite would be $35 \times 10^{-7} \circ C^{-1}$ (assuming a direct additive

relationship). This is considerably more than the measured quantity and

is probably a reflection of the inaccuracy in the determination of phase

content for enstatite using XRD results.

C4 material (no added B_2O_3) has low strength and a higher expansion

coefficient due to the presence of μ cordierite which has a measured

expansion of $\sim 47 \times 10^{-7} \circ C^{-1}$ (114). C6 was estimated to contain even more μ

phase plus an observable amount of residual glass and again gives rise

to a noticeably increased expansion coefficient. Strength is not much

reduced but values display increased scatter.

5.2   RELATIONSHIP BETWEEN PROPERTIES AND MICROSTRUCTURE

The overall dependance of material properties is related to the phases

present and consequently to the final firing temperature. This is

evident from Fig.5.4 which shows the variation in properties as a

function of firing temperature. The variation is quite noticeable and

Fig.5.4 clearly shows that the presence of μ cordierite within the

microstructure at lower temperatures has deleterious effects on a whole

range of properties. Furthermore, firing to higher temperatures

favours the development of protoenstatite and this, along with the

general coarsening of the microstructure and increase in porosity, also

has deleterious effects. This is especially noticeable for Tanδ since

this will be sensitive to small changes in microstructure e.g. different

potential well arrangement. As the amount of enstatite present appears

to show little variation up to $\sim 1000°C$ the variation in properties up to

this point is due to the ratio of μ to α present within the sample. Consequently for this cordierite material the avoidance of large quantities of μ phase at low temperatures is required for device packaging applications (see also Davies and Loftus (357)) as is the presence of protoenstatite, which is accompanied by a general microstructural degradation and which occurs at higher processing temperatures.

DeVekey and Majumdar (154) examined the variation in properties as a function of final heat treatment time for a titania nucleated MAS glass containing a small addition of CaO. They found a close correlation with the cordierite content except for permittivity and loss angle which, although being related to each other, did not follow so closely other parameters such as density or thermal expansion. This would also appear to be the case for this work, both Tanδ and, to a lesser extent, K showing fairly rapid variations with heat treatment. The authors also noted that the detrimental effects that occurred in their materials, such as coarsening and porosity, were partially due to zoning effects of Mg^{2+} and Ca^{2+} during phase separation.

In the mass production of any product, consistency and quality control are essential. This is particularly so in the semiconductor industry where close specifications and tolerances are required. Thus it was decided to repeat the property measurements made on C1 with a material of the same composition but made up from a different batch. Absolute values were found to be less than 10% different over the heat treatment range considered and usually less than 5%. The only exception was for

the Youngs Modulus measurements where, although the absolute values were of the same order as C1 (i.e. 70-90 GPa), a considerable degree of scatter across the heat treatment range made any trends difficult to see.

5.2.1 Difference Between Liquid and Dry Milled Powders

Table 5.3 gives some material properties for sintered specimens of powders milled in a dry environment or in the presence of methanol i.e. powders of differing size and size distribution. Examination of the thermal expansion coefficients show little dependency on the initial powder morphology compared with the influence of final firing temperature (i.e. crystal phases present). Expansion coefficients are also unchanged by the addition of binder to the powder prior to firing.

Mechanical properties on the other hand do appear to be influenced by the initial character of the powder. For strength, comparison of results for the air and methanol milled powders fired to 975°C show little variation within each group, i.e. average particle size has little effect. Comparison between the two groups however shows that air milled powders have strengths typically 20 MPa less than those milled in methanol, that is size distribution exerts a small influence. Insufficient samples were measured to ascertain whether the addition of lwt% binder affects the strength although the higher concentrations present in green sheets (typically 5-10% binder solids) would be expected to give rise to some reduction as particle packing is much less efficient. Also isolated regions of high binder concentration will leave large residual pores after the burn out stage. Bearing in mind

TABLE 5.3 Comparison of properties for dry and liquid milled powders

B = Binder, NB = No Binder

Specimen plus final firing temperature (°C)	Strength (MPa)	Young's Modulus (GPa)		Thermal Expansion $(\times 10^{-7} \,°C^{-1})$
A12,975 B	129±6	88±13	30-100°C	15.8±0.6
			30-200°C	19.6±1.4
A12,975 NB	110±6	69±4		17.1±2.7
				19.9±1.7
A24,975 B	141±11.5	88±3		17.2±0.7
				22.0±1.7
A36,975 B	126±1	90±5		17.9±1.7
				20.2±1.3
M36,875 B	86	77		28.0±2.2
				31.6±2.1
M36,875 NB	100	120		28.7±1.2
				31.6±1.5
M12,975 B	148±4	88±5		18.3±1.2
				21.9±1.2
M24,975 B	137±6	98±3		22.1±1.2
				24.5±1.5
M36,975 B	141±8	111±6		17.1±1.6
				21.1±1.4
M36,975 NB	141±8	111±10		17.1±2.6
				21.6±2.1
M36,1075 B	147	139		19.9±1.5
				23.8±1.7
M36,1075 NB	158	133		19.7±3.7
				22.5±2.5
Bulk Glass	147±13	193±43		33.3±1.0
				38.3±2.8

the scatter of results obtained for the Young's modulus results outlined
in Section 5.2 there does appear to be an influence on E by the initial
state of the powder, i.e. liquid milled powders yield specimens with a
higher moduli. Also powders with a smaller average size give higher
values.

Finally, careful analysis of Table 5.3 shows a discrepancy between the
overall values obtained here for σf and E with those given in Table 5.1,
which are generally smaller. A contribution to this difference may be
due to the packing of the particles during the initial pressing of the
rods. Typical specimen lengths used here were less than ⅜ of those used
in the various property determinations outlined in section 5.1. Thus
the initial stress distributions within the unsintered pellets may have
been sufficiently different to alter the sintering behaviour and hence
final physical properties.

5.3   IMPROVEMENT OF THERMAL EXPANSION

Considering that the thermal expansion coefficient of Si chips is in the
region $30 \times 10^{-7} {}^\circ C^{-1}$ it was felt that the expansion of the C1 material was
a little on the low side. One has to bear in mind however that MLC
substrates contain a fair proportion of metal conductors etc. surrounded
by the dielectric matrix. For example, again assuming a linear additive
relationship between expansion coefficients, it only requires ~21%
copper within the 'composite' to give the required expansion match.
Nevertheless it was decided to investigate the properties of two further
glass ceramics, C9 and C10, which had added MgO at the expense of Al_2O_3.
The idea behind this was to try to increase the amount of the higher
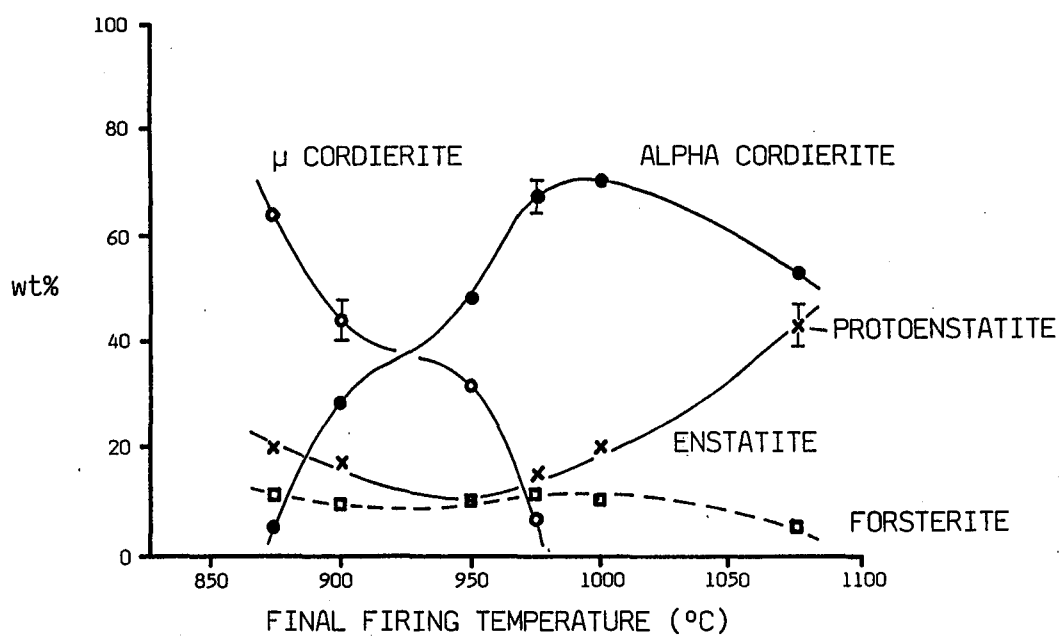
FIG.5.5 Phase evolution for composition C10

TABLE 5.4   Bulk properties of C9 and C10

PROPERTY	FINAL FIRING TEMPERATURE (°C)	C9	C10
RESISTIVITY (Ωcm)	900	-	$3\pm1 \times 10^{13}$
THERMAL EXPANSION ($\times10^{-7}$°C^{-1})	900-1000	19.1±0.9	28.9±0.8
DIELECTRIC CONSTANT (1MHz)	900	5.4±0.15	5.6±0.15
STRENGTH (MPa)	900-1075	110±7	109±4
YOUNGS MODULUS (GPa)	900-1000	187.5±2	205±2
DENSITY (g/cc)	975	2.612	2.690

expansion magnesium silicate subsiduary phase. Basta and Said (358) have already showed that addition of 10wt% Al_2O_3 to the stoichiometric composition gives a reduced expansion coefficient of $4.2 \times 10^{-7} °C^{-1}$ (20-400°C).

Examination of Fig.5.5 confirms that the goal of increasing the minor phase has been achieved, about 10% forsterite ($\alpha = 94 \times 10^{-7} °C^{-1}$) also forming in C10. This phase also has a higher density (3.27g/cc) compared with cordierite and this is reflected in Fig.4.8 when compared with the C1 material. Also noticeable is the rapid increase in enstatite content from about 950°C onwards. This could be partially aided by exsolution from the α phase. At 950°C the XRD pattern showed a 2θ shift of 0.2-0.25° to higher 2θ values for the α phase but by 1075°C it was of the order 0.1-0.15°. Table 5.4 gives some of the general properties for C9 and C10 glass ceramics. It can be seen that increased MgO content is not detrimental to the bulk properties from a packaging point of view. Firing to slightly higher temperatures than C1 is required to develop entirely α cordierite since the μ to α transition is not so rapid. This may be aided by the further addition of P_2O_5 and B_2O_3 . Both C9 and C10 had their initial glass powders dry milled and so further improvements to the material properties may be possible if the milling is done in a liquid medium.

CHAPTER SIX - APPLICATION TO DEVICE PACKAGING

In the late sixties, when MLC's were beginning to be developed, several areas were identified where improvements on the current technology were necessary. These included dimensional control and metallization techniques (359). Today, many of these basic problems have been overcome, the current market for thick film microcircuits being well over $4 billion worldwide and growing at 10-15% per year (360). To a certain extent such improvements have been possible through appropriate formulation, handling and processing of the green sheets plus a better understanding of the interactions both within a thick film paste and with the surrounding dielectric medium.

6.1   PREPARATION OF GREEN SHEET

6.1.1 Binder Formulation

The production of multilayer substrates is heavily dependant on the green sheet fabrication stage since the properties of the sheet often dictate the performance of the package as a whole. Although several methods exist for producing thin, flat ceramic parts such as pressing, extrusion or roll compaction (361), for multilayer applications slip casting, and more particularly doctor-blade tape-casting, is more appropriate. This places certain restrictions on the binder system used: i) it must be of the right viscosity for tape casting - typically 1-1.5 poise, about the consistancy of paint. ii) It must form a tough,

flexible film when dried but be present in as small a concentration as possible, generally less than 10wt%. iii) When fired, the binder should completely burn off leaving no residues within the powder. iv) Ideally the binder should be composed of cheap constituents and have a reasonable shelf life.

There are principally two types of binder mixes, those based on organic liquids and those formulated for aqueous solutions. As mentioned in section 3.1.2, milling in water can lead to aggregation problems if the slurry is dried. Aqueous binder mixes also take longer to form dry tape as the evaporation rate is slower and they generally form tapes of lower density (362). The exact choice of system however is also governed by factors such as the required tape thickness and casting surface. The typical constituents of a binder mix can be divided into several categories (see also Park (51) and Anderson et al (363)).

i)   Binders

The purpose of the binder is to retain the ceramic or glass particulate in a form in which it may be processed after the solvents have evaporated and to give green strength to the article as a whole. Typical binders for organic solvents include polymethacrylates, polyvinyl butyrol, polyvinyl chloride/acetate and various polyacrylamides. Water soluble ones include various starches and dextrins, polyvinyl alcohol and methyl cellulose. A more comprehensive list is given by Onoda (364).

ii)   Plasticizers

Generally the binder alone gives a dry film which is too hard and stiff. Addition of compatible, low molecular weight plasticizers (which may be present in concentrations greater than the binder itself) break up bonds within the binder to yield greater flexibility. Such additions may be at the expense of overall strength however. Organically soluble plasticizers include alkyl phthalates and various glycols whilst polyethylene glycol and glycerin are water soluble.

iii)   Solvents

The action of added solvents is to dissolve the above components, to be easily evaporated and to give the correct slip rheology. Two or more solvents are usually added since the solubility of a polymer is generally greater in a optimized mixed system than in any individual pure solvent (365). Solvents with high vapour pressures would appear to favour the production of thinner films. For example, Mistler et al (366) suggest for tapes, up to ~0.25mm thick, a polyvinyl acetate/chloride copolymer with MEK (methylethyl ketone) whilst using polyvinyl butyral with toluene or trichloroethylene for thicker casts.

iv)   Wetting agents

Addition of only a fraction of a percent of such chemicals as ethyl phenyl glycol, polyoxyethylene acetate or alkyl ethers of polyethylene glycol, reduces the mixing period and aids the slip characteristics due to enhanced wetting of the powder surfaces. Park (51) also noticed that

without wetting agents the production of uniform films, that were free of imperfections, was extremely difficult.

v)   Dispersants or deflocculants

In order to reduce agglomeration and aggregation of particles during the processing of the slip various additives are used so that individual particles repel each other, either by steric hindrance or charge repulsion. Shanefield and Mistler (367) found that ideally a deflocculent should contain a combination of double carbon bonds, a molecular weight above 357 and an ester group. Traditionally, natural extracts have been found to form the best deflocculents such as Menhaden fish oil or corn oil, although glyceryl trioleate has also proved to be satisfactory.

Due to the diverse constituents of a binder mix as a whole the most suitable formulation can only be really perfected on a trial and error basis. As a guideline however, Gardner and Nufer (62) identified several critical properties that are important in the production of green sheets. These include : i) Powder particle size - a small size with a high surface area being more suitable since the yield strength was found to be higher. ii) Interlaminar bond strength as outlined in section 1.2.2. iii) Permeability - gases generated during binder burn out must be able to escape during the heat treatment since entrapped vapour can damage the article due to excessive build up of pressure. iv) Compressibility - the materials must flow under laminating conditions in order to completely envelop the enclosed metallization.

v) Density - sheet density must be well controlled in order to maintain consistant shrinkage and fired density. Green density for various alumina powders can range from 2.0-2.6 g/cc (367).

6.1.2 Doctor Blade Tape Casting

Although tape casting is a relatively simple technique, care has to be exercised in producing thin films, this being particularly so during the drying stage. The process starts with thorough mixing of the slip followed by degassing and filtering to remove the milling debris etc. The slip is then pumped into a suitable chamber and is pushed out through a gap in the bottom of one of the walls. The size of this gap is controlled by micrometers which move the wall (or doctor blade) vertically up or down. Then either the chamber is moved over a fixed flat bed, usually made of glass or, as is more common, the chamber is fixed and the slurry is cast onto a plastic sheet which moves under the chamber. The latter method is favoured since, after drying, the tape can be stripped from the carrier in a continuous manner.

Typical carriers are of polyethylene, cellulose acetate, glycol terephthalic acid polyester ('Mylar') or polytetrafluroethylene ('Teflon'). The exact choice of carrier is governed by the ability of the slip to stick to the surface during drying so that shrinkage only occurs in the thickness of the cast film. This adherence must not be too excessive however or the dry tape will not strip off correctly. This is less of a problem if deflocculents are added to the slip.

After the slurry has passed under the doctor blade the tape thickness can be monitored via X-ray transmission or gamma ray backscatter etc, a feedback circuit adjusting the doctor blade as necessary. Apart from doctor blade height several other factors however can also influence the thickness of the wet cast film including slip viscosity, hydrodynamic head in the slip reservoir and casting speed (366). Several methods exist for drying the film after casting, a common one being the use of dry air blown in a direction opposite to the moving tape. This produces a vapour gradient above the slip and down the length of the table so that freshly cast material has above it a vapour saturated atmosphere. Air blown too fast however leads to excessive evaporation of the volatile components at the top of the slip which in turn leads to a deleterious skin formation. Too slow and the air above the slip becomes saturated and drying is thus retarded.

Several authors discuss slip preparation and the tape casting process in more detail (361, 362, 366, 367).

6.2   ASPECTS OF THICK FILM TECHNOLOGY

6.2.1 Thick Film Pastes

Metallization of the green sheet is usually brought about by screen printing a suitable thick film paste onto the substrate surface. This offers considerable advantages over other depositional methods (e.g. thin films) due to its simplicity, low cost and high turnover rate, an

automated machine being capable of up to 2000 substrates an hour. Obviously a prime requirement for a conductive paste is that the fired conductor has a low resistivity. For MLC applications this allows for narrower lines and wider spacings, thus reducing capacitive and any diffusional effects. Good bonding to the substrate is also required, as is line definition. On the top layer of a multilayer substrate the conductor must be able to electrically connect with the solder and this may require a paste of slightly differing composition. For instance, a few percent of Pt or Pd is usually added to Au pastes in order to reduce intermetallic compounds degrading the solder interface.

As with green sheets, a thick film paste can be divided into a number of discrete components, each of which has a marked effect on the overall character and final electrical performance of the conductor. Briefly these components are:-

i)   The functional phase

This dominates the electrical properties of the thick film and takes the form of a fine (generally very much less than $50\mu m$) pure metal or metal alloyed powder. Chance (368) has shown that to a certain extent particle size governs shrinkage of the metal layer whilst an appropriate choice of size distribution aids the adhesive properties by reduction in residual stress.

ii)   The binder

Unlike that for greensheets, here the binder is permanent as it is responsible for bonding the conductor to the substrate. Apart from mechanical keying there are three other means of improving bonding (369).

(a) Addition of up to 1% metallic oxides to form an interfacial compound - e.g. CdO and Al_2O_3 form a cadmium spinel.

(b) Addition of ~5% oxide to form a metal wetting eutectic liquid with the substrate, such as Bi_2O_3 and Al_2O_3 ,which form a liquid at 820°C

(c) The most common approach, addition of up to 10% glass frit which may also be combined with a fluxing agent to improve substrate wetting. Lead borate glasses have been extensively used for this purpose but this has caused problems when cofiring with Cu due to the reduction of PbO to Pb. A similar problem occurs with Bi_2O_3.

iii) The vehicle

This is usually a high molecular weight organic polymer plus a suitable solvent and is formulated to give the paste the required 'spreadability' although the rheological properties are strongly influenced by the other constituents. The paste must have a degree of both thixotropy and pseudo-plasticity (364) since it is required to flow through the screen on the application of a high shear rate, stay runny enough to form a continuous line and yet show a rapid return to the original viscosity so as not to spread over the substrate. The vehicle is removed during

firing although the solvent is required to have a low vapour pressure as the paste spends a long time spread thinly over the screen. Consequently pastes require drying thoroughly before firing. A typical vehicle is ethyl cellulose dissolved in butyl carbitol.

Thick film pastes are covered in greater detail by Vest (369), Larry et al (370) and Verma and Roberts (371).

The advent of low firing dielectric pastes, plus increasing costs, has lead to interest in Au, Ag and Cu conductors. (Al and Ni have also been investigate but gave generally poor results (372)). Unfortunately Ag tends to migrate easily and readily dissolves in some commercial solders. Thus it is more usually alloyed with one of the more refractory metals. Au offers excellent properties and has been used for many years but considerable cost savings are available, with little loss in performance, by using Cu. (Pitkanen et al (373) cited a 36% saving when comparing multilayer Au and Cu hybrid circuits). Thus there has been much work in recent years in the development of Cu based pastes which offer excellent adhesion, good solderability and low resistivity (372-377).

A complication in the processing of Cu thick film pastes is the need for an inert furnace atmosphere during firing. The paste is particularly prone to oxidation above ~150°C and before sintering because of the large surface area involved and thus O_2 levels must be kept in the order of a few ppm. After sintering, levels up to 600 ppm can be tolerated with only slight oxidation of the surface (378). Wu et al (379) however

have suggested a technique for firing Cu pastes in normal atmospheres. Here the substrate is placed within a low carbon steel vessel, the principal being that the oxygen will preferentially combine with Fe (ΔH = -1097 KJmol^{-1}) rather than with Cu (ΔH = -155 and -167.5 KJmol^{-1} for CuO and Cu$_2$O respectively). The physical properties of the air fired paste were found to be comparible with those fired in N$_2$.

6.2.2 Screen Printing

Although the final physical properties of a conductor are a function of both composition and firing, the overall nature of the pattern (line definition, thickness etc.) is dependant on the printing conditions, see Giesfeldt (380). To print a certain pattern a photopositive is made of an accurate drawing and this is then used to expose a screen covered in a light sensitive emulsion. The exposed emulsion can then be removed and the remaining coating hardened off. After positioning the screen above the substrate it is covered with the desired paste. A semi flexible squeegee is then made to push the pattern onto the substrate and ink into the gaps in the screen. As the screen peels off behind the squeegee, ink is drawn through the screen by surface tension onto the substrate below.

The printed line is dependant on a number of variables such as i) emulsion thickness, typically 10-25 μm. ii) screen type e.g. polyester, nylon or stainless steel. The latter is particularly suitable (381) for the fine line work encountered in multilayer substrates as the filaments

can be drawn finer than the others although the flexibility of the screen as whole is reduced. iii) screen orientation, typically 90, 45 or 22.5°. A 45° screen can lead to lines with serrated edges if lines lie in the direction of the squeegee track or 90° to it. A 90° mesh however can cause fine lines to disappear if they coincide with the position of a filament and thus 22.5° screens are usually a good compromise. iv) Pattern orientation. Kurzweil and Loughran (382) noted that the direction in which narrow conductors are printed has a significant effect on their definition and quality. The best results were obtained when the squeegee motion was parallel to the conductor length. v) nature of squeegee pressure, approach angle etc. - see Atkinson (383).

6.3   EXPERIMENTAL METHOD

In order to obtain optimum green sheet properties a number of possible binder formulations were investigated. A range of binders were used that represented a number of chemical types, some of which required aqueous solutions. In such cases a proprietary deflocculent was also used. Organic binders were usually dissolved in a mix of toluene and methanol although many other solvents could have been used. Excessive use of acetone in the mix however sometimes gave problems with rapid skin formation on the cast film. Two plasticizers that appeared to work well were di-n-butyl phthalate and polypropylene glycol and these were used exclusively.

In industrial processes the method of mixing is first by milling the coarse powder in the solvents and dispersants followed by the addition of the binder/plasticizers etc. and milling for a further 24 hours. This yields and homogeneous mix of the correct rheology. This approach is unsuitable for the large number of differing compositions studied here so mixing was performed by vigorously shaking together all the consitutents for about 15 minutes. A light vacuum was pulled over the slip until bubbling ceased so as to reduce the risk of 'pinholes' in the cast film. For suitable mixes the mixing method was satisfactory although small agglomerates were noticeable in the dry tape.

Casting was performed by pouring the slip onto a piece of Mylar sheet taped to a flat glass bed. (It was found that a very thin coat of Si grease spread over the Mylar before casting facilitated the removal of the dry tape). A stainless steel blade with a polished edge was drawn through the slip, guided by two pieces of brass shim 0.25mm thick. These dictated the final width (~40mm) and height (~0.1mm) of the tape. Drying was performed by blowing vapour saturated air over the length of the tape until the solvents had evaporated. After leaving for a further half an hour the successful mixes could be peeled from the carrier and cut to the desired shape.

The various experimental components used in the binder formulation along with the compositions studied are given in Appendices III and IV respectively. It was found that the water soluble binders did not wet the Mylar too well although this was not such a great problem with HA4. The best results were obtained with ethyl cellulose N-200 mix and, to a

lesser extent, polyvinyl acetate. (This may have been through a fortutious selection of the other components and does not imply that these two are the only effective binders). The dry density of the N-200 sheet was 1.72g/cc, calculated by measurement of dimensions and the mix was used in the next processing stages i.e. printing, laminating and firing.

The printed test pattern consisted of a series of lines of differing width and spacing in order to determine the most suitable combination and to check line definition. Some of these lines connected with smaller squares to enable electrical tests to be made whilst two isolated larger squares were for surface resistivity and peal strength measurements. Printing was performed on a DEK 240 screen printer using a 325 stainless steel mesh set at 22.5° and with an emulsion thickness of 18 μm. The green substrate was held in place by a vacuum bed with the squeegee pressure and print gap determined on a trial and error basis. A squeegee speed of ~5cm per second was found to be suitable. The print medium was DuPont 9924, a glass-bonded, nitrogen-fireable copper paste especially formulated for the inner layer conductors in high density multilayer interconnects. The printed green sheets were dried at ~100°C for 10 minutes to completely evaporate all volatile constituents in the paste and then stored in a N_2 atmosphere prior to use. Optical micrographs of part of the printed green sheet are shown in Fig.6.1. It can be seen that there is still good line definition even for the narrowest lines (~100μm) and no shorts were visible even for lines 100μm apart. The 'bumps' on the lines are due to the effects of screen orientation.
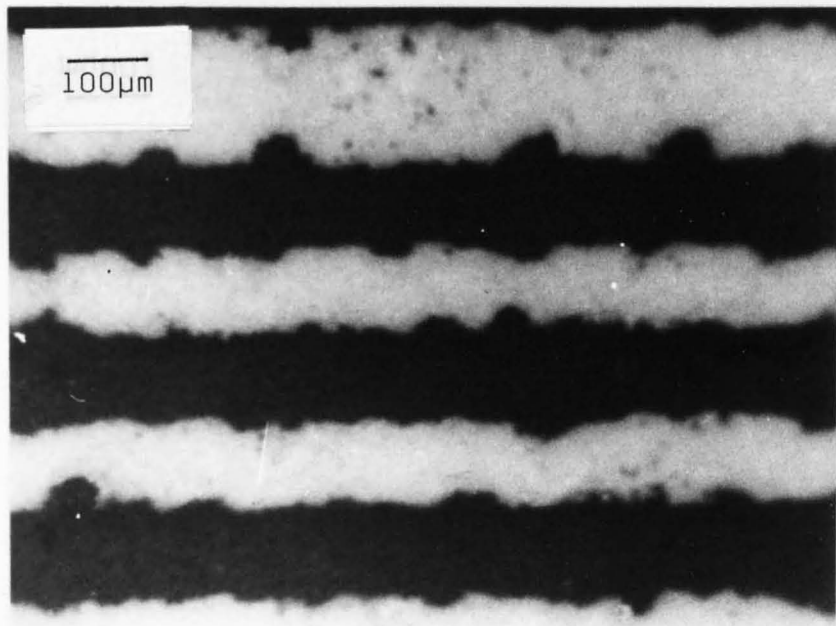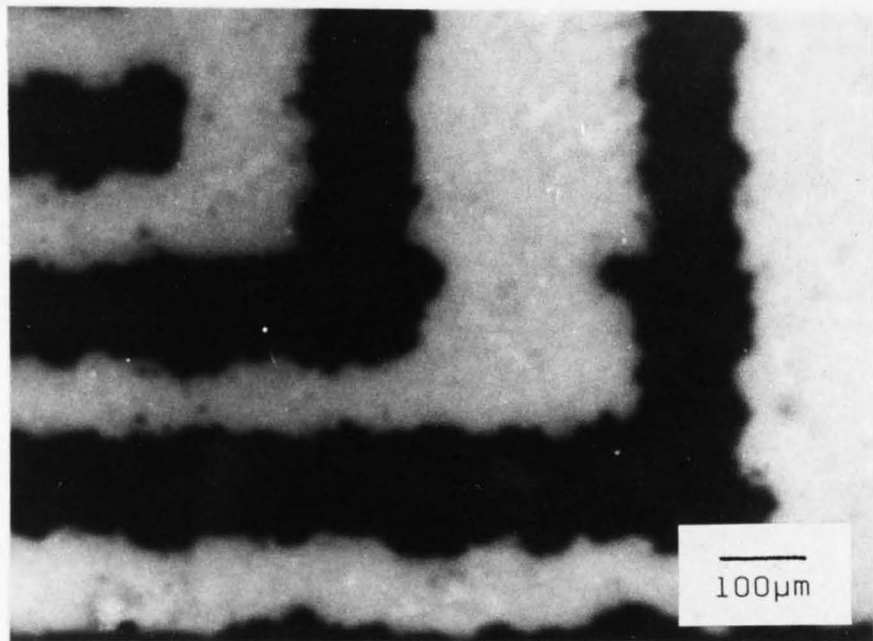
FIG.6.1 Optical micrographs showing freshly printed
copper conductors on the green ceramic

FIG.6.2 Change in weight versus temperature for N-200 mix heated at 3°C/min. in dry N_2
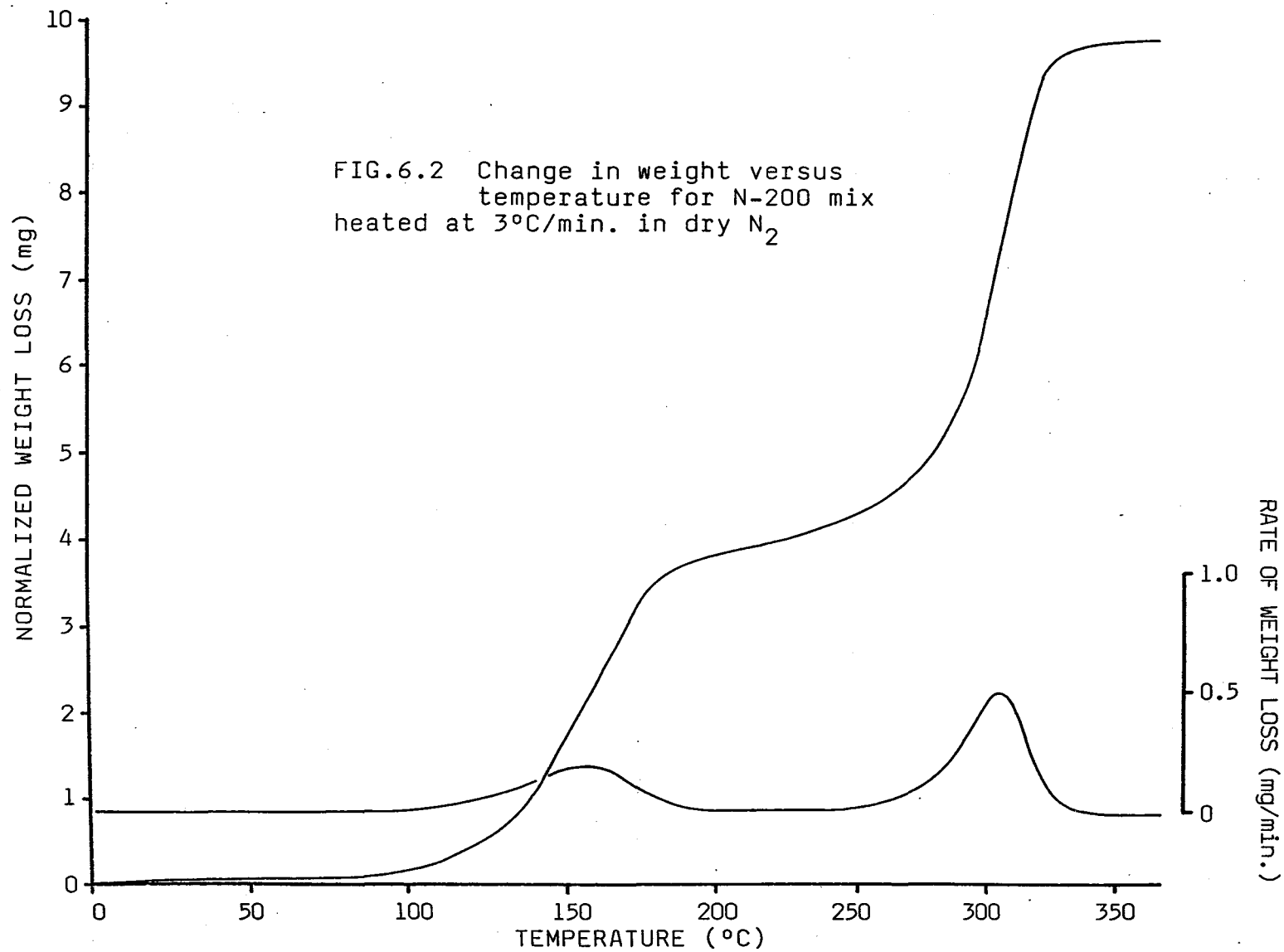
The laminating process involved the pressing together of a printed and unprinted green sheet at ~35 MPa and 100°C. This was made possible by two hollowed out stainless steel blocks through which steam was passed. The contact surfaces were polished to 1200 grit and again a thin layer of Si grease aided the removal of the sheets after pressing. The elasticity of the binder/powder mix was reflected in a negligible change in dimensions of the laminate after pressing was completed.

Ordinarily pastes are deposited on prefired substrates or dielectric films so that in the firing process the ramp rate can be fairly rapid (e.g.~80°C/min.) with a short upper dwell time (e.g. ~10 minutes at 900°C). Such a profile is suitable for belt furnaces which allow for a rapid turnover of substrates. For multilayer green sheets however this firing sequence would yield very poor articles as temperature gradients would give rise to distortion, a heating rate of 2-5°C/min. is usually more suitable. Added to this are the various dwell stages for binder burn out etc. A further complication is the change in furnace atmosphere necessitated by the need to remove carbon residues which impede densification and are a remnant of the binder burn out stage. Thus the innert atmosphere must be changed to one which is oxidising to C, to give CO and CO_2, but is still neutral to Cu. A suitable ambient for the cofiring of Cu and cordierite based glass ceramics is H/H_2O, a specific ratio of ~10^{-1} being sufficient to remove the carbon whilst the Cu is in a slight reducing atmosphere (384).

The TGA/DTG curves for the N-200 mix fired at 3°C/min. in dry N_2 are shown in Fig.6.2 and clearly show the temperatures at which the constituents of the binder evaporate. The peak at 307°C corresponds to
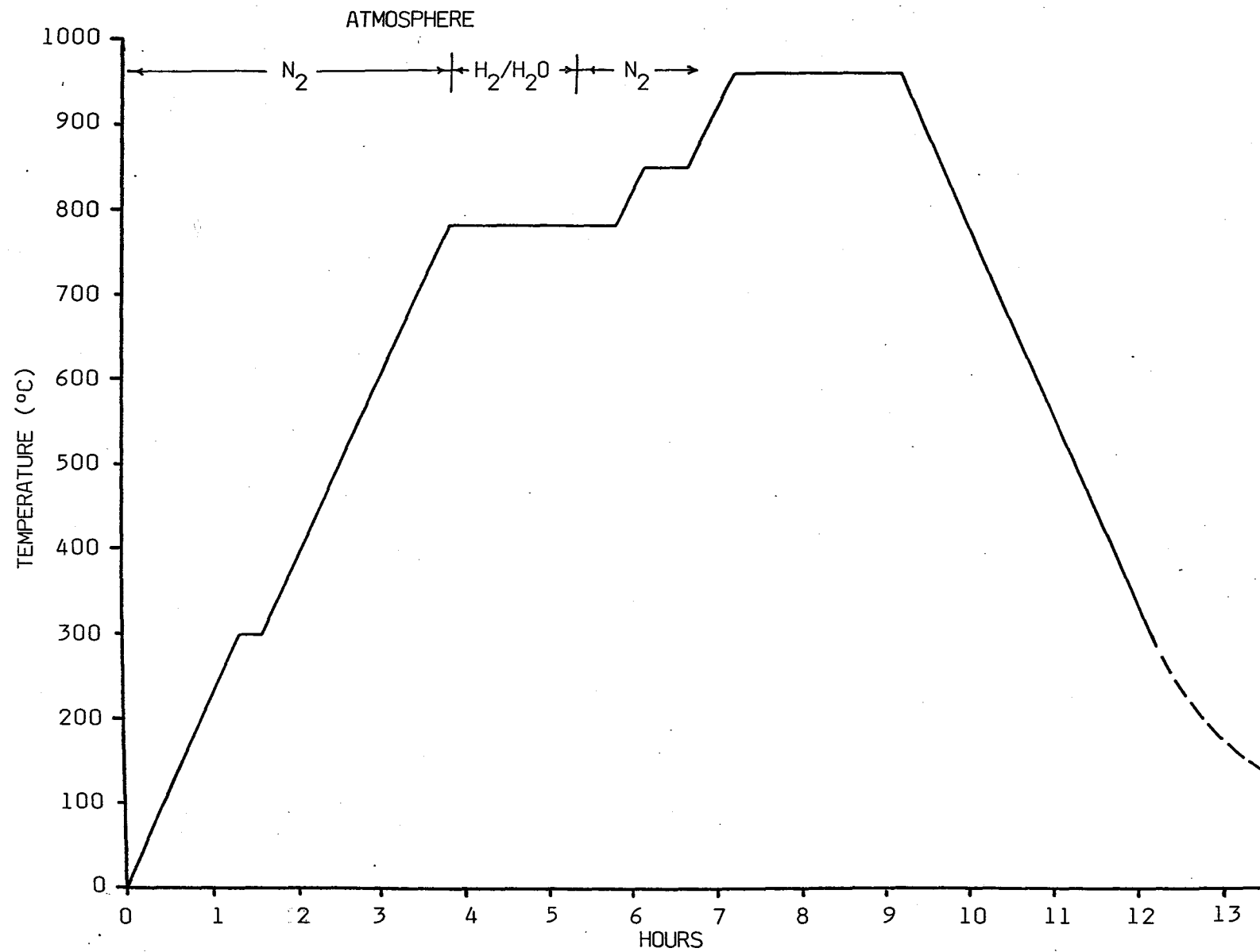
FIG.6.3 Heat treatment profile

FURNACE   SAMPLES

VENT

O RING SEAL   ALUMINA TUBE   MULLITE   THERMOCOUPLES   FLOW
                                             TUBE   METER

N_2

H_2O

H_2
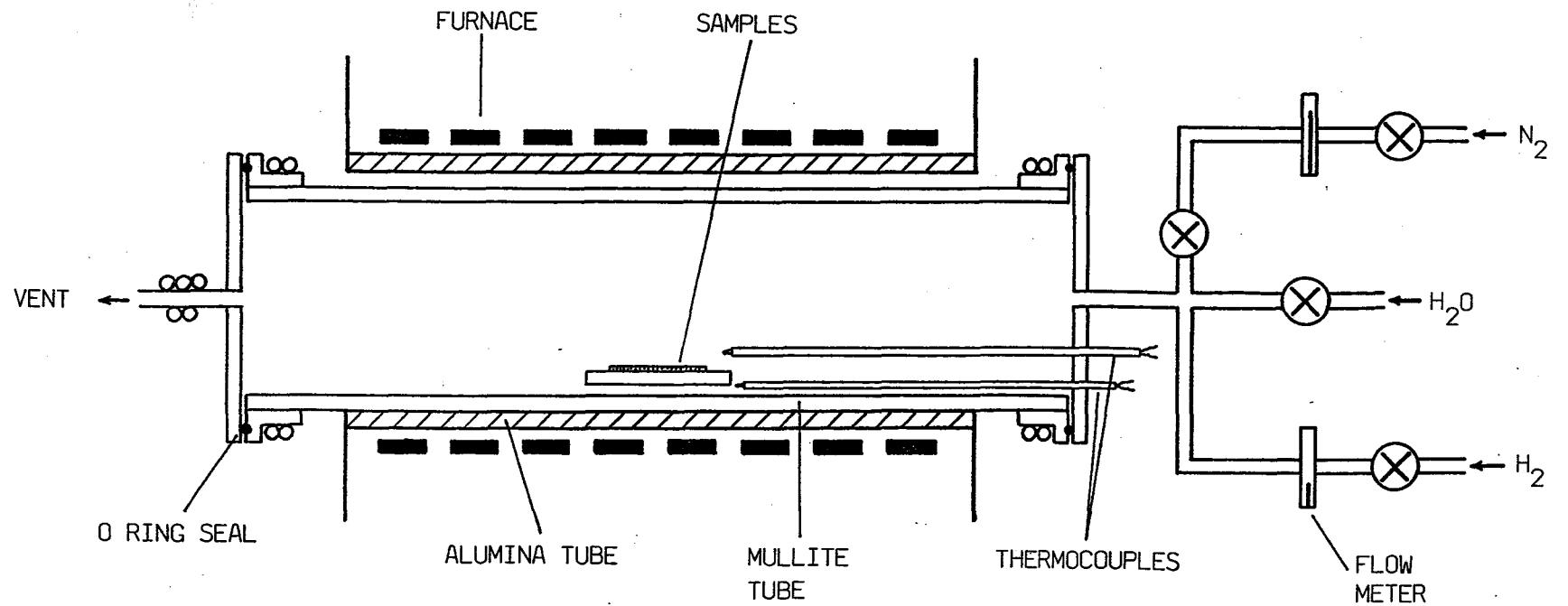
FIG.6.4   Inert atmosphere furnace

a weight loss of 0.5mg/min. Faster heating rates displaced both peaks to higher temperatures and increased the rate of weight loss. At 20°C/min the second peak was at 345°C and gave a weight loss of 3mg/min. Taking the TGA results into account and bearing in mind all the other requirements the heat treatment profile outlined in Fig.6.3 was adopted for firing the laminated green sheets. The hold at 300°C is to aid binder removal and the one at 780°C is to remove the residual carbon deposits. This temperature is suitable since the glass is still sufficiently porous to allow easy passage of the H_2/H_2O atmosphere throughout the substrate. Towards the end of the hold the H_2/H_2O atmosphere is again replaced by N_2 and sufficient time is left to remove any entrapped or dissolved water. The other two dwell times are concerned with powder consolidation and phase development.

A diagramatical representation of the furnace arrangement is shown in Fig.6.4. Cooled rubber O rings provided a gas tight seal for the two differing atmospheres used. After the H_2/H_2O mix had passed through the furnace the steam was condensed out before allowing the H_2 to be vented to a suitable outlet.

6.4   RESULTS AND DISCUSSION

After firing, the final product consisted of a white, sintered ceramic sheet with the copper test pattern embedded within it. The overall thickness of the laminate was ~0.19mm suggesting a negligible shrinkage in this direction although the other two lengths shrank by about 16%, not uncommon for these sort of substrates. Shimada et al (15) however,

for their lead borosilicate - alumina glass ceramic, found that shrinkage was dependant on the surface area of the glass powder, levelling off at ~12.5% above $40m^2/g$. It was noticed that the thin ceramic had deformed around the larger test pads, the thermal expansion mismatch over the large area concerned (10mm x 10mm) being sufficient to distort the adjacent regions, forcing them to curl upwards. Thus it would appear that this type of general test pattern is unsuitable for such thin substrates and that one of plain parallel straight lines would have been a better choice. Any tendency to distort would then be counteracted by the next two adjacent Cu layers orientated at 90° to it.

The firing of a single ceramic layer with the copper pattern screened onto it yielded very poor results with many parallel cracks running perpendicular to the conductors and thus impeding any electrical measurements. The nature of these cracks suggest that they have been caused by the expansion difference between the Cu and cordierite, the single ceramic layer being insufficiently strong to withstand the interfacial stress produced on cooling. No such cracks were found for the completely encapsulated conductors suggesting that in this case adhesion around the periphery of the conductor is greater than the shear stress at the interface and so cracks were not propagated. It was noticed however that this stress was able to distort the surrounding ceramic in that the overall thickness of the substrate was greater in the regions beween the conductors (180-190μm) than it was either side (135μm). Again this rippled effect is expected to be reduced in a more complete substrate where the other conductor and reference planes will dictate a more uniform stress distribution.

Of the two batches of substrates that were processed, the second set showed signs that a degree of oxidation of the copper had occurred. Careful examination of a section taken through the ceramic confirmed this to be so. Observation under the optical microscope clearly showed the Cu conductor, around which a reddish halo could be seen. Beyond this was a thin ($\sim5\mu m$) blackish region. The red halo appeared thicker ($25\mu m$) in the ceramic on which the pattern was printed than in the ceramic laminated on top ($\sim15\mu m$). Thus it would seem that during firing Cu diffused into the substrate and that at some stage an oxygen gradient existed across the substrate with CuO (black) forming near the surface and Cu_2O (red) nearer the middle. It was unclear from the optical examination whether the conductor itself exhibited any oxidation.

The exact cause of the anisotropic Cu_2O distribution is unclear but it may have been caused by some solvent in the freshly screened Cu paste dissolving the adjacent binder in the green sheet. This would create a low viscosity region enabling the Cu to diffuse slightly. If this was entirely true however one would expect the Cu/cordierite interface to be more diffuse than was actually observed. The oxidation problem as a whole most likely arose through an imbalance in the H_2/H_2O ratio. This was determined by measuring the output from the steam generator in a separate experiment and then during the heat treatment adding H_2 in the desired quantity by counting the number of bubbles passing through water. It may have been that the quantity of steam varied too much and thus this stage in the process would have benefitted from a more precise 'in situ' monitoring of the amount of steam passing into the furnace.

Pitkanen et al (385-387) examined the compatibility of various Cu thick film/dielectric thick film systems. They observed that, apart from compositional effects, the amount of pre oxidation that occurred during the drying stage of the paste controlled both blistering and diffusion such that the temperature at the onset of blistering, the threshold temperature for diffusion and the density of the dielectric films are established in the early stages of processing (386). A surface covering of cupric oxide is the principal contamination which converts to Cu_2O during the high temperature processing inhibiting both sintering and adhesion. Addition of H_2 at 100 ppm removed the oxide film but brought on delamination whilst at 1000 ppm total loss of conductor adhesion occurred (385).

In the first set of fired substrates an optical examination gave no indication of oxidation but back scattered SEM imaging of a typical section showed copper diffusion into the dielectric. This can be seen in Fig.6.5 which shows a distinct halo around the conductor. EDAX spot analysis confirmed that these white particles contained mostly copper. Obviously Cu in some form has diffused from the conductor and precipitated out to form crystallites less than 1μm in size. These areas of Cu precipitation appeared fairly symmetric around the conductor which would not be expected if partial solution of the copper phase had occurred during printing. Generally two observations can be made. Firstly there appears to be a region approximtely 5μm wide around the periphery of the conductor which shows little sign of copper precipitates. Secondly, many of the larger crystallites appear to have an elongated form. The latter may be due to preferred orientation
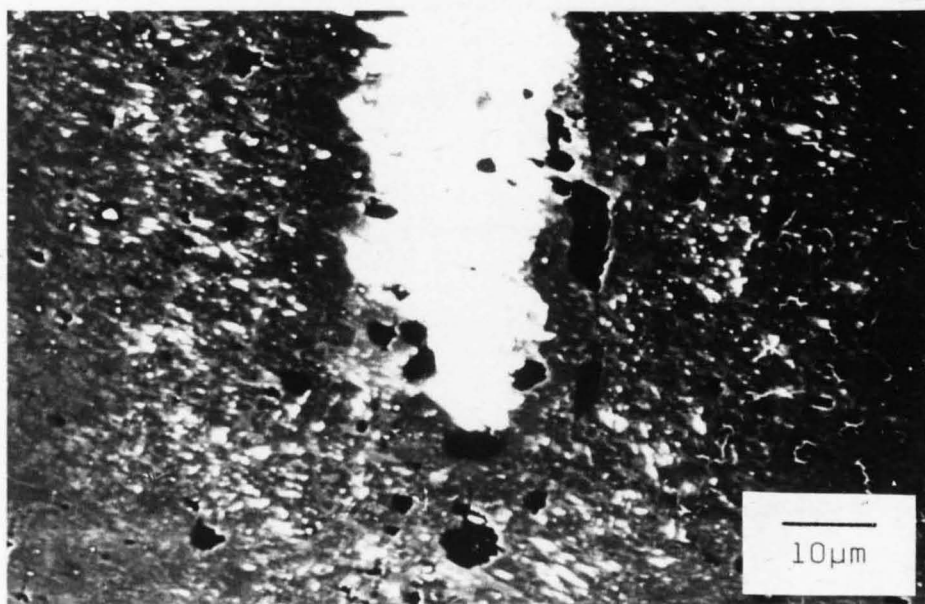
FIG.6.5 Section of a copper conductor and the
surrounding copper precipitation
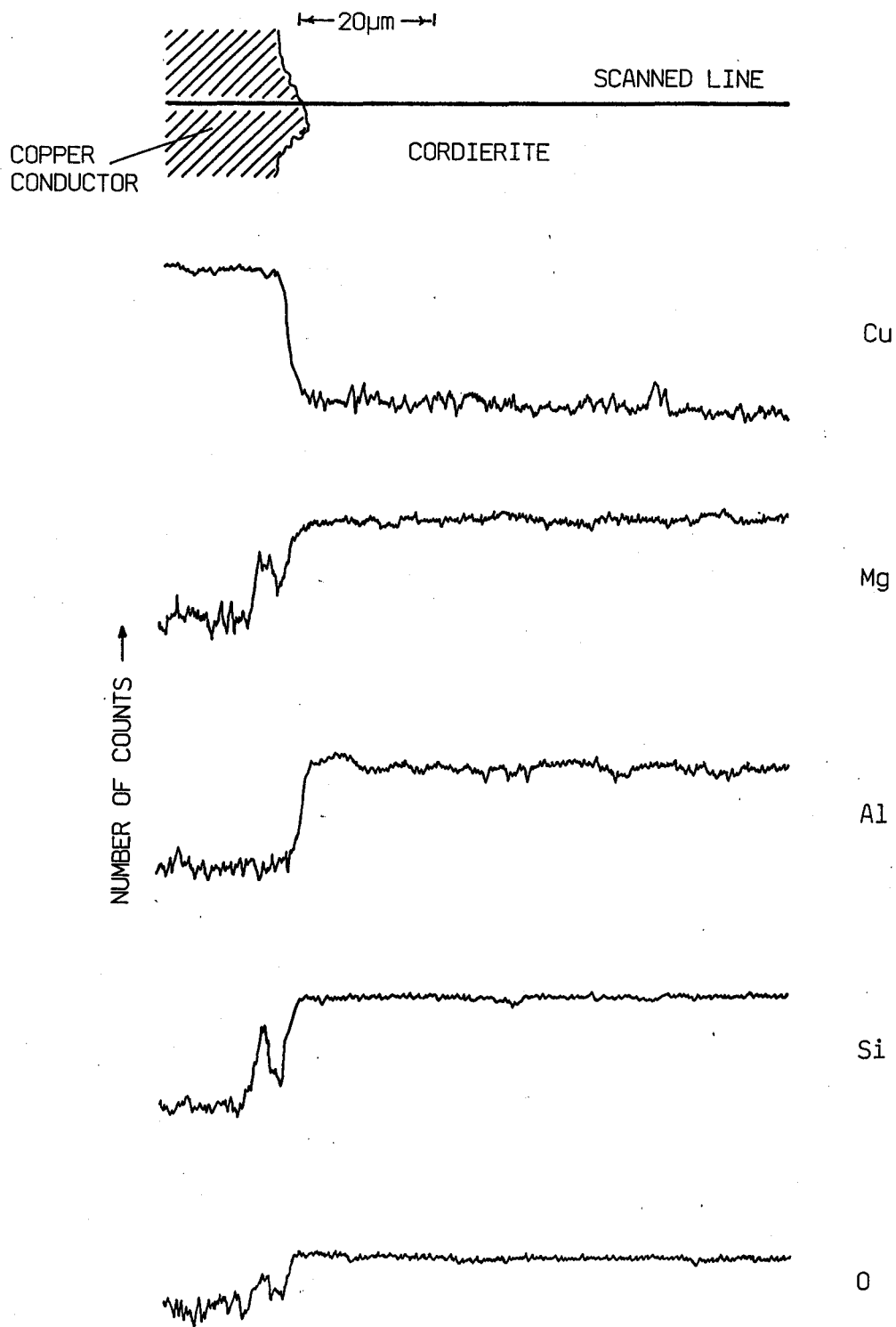
FIG.6.6 EDAX line scans across the copper/cordierite interface

effects brought about by the residual stress field associated with the Cu/dielectric interface or possibly 'smearing' during the polishing stage.

The cause of the denuded zone around the conductor is due to a compositional change of the dielectric in this region. This leads to a greater solubility of copper although its limited extent does not inhibit Cu diffusion through it. There are probably two factors which affect the composition of this interfacial region -

i) interaction between the cordierite glass and the lead borosilicate frit present in the 9924 conductor paste.

ii) interdiffusion between the Cu in the conductor and ions from the surrounding glass ceramic.

In the first case the frit was present at only ~10 volume % and any interactions will be much reduced once the glass has crystallized. In the second case EDAX spot analysis of the denuded zone showed that ~2μm from the interface there was a ~4% depletion in both MgO and SiO_2 (with a corresponding 8% enrichment of Al_2O_3) with there being no disparity at 5μm.

Evidence for the diffusion of Mg and Si into the conductor is shown in Fig.6.6 which gives typical EDAX line scans across a Cu/dielectric interface for the major elements present in the system. Increased concentrations of both Mg and Si can be clearly seen ~10μm into the

conductor. The amount of Cu falls off rapidly at the interface to a low level although a few slightly larger than average Cu peaks appear at varying distances from the interface and these may be due to groups of precipitated crystals. The general noise of this part of the Cu trace however is more likely because of random fluctuation in the X-ray statistics due to the low level of Cu present rather than an inhomogeneous distribution of Cu. Careful analysis of the mean line drawn through this noise does show a slight decrease in Cu content away from the interface, an observation which was also made on other Cu line scans. EDAX spot analysis gave a Cu concentration of ~1.5% for distances between 2 and 30μm although this sometimes rose to nearer 4%, again presumably due to precipitated Cu containing crystals. No Cu was detectable ~45μm from the interface.

Copper diffusion in cordierite has been briefly studied by Poetzinger and Risbud (388) and Kriven and Risbud (389). As with this work, they found (389) that at an oxygen partial pressure $pO_2 = 10^{-4}-10^{-1}$ Pa there existed a denuded zone 20μm from the interface and dispersed Cu precipitates from 20-50μm distance, the larger dimensions being due to increased heat treatment times. Using a variety of techniques they showed that at 800°C Cu diffuses as Cu^+, which is to be expected thermodynamically (see also Singh and Nath (390)). By 1000°C however, TEM diffraction analysis suggested that the precipitated particles were mainly metallic copper. The most likely mechanism for this would be the breaking of Cu-O bonds to form Cu_2O followed by reduction of this oxide, i.e.

$$2 \; (\equiv Si-O-Cu \;) \quad \rightarrow \quad \equiv Si-O-Si \equiv \; + \; Cu_2O$$

followed by $\qquad 2Cu_2O \; \rightarrow \; 4Cu + O_2\uparrow$
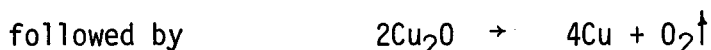
At 1000°C and $pO_2 \sim 10^{-5}$Pa reduction of Cu_2O is favourable since this gives a reduction in free energy of 165KJ (388). For this work where T = 970°C and $pO_2 \sim 10^{-1}$Pa the reduction is 88KJ and thus there would appear to be no reason why the same diffusion and reduction mechanisms should not occur here. Finally, to confirm that the observed precipitates were chemically different to the surrounding matrix, part of the exposed section was ultrasonically etched in 10% nitric acid for 15 seconds. Re-examination of the etched region showed that the majority of the precipitates had been removed although it was noticeable that the few remaining crystals showed no sign of etch pits around them. Attack of the conductor had also occurred - this being most prominent around the interface region where etching had been aided by the associated interfacial stresses.

CHAPTER SEVEN - FINAL SUMMARY AND CONCLUSIONS

The preceding chapters have covered in detail many of the aspects concerning MLC fabrication, from powder production through to lamination and firing. Also investigated was the nature of the cordierite based glass ceramic used, its phase evolution and material properties. The purpose of this chapter is to look in more detail at some of the areas that have shown themselves to be of importance, either from a fabrication or from a materials science viewpoint, and to discuss the feasability of using cordierite dielectric layers for multilayer packaging applications.

7.1   THE EFFECTS OF MILLING

In section 3.1 the milling operation was investigated and it was shown that MAS NMR represents a convenient method of quantifying and pinpointing sources of contamination that occur. This is particularly so for ^{27}Al resonances due to the speed by which spectra can be obtained having an acceptable signal to noise ratio. However, for the milling arrangement used here ^{27}Al analysis alone does not yield information on whether the contamination is from the grinding media (alumina and magnesium silicate) or from the jar lining (aluminous porcelain). The absence of quartz peaks in the ^{29}Si spectrum however would confirm that the majority of the wear is from the alumina balls.

If contamination proves to be a problem then there are several possible ways to reduce it. Analysis of the alumina media used showed it to be

only 88% Al_2O_3 (the rest being mostly MgO and SiO_2) and this may partly account for the ~8% observed contamination. This figure could be much reduced by using harder balls of higher alumina content. Another approach would be to do away with the proprietary media altogether and use media of the same composition as the powder being milled. For example, the cordierite powder used here could be milled using larger glass blocks made from the same melt. Slabs of glass could be poured, annealed and then varying sized cylinders trepanned out, thereby reducing the source of contamination to the jar lining alone. This in turn can be reduced by using rubber or dense polyurethane lined mills and preheating the resulting powder prior to use. Steel fragments from steel lined mills can be removed by acid leaching.

An alternative comminutive technique which gives rise to low levels of contamination is that of fluid energy (jet) milling. In this method the coarse powder is fed into one of two diametrically opposed fluid jets (usually compressed air but can also be water, steam or N_2 etc.). The powder is deflected out of the grinding chamber and into a round processing chamber, finer particles being drawn off at the centre whilst the larger ones traverse the chamber wall to be fed into the second jet. Thus comminution is solely via impaction between powder particles and contamination only occurs from the chamber walls.

The powders so produced by either comminutive method are fairly active which is desirable since in the firing process as short a period as possible at high temperatures is required. Section 3.3 showed that the effects of differing particle sizes and shapes gives rise to deviations from the expected theoretical shrinkages. The initial contraction of

compacts is linear however whilst during the later stages sintering rate slows due to the effect of isolated pores. The results of section 3.3 also show that there exists a shrinkage anisotropy for compacted pellets which complicates the shrinkage of more complex shapes. Fortunately this is not a problem in green sheet processing since the powder is initially held in suspension.

7.2   SURFACE CRYSTALLIZATION

Part of a larger liquid milled particle is shown in Fig.7.1 and it is possible that the milling operation may exert an influence on the crystallization kinetics. From Fig.7.1 it can be seen that although exposed regions are relatively smooth, presumably due to the polishing effect of submicron particles in suspension, other less exposed surfaces are quite rough and undoubtedly contain numerous surface cracks. Such regions would be expected to catalyse crystallization as suggested by Helgesson (159) although the slow heating rate used in this study would reduce the effects of the associated stress fields as the particle is heated through the annealing point.

That surface crystallization is readily nucleated by surface defects has been shown by Adams and McMillan (391). They polished glass specimens to 6μm diamond paste and then subjected the surfaces to an increasing severity of abrasion prior to crystallization. It was found that the proportional increase in the modulus of rupture was related to the improvement in surface nucleation density. Also Partridge and McMillan (392) found that in some cases applying a prior high surface abrasion to $ZnO.Al_2O_3.SiO_2$ glass lead to a strength increase of ~50%. Thus these
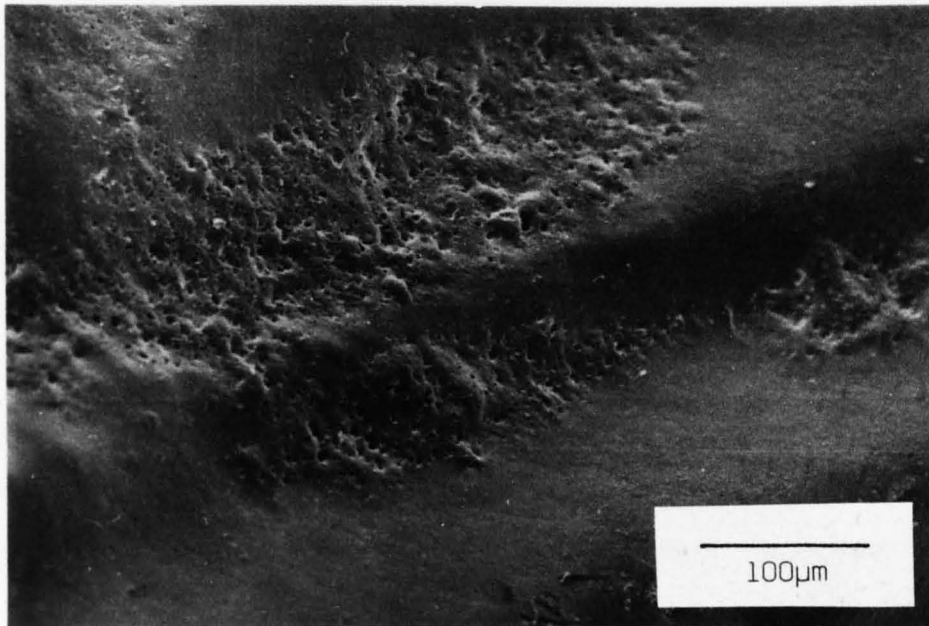
FIG.7.1 Surface of a glass particle milled in methanol

rough regions on the individual glass particles would be expected to act as nucleation sites for the crystals shown in Fig.4.2. Zdaniewski(279) observed that in his material these pseudo spherical crystals of μ cordierite were possibly composed of a number of smaller (50-100nm) crystallites and this may also partly account for the XRD size discrepancy outlined in section 4.1.2.

Chapter four also raised some interesting points about the crystallization mechanism generally. For instance, in the larger pieces of glass a quartz like phase appeared to be the precursor to α cordierite development whilst in the powder form the precursor was μ cordierite. A possible reason for this could be difference in oxygen partial pressure above the glass surface for the larger specimens and within the compacts, where it may be much lower. Such conditions exist in thick films and is the likely cause of reduction of PbO and Bi_2O_3 (which is present in the frit) to metallic Pb and Bi (369). The mechanisms of nucleation can be altered if oxygen recombines with any oxygen deficient sites that occur at the glass surface. The effect of furnace atmosphere has been shown by Partridge and McMillan (392) for their glasses where surface crystallization was inhibited for oxygen and water vapour deficient environments.

Further to this surface modification, it is also possible that a certain degree of P_2O_5 and B_2O_3 volatilization occurs during the heat treatment process to leave powder particles with a thin surface layer deficient in these additives. (This statement could be checked by using secondary ion mass spectrometry which detects concentration changes of elements as a function of depth and has a typical resolution of ~10nm). If such a

scenario existed then it might be expected that crystallization could occur in this defi cient layer before it would for the rest of the bulk glass and this has been shown by the DSC results, Fig.4.22. This is particularly so for C6 glass, which contains no P_2O_5 and B_2O_3, and where the onset and maximum rate of crystallization occurs some 20°C below that for C1.

7.3   PHASE DEVELOPMENT

In order to further investigate the occurance of the quartz like phase, careful examination was made of the initial stages of crystallization using XRD.   It was found that for pressed compacts of C1(M36) glass μ cordierite indeed appeared to be the first phase to crystallize but for loosely stacked powder the quartz-like phase was also present. This is shown in Fig.7.2 which is for a heat treatment up to 865°C followed by air quenching. The quartz like phase only existed for a few minutes before disappearing to leave just μ cordierite but it was not possible to discern which phase appeared first. The co-existance of these two phases was also found to occur initially for compositions C3 and C5. This difference between well compressed and loosely stacked powders would further support the idea that pO_2 plays a role in the nucleation of this unknown phase. (It has already been mentioned that firing in N_2 has an effect on the phase evolution generally). There is also a large difference in the stability of the phase, it being shown to exist for over two hours heat treatment at 850°C for larger surface areas but for only a few minutes for bulk specimens. Thus diffusional mechanisms from depleted regions around the crystal phase may also play a role in dictating the existance and duration of this phase.
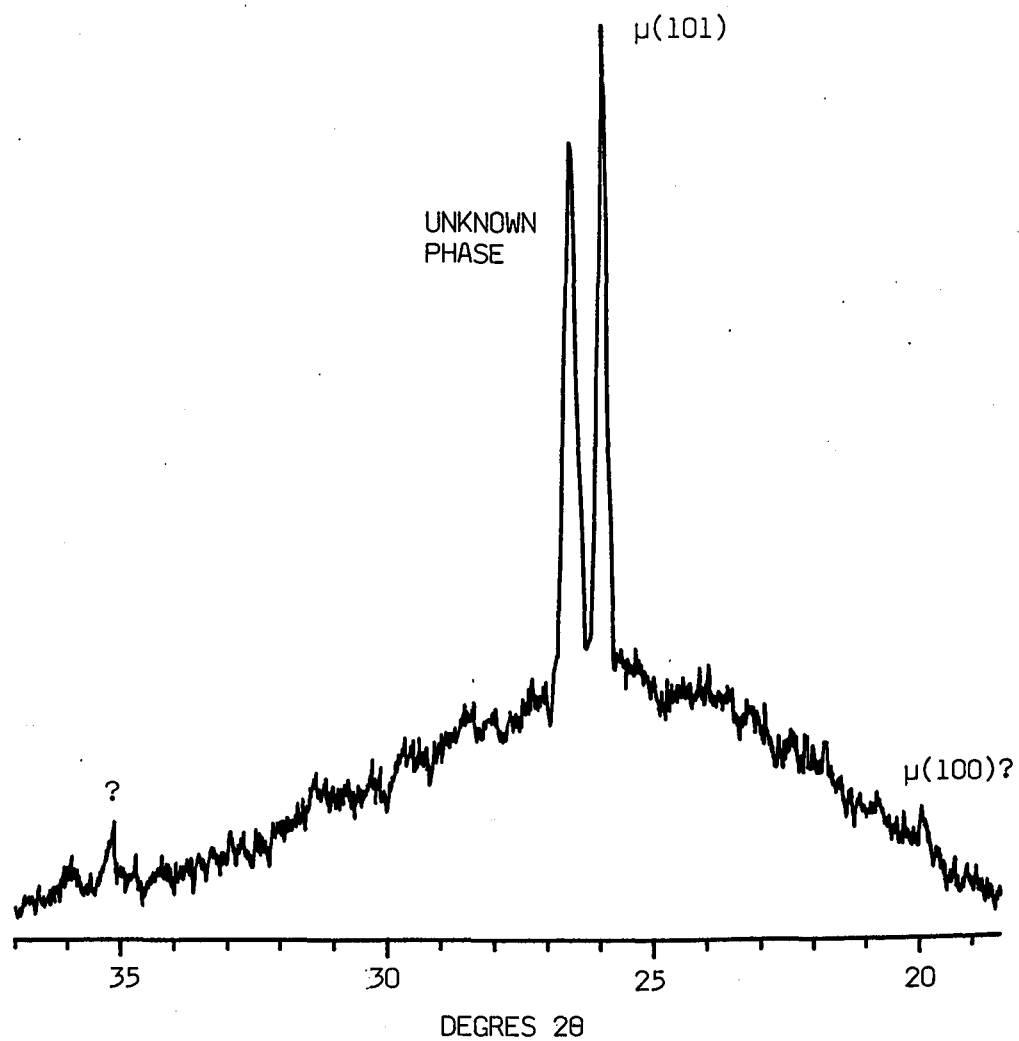
FIG.7.2 XRD pattern for loosely stacked C1
powder fired to 865°C and quenched

In the introduction it was noted that the phase development and physical properties of MAS and $Li_2O.Al_2O_3.SiO_2$ based glass ceramics are comparable due to the similarity in size of the Mg^{2+} and Li^+ ions. Recently Headly and Loehman (393) have looked specifically at the role of P_2O_5 in crystal nucleation and growth in the latter glass system. They were able to show using TEM that crystal formation is via an epitaxial growth on tiny Li_3PO_4 crystallites which precipitated out at lower temperatures. Thus if bulk nucleation occurs it may be that a magnesium phosphate phase acts as the precursor to crystal growth.

7.4   THE EFFECT OF THE DIELECTRIC

In a MLC, the sintering and phase changes that occur during firing cannot be assumed to occur independently since the package is in fact a 'two phase' system, the thick film conductor forming a continuous second phase. Even slight variations in dielectric behaviour can have measurable effects on device performance. As previously mentioned alumina is the most common substrate material and thick film properties are usually quoted by the manufacturers in conjunction with it, 96% alumina being the usual standard. Hailes and Crossland (394) have shown however that even the nature of the remaining 4% (either MgO/SiO_2 or CaO/SiO_2) can have a significant effect and thus the substrate plays a vital role in maintaining a delicate balance between chemical and physical reactions that occur at the thick film/dielectric interface during the firing cycle.

7.5   THE EFFECT OF THE CONDUCTORS

One of the advantages of copper thick film pastes is their good adhesion

and this was certainly found to be so for this system with very little sign of disruption of the Cu/cordierite interface. The stress at this interface is expected to be quite large due to the difference in thermal expansion between the cordierite ($\sim 16 \times 10^{-7} °C^{-1}$) and the copper ($\sim 170 \times 10^{-7} °C^{-1}$). However the bond between the two via the permanent binder, is sufficiently strong to withstand this stress. That a stress field does exist is manifested in two ways:-

(a) Distortion and enlargement of pores in the neighbourhood of the conductor, Fig.6.6 being a more extreme case. Most pores were found to be elongated in a direction parallel to the interface.

(b) Distortion of the final ceramic surface to give a rippled effect (see section 6.4). Taking E for the cordierite to be 80 GPa and assuming E = stress/strain then the stress required to give rise to this distortion is of the order 10 GPa. Since this is nearly two orders of magnitude greater than the measured fracture stress it is more likely that these distortions occurred during the initial heating period when the dielectric was far more easily deformed thereby allowing stress relief.

The residual stress found in metal/ceramic systems has been examined both theoretically and experimentally for a copper conductor in a cordierite matrix by Hsuech and Evans (395). They found that for metals that exhibit a large work hardening rate the axial stress is enhanced and the interfacial stress is reduced. Moreover, the presence of porosity in the metal can have a dramatic effect in that the effective expansion coefficient of the metal is reduced. This occurs through

plastic dilation of the pores, a volume fraction of only 0.01 being sufficient to lower the effective expansion coefficient from 170 to $40 \times 10^{-7} °C^{-1}$. This dilational effect is enough to reduce the stress by a factor of ~8 and may largely account for the difference between the calculated bulk interfacial stress (1500 MPa) and the measured surface value (130 MPa). (Measurements were made by investigating the effects of the residual stress field on the radial cracks eminating from Vickers indentations placed close to the copper/cordierite interface). Thus whilst a certain degree of metal porosity is to be favoured this porosity should distribute itself homogeneously since void clusters can initiate premature ductile rupture.

Chapter six also dealt with the observed Cu diffusion which occurred in the dielectric during firing. The rate of change of concentration, c, is given by Ficks second law, i.e.

$$\delta c / \delta t = D \delta^2 c / \delta x^2 \qquad (7.1)$$

where D is the diffusion coefficient and x is distance. As the diffusion of an atom/ion is dependant on overcoming a potential energy barrier and is also a function of temperature the diffusion coefficient may be written in Arrhenius form -

$$D = D_0 \exp(-Q/RT) \qquad (7.2)$$

where D_0 is the pre exponential factor, essentially D at 1/T = 0. Thus Q can be calculated from the plot of lnD versus 1/T. To a first

approximation however D can be estimated from the relation (396)

$$x^2 \sim Dt \qquad (7.3)$$

If it is assumed for this work that diffusion only occurred during the upper heat treatment period, i.e. above 875°C, then the total time the sample was at or above this temperature was ~210 minutes. Taking the periphery of the precipitated zone around the conductors to be the extent of copper diffusion then this gives from equation 7.3 a diffusion coefficient of ~6 x 10^{-14} m^2s^{-1}. This is to be compared to ~10^{-15} m^2s^{-1} quoted by Poetzinger and Risbud (388) for Cu diffusion in Ti nucleated MAS glass at 800°C. Using hot stage microscopy, Pitkanen et al (397) noticed that with dielectrics having a high glass to refractory ratio Cu diffusion started abruptly and progressed rapidly into the surrounding dielectric. Such behaviour is indicative of liquid rather than solid state diffusion and thus it is possible that in this system most of the Cu diffuses before the glass crystallizes, diffusion after this point being limited to grain boundary and slower solid state mechanisms.

The electrical performance of a conductor used for high speed signal processing is not only a function of its properties but also of the surrounding dielectric medium. Table 5.1 compares the relevant material properties determined for C1 glass ceramic with those of alumina. As can be seen, in most cases the C1 material proves to be a superior alternative to the standard substrate. Through adjustment of the $MgO:Al_2O_3$ ratio the thermal expansion can be matched to that of silicon although the role of the internal Cu network has to be taken into

account. Larry et al (370) in their substrate fabrication, which was bonded to an alumina base, chose a net expansion coefficient just below that of the base so as to place the dielectric in a slightly compressive stress so as to give maximum strength.

7.6 THERMAL MANAGEMENT

One of the biggest issues in device packaging as a whole is that of heat dissipation, with the trend towards more power in an ever decreasing space. The importance is demonstrated by Keyes (398) who has shown that signal time delay in a package is inversely proportional to the maximum thermal energy that can be removed in unit time from unit area in planar packaging technology. Thus it would appear that the biggest drawback with this material is its low thermal conductivity and, as mentioned in section 5.1.1, there is little scope for improvement from a materials point of view whilst retaining the other beneficial properties. IBM have got round this problem by taking heat out via the chip and not through the MLC by the use of the Thermal Conduction Module outlined in section 1.2.3. This represents however an engineering solution to a particular problem and consequently a more universal approach to heat dissipation is required.

One such approach is to use microchannel cooling of the silicon wafer which again has the advantage that heat flow is through the chip rather than the substrate. Here channels $\sim 20 \mu$m wide and $\sim 170 \mu$m deep are mechanically cut into the back of the chip, the channels being covered over by a cover plate thereby allowing the passage of various cooling media. For a typical superchip ~ 40mm square and dissipating 1KW this

gives a junction temperature ~30°C higher than the inlet fluid temperature even for a low flow rate of 12cc per second. This cooling mechanism and thermal management generally is discussed further by Mahalingam (399).

Alternatively a composite ceramic may give improved results. For instance, Greenwald and Payne (400) investigated SiO_2 and $SiO_2.B_2O_3$ derived glasses with SiC and AlN additions as a suitable substrate having a low dielectric constant and high thermal conductivity. Such an approach may be possible here utilising the MAS based glass ceramics. Finally cooling of the MLC itself may be possible by constructing open channels through it. Such technology to produce microchannels already exists, the channels normally being infilled by conducting pastes see (section 1.2.2).

CONCLUSIONS

In chapter one the aims of this research work were outlined. Specifically these were to develop a glass ceramic alternative packaging material to alumina that could be processed below 1000°C, to study the phase development, the properties and the process variables. Cordierite was chosen as a suitable candidate material although other glass ceramic phases may also have suitable applications.

Chapter five covers the basic material properties of the compositions studied and, compared with alumina, the glass ceramic offers distinct advantages. Two cordierite phases were found to occur, an unstable μ

phase and a stable α phase. The former was the first to crystallize and was found to be unacceptable from a packaging point of view. Fortunately the latter, which had beneficial properties, could be fully crystallized by ~960°C. The benefits of having α cordierite as a major phase are low dielectric constant (5.35) and loss angle (~5 x 10^{-4}), reasonable strength (130 MPa) and high resistivity (~10^{15} Ωcm). The only serious drawback of the material is its low thermal conductivity (~2Wm^{-1}K^{-1}) and this will require careful consideration in the design of a multilayer system.

All the compositions studied were rich in MgO and SiO$_2$ compared to the stoichiometric cordierite composition and as a result enstatite also occurred as a minor phase. The amount of this high expansion phase could be adjusted by altering the MgO/Al$_2$O$_3$ ratio, forsterite also forming with higher MgO additions. For material fired to 970°C the net expansion coefficients varied from 15 to 29 x 10^{-7}°C^{-1} for MgO contents between 22 and 25 wt% resectively. At processing temperatures greater than about 1050°C enstatite converted to protoenstatite bringing about a general degradation in properties.

Crystallization starts at the surfaces of glass particles during the final stages of sintering, probably being nucleated by the numerous surface flaws generated during the milling operation. The exact crystallization onset temperature however is dependant on the amount of B$_2$O$_3$ and P$_2$O$_5$ additions, these oxides also having a pronounced effect on phase evolution generally. When B$_2$O$_3$ and P$_2$O$_5$ are mutually excluded μ

cordierite does not transform to α cordierite until ~1175°C final firing temperature. Other factors such as furnace atmosphere and glass surface area can also have an effect on the crystallization kinetics.

Upon crystallization μ cordierite takes the form of roughly spherical crystals (or clusters of smaller crystallites) which link together to give a skeletal framework within the body, this helping to prevent deformation of the body via viscous flow at these high temperatures. μ cordierite may also form via a bulk nucleation route, being aided by prior spinodal phase separation. Evidence for this comes from a descrepancy in the activation energy determinations and crystal size determinations although the effectiveness of the bulk nucleation may also depend on heating rate. Further heating of the μ phase leads to exsolution of Mg and Si (further aiding the formation of enstatite) and then conversion to α cordierite. MAS NMR studies on this phase show that initially Si atoms prefer ring sites and that the Al tetrahedral sites are rather distorted. There is also evidence that initially some Al's may also occupy six fold co-ordination.

In the manufacture of MLC's several critical processing steps are involved, some of which were studied here. Milling in a liquid medium was found to give a powder more suitable for sintering although MAS NMR showed that this gave rise to contamination of the powder. Sintering of the dried powder followed to a degree the theoretical curves proposed by Frenkel (239) and Mackenzie and Shuttleworth (244), variation being due to average particle sizes, size distributions and the effects of

particle compaction.

Copper was chosen as a suitable conductor material and was screenprinted onto thin green ceramic sheets formed by doctor blading a glass powder/binder slurry. Firing the printed sheets showed that copper diffused into the surrounding dielectric, probably as Cu^+, before precipitating out as metallic copper via Cu_2O. Compositional changes in the dielectric just around the periphery of the conductor formed a region where precipitation did not occur. Thermal expansion mismatch between the copper and the cordierite glass ceramic gave rise to sufficient stress to distort the pores close to the interface and distort the dielectric surface although interfacial integrity was rarely impaired.

SUGGESTIONS FOR FUTURE WORK

Throughout the course of this work it has become apparent that certain areas may warrant further investigation if cordierite is to be considered as a viable contender to alumina. Although not exhaustive, some of these areas include:-

1.   Sintering experiments for powders loosely packed within a flexible binder system. Of particular interest here is powder in the form of thin sheets since a closer understanding of how they behave when fired may give rise to the ability to stipulate shrinkage tolerances more closely.

2.   Investigation of the unknown quartz like phase e.g. its crystallographic characteristics, stability, etc. Coupled with this is the need for a more systamatic study of the crystallization of the MAS glasses used in this study, areas of interest being surface area and surface finish, furnace atmosphere (particularly pO_2) and glass surface composition. A high temperature X-ray camera would greatly aid such a study.

3.   Existance of a magnesium phosphate phase as the precursor to crystal growth during bulk nucleation just as Li_3PO_4 is for $Li_2O.Al_2O_3.SiO_2$ glasses containing P_2O_5.

4.   Stress distributions in several laminated printed sheets since this will help to identify areas of either poor design or likely premature failure.

5.   Ways of reducing the upper firing temperature. This is shown to be necessary in order to minimise copper diffusion into the surrounding dielectric and reduce the risk of oxidation. A way of reducing sintering times is to use finer powders and thus production of glasses of the composition used here but via a sol gel route may offer an alternative approach. This also eliminates the contamination problem that occurs during ball milling. Pre-seeding the glass with the desired phase (α cordierite in this case) would also be expected to reduce processing times if it acted as a selective

nucleating agent. Preliminary experiments were encouraging.
Adding 10wt% of finely ground α cordierite to the powdered
glass was sufficient to develop a glass ceramic composed of
only α cordierite and enstatite after only 40 minutes at
910°C.

APPENDIX I - PHASE SEPARATION

For some liquids it is found that upon cooling it is energetically favourable that separation into two, or sometimes more, immiscible phases occurs. Such a mechanism can exert a marked influence on the crystallization kinetics of a glass system since one can now be dealing with two intimately mixed phases, probably of quite differing compositions, rather than the original continuous single phase material. If separation occurs above the liquidus then it is described as stable immiscibility whilst if it occurs below it is metastable, that is the equilibrium phases should be crystalline. The latter is also known as glass-in-glass phase separation and the generally slow kinetics associated with it makes it a potentially useful technique as demonstrated in the Vycor process (401). A review of liquid phase separation in glass forming systems is given by James (402) and is covered in more detail in the book by Mazurin and Porai-Koshits (403)

An understanding of the kinetics of phase separation comes from the consideration of a free energy versus composition curve that exhibits two minima (Fig.I.1) which get closer together as the temperature is increased. At what is termed the upper consolate temperature, Tc, the two coincide. The loci of points A and B as a function of temperature trace out two curves which meet at Tc, Fig.I.2. This is known as the binodal. Between compositions A and B two liquids are more stable than one and thus phase separation occurs. Two more curves however can also be drawn which represent the loci of the points of inflections C and D.
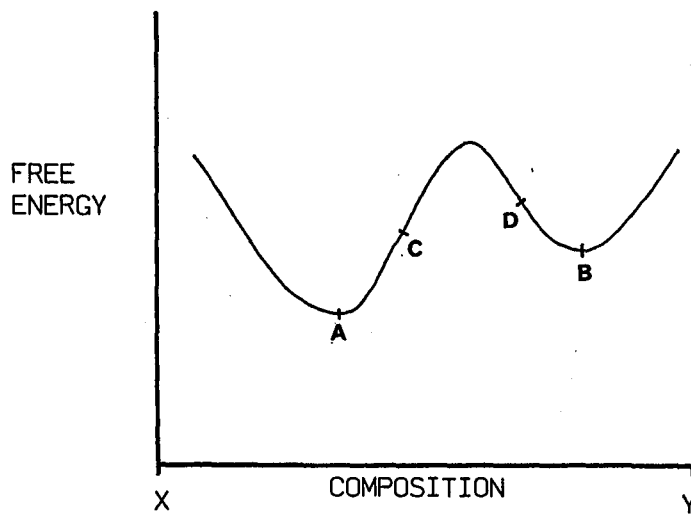
FIG.I.1 A typical free energy curve
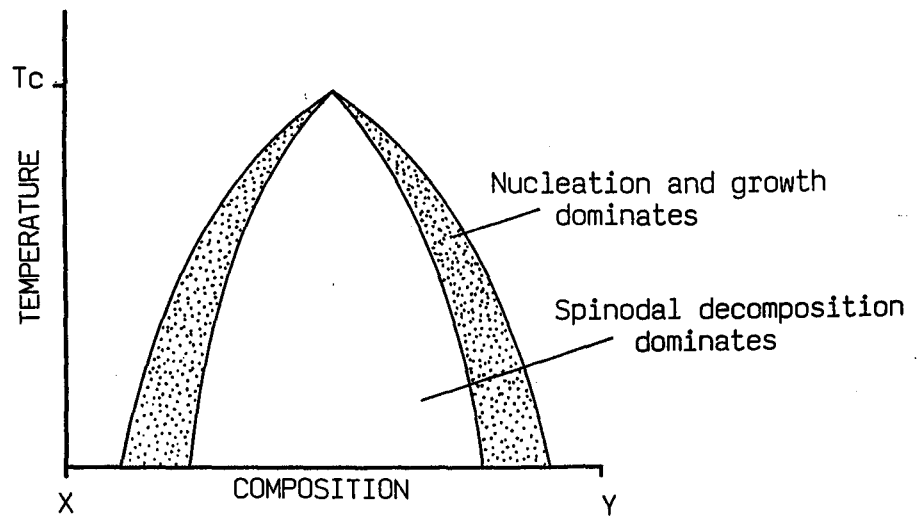
FIG.I.2 Immiscibility curves

This gives the spinodal curve which also has a maximum at Tc. The spinodal represents the second derivative of the free energy of mixing (ΔG) with respect to composition (c), i.e. $\delta^2\Delta G/\delta c^2 = 0$. Thus the binodal and spinodal lines dictate the two mechanisms by which phase separation occurs.

Between the two curves $\delta^2\Delta G/\delta c^2$ is positive and thus any compositional fluctuation will increase the free energy of the system i.e. very small nuclei that form will be unstable. If a nucleus is greater than some critical radius however then it will be stable and can then act as a nucleation site for a suitable crystal phase if the glass is going to crystallize. Thus compositions between AC and DB form solids by a nucleation and growth process, the mechanisms of which are similar to those outlined in section 1.3.2. Beneath the spinodal $\delta^2\Delta G/\delta c^2$ is negative and compositional fluctuations decrease the free energy such that compositions between CD will spontaneously phase separate (spinodal decomposition).

Spinodal decomposition is characterized by phases of high connectivity with initially very diffuse boundaries. This is due to a continuous sinusoidal variation of both extremes in composition and leads to the assigning of a value λ, the wavelength of the microstructure. The theoretical treatment of this type of phase separation is attributed to Hillert (404) and Cahn (405 - 407). The predicted structure can be described by the superposition of sinusoidal composition modulations of fixed wavelength but random amplitude, orientation and phase. On commencement of separation the initial distribution of fluctuations

changes with time. The dimensions of the fluctuation are governed by interfacial energy, favouring larger scales and diffusioned processes, favouring smaller scales. The two opposing mechanisms account for the eventual observed optimum wavelength.

APPENDIX II - CHEMICAL PURITIES

CHEMICAL	MANUFACTURER	IMPURITIES (ppm)
SiO_2(Limoze)	CP*	Fe_2O_3(10) K_2O(40) Al_2O_3(160) Na_2O(60) Li_2O(2)
MgO	BDH**	Fe(300) SO_4(1×10^3) Cl(100) Pb(20)
Al_2O_3	BDH	Fe, SO_4, Cl(50)
$AlPO_4$	BDH	Fe(100) SO_4(500) Cl(50)
H_3BO_3	BDH	K, PO_4, SO_4, Ca, Cr(10) Na(20)
ZnO	BDH	>99%
Fe_2O_3	N&W***	-

* Chance Pilkington Ltd.
   Glascoed Road
   St. Asaph

** BDH Ltd.,
   Carlyon Industrial Estate,
   Atherstone.

*** Hopkins and Williams Ltd.,
   Freshwater Road,
   Dagenham.

APPENDIX III - BINDER MATERIALS USED

NAME/CODE	COMPANY	DESCRIPTION	NOTES
Versicol W14	Allied Colloids Ltd. PO Box 38, Bradford	BINDER - Soln. of Polyacrylamide	Water Soluble Active content 70%
Glascol HA14	"	BINDER - Soln. of the ammonium salt of acrylic copolymer	Water soluble Active content 30%
Versicol KA21	"	BINDER - Soln. of the ammonium salt of polymethacrylic acid	Water soluble Active content 15%
Dispex A40	"	DEFLOCCULENT - Soln of the ammonium salt of polycarboxylic acid	Water soluble Active content 40%
N-10	Hercules Ltd. 20 Red Lion St. London	BINDER - Ethyl cellulose	η = 10 cps in 5% soln.
N-50S	"	BINDER - Ethyl cellulose	η = 50 cps in 5% soln.
N-200	"	BINDER - Ethyl cellulose	η = 200 cps in 5% soln.
Kraton G1652	Shell Chemicals Ltd. 1 Northumberland Ave. Trafalgar Sq, London.	BINDER - Thermoplastic rubber	η = 500 cps in 20% soln.
D4426	Deancraft Ltd. Lovatt St., Stoke on Trent	BINDER ?	

Mylar	Dupont (UK) Ltd. Maylands Ave., Hemel Hempstead.	CARRIER - glycol terephthalic acid polyester	~0.12mm thick sheet
5200	"	BINDER - formulated for MLC's	
PVA	BDH Ltd., Carlyon Ind. Est., Atherstone.	BINDER - polyvinyl acetate	MW ~ 33,000
PPG	"	PLASTICIZER - polypropylene glycol	MW = 2025
DNBP	"	PLASTICIZER - Di-n- butyl phthalate	MW = 278

APPENDIX IV - BINDER FORMULATIONS (in g for 100g of Powder)

BINDER	DNBP	PPG	ACETONE	METHANOL	TOLUENE	DISPEX A40	H_2O	COMMENTS (ρ in g/cc)
N-200(A)	4.0	4.33	3.77		10.0	43.3			Just too flexible $\rho = 1.27$
N-200(B)	4.0	2.3	2.0		15.7	41.4			Satisfactory $\rho = 1.72$
N-50(A)	4.0	3.4	2.9		15.7	41.4			Too flexible
N-50(B)					15.7	41.4			Too stiff - difficult to peel off
N-10	4.0				15.7	41.4			Too stiff - difficult to peel off
PVA(A)	28	1.4		34.8					Failure
PVA(B)	4.0	1.1	1.0		15.7	41.4			Just too flexible $\rho = 1.32$
5200	50.0								Too brittle
D4426	5.4	2.3	2.0	6.8			0.7		Failure
G1652(A)	4.0	2.0	1.7			20			Poor formulation
G1652(B)	4.0	5.7				57.1			Failure

W14(A)	15.0	0.4	0.3	0.7	5.0	Slow evaporation. A little too brittle. $\rho = 1.97$
W14(B)	15.0	2.0	1.7	0.7	1.4	Still too brittle
HA4(A)	10.0	2.0	1.7	0.7	1.4	Slightly better than W14 $\rho = 1.85$
HA4(B)	10	3.0	2.6	0.7	1.4	Little change
KA21	20.0	2.0	1.7	0.7	5.7	Poor wetting of Mylar sheet

APPENDIX V - PUBLISHED PAPERS

Development of the alpha-cordierite phase in glass ceramics for use in electronic devices*

D. R. Bridge, D. Holland & P. W. McMillan†

Department of Physics, University of Warwick, Coventry CV4 7AL, England

The manufacture of multilayer packages for VLSI devices requires an encapsulation material with specific properties such as high electrical resistivity, low dielectric constant, and a thermal expansion coefficient which matches that of silicon. Glasses based on the cordierite composition have been used to produce glass ceramic substrates with properties superior to those of alumina. Careful choice of composition allows sintering to near-theoretical density and crystallisation to give the preferred α-cordierite phase at temperatures below 1000°C. This has the additional advantage of allowing the use of copper paste for the conductor tracks.

Multilayer packaging is a viable prospect for increasing the net computation speed of large computers by reduction of the inter chip distance by means of increased density of the VLSI chips.[1,2] These modules allow for sufficient heat dissipation, make the best use of the available space for the linking conductor networks, and avoid excess electrical distortion of transmitted signals.

A more detailed description of a multilayer package may be obtained elsewhere[3] but a brief summary of the fabrication process is outlined here. Suitable ceramic powders, such as alumina, are mixed with organic binders and plasticisers to form a flexible 'green' sheet. After cutting to size, location holes and vias are punched, followed by metallisation of the conductor tracks with either noble or refractory metals, usually by means of thick film technology. Individual sheets or layers are stacked and then laminated at about 2 MPa and 100°C to drive off solvent and to fuse the individual layers into a coherent block. Higher temperature firing drives off residual binder and sinters the ceramic to produce a dense article filled with a three dimensional network of conductors.

A typical multilayer package has been developed for the IBM 3081 processor.[4] Here up to 133 VLSI chips are placed on an area approximately 80 mm square with a substrate of 33 layers and about 130 m of wiring. Total substrate depth is 5 mm and includes some 350 000 linking vias.

In the past alumina has been extensively used as the main substrate material because of its high electrical resistance, good thermal properties, and high strength. However, alumina also has some undesirable properties which severely limit its effectiveness. Its high sintering temperature (> 1500°C), for example restricts the associated conductor material to high melting, costly, and generally high resistivity metals such as tungsten, molybdenum, or platinum. Ability to sinter at temperatures below 1000°C would enable more conducting metals with lower melting temperature to be used. Copper is particularly suitable because of its high cohesive strength, good conductivity, and good solderability.

The high dielectric constant (~10) introduces significant signal propagation delays since velocities down a conductor are reduced by a factor proportional to the square root of the dielectric constant of the surrounding material. Finally, the thermal expansion coefficient is large ($52–74 \times 10^{-7}$ degC^{-1}, 20–200°C) compared to that of silicon ($25–32 \times 10^{-7}$ degC^{-1}, 20–125°C). This introduces stresses at the chip interface resulting in a reduction of reliability.

Possible alternative materials have been proposed. Kumar & McMillan[5] have suggested a composition based on β-spodumene ($Li_2O.Al_2O_3.4SiO_2$) as the principle crystalline phase whilst Shimada et al.[6] have developed an alumina – lead borosilicate mix. Both have improved properties over pure alumina but one of the most promising materials for electronic device packaging is based on cordierite ($2MgO.2Al_2O_3.5SiO_2$) due to its low dielectric constant, low thermal expansion, high bulk resistivity, and good strength.

The general cordierite system was first extensively studied by Rankin & Merwin[7] who identified the existence of two polymorphs, a stable α phase and a metastable μ phase. It was found that the μ form transformed to the α form at temperatures above 1050°C, the exact transformation temperature depending upon composition and previous heat treatment: the transformation is irreversible.[8] Since this early work, Yoder[9] has found another stable form,

denoted β-cordierite, which can be produced hydro-thermally from the other two forms. More recently work on the cordierite system has been reviewed by Gregory & Veasey.[10]

Achieving bulk nucleation in preference to surface nucleation in cordierite glass has proven very difficult. However, Stookey[11] was able to produce a glass ceramic with high chemical and thermal shock resistance by the addition of up to 11·5 w% TiO_2. Later, DeVekey & Majumdar[12] showed that further additions of up to 5 wt% CaO greatly improved the melt and crystallisation characteristics. Since Stookey's early discovery much work has been done on these titania nucleated cordierites.[10,13] For this work, in which high surface area powders are employed, bulk nucleation/crystallisation is not required. Moreover, the addition of large quantities of nucleating agent is likely to have deleterious effects upon material properties for this particular application. However, fluxing agents are necessary to produce melts of low viscosity and good homogeneity and further additions are generally required to aid surface nucleation and for good sintering. Miller[14] was unable fully to sinter a powder of stoichiometric composition (13·7MgO, 34·9Al_2O_3, 51·4SiO_2 wt%) until 0·5–2·5% K_2O and/or Cs_2O has been added to the melt. Other typical additives are P_2O_5, Li_2O, B_2O_3, ZrO_2, and ZnO.

Experimental details

Glass forming procedure

The compositions studied are given in Table 1 although most of the work reported is for material number 1. P_2O_5 was added as a nucleating agent and B_2O_3 aided in the formation of a homogeneous melt of acceptable viscosity. P_2O_5 was added in the form $AlPO_4$ and B_2O_3 as H_3BO_3.

The required powders were mixed thoroughly for about 24 h and then melted at 1500°C in a ZGS 95%Pt 5%Au crucible for 5 h. A glass frit was produced by pouring into demineralised water and drying. The frit was then mixed and the procedure repeated. This ensured good homogeneity of the melt.

Production of a fine powder was achieved by crushing the frit with alumina balls for 36 h in a ball mill jar followed by sieving to 180 μm. Bulk chemical analysis by energy dispersive x-ray analysis suggested that Al_2O_3 contamination from the milling process was minimal and that compositions were within 1% of the desired proportions.

Care was taken to avoid metal contamination and to standardise the preparation procedure for all samples since cordierites have been shown to be sensitive to preparative conditions.[15]

Sample preparation

In the production of multilayer packages it is necessary to bind the glass powder together in order to form the thin pliable sheets used in the manufacturing process. Although material characterisation was not performed on samples in this form a suitable binding mix was added to keep the pressed pellets together before firing and to give more realistic results. The mix consisted of 1 wt% polyvinyl acetate dissolved in 0·2 wt% ethyl ether (a wetting agent) and 25 wt% acetone, the remainder being glass powder. This is based on a formulation by Park.[16]

Pellets weighing 1 g and about 16 mm in diameter were used for x-ray, density, and scanning electron microscope analysis whilst 1·5 and 2·5 g samples about 25 mm in diameter were used for dielectric and resistivity measurements. Strength and thermal expansion were measured on uniaxially pressed cylinders approximately 25 mm in length and 5 mm in diameter. Cylinders were pressed to ~300 MPa and the other specimens to ~150 MPa. Grinding and polishing of surfaces after firing removed the effects of surface contamination.

Firing procedure

Using thermogravimetric analysis it was found that most of the binder burned off at about 340°C. Sintering was found to occur in the region 825–875°C and consequently the following heat treatment process was adopted. A heating/cooling rate of 3 degC/min with holds at 340°C for 1·5 h, 875°C for 2 h, and at the desired firing temperature for 2·5 h. These holding times were lengthy in order to obtain maximum burn off of binder and complete sintering, although in industrial applications these times may be much reduced.

Measurements of material properties

Differential thermal analysis was used to determine the temperatures of maximum phase development although rate of reaction has been shown to depend upon heating rate[17] and, for powders, on particle size.[18,19] X-ray diffraction was used to identify crystal phases within the sintered material and to follow phase evolution. The intensity of the diffracted x-rays was taken, to a first approximation, as being representative of the total wt% of phase present. A calibration graph of experimentally determined contents against known contents for mixes of pure μ and α cordierite enabled results for these two phases to be adjusted accordingly. A visual indication of phase development was obtained by scanning electron microscopy.

Thermal expansion coefficients were measured in the range 30–100°C using a dilatometer with a heating rate of ~2 degC/min. Samples were subsequently used in strength tests using three point loading.[20]

Resistivity values for cordierite are high and measurement required the use of a specially built amplifier.

Table 1. *Composition of materials studied (wt%)*

Material	MgO	Al_2O_3	SiO_2	P_2O_5	B_2O_3
1	22·0	22·0	53·0	2·0	1·0
2	23·5	20·5	53·0	2·0	1·0
3	25·0	19·0	53·0	2·0	1·0

This monitored the current through a specimen with evaporated gold electrodes, under a known applied voltage, the amplifier also compensating for surface capacitances and contact potentials. Measurements were taken in the range 100–400°C and extrapolated back to 80°C, a typical operating temperature for a VLSI chip. Float glass of known resistivity was used to check the system.

Dielectric measurements were made using a parallel plate method in conjunction with two Wayne Kerr Universal RF Bridges for measurements at 1 MHz and 1 kHz. Samples were contained within a specially built jig which supplied an earth for the guard ring and also prevented interference from external fields. The system was tested using an alumina standard ($K = 9.381$) and this was measured to within 1%. Great care was taken in preparing specimen surfaces prior to electrode evaporation.

Thermal conductivity was measured on a specimen of composition 1 fired to 975°C using Lee's disk method for comparison with typical values for alumina. Density was measured using glycerol as the immersion fluid.

Results and discussion

Phase development

Differential thermal analysis of all three compositions yielded two characteristic exothermic peaks, at about 890 and 950°C, for material 1. Comparison with x-ray diffraction results for materials fired to these temperatures showed that these two peaks were attributable to the formation of μ and α cordierite respectively. On some runs for compositions 2 and 3 a small peak was just discernible at ~930°C. This was taken to be due to the formation of enstatite (MgSiO$_3$).

Phase evolution in composition 1 is shown in more detail in Figure 1 which gives the results for x-ray diffraction studies. Enstatite was present as a minor phase, converting to the high temperature stable form protoenstatite at about 1050°C. It should be noted that no residual glass phase could be detected by x-ray
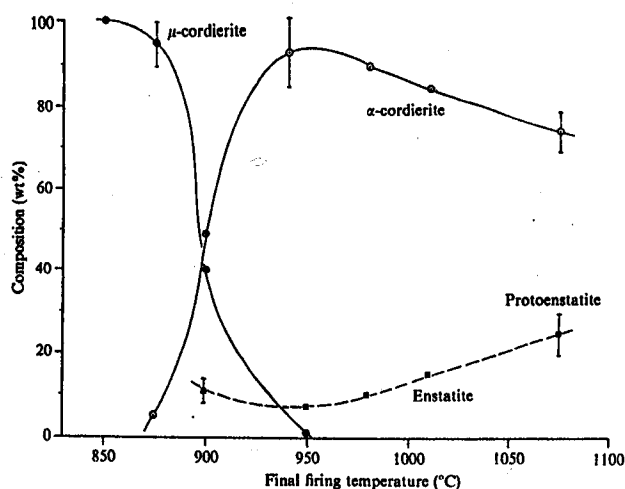
diffraction on samples prepared at temperatures above ~900°C. Development of μ-cordierite at lower temperatures can clearly be seen, transformation to the stable α form occurring rapidly in the region 875–925°C. This is in contrast to observations made on magnesium aluminosilicate glasses with no additives where more than 50 h of heat treatment are required to induce crystallisation[7,21] and the transformation itself is rather sluggish. Consequently it would appear that P$_2$O$_5$ and B$_2$O$_3$, both glass formers themselves, exert a marked influence on the crystallisation kinetics. Recently, Watanabe et al.[22] have looked at the crystallisation mechanism in bulk glass of similar composition yet make no mention of the role played by P$_2$O$_5$ and B$_2$O$_3$.

The formation of the μ-cordierite phase is thought to occur by the precipitation of a silica rich solid solution into which isomorphous substitution of Al^{3+} and Mg^{2+} occurs.[23] The Al^{3+} ions occupy silicon sites and the Mg^{2+} ions interstitial sites.[24] It has been found that the structure of the μ phase is related to that of β-quartz, the unit cell of the μ phase being slightly larger.[25,26] More recently, Carpenter et al.[27] have shown from a thermodynamic viewpoint that crystallisation of the β-quartz phase of cordierite composition is energetically similar to that of pure β-quartz from silica. The μ phase also exhibits a range of possible solid solutions[7,28] and is sometimes referred to as a β-quartz solid solution. In all three compositions studied for this work the β-quartz phase had a cordierite composition.[28]

α-Cordierite is isostructural with beryl[29] and is based on hexagonal symmetry. It consists of superimposed Al$_2$Si$_4$O$_{18}$ rings[30] linked both vertically and horizontally by two Al and one Si tetrahedra and two Mg octahedra. The region between facing hexagonal rings takes the form of a pseudo spherical cavity ($r = 2.2$ Å)[31] in which impurities such as Na$^+$, Fe^{2+}, and H$_2$O can be accommodated. The crystal structure gives rise to a positive thermal expansion in the plane of the hexagonal rings and a negative expansion in a perpendicular direction.[32] Again, the phase developed for all three compositions had stoichiometric composition.[33]

P$_2$O$_5$ is preferably added in the form AlPO$_4$ as it can be easily accommodated into the silica based glass network.[34,35] AlPO$_4$ was also used to reduce the viscosity of the melt and helped prevent volatilisation of P$_2$O$_5$. Besides acting as a nucleating agent, AlPO$_4$ has been shown to have a marked influence on phase development. Topping & Murphy,[36] investigating the effect of AlPO$_4$ substitution for SiO$_2$ in synthetic cordierite, found that the μ to α transformation occurred at about 25 degC lower if about 10% P$_2$O$_5$ was present. This would appear to be verified by the above results although at lower temperatures and with a lower concentration of P$_2$O$_5$. However, inclusion of P$_2$O$_5$ alone requires more prolonged heating fully to develop the α phase.[36,37]

Consequently the action of B$_2$O$_3$ is also important in phase development and also in helping to regulate the nature of the crystal phase formed. B$_2$O$_3$ can also

Figure 1. *Phase development for material based on composition 1*

be shown to play a prominent role in sintering. Due to premature surface crystallisation during sintering, Helgesson[37] was unable fully to sinter a glass powder of similar composition but containing only CaF_2 (a fluxing agent) and P_2O_5. In this work, however, glasses of the above compositions have been made to sinter leaving a completely glassy product with a low porosity of $3.9 \pm 0.6\%$. This indicates that B_2O_3, acting at the surface of a power particle, delays the onset of crystallisation until sintering is near completion although the exact mechanism for this is uncertain.

Sintering and final crystal morphology have been studied extensively by scanning electron microscopy. By comparison with the above results, an indication of how phases develop can be obtained. In common with other authors[23,37,38] it was appreciated that the crystallographic nature of the structure was complex.

The binder burns away at about 340°C to leave an unsintered product with much porosity. Firing in air aids the removal of residual carbon deposits, a potential problem when firing in inert atmospheres such as nitrogen (a requirement when firing multilayer packages with copper conductors). Sintering occurs rapidly in the region 850–875°C, yielding a dense product of low porosity. It should be noted that the average particle size in the powder of composition 1 was 10.1 μm prior to sintering. The presence of B_2O_3 at the glass particle boundaries delays crystallisation until sintering is near completion.

Development of the μ phase takes the form of roughly spherical crystals, a few μm in diameter, concentrating at the original boundaries between the glass particles, Figure 2. This would indicate that surface nucleation has occurred, aided by B_2O_3 and P_2O_5, on the surfaces of the particles before the sintering. The formation of this partially interconnected network helps prevent deformation of the article by viscous flow of the remaining glass phase. This is a major requirement in the firing of multilayer packages in which close tolerances are required.

Shortly after the formation of crystals at the interfaces between the particles a much finer crystal microstructure appears by internal nucleation and crystallisation of the remaining glassy 'islands', this possibly being aided by phase separation which has been reported in glasses of similar composition[5] but not directly observed here. The delay in the onset of bulk nucleation and crystallisation compared with that at the surface is aided by the absence of a well defined nucleation hold in the heat treatment schedule.

Transformation to the stable α phase occurs rapidly in the region 875–925°C with a corresponding decrease in density, Figure 3, from around 2.62 to about 2.55 g/cm³ (the density of the base glass was 2.652 g/cm³) due to a small increase in volume during the transformation.[39] The formation of enstatite occurs at this point although only in small quantities. The theoretical density of a 95% α-cordierite, 5% enstatite composite with no pores is 2.564 g/cm³.

The bulk of the enstatite is likely to be associated with the region of initial growth of the crystal phase since the growing solid/liquid interface will have associated with it a liquid rich in rejected magnesia and silica. The ratio of excess MgO to SiO_2 is 1:1.6, with the ratio required for formation of enstatite 1:1.5. Energy dispersive x-ray analysis in conjunction with electron microprobe analysis has indicated that this is indeed the case, the region at the edge of the original glass particle being considerably richer in Mg than the centre which has a concentration similar to that of stoichiometric cordierite. Firing to 975°C favours the growth of the large cordierite crystals, Figure 4.

Firing to 1075°C has marked effects upon crystal morphology, cordierite crystals present at grain boundaries growing quite large and taking on a more faceted appearance, Figure 5. Enstatite develops into protoenstatite at around 1050°C and also appears to be present in greater quantities, Figure 1. Foster[40] found that enstatite converted slowly to protoenstatite at about 1260°C although Sarver & Hummell[41] found that this could be reduced to 1042°C by adding 3% LiF. Again it would appear that P_2O_5 and B_2O_3 exert a marked influence on the kinetics of phase transformation.
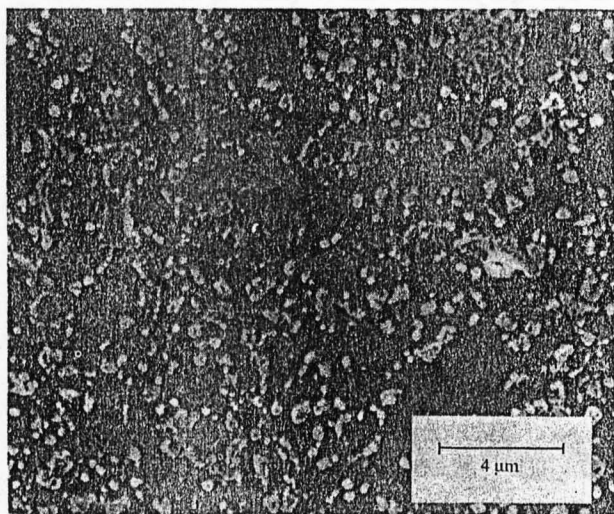

Figure 2. *Scanning electron micrograph showing initial crystallisation around the old glass particle boundaries. Material etched in 5% HF solution after firing to 875°C*
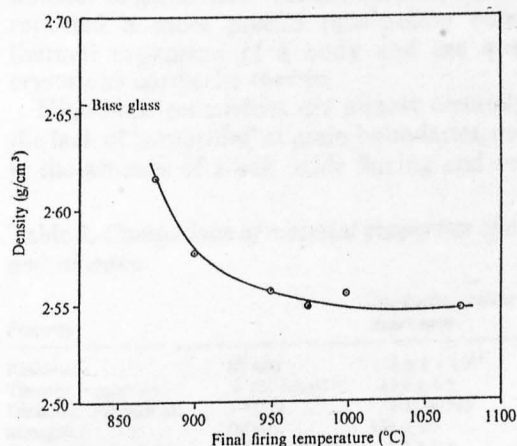
Figure 3. *Change in density with final firing temperature for material I*
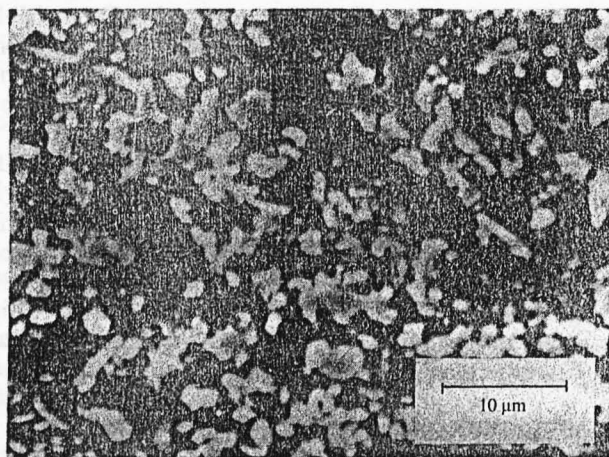
Figure 4. *Scanning electron micrograph of material 1 fired at 975°C. Pores are due to etching*
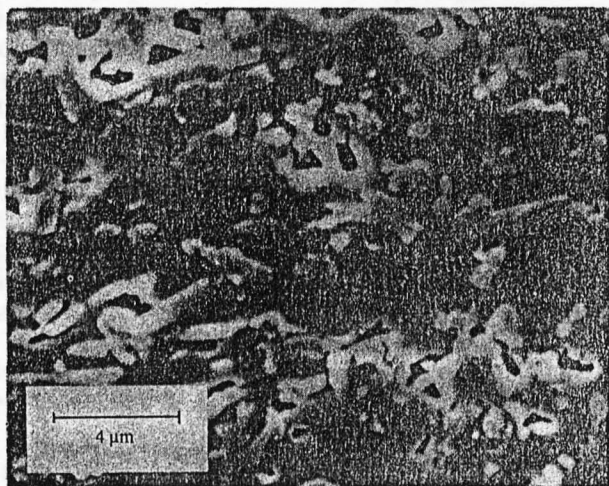
Figure 5. *Scanning electron micrograph of material 1 showing the growth of α-cordierite crystals after firing to 1075°C*

At these higher temperatures there also appears to be an increase in porosity of the material and this is the most likely explanation of why the density does not appear to rise as one would expect for an increase in protoenstatite content. The required porosity to keep this figure down is ~5%. The cause for this is uncertain; it may be attributable to cracking during the μ or enstatite inversions or to density changes. More likely it is due to the thermal expansion mismatch between low expansion cordierite and the high expansion residual glass and protoenstatite ($\alpha = 98 \times 10^{-7}$ degC^{-1}).[41] Indeed, many of the pores appear to be associated with the edges of the large cordierite crystals.

Relation between phase content and properties

The general properties of samples based on composition 1 are shown in Figure 6. Quite clearly the presence of μ-cordierite at lower temperatures within the microstructure has deleterious effects, especially upon strength, resistivity, and dielectric constant. Protoenstatite at higher temperatures also affects
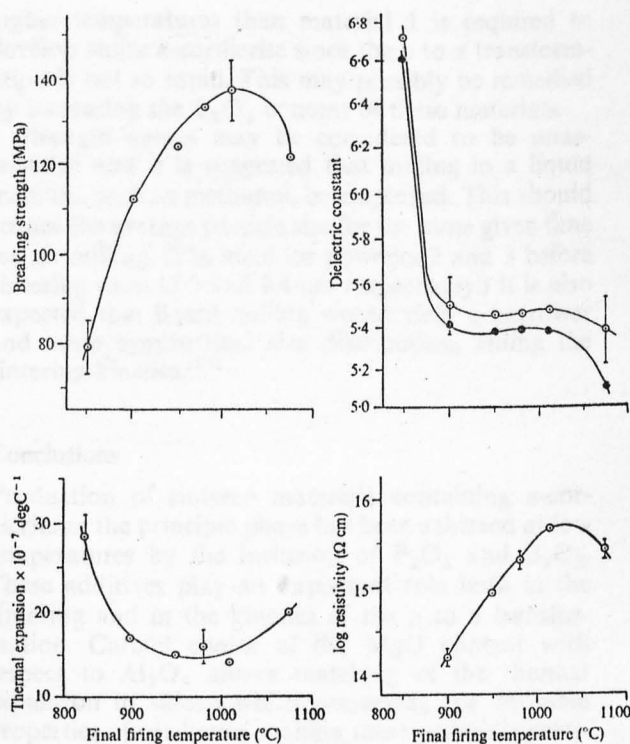
Figure 6. *Some material properties of composition 1 as a function of final firing temperature*

material properties, yielding an expected increase in thermal expansion but giving lower strength values. The cause of both this and the slight decrease in dielectric constant is most probably due to porosity, especially at the α boundaries.

Consequently, the inclusion of α-cordierite as a major phase is advantageous, yielding strong materials of high bulk resistivity yet with low dielectric constant. A comparison between the material properties of alumina and specimens fired to 975°C is given in Table 2 and clearly shows the improvement in properties for the packaging of devices.

The low thermal expansion coefficient and dielectric constant are attributed directly to the presence of α-cordierite, values of dielectric constants being typically 4·5–5·5.[42] Beals & Cook[43] have studied a number of materials in the cordierite system and have reported a more precise relationship between the thermal expansion of a body and the quantity of crystalline cordierite therein.

High bulk resistivities are almost certainly due to the lack of 'impurities' at grain boundaries, particularly the absence of alkali oxide fluxing and nucleation

Table 2. *Comparison of material properties of cordierite and alumina*

Property		Cordierite, present experiment	Alumina
Resistivity	(Ω cm)	$3 \pm 1 \times 10^{15}$	10^{11}–10^{14}
Thermal expansion	$\times 10^{-7}$ degC^{-1}	$15·5 \pm 1·5$	65–70
Dielectric constant at	1 MHz	$5·35 \pm 0·15$	~10
Strength	(MPa)	133 ± 10	~150
Thermal conductivity	(W m^{-1} K^{-1})	$1·9 \pm 0·4$	~29
Density	(g cm^3)	2·548	~3·96

additives. Good strength is attributed to the dual microstructure, that is of large (~ 2 μm) framework forming crystals enclosing areas of finer crystal growth.

The value of thermal conductivity is relatively low although not untypical for glass ceramics which generally yield values much lower than those for pure oxide ceramics[44] but this is not a great problem. In the thermal conduction module designed for the IBM 3081 processor[4] heat was conducted away from the chip by means of a metal, water-cooled piston pressing onto the rear surface of the chip. Thus heat conduction through the package itself was rendered unnecessary.

It was considered that the thermal expansion of material 1 was possibly too low for packaging applications, although one has to take into account the internal conductor network which is likely to increase the net expansion of the multilayer package. Consequently, experimentation was conducted on two further compositions (2 and 3, Table 1) which had a higher MgO content at the expense of Al_2O_3, the intention being to increase the minor phase content.

Examination of Figure 7, which shows the phase development of material 3, indicates that this was indeed the case; small quantities of forsterite (Mg_2SiO_4) also being present. Forsterite also has a high expansion coefficient (94×10^{-7} degC^{-1}) and this is reflected in the higher expansion for these two materials.

Table 3 gives the general properties for materials 2 and 3. It can be seen that increased MgO content is not detrimental to bulk properties. Firing to slightly higher temperatures than material 1 is required to develop entire α-cordierite since the μ to α transformation is not so rapid. This may possibly be remedied by increasing the B_2O_3 content of these materials.

Strength values may be considered to be unacceptable and it is suggested that milling in a liquid medium, such as methanol, be employed. This should reduce the average particle size for the same given time for air milling. (The sizes for powders 2 and 3 before sintering were 15·2 and 9·4 μm respectively.) It is also expected that liquid milling would yield a narrower and more symmetrical size distribution, aiding the sintering kinetics.[45]

Conclusions

Production of sintered materials containing α-cordierite as the principle phase has been achieved at low temperatures by the inclusion of P_2O_5 and B_2O_3. These additives play an important role both in the sintering and in the kinetics of the μ to α transformation. Careful choice of the MgO content with respect to Al_2O_3 allows matching of the thermal expansion to silicon whilst preserving the desirable properties of cordierite, making these materials particularly suitable for the packaging of devices.

The ability to produce dense, sintered material of low porosity at temperatures below 1000°C enables low melting metals to be used as the conductor network in multilayer packages.

References

1. Schwartz, B. & Wilcox, D. L. (1967). *Proc. 17th Electronic Components Conf.*, IEEE. New York. P. 17.
2. Kaiser, H. D., Pakuiski, F. J. & Schmeckenbecher, A. F. (1972). *Solid St. Technol.* 5, 35.
3. Blodgett, A. J. (1983). *Scient. Am.* 249, 30.
4. Blodgett, A. J. & Barbour, D. R. (1982). *IBM Jl Res. Dev.* 26, 30.
5. Kumar, A. H. & McMillan, P. W. (1981). USP 4, 31, 324.
6. Shimada, Y. *et al.* (1983). *IEEE Trans. CHMT* 6, 382.
7. Rankin, G. A. & Merwin, H. E. (1918). *Am. J. Sci.* 45, 301.
8. Toropov, N. A. & Borzokovski, V. P. (1963). *High temperature chemistry of silicates.* Consultants Bureau, N.Y.
9. Yoder, H. S. (1952). *Am. J. Sci.* 250, 569.
10. Gregory, A. J. & Veasey, T. J. (1971). *J. Mater. Sci.* 6, 1312.
11. Stookey, S. D. (1960). USP 2, 920, 971.
12. DeVekey, R. C. & Majumdar, A. J. (1970). *Mineralog. Mag.* 37, 771.
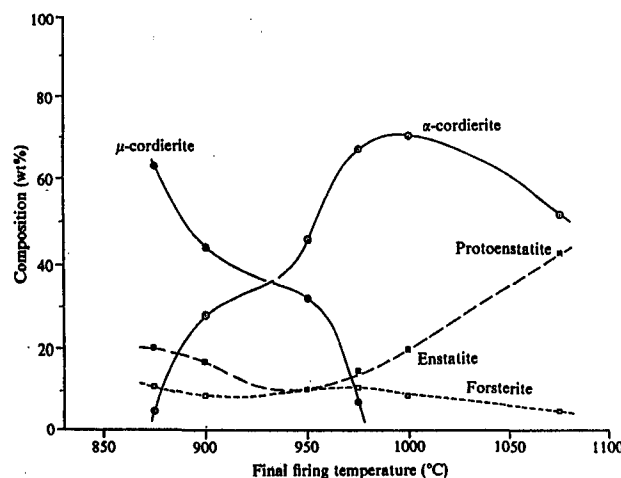
Figure 7. *Phase development in material based on composition 3*

Table 3. *Bulk properties of materials 2 and 3*

Property		Final firing temperature (°C)	2	3
Resistivity	(Ω cm)	900	—	$3 \pm 1 \times 10^{13}$
Thermal expansion	$\times 10^{-7}$ degC^{-1}	900–1000	$19 \cdot 1 \pm 0 \cdot 9$	$28 \cdot 9 \pm 0 \cdot 8$
Dielectric constant	1 MHz	900	$5 \cdot 4 \pm 0 \cdot 15$	$5 \cdot 6 \pm 0 \cdot 15$
Strength	(MPa)	900–1075	110 ± 7	109 ± 4
Density	(g cm^3)	975	$2 \cdot 612$	$2 \cdot 69$

13. Todhunter, R. (1984). *Ph.D Thesis*, University of Warwick.
14. Miller, D. M. (1975). USP 3, 926, 648.
15. Barry, T. I., Lay, L. A. & Morrell, R. (1978). *Sci. Ceram.* 8, 331.
16. Park, J. L. (1961). USP 2, 966, 719.
17. Hench, L. L. & Gould, R. W. (1971). *Characterization of ceramics.* Marcel Dekker, New York, P. 273.
18. Norton, E. H. (1939). *J. Am. Ceram. Soc.* 22, 54.
19. Grimshaw, R. W. *et al.* (1945). *Trans. Br. Ceram. Soc.* 44, 87.
20. Hing, P. (1975). *Proc. Br. Ceram. Soc.* 25, 13.
21. Karkshanavola, M. D. & Hummel, F. A. (1953). *J. Am. Ceram. Soc.* 36, 373.
22. Watanabe, K., Giess, E. A. & Schafer, M. W. (1985). *J. Mater. Sci.* 20, 508.
23. Zdaniewski, W. (1975). *J. Am. Ceram. Soc.* 58, 163.
24. Beall, G. H., Karsetter, B. R. & Rittler, H. L. (1967). *J. Am. Ceram. Soc.* 50, 181.
25. Schreyer, W. & Schairer, J. F. (1957). *Yb. Carnegie Instn Wash.* 58, 197.
26. Roy, R. (1959). *Kristallografiya* 111, 185.
27. Carpenter, M. A., Putnis, A., Navrotsky, A. & McConnell, J. D. C. (1983). *Geochim. cosmochim. Acta* 47, 899.
28. Schreyer, W. & Schairer, J. F. (1961). *Kristallografiya* 16, 60.

29. Bragg, L. & Claringbull, G. F. (1965). *Crystal structure of minerals.* G. Bell & Sons, London. P. 217.
30. Gibbs, G. V. (1966). *Am. Miner.* 51, 1068.
31. Selkregg, H. R. & Bloss, F. D. (1980). *Am. Miner.* 65, 522.
32. Evans, D. L., Fischer, G. R., Geiger, J. E. & Martin, F. W. (1980). *J. Am. Ceram. Soc.* 63, 629.
33. Schreyer, W. & Schairer, J. F. (1981). *J. Petrol.* 2, 334.
34. McMillan, P. W. (1964). *Glass ceramics.* Academic Press, London. P. 68.
36. Topping, J. A. & Murthy, M. K. (1977). *J. Can. Ceram. Soc.* 46, 19.
37. Helgesson, C. I. (1976). *Sci. Ceram.* 8, 347.
38. DeVekey, R. C. & Majumdar, A. J. (1973). *Glass Technol.* 14(5), 125.
39. Zdaniewski, W. (1973). *J. Mater. Sci.* 8, 192.
40. Foster, W. R. (1951). *J. Am. Ceram. Soc.* 34, 255.
41. Sarver, J. F. & Hummel, F. A. (1962). *J. Am. Ceram. Soc.* 45, 152.
42. Kingery, W. D., Bowen, H. K. & Uhlmann, D. R. (1960). *Introduction to ceramics.* John Wiley & Sons, New York. P. 727.
43. Beals, R. J. & Cook, R. L. (1952). *J. Am. Ceram. Soc.* 35, 53.
44. McMillan, P. W. (1964). *Glass ceramics.* Academic Press, London. P. 188.
45. Yan, M. F. (1982). In *Advances in powder technology.* Edited by G. Y. Yin, American Society of Metals, Ohio. P. 107.

REFERENCES

1.   BLODGETT, A.J., Sci. Amer. 249(1), 76 (1983)

2.   STANGHAN, C.J., Microwave Packaging Colloq.,
        I.E.E.E., London (1986)

3.   FOGIEL, M. 'Modern Microelectronics' Research and
        Education Assoc. New York (1972)

4.   HO, C.W. in 'Microstructure Science, Vol. 5, VLSI
        Electronics' Ed. G.E. Einspruch. Academic Press,
        London (1982)

5.   GIESS, E.A., TU, K.N. and UHLMANN, D.R. 'Material Research
        Society, Vol. 40, Electronic Packaging Material Science'.
        Material Research Society, Pittsburgh (1985)

6.   FLOCK, W. in 'Material Research Society, Vol. 40, Electronic
        Packaging Material Science' Ed.E.A. Giess, K.N. Tu and
        D.R. Uhlmann Material Research Society Pittsburgh (1985)

7.   ANONYMOUS, Ceram. Forum. Int./Ber. DKG 58(7), 553 (1980)

8.   CARLSON, R.O., GLASCOCK, H.H., WEBSTER, H.F. and NEUGEBAUER,
        C.A. in 'Material Research Society, Vol. 40, Electronic
        Packaging Material Science' Ed. E.A. Giess, K.N. Tu and
        D.R. Uhlmann. Material Research Society, Pittsburgh (1985)

9.   TOSAKI, H., SUGISHITA, N. and IKEGAMI, A., Int. J. Hybrid
        Microelectronics (U.S.A.) 4(2), 100 (1981)

10.   WILCOX, D.L., Sol. St. Technol. 41(1), 40 and 41(2),
        55 (1971)

11.   McMILLAN, P.W., HODGSON, B.P., LOLE, J.D. and DAVIES, S.B.,
       U.K. Patent No. 1,232,621 Feb. (1968)

12.   BYER, M., O'LEARY, G. and REED, T.L., U.S. Patent
       No. 3,040,213 June (1962)

13.   GREENSTEIN, B., LANGSTON, P.R., NARKEN, B. and
       TURETZKY, M.N., U.S. Patent No. 3,726,002 Apr. (1973)

14.   LANGSTON, P.R. and TURETZKY, M.N., U.S.Patent No.
       3,968,193 Sep. (1980)

15.   SHIMADA, Y. et al, I.E.E.E. Trans. CHMT-6(4), 382 (1983)

16.   LAU, J.W., ENLOE, J.H. and RICE, R.W., presented at the
       88th American Ceramic Society Meeting, Chicago (1986)

17.   WAKINO, K., MURATA, M., MANDAI, H. and SUGOH, K., presented
       at the 88th American Ceramic Society Meeting, Chicago (1986)

18.   NARKEN, B. and TUMMALA, R.R., U.S. Patent No. 4,221,047
       Sep. (1980)

19.   KUMAR, A.H., McMILLAN, P.W. and TUMMALA, R.R., U.S. Patent
       No. 4,301,324 Nov. (1981)

20.   VILKELIS, W.V., IBM J. Res. Dev. 26(3), 342 (1982)

21.   LANDMAN, B.S. and RUSSO, R.L., I.E.E.E. Trans. C-20(12)
       1469 (1971)

22.   AMEY, D.I., MOORE, R.P. and WALKER, D.S., Proc. Int.
       Microelectronics Conf. Anaheim (1977)

23.   STAFFORD, J.W., I.E.E.E. Trans. CHMT-3(2), 195 (1980)

24.   MATHER, J.C., Proc. 30th Electronic Compnts. Conf. San
       Francisco (1980)

25.   WERBIZKY, G.G., WINKLER, P.E. and HAINING, F.W., 20th
       I.E.E.E. Comp. Conf. San Francisco (1980)

26.   CLARK, B.T. and HILL Y.M., I.E.E.E. Trans. CHMT-3(1),
         89 (1980)

27.   BLODGETT, A.J., I.E.E.E. Trans. CHMT-3(4), 634 (1980)

28.   BLODGETT, A.J. and BARBOUR, D.R., IMB J. Res. Dev. 26(1),
         30 (1982)

29.   BLODGETT, A.J., Proc. 30th Electronic Compnts. Conf. San
         Francisco (1980)

30.   PITTLER, M.S., POWERS, D.H. and SCHNABEL, D.L., IBM J. Res.
         Dev. 26(1), 2 (1982)

31.   WATARI, T. and MURANO, H., I.E.E.E. Trans. CHMT-8(4),
         462 (1986)

32.   SERAPHIM, D.P. and FEINBERG, I., IBM J. Res. Dev. 25(5),
         617 (1981)

33.   SCHWARTZ, B., Bull. Amer. Ceram. Soc. 63(4), 577 (1984)

34.   CHAMBERS, J. and MORRIS, M., Microwave Packaging Colloq.
         I.E.E.E. London (1986)

35.   BARKER, G.K., MUN, J., YOUNG, Y.M. and McQUART, R.,
         Microwave Packaging Colloq. I.E.E.E. London (1986).

36.   FERRY, D.K., I.E.E.E. CD-M1(4), 39 (1985)

37.   MURASE, T., HIRATA, H. and VENO, S., Proc. 32nd Electronic
         Compnts. Conf. San Diego (1982)

38.   SERAPHIM, D.P., IBM J. Res. Dev. 26(1), 37 (1982)

39.   BALDE, J.W., I.E.E.E. Trans. CHMT - 7(3), 257 (1984)

40.   SCHWARTZ, B. and WILCOX, D.I., Proc. 17th Electronic
         Components Conf. Jackson U.S.A. (1967)

41.   STETSON, H.W. and SCHWARTZ, B., Electronics Div. Mtg.
        Amer. Ceram. Soc. San Francisco U.S.A. (1961). Abs. Amer.
        Ceram. Soc. Bull. 40(9), 584 (1961)

42.   KAISER, H.D., PAKULSKI, F.J. and SCHMEKENBECHER, A.F.,
        Sol. St. Technol. 15(5), 35 (1972)

43.   STETSON, H.W., U.S. Patent No. 3,189,978 June (1965)

44.   BREEDLOVE, J.G., U.S. Patent No. 3,379,943 Apr. (1968)

45.   BENNETT, M., BOYD, W.E. and NOBILE, J.C., U.S. Patent
        No. 3,518,756 July (1970)

46.   SCHWARTZ, B., U.S. Patent No. 3,502,520 Mar. (1970)

47.   HARGIS, B.M., U.S. Patent No. 3,549,784 Dec. (1970)

48.   ARRHENIUS, G., U.S. Patent No. 3,423,517 Jan. (1969)

49.   THEOBALD, P.R. and BAILEY, J.T., U.S. Patent
        No. 3,723,176 Mar. (1973)

50.   BLAZICK, L.A. and MILLER, F., U.S. Patent No. 4,109,377
        Aug. (1978)

51.   PARK, J.L., U.S. Patent No. 2,966,719 Jan. (1961)

52.   HALL, A.V. and ZYKOFF, F.B., I.E.E.E. Trans. CHMT-5(4),
        374 (1982)

53.   IWAMURA, R., MURAKAMI, H., ICHIMOTO, K., TAKASAKI, M.
        presented at the 88th Amer. Ceram. Soc. Meeting,
        Chicago 1986.

54.   WRENNER, W.R., IBM J. Res. Dev. 27(3), 285 (1983)

55.   DOUGHERTY, W.E. and GREER, D.E., Proc. 32nd Electronic
        Compnts. Conf. San Diego (1982)

56.   DELIO, R.C., IBM Tech. Discl. Bull 22(3), 1002 (1979)

57.   DOHYA, A., WATARI, T., TAMURA, T. and MURANO, H.,
        I.E.E.E. Trans. CHMT - 6(2), 168 (1983)

58.   HO, L.W., CHANCE, D.A., BAJOREK, C.H. and ACOSTA, R.E.,
        IBM J. Res. Dev. 26(3), 286 (1982)

59.   CHANCE, D.A. and WILCOX, D.L., Proc. I.E.E.E. 59(10),
        1455 (1971)

60.   CHANCE, D.A. and WILCOX, D.L., Met. Trans. 2(3), 733 (1971)

61.   RUTT, T.C., U.S. Patent No. 3,679,950 July (1972)

62.   GARDENER, R.A. and NUFER, R.W., Sol. St. Technol.
        17(5), 38 (1974)

63.   ETTRE, K. and CASTLES, G.R., Ceram. Bull 51(5),
        482 (1972)

64.   EGGERDING, C.L., MANSURIN, M.S. and OKTAY, S., IBM Tech.
        Discl. Bull. 21 (12), 4839 (1979)

65.   BABUKA, R., SAXENMEYER, G.J. and SCHULTZ, L.K., IBM J. Res.
        Dev. 26(3), 18 (1982)

66.   MILLER, L.F., Proc. Int. Hybrid Microelectronics Symp.
        Chicago (1968)

67.   MILLER, L.F., IBM J. Res. Dev. 13(5), 239 (1969)

68.   GOLDMAN, L.S., IBM J. Res. Dev. 13(5), 251 (1969)

69.   BURGER, W.G. and WEIGEL, C.W., IBM J. Res. Dev. 27(1)
        11 (1983)

70.   SCHWARTZ, B., J. Phys. Chem. Sol. 45(10), 1051 (1984)

71.   KEYS, L.K., RUSSO, A.J., FRANCIS, F.J. and HERRING, S.,
        Proc. Int. Hybrid Microelectronics Symp. Beverly Hills
        (1970)

72.   CHU, R.C., UWANG, U.P. and SIMONS, R.E., IBM J. Res. Dev. 26(1), 45 (1982)

73.   DIETZEL, A., Elektrochem 48, 9 (1942)

74.   DIETZEL, A., Glastechn. Ber. 22, 279 (1948/49)

75.   ZACHARIASEN, W.H., J. Amer. Chem. Soc. 54, 3841 (1932)

76.   GOLDSCHMIDT, V.M., Geochem Vert. der Elem., vii Vid. Akad (1926)

77.   WARREN, B.E., J. Amer. Ceram. Soc. 17(8), 249 (1935)

78.   ELLIOTT, S.R., 'Physics of Amorphous Materials' p.104 Longman, London (1982)

79.   VOLF, M.B., 'Glass Science and Technology, Vol. 7. Chemical Approach to Glass' p.30 Elsevier, Amsterdam (1984)

80.   LEBEDEV, A.A., Izr. Optic Inst. 2, 1 (1921)

81.   EVSTROPYEV, K.S., in 'The Structure of Glass' Consultants Bureau, New York (1958)

82.   RANDALL, T.J., ROOKSBY, N.P. and COOPER, B.S., Z. Kristallogr. 75(3-4), 196 (1930)

83.   VALENKOV, N.N. and PORAI-KOSHITS, E.A., Z. Kristallogr. 95, 195 (1936)

84.   GASKELL, P.H. and SMITH, D.J., J. Microscopy 119(1), 63 (1980)

85.   BOCKRIS, J.M., TOMLINSON, J.W. and WHITE, J.C., Trans. Faraday Soc. 52, 299 (1956)

86.   GOODMAN, C.H.L., Nature 257, 370 (1975)

87.   GOODMAN, C.H.L., Phys. Chem. Glasses 26(1), 1 (1985)

88.   SINCLAIR, R.N., DESA, J.A.E., ETHERINGTON, G.,
JOHNSON, P.A.V. and WRIGHT, A.C., J. Non Crystalline
Sol. 42, 107 (1980)

89.   RAWSON, H., 'Inorganic Glass Forming Systems' Academic
Press, London (1967)

90.   JONES, G.O., 'Glass' Chapman and Hall, London (1971)

91.   VOGEL, W., 'Structure and Crystallization of Glasses'
Pergamon Press, Leipzig (1971)

92.   MACKENZIE, J.D., 'Modern Aspects of the Vitreous State,
Vols 1-3' Butterworths, London (1960)

93.   PYE, L.D., STEVENS, H.J. and LaCOURSE, W.C., 'Introduction
To Glass Science' Plenum Press, New York (1972)

94.   PAUL, A., 'Chemistry of Glasses' Chapman and Hall,
London (1982)

95.   RAWSON, H., 'Glass Science and Technology Vol. 3. Properties
and Applications of Glass' Elsevier, Amsterdam (1984)

96.   JAMES, P.F., in 'Nucleation and Crystallization of Glasses'
p.1 Ed. J.H. Simmons. Amer. Ceram. Soc. Ohio (1982)

97.   JAMES, P.F., J. Non Crystalline Sol. 73, 517 (1985)

98.   TURNBULL, D. and COHEN, M.H., J. Chem. Phys. 29, 1049 (1958)

99.   STOOKEY, S.D. and MAURER, R.D. in 'Progress in Ceramic
Science, Vol. 2' p.78 Ed. J.E. Burke. Plenum Press, London
(1962)

100.   THAKUR, R.L. and THIAGARAJAN, S., Cent. Glass Ceram. Res.
Inst. Bull. 13(2), 33 (1966)

101.   McMILLAN, P.W., J. Non. Crystalline Sol. 52, 67 (1982)

102.   JOHNSON, W.A. and MEHL, R.F., Trans. A.I.M.E. 135,
        416 (1939)

103.   AVRAMI, M., J. Chem. Phys. 7 1103 (1939), 8, 212 (1940)
        and 9, 177 (1941)

104.   McMILLAN, P.W., 'Glass Ceramics' Academic Press,
        London (1964)

105.   HLAVAC, J., 'Glass Science and Technology, Vol. 4.
        The Technology of Glass and Ceramics' Elsevier,
        Amsterdam (1983)

106.   LEVIN, E.M., ROBBINS, C.R. and McMURDIE, H.F., 'Phase
        Diagrams for Ceramists' No. 712. Amer. Ceram. Soc.
        Ohio (1964)

107.   SCUREYER, W. and SCHAIRER, J.F., J. Petrol 2(3),
        361 (1961)

108.   ITO, K. et al, UK Patent No. 2,091,239 Nov. (1981)

109.   INOGUCHI, K., NAKANISHI, T., OKAMOTO, K. and ASANO, M.,
        U.S. Patent No. 4,385,129 Aug. (1981)

110.   LACHMAN, M. and LEWIS, R.M. U.S. Patent No. 3,885,977
        May (1975)

111.   STOOKEY, S.D., Ind. Eng. Chem. 51(7), 805 (1959)

112.   McMILLAN, P.W., 'Glass Ceramics' p.262 Academic
        Press, London (1964)

113.   RANKIN, G.A. and MERWIN, H.E., Amer. J. Sci 45,
        301 (1918)

114.   KARKHANAVALA, M.D. and HUMMEL, F.A., J. Amer. Ceram.
        Soc. 36(12), 389 (1953)

115. SCHREYER, W. and SCHAIRER, J.F., Carn. Inst. Wash. Year Book, 197 (1958)

116. ROY, R., Z. Kristallogr. 111, 185 (1959)

117. SCHREYER, W. and SCHAIRER, J.F., Z. Kristallogr. 116, 60 (1961)

118. YODER, H.S., Amer. J. Sci 250, 569 (1952)

119. SCHREYER, W. and SCHAIRER, J.F., Amer. Mineral. 47, 90 (1962)

120. WINKLER, H.G., Acta Crystallogr. 1, 27 (1948)

121. RAY, S. and MUCHOW, G.M., J. Amer. Ceram. Soc. 51(12), 678 (1968)

122. BEALL, G.H., KARSETTER, B.R. and RITTLER, H.L., J. Amer. Ceram. Soc. 50(4), 181 (1967)

123. ZDANIEWSKI, W., J. Amer. Ceram. Soc. 58(5-6), 163 (1975)

124. CARPENTER, M.A., PUTNIS, A., NAVROTSKY, A. and McCONNELL, J.D.C., Geochim. Cosmochim. Acta 47, 899 (1983)

125. NAVROTSKY, A., PERAUDEAU, G., McMILLAN, P. and COURTURES, J.P., Geochim. Cosmochim. Acta 46, 2039 (1982)

126. TOROPOV, N.A. and BARAZOKOVSKI, V.P., 'High Temperature Chemistry of Silicates' p.32 Invest. A. Kad. Nauk. Moscow (1963)

127. NEGRO, A., MURAT, M. and SASSI, F., Ceram. Int. 2(3), 131 (1976)

128. PUTNIS, A., Nature 287 , 128 (1980)

129. WATANABE, K., GIESS, E.A. and SCHAFER, W., J. Mat. Sci. 74, 508 (1985)

130.   BRAGG, W.L. Z Kristallogr 74, 237 (1930)

131.   BYSTROM, A., Arkiv. Kemi. Mineral. Geol. 15B(12),

         1 (1941)

132.   GIBBS, G.V., Amer. Mineral. 51(7), 1068 (1966)

133.   MEAGHER, E.P. and GIBBS, G.V., Can. Mineral. 15(1),

         43 (1977)

134.   COHEN, J.P., KOSS, F.K. and GIBBS, G.V., Amer. Mineral.

         62(1-2), 67 (1977)

135.   BRAGG, L. and CLARINGBULL, G.F., 'The Crystalline State

         Vol. IV. Crystal Structure of Minerals' p.217

         G. Bell and Sons, London (1965)

136.   TOROPOV, N.A., ZHUKAUSKAS, R.S.M. and ALEINIKOV, F.K.,

         Inorg. Mat. 2(2), 307 (1966)

137.   PUTNIS, A. and BISH, D.L., Amer. Mineral. 68(1-2),

         60 (1983)

138.   McMILLAN, P., PUTNIS, A. and CARPENTER, M.A., Phys. Chem.

         Min. 10(6), 256 (1984)

139.   SORRELL, C.A., J. Amer. Ceram. Soc. 43(7), 337 (1960)

140.   LOWENSTEIN, W., Amer. Mineral. 39, 92 (1954)

141.   FYFE, C.A., GOBBI, G.C., KLINOWSKI, J., PUTNIS, A. and

         THOMAS, J.M., J. Chem. Soc. Comm., 556 (1983)

142.   MIYASHIRO, A., IIYAMA, T., IAMASKA, M. and MIYASHIRO, T.

         Amer. J. Sci. 253, 185 (1955)

143.   MIYASHIRO, A., Amer. J. Sci. 255, 43 (1957)

144.   SCHREYER, W. and YODER, H.S., Neues. Jahrb. Mineral Akstr.

         101, 271 (1964)

145.   FOLINSBEE, R.E., Amer. Min. 26, 485 (1941)

146.   SELKREGG, K.R. and BLOSS, F.D., Amer. Mineral.
         65, 522 (1980)

147.   FARRELL, E.F. and NEWNHAM, R.E., Amer. Mineral 52, 380
         (1967)

148.   GOLDMAN, D.S., ROSSMAN, G.R. and DOLLASE, W.A.,
         Amer. Mineral. 62, 1144 (1977)

149.   ARMBUSTER, T. and BLOSS, D.F., Nature 286, 140 (1980)

150.   HOCHELLA, A., M.F. BROWN, G.E., ROSS, F.K. and GIBBS, G.V.,
         Amer. Mineral. 64, 337 (1979)

151.   LEAKE, B.E., Amer. Mineral. 45, 282 (1960)

152.   STOOKEY, S.D., U.S. Patent No. 2,920,971 Jan. (1960)

153.   GREGORY, A.G. and VEASEY, T.J., J. Mat. Sci. 6(10),
         1312 (1971), 7(11), 1327 (1972), 8(3), 324 (1973) and
         8(3), 333 (1973)

154.   DeVEKEY, R.C. and MAJUMDAR, A.J., Glass Technol. 14(5),
         125 (1973) and 15(3), 71 (1974)

155.   BARRY, T.I., LAY, L.A. and MORRELL, R., Sci. Ceram. 8,
         331 (1976)

156.   BARRY, T.I., COX, J.M. and MORRELL, R., J. Mat. Sci.
         13(3), 594 (1978)

157.   TODHUNTER, R., PhD. Thesis, University of Warwick
         Jan. (1984)

158.   RABINOVICH, E.M. in 'Nucleation and Crystallization in
         Glasses' p.327. Ed. J. H. Simmons. Amer. Ceram. Soc.
         Ohio (1982)

159.   HELGESSON, C.I., Sci. Ceram. 8, 347 (1976)

160.   MORRELL, R., Brit. Ceram. Soc. Proc. 28, 53 (1979)

161.   MILLER, D.M., U.S. Patent No. 3,926,648 Dec. (1975)

162.   STONG, G.E., U.S. Patent No. 3,450,546 June (1969)

163.   MUSSLER, B.H. and SHAFER, M.W., Bull. Amer. Ceram. Soc.
         63(5), 705 and 714 (1984)

164.   RUSCONI, D.M., ANDERSON, R.M. and WACHTMAN, presented at the
         88th American Society Meeting, Chicago (1986)

165.   THOMPSON, R.G., presented at the 88th American Society
         Meeting, Chicago (1986)

166.   McMILLAN, P.W. and PARTRIDGE, G., U.K. Patent No.
         924, 996 May (1963)

167.   PARTRIDGE, G. and McMILLAN, P.W., Glass Technol. 4(6)
         173 (1963)

168.   GOSTELOW, C.R. and RESTALL, J.E. in 'Special Ceramics,
         Vol. 6' p.23 Ed. P. Popper. Brit. Ceram. Res. Ass.
         July (1974)

169.   PAVLUSHKIN, N.M. and KHODAKOVSKAJA, R.J., Sci. Tech.
         Comm. 2, 1051 (1971)

170.   KINGERY, W.D. in 'Ceramic Fabrication Processes' p.55
         Ed. W.D. Kingery. M.I.T. Press, J. Wiley and Chapman and
         Hall, New York (1958)

171.   REED, J.S. and RUNK, R.B. in 'Treatise on Materials Science
         and Technology Vol. 9 Ceramic Fabrication Processes' p. 71
         Ed. F.F.Y. Wong. Academic, Press London (1976)

172.   STRIJBOS, S. and VERMEER, P.A. in 'Materials Science
        Research, Vol. 11. Processing of Crystalline Ceramics'
        p.113 Ed. H. Palmour, R.F. Davis and T.M. Hare. Plenum
        Press, New York (1978)

173.   KLUG, H.P. and ALEXANDER, L.E., 'X-Ray Diffraction
        Procedures' J. Wiley, New York (1954)

174.   SCHERRER, P., Gott. Nach. $\underline{2}$, 98 (1918)

175.   WARREN, B.E. and BISCOE, J., J. Amer. Ceram. Soc. $\underline{21}$, 49
        (1938)

176.   WARREN, B.E., J. Appl. Phys. $\underline{12}$, 375 (1941)

177.   JONES, F.W., Proc. Roy. Soc. (London) $\underline{166A}$, 16 (1938)

178.   BRAGG, L., 'The Crystalline State, Vol. 1. A General
        Survey' p. 189 G. Bell and Sons, London (1919)

179.   MURDOCH, C.C., Phys. Rev. $\underline{31}$, 304 (1928) and $\underline{35}$, 8 (1930)

180.   WARREN, B.E., Z Kristallogr. $\underline{99}$, 448 (1938)

181.   BORCHARDT, H.J. and DANIELS, F., J. Amer. Chem. Soc.
        $\underline{79}$(1), 41 (1957)

182.   SKVARA, F. and SATAVA, V., J. Thermal Anal. $\underline{2}$(3), 325 (1970)

183.   KISSINGER, H.E., J. Res. Nat. Bur. Stand. $\underline{57}$(4), 217 (1956)

184.   KISSINGER, H.E., Anal. Chem. $\underline{29}$(11), 1702 (1957)

185.   AKITA, K. and KASE, M., J. Phys. Chem. $\underline{72}$, 906 (1968)

186.   REED, R.L., WEBER, L. and GOTTFRIED, B.S. Ind. Eng. Chem.
        Fund. $\underline{5}$, 286 (1966)

187.   HENDERSON, D.W., J. Non. Cryst. Sol. $\underline{30}$, 301 (1979)

188.   MATUSITA, K. and SAKKA, S., Phys. Chem. Glasses $\underline{20}$(4),
        81 (1979)

189.   BOWEN, D.K. and HALL, C.R., 'Microscopy of Materials'
        MacMillan London (1975)

190. WONG, J. and ANGELL, C.A., 'Glass Structure by Spectroscopy'
      Dekker, New York (1976)

191. FARMER, V.C., 'The Infrared Spectra of Minerals'
      Mineralogical Society, London (1974)

192. SIMON, I. in 'Modern Aspects of the Vitreous State, Vol. 1'
      p.120 Ed. J. D. Mackenzie.Butterworths, London (1960)

193. WHITE, R.G., 'Handbook of Industrial Infrared Analysis'
      Plenum Press, New York (1964)

194. FRIDMANN, S.A., Prog. Infrared Spectrosc. 3, 1 (1967)

195. DACHILLE, F. and ROY, R., Nature (London) 186, 34 and
      71 (1960)

196. SCHAEFFER, C. and MATOSSI, F. 'Ultrarote Spekrum'
      Springer, Berlin (1930)

197. RUBENS, H. and NICHOLS, F., Wied. Ann. 60, 418 (1897)

198. PAO, M.A. and KLAR, E. in 'Metals Handbook Vol. 7. Powder
      Metallurgy (9th Edition)' p.221 ASM, Ohio (1984)

199. RAYLEIGH, J.W.S., Phil. Mag. 41(4), 107 and 274 (1871)

200. MIE., G., Ann. Physik. 25, 377 (1908)

201. PURCELL, E.M., TORREY, H.C. and POUND, R.V., Phys.
      Rev. 69, 37 (1946)

202. BLOCH, F., HANSEN, W.W. and PACKARD, M., Phys. Rev.
      69, 127 (1946)

203. SLICHTER, C.P., 'Solid State Sciences Vol. 1. Principles
      of Magnetic Resonance' Springer, Berlin (1980)

204. ABRAGHAM, A., 'The Principles of Nuclear Magnetism'
      Clarendon Press, Oxford (1961)

205.   BRAY, P.J. and SILVER, A.H. in 'Modern Aspects of the
        Vitreous State, Vol. 1' p.92 Ed. J.D. Mackenzie.
        Butterworths, London (1960)

206.   HARRIS, R.K. 'NMR Spectroscopy' Pitman,London (1983)

207.   MARCIEL, G.E., Science 226, 282 (1984)

208.   OLDFIELD, E. and KIRKPATRICK, R.J., Science 227, 1537 (1985)

209.   ANDREW, E.R., BRADBURY, A. and EADES, R.G., Nature (London)
        182, 1659 (1958)

210.   ANDREW, E.R., Int. Rev. Phys. Chem. 1, 195 (1981)

211.   KLINOWSKI, J. and THOMAS, J.M., Endeavour 10(1), 2 (1986)

212.   DOUGLASS, R.W., ARMSTRONG, W.L., EDWARD, J.P. and HALL, D.,
        Glass. Technol. 6(2), 52 (1965)

213.   LEES, C.H., Phil. Trans. Roy. Soc. (London) 191, 399 (1898)
        and 208, 381 (1908)

214.   JERRARD, H.G. and McNEILL, D.B., 'Theoretical and
        Experimental Physics' p.261 Chapman and Hall, London (1960)

215.   ESTERMANN, I. 'Methods of Experimental Physics, Vol. 1
        Classical Methods' p. 496 Academic Press London (1959)

216.   AMERY, W.G. and HAMBURGER, F., Amer. Soc. Test. Mat.
        49, 1079 (1949)

217.   FIELD, R.F., Amer. Soc. Test. Mat. 54, 456 (1954)

218.   STEVELS, J.M., 'Hanbuck der Physik, XX' p. 372 Springer,
        Berlin (1957)

219.   MULAR, A.L., Con. Metall. Q. 4(1), 31 (1965)

220.   SOMASUMDARAN, P. in 'Ceramic Processing Before Firing'
        p.105 Ed. G.V. Onada and L.L. Hench. Wiley, New York (1978)

221.   RYSHKEWITCH, E., 'Oxide Ceramics' p.12 Academic Press,
        New York (1960)

222.   A.S.M. Committee on Milling in 'Metals Handbook, Vol. 7.
        Powder Metallurgy (9th Edition)' p.56 American Society
        for Metals, Ohio (1984)

223.   FRANCIS, T.L., MacZURA, G., MARHANKA, J.E. and PARKER, H.J.,
        Bull. Amer. Ceram. Soc. 51(6), 535 (1972)

224.   DUPREE, R., FARNAN, I., FORTY, A.J., EL-MASHRI, S. and
        MOTTYAN, L. in 'The Structure of Non Crystalline Materials'
        Ed. C. Janot and A. F. Wright. J. Phys. Paris (to be
        published)

225.   MULLER, D., GESSNER, W., BIHRENS, H.J. and SCHELER, G.,
        Chem. Phys. Lett. 79(1), 59 (1981)

226.   MARICQ, M.M. and WAUGH, J.S., Chem. Phys. Lett. 47(2),
        327 (1977)

227.   MARICQ, M.M. and WAUGH, J.S., J. Chem. Phys. 70(7),
        3300 (1979)

228.   WAUGH, J.S., MARICQ, M.M. and CANTOR, R., J. Magn. Res.
        29(2), 183 (1978)

229.   RICHERSON, A.W., 'Modern Ceramic Engineering' p.161
        Marcel Dekker, New York (1982)

230.   BRAGG, L. and CLARINGBULL, C.F., 'The Crystalline State,
        Vol. IV. The Crystal Structure of Minerals' p.196
        G. Bell and Sons, London (1965)

231.   SMITH, K.A., KIRKPATRICK, R.J., OLDFIELD, E. and HENDERSON
        D.M., Amer. Mineral. 68(11-12), 1206 (1983)

232. LIPPMAA, E., MAGI, M. SAMOSON, A., ENGELHARDT, G. and
      GRIMMER, A.R., J. Amer. Chem. Soc. 102, 4889 (1980)

233. GRESKOVICH, C. in 'Treatise on Material Science and
      Technology, Vol. 9. Ceramic Fabrication Processes'
      p. 915 Ed. F.F.Y. Wang. Academic Press, New York (1976)

234. QUATINETZ, M., SCHAFER, R.J. and SMEAL, C.R. in
      'Ultrafine Particles' p.271 Ed. W.E. Kuhn. Wiley,
      New York (1963)

235. GRIFFITH, A.A., Phil. Trans. Roy. Soc. A221, 163 (1920)

236. NIESZ, D.E. and BENNETT, R.B. in 'Ceramic Processing Before
      Firing' p.61 Ed. G.Y. Onoda and L.L. Hench. Wiley,
      New York (1978)

237. REED, J.S., CARBONE, T., SCOTT, C. and RUKASIEWICZ, S. in
      'Materials Science Research, Vol. 11. Processing of
      Crystalline Ceramics' p.171 Ed. H. Palmour, R.F. Davies and
      T.M. Hare. Plenum Press, New York (1978)

238. KIESSKALT, S.Z., Ver. Dunt. Ing. 91, 313 (1949)

239. FRENKEL, J., J. Phys. (U.S.S.R.) 9(5), 385 (1945)

240. KUCZYNSKI, G.C., J. Appl. Phys. 20(12), 1160 (1949)

241. KINGERY, W.D. and BERG. M., J. Appl. Phys. 26(10),
      1205 (1955)

242. KUCZYNSKI, G.C. and ZAPLATYNSKIJ, I., J. Amer. Ceram. Soc.
      349(10), 349 (1956)

243. ESHELBY, J.D., Trans. A.I.M.E. 185(11), 806 (1949)

244. MACKENZIE, J.K. and SHUTTLEWORTH, R., Proc. Roy. Soc.
      (London) 62(12-B), 833 (1949)

245.   KINGERY, W.D., BOWEN, H.K. and UHLMANN, D.R., 'Introduction to Ceramics' p.493 Wiley, New York (1960)

246.   SCHERER, G.W., J. Amer. Ceram. Soc. 60(5-6), 236 (1977)

247.   SCHERER, G.W. and BACHMAN, D.L., J. Amer. Ceram. Soc. 60(5-6), 239 (1977)

248.   SCHERER, G.W., J. Amer. Ceram. Soc. 60(5-6), 243 (1977)

249.   EXNER, H.E., PETZOW, G. and WELLNER, P. in 'Sintering and Related Phenomena' p.351 Ed. G.C. Kuczynski. Plenum Press, New York (1973)

250.   GUTMANAS, E.Y., RABINKIN, A. and ROITBERG, M., Scripta. Metall. 13(1), 11 (1979)

251.   GUTMANAS, E.Y., Powder Met. Int. 12(4), 178 (1980)

252.   OCCHIONERO, M.A. and HALLORAN, J.W. in 'Materials Science Research, Vol. 16. Sintering and Heterogenious Catalysis' p.89 Ed. G.C. Kuczynski, A.E. Miller and G.A. Sargent.Plenum Press, New York (1984)

253.   HERRING C., J. Appl. Phys. 21(4), 301 (1950)

254.   EVANS, C. in 'Metals Handbook, Vol. 7. Powder Metallurgy (9th Edition)' p.288. American Society for Metals, Ohio (1984)

255.   CHOWDHRY, U. and CANNON, R.M. in 'Materials Science Research Vol. 11. Processing of Crystalline Ceramics' p.443 Ed. H. Palmour, R.F. Davis and T.M. Hare. Plenum Press, New York (1978)

256.   CUTLER, I.B. and HENRICHSEN, R.E., J. Amer. Ceram. Soc. 51(10), 604 (1968)

257.   CAHN, I.W. and HEADY, R.B., J. Amer. Ceram. Soc. 53(7), 406 (1970)

258.   NII, K.H., Z. Metall. 61, 935 (1970)

259.   YAN, M.F. in 'Advances in Powder Technology' p.107 Ed. G.Y. Chin. Amer. Soc. Test. Mats., Ohio (1982)

260.   KOLAR, D., KUCZYNSKI, G.C. and CHIANG, S.K. in Materials Science Research, Vol. 16. Sintering and Heterogeneous Catalysis' p.81 Ed G.C. Kuczynski, A.E. Miller and G.A. Sargent. Plenum Press, New York (1984)

261.   FULCHER, G.S., J. Amer. Ceram. Soc. 8(6), 339 (1925)

262.   LAKATOS, T., JOHANSSON, L.G.and SIMMINGSKOLD, B., Glass Technol. 13(3), 88 (1972)

263.   LYON, K.C., J. Res. Nat. Bur. Stand. 78A(4), 497 (1974)

264.   GIESS, E.A. and KNICKERBOCKER, S.H., J. Mat. Sci. Lett. 4, 835 (1985)

265.   SONG, H., COBLE, R.L. and BROOK, R.J. in 'Materials Science Research, Vol. 16. Sintering and Heterogeneous Catalysis' p.63 Ed. G.C. Kuczynski, A.E., Miller and G.A. Sargent. Plenum Press New, York (1984)

266.   DIETZEL, A., Sprechsaal 75, 82 (1942)

267.   GIESS, E.A., FLETCHER, J.P. and HERRON, L.W., J. Amer. Ceram. Soc. 67(8), 549 (1984)

268.   PERROT, G.J. and KINNEY, S.P., J. Amer. Ceram. Soc. 6, 417 (1923)

269.   GIESS, E.A., GUERCI, C.F., WALKER, G.F. and WEN, S.H., J. Amer. Ceram. Soc. 68(12), C-328 (1985)

270.   EXNER, H.E. and PETZOW, G. in 'Materials Science Research Vol. 10. Sintering and Catalysis' p.279 Ed. G.C. Kuczynski. Plenum Press, New York (1975)

271.   WILDER, D.R. and FITZSIMMONS, E.S., J. Amer. Ceram. Soc. 38(2), 66 (1955)

272.   NORTON, F.H., KINGERY, W.D., HALDEN, F.A. and BERG, M., Atom. En. Comm. Rept. No. NYO-6289 SEP-80 Nov. (1951)

273.   AMATO, J. and NEGRO, A., Ceram. 4(4), 237 (1974)

274.   TODHUNTER, R., Ph.D. Thesis p.38 University of Warwick (1984)

275.   MATUSITA, K., SAKKA, S., and MATSUI, Y., J. Mat. Sci. 10(1), 961 (1975)

276.   MATUSITA, K. and SAKKA, S., Thermochim. Acta 33, 351 (1979)

277.   MATUSITA, K. and SAKKA, S., J. Non Crystal. Sol. 38 and 39 (Part 2), 741 (1980)

278.   WATANABE, K. and GEISS, E.A., J. Amer. Ceram. Soc. 68(4), C102 (1985)

279.   ZDANIEWSKI, W., J. Mat. Sci. 8, 192 (1978)

280.   HUTTON, W. and THORP, J.S., J. Mat. Sci. 20, 542 (1985)

281.   SEIFERT, F., MYSEN, B.O. and VIRGO, D., Amer. Mineral. 67, 696 (1982)

282.   SIMMONS, J.H., J. Non Crystal. Sol. 24, 77 (1977)

283.   TAKHER, E.A., POPIL 'SKII, R.Y., DAIN, E.P.,
        LUKOPEROVA, M.G. and KIR'YANOVA, N.A., Glass and
        Ceramics 7, 445 (1977)

284.   SARVER, J.F. and HUMMEL, F.A., J. Amer. Ceram. Soc.
        45(4), 152 (1962)

285.   GOSSNER, B., Centr. Mineral. Geol. 1928A, 204 (1928)

286.   IIYAMA, T., Proc. Imp. Acad. Jap. 31, 166 (1955)

287.   IKAWA, H., OTAGIRI, T., IMAI, O., URABE, K. and VDAGAWA, S.,
        J. Ceram. Soc. Jap. 64(3), 344 (1986)

288.   J.C.P.D.S. File No. 13-293 (1984)

289.   LANGER, K. and SCHREYER, W., Amer. Mineral. 54, 1442 (1969)

290.   DACHILLE, F. and ROY, R., Z. Kristallogr. 111, 462 (1959)

291.   TARTE, P., Bull. Ceram. Fr. Soc. 58, 13 (1963)

292.   FARMER, V.C., 'The Infrared Spectra of Minerals' p. 293
        Mineralogical Soc., London (1974)

293.   CROZIER, D. and DOUGLASS, R.W., Phys. Chem. Glasses
        6(6), 240 (1965)

294.   ESTEP, P.A., KOVACH, J. and KARR, C., Proc. 2nd Lunar
        Sci. Conf. Geochim. Cosmochim. Acta. Supp.3 2, 21377 (1971)

295.   SANDERS, D.M., PERSON, W.B. and MENCH, L.L., Appl. Spec.
        28(3), 246 (1974)

296.   ESTEP, P.A., KOVACH, J., WALDSTEIN, P. and KARR, C.,
        Proc. 3rd Lunar Sci. Conf. Geochim. Cosmochim. Acta.
        Supp.3 3, 3047 (1972)

297.   TODHUNTER, R., Ph.d. Thesis p.49 University of Warwick
        (1984)

298.   PLIUSNINA, I.J. and BOKII, G.B., Sov. Phys. Cryst.
        3, 761 (1958)

299.   WYCKOFF, R.W.G. 'Crystal Structures, 2nd Edition,

        Vol. 1' p.313 Interscience, New York (1963)

300.   BACHIORRINI, A., Ceram. 8(2), 81 (1978)

301.   KLINOWSKI, J., RAMDAS, S., THOMAS, J.M., FYFE, C.A.

        and HARTMAN, J.S., J. Chem. Soc. Faraday Trans II

        78, 1025 (1982)

302.   THOMAS, J.M., FYFE, C.A., RAMDAS, S., KLINOWSKI, J. and

        GOBBI, G.C., J. Phys. Chem. 86, 3061 (1982)

303.   FYFE, C.A., THOMAS, J.M., KLINOWSKI, J. and GOBBI, G.C.,

        Angew. Chem. Int. Ed. Engl. 22(4), (1983)

304.   FYFE, C.A., GOBBI, G.C., and PUTNIS, A., J. Amer. Chem.

        Soc. 108(12), 3218 (1986)

305.   DUPREE, R. HOLLAND, D., McMILLAN, P.W. and PETTIFER, R.F.,

        J. Non. Crystal. Sol. 68, 399 (1984)

306.   DUPREE, R., HOLLAND, D. and WILLIAMS, D.S., 3rd Int. Conf.

        on Structure of Non Crystal. Mats. Grenoble (1985),

        J. de Phys. Colloq. C8(12), 119 (1985)

307.   MULLER, D., GESSNER, W., BEHRENS, H.J. and SCHELER, G.,

        Chem. Phys. Lett. 79(1), 59 (1981)

308.   FOSTER, W.R., J. Amer. Ceram. Soc. 34(9), 255 (1951)

309.   ATLAS, L., J. Geol. 60(2), 125 (1952)

310.   MORIMOTO, N., Carn. Inst. Wash. Year Book 58, 197

        (1958-59)

311.   SMITH, J.V., Acta Cryst. 12(7), 515 (1959)

312.   LACHMAN, I.M., BAGLEY, R.D. and LEWIS, R.M., Bull. Amer.

        Ceram. Soc. 60(2), 202 (1981)

313.   RUSS, J.C., EDAX Edit. 3(5), 10 (1973)

314.   J.C.P.D.S. File No. 19-768 (1984)

315.   J.C.P.D.S. File No. 22-714 (1984)

316.   SCHULZ, H., MUCHOW, G.M., HOFFMAN, W. and BAYER, G.,
        Z. Kristallogr. 133, 91 (1971)

317.   SCHULZ, H., HOFFMAN, W. and MUCHOW, G.M., Z. Kristallogr.
        134, 1 (1971)

318.   DIETZEL, A., Glasstech. Ber. 21, 198 (1943)

319.   VOLF, M.B., 'Glass Science and Technology, Vol. 7. Chemical
        Approach to Glass' p.194 Elsevier, Amsterdam (1984)

320.   KONIJNENDIJK, W.L., 'The Structure of Borosilicate Glasses'
        Philips Res. Repts. Suppl. No.1. Philips Res. Labs. (1975)

321.   McMILLAN, P.W., 'Glass Ceramics' p.68 Academic Press,
        London (1964)

322.   TOPPING, J.A. and MURPHY, H.K., J. Can. Ceram. Soc.
        46, 19 (1977)

323.   KINGERY, W.D., BOWEN, H.K. and UHLMANN, D.R.,
        'Introduction to Ceramics' p.955 Wiley, New York (1976)

324.   GELLER, R.F. and INSLEY, H., U.S. J. Res. 9(1), 35 (1932)

325.   HUMMEL, F.A. and REID, M.W., J. Amer. Ceram. Soc.
        34(10), 319 (1951)

326.   BEALS, R.J. and COOK, R.L., J. Amer. Ceram. Soc. 35(2),
        53 (1952)

327.   LEE, J.D. and PENECOST, J.L., J. Amer. Ceram. Soc. 59
        (3-4), 183 (1976)

328.   MILBERG, M.E. and BLAIR, H.D., J. Amer. Ceram. Soc.
        60(7-8), 372 (1977)

339.   IKAWA, H. et al, J. Amer. Ceram. Soc. 69(6), 492 (1986)

330.   MOROSIN, B., Acta Crystallogr. (Sect. B) 28(6), 1899 (1972)

331.   ROY, R. and AGRAWAL, D.K. in 'Materials Research Society,
        Vol. 40. Electronic Packaging Materials Science' p.83.
        Ed. E.A. Geiss, K.N. Tu and D.R. Uhlmann. Mat. Res. Soc.
        Pittsburgh 1985

332.   HOCHELLA, M.F. and BROWN, G.E., J. Amer. Ceram. Soc.
        69(1), 13 (1986)

333.   EVANS, D.L., FISCHER, G.R., GEIGER, J.E. and MARTIN, F.W.,
        J. Amer. Ceram. Soc. 63(11-12), 629 (1980)

334.   KINGERY, W.D. in 'Progress in Ceramic Science, Vol. 2'
        p.181 Ed. J.E. Burke. Plenum Press, New York (1962)

335.   KITTEL, C., Phys. Rev. 75, 972 (1949)

336.   BASKARAN, S., BHADURI, S.B. and HASSELMAN, D.P.H.,
        J. Amer. Ceram. Soc. 68(3), 112 (1985)

337.   WATANABE, M., CAPORALI, R.V. and MOULD, R.E. in
        'Symposium on Nucleation and Crystallization of Glasses'
        p.23 Ed. M.K. Reser. Amer. Ceram. Soc., Ohio (1962)

339.   HING, P., Proc. Brit. Ceram. Soc. 25, 13 (1975)

339.   HING, P. and McMILLAN, P.W., J. Mat. Sci. 8(7),
        1041 (1973)

340.   DUCKWORTH, W., J. Amer. Ceram. Soc. 36(2), 68 (1953)

341.   EVANS, A.G., J. Amer. Ceram. Soc. 63(3), 127 (1982)

342.   PLETKA, B.J. and WIEDERHORN, S.M., J. Mat. Sci. 17(5),
        1247 (1982)

343.   KATZ, R.N. and LENOE, E.M. in 'Treatise on Materials
        Science and Technology, Vol. 9. Ceramic Fabrication

Processes' p.241 Ed. F.F.Y. Wang. Academic Press, New York (1976)

344. BANSAL, G.K., DUCKWORTH, W. and NIESZ, D.E., Bull. Amer. Ceram. Soc. 55(3), 289 (1976)

345. LEWIS, D., Bull. Amer. Ceram. Soc. 61(11), 1208 (1982)

346. PICKETT, G., Proc. Amer. Soc. Test. Mats. 45, 846 (1945)

347. CHOW, L., CONWAY, H.D., WINTER, G. and ASCE, M., Amer. Soc. Civ. Eng. Trans. 118, 686 (1957)

348. KAAR, P.H., Proc. Soc. Expt. Stress Anal. 15(1), 77 (1957)

349. SAAD, S. and HENDRY, A.W., Expt. Mech. Proc. Soc. Expt. Stress Anal. 19(1), 192 (1961)

350. DUCKWORTH, W.H., J. Amer. Ceram. Soc. 34(1), (1951)

351. HOAGLAND, R.G., MARSCHALL, C.W. and DUCKWORTH, W.H., J. Amer. Ceram. Soc. 59(5-6), 189 (1976)

352. ROARK, R.J. and YOUNG, W.C., 'Formulas for Stress and Strain, 5th Edition' p.189 McGraw Hill, Tokyo (1975)

353. KITTEL, C., 'Introduction to Solid State Physics, 6th Edition' Wiley, New York (1986)

354. MASHKOVICH, M.D. and UDOVENKO, N.G., Sov. Phys. Sol. St. 7(2), 417 (1965)

355. McMILLAN, P.W., 'Glass Ceramics' p.117 Academic Press, London (1964)

356. FEKELDJIEV, G. and ANDREEVA, V., Int. Wiss. Kolloq. Tech. 28(4), 183 (1983)

357. DAVIES, M.J. and LOFTUS, J.P., Symp. Vit. Phase in Tech. Mats. p.1 Leeds (1972)

358.   BASTA, E.Z. and SAID, M.K.A., Brit. Ceram. Soc. Trans. J. 72(2), 69 (1973)

359.   SWARTZ, B. in 'Electronic Ceramics' p.12 Ed. O.J. Whittemore. American Ceramic Society, Ohio (1969)

360.   McCANDLISH, C.S. and DOW, A.L., Bull. Amer. Ceram. Soc. 64(4), 547 (1985)

361.   HYATT, E.P., Bull. Amer. Ceram. Soc. 65(4), 637 (1986)

362.   SHANEFIELD, D.J. in 'Materials Research Society, Vol. 40. Electronic Packaging Materials Science' p.69 Ed. E.A. Giess, K.N. Tu and D.R. Uhlmann. Materials Research Society, Pittsburgh (1985)

363.   ANDERSON, L.L., NUFER, R.W. and PUGLIESE, F.G., U.S. Patent No. 4,080,414 Mar. (1978)

364.   ONODA, G.Y. in 'Ceramic Processing Before Firing' p.235 Ed. G.Y. Onoda and L.L. Hench. Wiley, New York (1978)

365.   BURRELL, H., Interchem. Rev. 14(1), 3 (1955)

366.   MISTLER, R.E., SHANEFIELD, D.J. and RUNK, R.B. in 'Ceramic Processing Before Firing' p.411 Ed. G.Y. Onoda and L.L. Hench. Wiley New, York (1978)

367.   SHANEFIELD, D.J. and MISTLER, R.E., Bull. Amer. Ceram. Soc. 53(4), 416 (1974)

368.   CHANCE, D.A., Metall. Trans. 1(3), 685 (1970)

369.   VEST, R.W., Bull. Amer. Ceram. Soc. 65(4), 631 (1986)

370.   LARRY, J.R., ROSENBERG, R.M. and UHLER, R.O., L.E.E.E. Trans. CHMT-3(2), 211 (1980)

371.   VERMA, K.K. and ROBERTS, A. in 'Ceramic Processing Before Firing' p.463 Ed. G.Y. Onoda and L.L. Hench. Wiley, New York (1978)

372.   KURZWEIL, K. and FRANCONVILLE, F., Proc. Int. Hybrid Microelectron. Symp. p.246 (1975)

373.   PITKANEN, D.E., CUMMINGS, J.P. and SPEERSCHNEIDER, L.J., Sol. St. Technol. 23(10), 141 (1980)

374.   GRIER, J.D., Proc. Int. Hybrid Microelectron. Symp. p.249 (1976)

375.   WOOD, J.H., Proc. Int. Hybrid Microelectron. Symp. p.257 (1976)

376.   COX, J.J., Sol. St. Technol. 23(10), 150 (1980)

377.   MITCHELL, J.D., DONOHUE, P.C., NEEDES, C.R., FUNER, R.E. and UHLER, R.O., Int. Microelectron. Conf. p.108 Tokoyo (1980)

378.   MITCHELL, J.D., DONOHUE, P.C. and PATTERSON, F.K., Proc. 29th Electronic Compnts. Conf. p.1 Cherry Hill (1979)

379.   WU, T.S., SHIRAMATSU, T. and CHEN, S.N., Proc. 29th Electronic Compnts. Conf. p.11 Cherry Hill (1979)

380.   GIESFELDT, W.O., 8th Int. Electronic Circt. Pack. Symp. p.1 San Fransisco (1967)

381.   STALNECKER, S.G., Electrocompnt. Sci. and Technol. 8(1-3), 47 (1979)

382.   KURZWEIL, K. and LOUGHRAN, J., I.E.E.E. Trans. PHP-9(4), 216 (1973)

383.   ATKINSON, R.W., Sol. St. Technol. 14(5), 51 (1971)

384.   HERRON, L.W., MASTER, R.N. & TUMMALA, R.R., U.S. Pat. No. 4,234,367 Nov. (1980)

385.   PITKANEN, D.E., CUMMINGS, J.P. and SARTELL, J.A., Int.
        J. Hybrid Microelectron. $\underline{2}$(2), 45 (1979)

386.   PITKANEN, D.E., CUMMINGS, J.P. and SARTELL, J.A., Int.
        J. Hybrid Microelectron. $\underline{3}$(1), 1 (1980)

387.   PITKANEN, D.E., CUMMINGS, J.P. and SARTELL, J.A., Int.
        Microelectron. Symp. p.148 (1979)

388.   POETZINGER, J.E. and RISBUD, S.H., J. de Phys. $\underline{C4}$(4),
        147 (1985)

389.   KRIVEN, W.M. and RISBUD, S.H. in 'Materials Research
        Society, Vol. 40. Electronic Packaging Materials Science'
        p.323 Ed. E.A. Giess, K.N. Tu and D.R. Uhlmann.
        Materials Research Society, Pittsburgh (1985)

390.   SINGH, S.P. and NATH, G.P., J. Amer. Ceram. Soc. $\underline{61}$
        (9-10), 377 (1978)

391.   ADAMS, R. and McMILLAN, P.W., J. Mat. Sci. $\underline{17}$(1),
        2727 (1980)

392.   PARTRIDGE, G. and McMILLAN, P.W., Glass Technol. $\underline{15}$(5),
        127 (1974)

393.   HEADLEY, T.J. and LOEHMAN, R.E. J. Amer. Ceram. Soc.
        $\underline{67}$(9), 620 (1984)

394.   HAILES, L. and CROSSLAND, W.A., Elect. Pack and Prod.
        $\underline{8}$(4), 3 (1972)

395.   HSUEH, C.H. and EVANS, A.G., J. Amer. Ceram. Soc. $\underline{68}$(3),
        120 (1985)

396.   FREER, R., Contrib. Mineral. Petrol. $\underline{76}$, 440 (1981)

397.   PITKANEN, D.E., CUMMINGS, J. and SARTELL, J., Int. Symp.
        Hybrid Microelectronics p.49 (1980)

398.   KEYES, R.W., I.E.E.E., J. Sol. St. Circuits SC-13, 265 (1978)

399.   MAHALINGAM, M., Proc. I.E.E.E. 73(9), 1396 (1985)

400.   GREENWALD, F.T. and PAYNE, D.A. presented at the 88th Amer. Ceram. Soc. Meeting, Chicago (1986)

401.   VOLF, M.D., 'Technical Glasses' p.176 Pitman, London (1961)

402.   JAMES, P.F., J. Mat. Sci. 10(10), 1802 (1975)

403.   MAZURIN, O.V. and PORAI-KOSHITS, E.A., 'Phase Separation in Glasses' North Holland, Amsterdam (1982)

404.   HILLERT, M., Acta Metall. 9, 525 (1961)

405.   CAHN, J.W., Acta Metall. 9, 795 (1961)

406.   CAHN, J.W., J. Chem. Phys. 42(1), 93 (1965)

407.   CAHN, J.W. and CHARLES, R.J., Phys. Chem. Glasses 6(5), 181 (1965)

POSTSCRIPT

This thesis conforms to PHYS/PG/2